Oral lubrication of alternative proteins

Ben Kew

Submitted in accordance with the requirements for the degree of

Doctor of Philosophy

The University of Leeds

School of Food Science and Nutrition

December 2023

The candidate confirms that the work submitted is his/her own, except where work which has formed part of jointly-authored publications has been included. The contribution of the candidate and the other authors to this work has been explicitly indicated below. The candidate confirms that appropriate credit has been given within the thesis where reference has been made to the work of others. Details of the jointly-authored publications and contribution of each authors are outlined on the next page

Chapter 2

Kew, B., Holmes, M., Stieger, M. and Sarkar, A. 2020. Review on fat replacement using protein-based microparticulated powders or microgels: A textural perspective. *Trends in Food Science & Technology*. 106, pp.457-468.

Chapter 3

Kew, B., Holmes, M., Stieger, M. and Sarkar, A. 2021. Oral tribology, adsorption and rheology of alternative food proteins. *Food Hydrocolloids*. 116, p106636.

Chapter 5

Kew, B., Holmes, M., Liamas, E., Ettelaie, R., Connell, S.D., Dini, D. and Sarkar, A. 2023. Transforming sustainable plant proteins into high performance lubricating microgels. *Nature Communications.* 14(1), p4743.

Details of authorship contributions:

Ben Kew : designed the question for literature search, selected and conducted experimentation on the proteins chosen for this manuscript, identified the knowledge gap, drafted and edited the manuscript and replied to the comments from reviewers.

Simon Connel and Evan Liamas: contributed in imaging atomic force microscopy

Yunqing Wang: conducted TR146 mucin cell line experiments

Melanie Burke: Coded statistical analysis for Near-frequency infrared spectroscopy final analysis

Melvin Holmes: Conducted preliminary R code for statistical analysis

Anwesha Sarkar, Melvin Holmes, Markus Steiger and Melanie Burke: provided supervision and feedback on the literature research and contributed to the proofreading and editing of the manuscripts

List of accepted conference abstracts:

Poster Presentation:

Kew, B., Sarkar, A. Adsorption of dairy vs plant proteins using QCM-D. (2019) - 6th Food Science and Nutrition conference, Leeds, UK (1st place poster prize)

Kew, B., Sarkar, A. Adsorption of dairy vs plant proteins using QCM-D. (2020) – 18th Food Colloids Conference, Leeds, UK

Kew, B., Holmes, M., Stieger, M. and Sarkar, A. 2021. Oral tribology, adsorption and rheology of alternative food proteins (2020) – 7th Food Science and Nutrition PGR conference – Leeds, UK

Kew, B., Holmes, M., Liamas, E., Ettelaie, R., Connell, S.D., Dini, D. and Sarkar, A. 2023. Alternative Protein Microgels - 11th International Colloids Conference (2021) – Online

Kew, B., Holmes, M., Stieger, M. and Sarkar, A. 2021. Oral tribology, adsorption and rheology of alternative food proteins (2021) – 4th Structure and Functionality Conference – Online

Kew, B., Holmes, M., Stieger, M. and Sarkar, A. Oral tribology, adsorption and rheology of alternative food proteins – 34th EFFOST (2022) – Runner up in student of the year award

Kew, B., Holmes, M., Liamas, E., Ettelaie, R., Connell, S.D., Dini, D. and Sarkar, A. 2023. Lubrication Performance of Alternative Proteins and Microgel Particles for Fat Replacement Applications - Bragg Materials Science Conference (2022) – Leeds, UK (1st place poster prize)

Kew, B., Holmes, M., Stieger, M. and Sarkar, A. Improving Plant Proteins by Microgelation– 35th EFFOST (2023) – Runner up in student of the year award

Kew, B., Holmes, M., Steiger, M., Burke, M., Wang, Y. Sensory, Neural and Cellular Properties of Plant Protein – Eurosense (2022) – Turku, Finland

Kew, B., Holmes, M., Liamas, E., Ettelaie, R., Connell, S.D., Dini, D. and Sarkar, A. 2023. Transforming Plant Proteins into High Performance Microgels – UK SPM/AFM Conference (2023) – Leeds, UK

Oral presentation:

Kew, B., Holmes, M., Stieger, M. and Sarkar, A. Oral tribology, adsorption and rheology of alternative food proteins – Food Structure and Functionality Symposium (2020) - Online

Kew, B., Holmes, M., Stieger, M. and Sarkar, A. Oral tribology, adsorption and rheology of alternative food proteins – NIZO Plant Protein Sustainability Conference (2021) – Online

Kew, B., Sarkar, A. Oral tribology, adsorption and rheology of alternative food proteins. (2021) – 5th International Biotribology Conference – Online

Kew, B., Sarkar, A. Adsorption of dairy vs plant proteins using QCM-D. (2021) – Food Oral Processing Conference (1st place poster prize)

Kew, B., Holmes, M., Liamas, E., Ettelaie, R., Connell, S.D., Dini, D. and Sarkar, A. 2023. Lubrication Performance of Sustainable Microgel Particles for Fat Replacement Applications (2021) – COLL summer Symposium – Online

Kew, B., Holmes, M., Liamas, E., Ettelaie, R., Connell, S.D., Dini, D. and Sarkar, A. 2023. Oral Tribology, Lubrication and Adsorption of Alternative Food Proteins and Microgels - 75th STLE (Society of Tribologist and Lubrication engineers) (2021) – Online

Kew, B., Holmes, M., Liamas, E., Ettelaie, R., Connell, S.D., Dini, D. and Sarkar, A. 2023. Oral tribology, adsorption and rheology of plant proteins and

microgels - 95th ACS Colloid and Surface Science Symposium (Society of Tribologist and Lubrication engineers) (2021) – Online

Kew, B., Holmes, M., Liamas, E., Ettelaie, R., Connell, S.D., Dini, D. and Sarkar, A. 2023. Lubrication Performance of Sustainable Protein Microgels for Fat Replacement Applications - European Colloids and Interface Society (ECIS) (2021) – Athens, Greece

Kew, B., Holmes, M., Liamas, E., Ettelaie, R., Connell, S.D., Dini, D. and Sarkar, A. 2023. Lubrication Properties of Plant Protein Structures - Plant-Food Industry Conference (2022) – Leeds, UK

Kew, B., Holmes, M., Liamas, E., Ettelaie, R., Connell, S.D., Dini, D. and Sarkar, A. 2023. Modifying Plant Proteins as Microgels for Fat Replacement Applications - 74th American Oil and Chemistry Society (AOCS) (2022) – Atlanta, Georgia, USA (European Travel Grant Award)

Kew, B., Holmes, M., Stieger, M. and Sarkar, A. Sensory, Neural and Cellular Aspects of Plant Protein and Improving Protein by Microgelation - 75th American Oil and Chemistry Society (AOCS) (2023) – Denver, Colorado, USA (Processing Division Honorarium Award)

Kew, B., Holmes, M., Liamas, E., Ettelaie, R., Connell, S.D., Dini, D. and Sarkar, A. 2023. Transforming Plant Proteins into Microgels– Bragg Material Science Conference (2023) – Leeds, UK

Kew, B., Holmes, M., Steiger, M., Burke, M., Wang, Y. Sensory, Neural and Cellular Properties of Plant Protein – 7th School of FSN Annual Conference (2023) – Leeds, UK

Kew, B., Holmes, M., Liamas, E., Ettelaie, R., Connell, S.D., Dini, D. and Sarkar, A. 2023. Transforming Plant Proteins into Microgels–SOFT COMP Conference (2023) – Ancona, Italy (Travel Grant Winner, Keynote speaker)

Kew, B., Holmes, M., Liamas, E., Ettelaie, R., Connell, S.D., Dini, D. and Sarkar, A. 2023. Transforming Plant Proteins into Microgels–UK Colloids (2023) – Liverpool, UK

Kew, B., Holmes, M., Steiger, M., Burke, M., Wang, Y. Sensory, Neural and Cellular Properties of Plant Protein – Pangborn Sensory Conference (2023) – Nantes, France (Travel Grant Winner)

Acknowledgements

Firstly, there are truly unaccountable amounts of people who have inspired my journey in Food Science and in the privilege that I got to learn, and have access to education from the past decade until now. From high school to university, you know who you are and I have never forgotten you in supporting me in my journey to where I am today.

I thank my ERC LUBSAT grant for funding in order to do my PhD where In particular I thank my supervisor Professor Anwesha Sarkar as one of the most inspiring people I know, not just in academia but whose work ethos, dedication and ambition to her students and research will forever make an impact on me for these values I will hope to attain in my continued path in education. I also thank my secondary supervisor Dr Melvin Holmes – who knew I would still be around 8 years from delivering my first lecture!

I owe my initial roots for my fascination of food and science to my cooking teacher Paul Giles Philips. In the years that followed an interest in university blossomed from a love for learning made possible by my enthusiastic biology, food technology and importantly my art teachers – where despite studying science, to this day I have kept my promise to involve art in whatever I do. In this respect I especially thank Launceston college for supporting me in my home challenges during A-levels which allowed me to fulfil my, what was unlikely at the time, dream of attending university. Of all people I truly thank Lisa and Guy Southard who cared for me during these times whose selflessness is truly inspiring, it was because of you I am here now and have been role models for my optimism, energy, positivity and making the most out of every opportunity in life.

I was able to attend university and thank my whole university experience to a number of scholarships from generous alumni donors as well as from the School of Food Science and Nutrition at the University of Leeds. This funding allowed me to focus on my studies but discover sports, societies and communities for which I found new friends, developed skills, attitudes and strengths that has

carried me throughout education. On this note I thank Leeds University: Swimming and water polo, Rowing/boat club and Sailing societies that provided me with new hobbies, well needed socials, fun activities and maybe one to many drinks during my undergraduate and PhD.

I finally want to thank the School of Food Science, all its staff and the University of Leeds in general, I have always felt welcomed, accepted and safe to be and grow to who I am today without barriers and couldn't be part of a better community. Leeds is a beautifully diverse place and I have loved every opportunity learning about new cultures, making amazing friends from all corners of the globe and from all walks of life and hope the university continues to empower students from diverse backgrounds. And one final note I must thank the LGBTQ+ community of Leeds and my close lifelong friends: James. K, Megan. O, Oliver. M, Jose. M and my PhD partner in crime Fran. B – Given me the best years of my life and sorry for my occasional antics!

Abstract

Alternative proteins are gaining significant prominence in food design, driven by sustainability which is underscored by substantial greenhouse gas emissions associated with food production, particularly stemming from animal protein sources. However, the utilisation of alternative proteins remain limited, marked by subpar sensory performance, off mouthfeel and limited solubility in aqueous phase. Often such poor mouthfeel performance is hypothesised to be linked with astringency and lubrication failure. Although there has been substantial work in recent years in sensory performance of alternative proteins in various food applications, mechanistic understanding of the lubrication performance of alternative proteins remain elusive. A thorough literature search identified key gaps in this thesis which include limited characterisation of a range of alternative proteins, particularly plant proteins in terms of surface interactions and lubrication, all of which could play a pivotal role in improving their mouthfeel and acceptability in food products. Also, there is limited understanding on the origin of such lubrication failure in alternative proteins. Finally, how to limit such off-mouthfeel also remain underexplored.

This thesis has combined in-vitro, ex-vivo and in vivo methodological approaches in elucidating these knowledge gaps on mechanism behind off-tactile perception of alternative proteins. In particular, this thesis has highlighted the usefulness of new characterisation techniques including quartz crystal microbalance with dissipation, tribology using biomimetic surfaces, functional near-infrared spectroscopy and cellular models with salivary coating, Rate-All-That-Apply and theoretical assessment of tribological mechanism. Alternative proteins, such as pea, potato, lupin, and insect proteins were selected which hold high regard for future application. However, it was shown these alternative proteins suffer from high friction with friction coefficients increasing with higher concentration, a behaviour contrasting with those of animal protein (whey protein) counterparts. Next, model plant proteins either as single proteins or in mixed state were comprehensively characterised in their sensory profiling (n=100) identifying their taste and texture characteristics. Lupin and potato proteins surpassed the more often used pea protein in sensory aspects signifying their greater suitability for use in food applications. However, astringency immediately or as an aftertaste underlined the sensory profile of all plant proteins. When subjected to neural analyses, this astringent quality elicited a marked prefrontal cortex response, akin to the response observed with well-known astringent compound i.e. tannic acid. Furthermore, the presence of salivary protein binding was observed in presence of plant proteins again similar to tannic acid in cell culture experiments, a characteristic notably absent even at high concentrations of whey protein. With such poor lubrication and astringency aspects identified, the next step was to explore a colloidal strategy “microgelation” to limit lubrication failure. This process, never before applied to plant protein in lubrication context was able to

enhance the lubrication performance of plant proteins remarkably irrespective of the type of plant proteins used. Using in-vitro methodology of biomimetic tongue-like surface as well as mathematical modelling, the microgels of plant proteins were found to be ultra-lubricating, highly dispersible, stable and heat resistant irrespective of type or concentration. Strikingly, the plant protein microgels demonstrated lubricity resembling that of an oil-in-water emulsion despite having no lipidic additives in the microgels. In summary, this thesis provides a mechanistic understanding of lubrication failure of alternative proteins focusing primarily on plant proteins and provides a unique microgelation approach to address off-mouthfeel perception with the insights gathered paving the way forward for sustainable food development limiting “dryness” and “astringency” to improve consumer acceptability of alternative proteins.

Table of contents

List of Tables

List of Figures

List of Abbreviations

AFM	Atomic force microscopy
ANOVA	Analysis of variance
BSA	Bovine serum albumin
CNF	Cellulose nanofiber
CATA	Check-All-That-Apply
Ctr	Control water
DLS	Dynamic light scattering
DLPFC	Dorsolateral prefrontal cortex
DMPFC	Dorsomedial prefrontal cortex
DMEM	Dulbecco's Modified Eagle Medium
DMSO	Dimethyl sulfoxide
DPBS	Dulbecco's Phosphate-Buffered Saline
DPF	Differential path length factor
EWP	Egg white protein
EDTA	Ethylenediaminetetraacetic
EHL	Elastohydrodynamic regime
FBS	Fetal bovine serum
FF	Full fat

FM	Fat mimetic
fNIRS	Functional near-infrared spectroscopy
FR	Fat replacer
FS	Fat substitute
GHG	Greenhouse gas
HBSS	Hanks' balanced salt solution
HbO	Oxygenated haemoglobin
HbR	Deoxygenated haemoglobin
HEPPES	4-(2-hydroxyethyl)-1-piperazineethanesulphonic acid
HMF	Haemodynamic response function
HPC	Hemp protein concentrate
HTST	High temperature short time
IPC	Insect protein isolate
IPC_{sol}	Insect protein isolate soluble fraction
LF	Low fat
LCA	Life cycle assessment
LPI	Lupin protein isolate
LPI_{sol}	Lupin protein isolate soluble fraction
MCP	Microparticulated canola protein
MEP	Melanisation engaging protein
MEWP	Microparticulated egg white protein
MHP	Microparticulated hemp protein
MSP	Microparticulated soy protein
MWP	Microparticulated whey protein
NIR	Near-infrared
NWP	Nanoparticulated whey
N/D	Native/ denatured
NF	No fat
OA	Overall acceptability
O/W	Oil in water emulsion
PCA	Principle component analysis
PDMS	Polydimethylsiloxane
PWP	Polymerised whey protein
PI	Protease inhibitor
PPI	Pea protein isolate
PPC	Pea protein concentrate

PPC_{sol}	Pea protein concentrate soluble fraction
PPM	Pea protein microgel
PoPI	Potato protein isolate
$PoPI_{sol}$	Potato protein isolate soluble fraction
PPM	Potato protein microgel
PFC	Prefrontal cortex
QCM-D	Quartz crystal microbalance with dissipation
RATA	Rate-All-That-Apply
SAXS	Small angle X-ray scattering
SDS-PAGE	Sodium dodecyl-sulfate polyacrylamide gel electrophoresis
SPAN-80	Sorbitan monolete
SPI	Soy protein isolate
SEM	Scanning electron microscopy
SE	standard error
STD	Water standard
SDG	Sustainable Development Goals
TA	Tannic acid
TEM	Transmission electron microscope
TPA	Texture profile analysis
TR146	squamous cell carcinoma cells
TR146+S	squamous cell carcinoma cells with saliva
WHC	Water holding capacity
WPI	Whey protein isolate
WPI_{sol}	Whey protein isolate soluble fraction
WPM	Whey protein microgels
XG	Xanthan gum
α-la	*α*-lactalbumin
β-lg	*β*-lactoglobulin

List of symbols

G’	Storage modulus
G’’	Loss modulus
G*	Complex shear modulus

C	Mass sensitivity constant
tan(δ)	Loss factor
μ	Shear modulus
η	Viscosity
K	Consistency coefficient
n	Flow behaviour
μ	Coefficient of friction
σ	Shear stress
γ	Shear strain
$\dot{\gamma}$	Shear rate
ϕ	Volume fraction
φ	Phase angle
r	Pearson's correlation
ΔD	Change in dissipation
f	Frequency
Δf	Change in frequency
A	Amplitude
A	Area
A_t	Cross sectional area
E	Energy
E^*	Elastic modulus
F	Force
F_t	Applied force
F_N	Normal force
l	Length
R	Plate radius
K	Spring constant
h	Distance (between two plates)
H_t	Height at a given time
M	Torque
n	Overtone number
t	Time
T	Decay time
T	Torque
v	Poisson ratio
v	Velocity

V_R	Linear speed
Ω	Angular speed
x	Cantilever deflection
k_B	Boltzmann constant
T	Temperature
D	Translational diffusion coefficient
ρ	Density
δ	Shear wave
ω	Frequency of oscillation
α	Specific molar absorption coefficient
λ	Wavelength
λ	Specific height
W	Normal load
ε0	Permittivity of a vacuum
εr	relative permittivity or dielectric constant
k	Electrical double layer thickness
fka	Henry's function
$\boldsymbol{\eta}_\infty$	Viscosity at shear rate of $1000s^{-1}$
$\mathbf{d_H}$	Hydrodynamic diameter

Chapter 1 : General Introduction

As we confront the consequences of global warming and increasing food insecurity, the importance of sustainable food systems cannot be overstated in shaping the future of food production. Of all human-caused greenhouse gas (GHG) emissions, one-third can be attributed to the food-related emissions, with animal-based food production alone accounting for over half of those GHG emissions within the food-related emissions (Crippa et al., 2021). Consequently, there is a pressure in the food industries to deliver more sustainable, lower carbon footprint foods particularly using alternative protein sources. Additionally, with the global rise in obesity and diabetes, protein consumption is being leveraged as a weight management strategy due to its high satiety per calorie and potential to act as a fat substitute. In particular, plant proteins offer additional health benefits through the presence of phytonutrients.

One common way of incorporating more protein into food is by fortification using protein powders ranging from protein flours (<60 wt% protein), concentrates (60-80 wt% protein) to isolates (>90 wt% protein) (Nehete et al., 2013). The methods used to produce protein powders involve initial extraction (removal of fibre/fat and other contaminants, filtering and drying), followed by isolation (advanced separation using acid precipitation, ion exchange, micro/ultra-filtration or hydrolysis) (Rothstein, 1994). Examples of high protein foods include protein drinks and bars, although currently only in significant quantities utilising dairy proteins *(i.e.* whey) as these are more sensorial acceptable at higher concentrations. These protein powders also include a number of functional properties including emulsification and fat-replacement by

mimicking rheology and lubrication. In recent times, there has been an increase in novel sustainable proteins being commercially available. This trend is especially evident in the emergence of proteins sourced from vegetable by-products, as well as insects utilising their efficient vertical farming techniques. Additionally, a significant emphasis is being placed on locally sourced proteins that come with a low carbon footprint. Nevertheless, the functionality of these new proteins has been limited to date. Additionally plant proteins suffer from challenges in their palatability when consumed, with astringency widely reported in sensory study (Yousseef et al., 2016; Colonges et al., 2022; Tanger et al., 2022) and lubrication failure and delubrication being a particular tactile issue that restricts application (Zembyla et al., 2021; Vlădescu et al., 2023). Astringency of protein structures themselves have not been investigated where previous literature suggests astringency arises from phenolic compounds. The understanding of frictional properties of plant proteins and potential effectiveness of transforming them to valuable functioning ingredient, to reduce their astringency is the subject of investigation of this thesis.

1.1 Overall research aim

The escalation in plant protein consumption is an inevitable requirement to address the sustainable protein demands of our future. Plants offer an effective protein source that not only aligns with ethical considerations and generates fewer than half the greenhouse gas emissions compared to animal protein (Xu et al., 2021) , but also boasts high cultivation efficiency. This makes it a well-suited remedy for fulfilling the dietary requirements of an expanding global population. However, incorporation of plant proteins create a major sensory challenge resulting in infrequent consumption with considerable effort and therefore current

plant-based products have achieved limited success with consumer acceptability. Even in cases of success these products often lack sufficient protein and are often over-formulated with additional fat, sugar and salt to mask such poor sensory aspects (Choudhury et al., 2020) . This in turn leads to overall unhealthy food design unable to compete with animal and dairy proteins. Despite a new wave of commercialised plant protein powders in recent years, the characterisation, of their physicochemical, adsorption, tribological and sensory aspects are poorly understood and is key to unlock their potential for successful and smarter application. Although *in vivo* (sensory) experimentation has been extensive focusing on taste, texture has traditionally been overlooked with recent studies highlighting this importance in providing pleasure, mouthfeel, and lubrication to food. In case of *in-vitro* experimentation, often rheology and size measurements have been used to characterise texture, however an important aspect that has been neglected is surface-related interactions and tribology research.

Tribology is the study of lubrication, wear, and friction and plays a critical role in food texture. The key to the success of plant proteins may lie in understanding of surface-related texture i.e. how plant protein interact with oral surfaces contributing to mouthfeel. Such knowledge is key to intelligent design of protein ingredients that may improve performance functionally and sensorially with plant proteins not only contributing to replace animal proteins for promoting planetary health but also acting as *i.e.* fat mimetics. Several gaps in knowledge were captured in the review phase, which led to experimental work involving understanding of surface interactions of plant proteins, their comprehensive sensory and lubrication failure analysis, understanding the origin behind such

astringency and exploring processing methods to improve the tactile performance.

Thesis object: The overall aim of this thesis was to characterise tribology, rheology and adsorption behaviour of alternative proteins, relating these to sensory performance and identifying mechanisms and solutions to improve astringency aspects through increased lubrication. New neural and cellular characterisation tools and use of more real-life-simulating 3D tongue-like tribological surfaces have been applied to better quantify and relate to the sensory outcomes. These advancements in methodology could also play an important role in improving screening techniques for novel ingredients to accelerate plant-based food product development process.

Historically, soybean has been the dominant source of plant protein alternatives in commercialisation. However, there is now a movement towards increased diversity and highlighting underutilised proteins to avoid relying on single sources of protein. The limitations of food proteins, particularly soy can be allergenicity, sustainability aspects from global exportation and deforestation as well as protein digestibility, oestrogenic activity, anti-nutritional factors and essential amino acid imbalance. A range of new commercial plant protein categories was thus investigated in this thesis including legumes (pea, lupin), tuber (potato) and insects as alternative sources of protein. At the beginning of this PhD there existed limited awareness of the alternative protein studies elucidated in chapter 4 and expanded upon by Brown et al. (2021). The trajectory of this thesis evolved from its initial focus on utilising proteins as fat mimetics to encompass a more expansive perspective. This broader approach considered characterising new sustainable proteins, comprehending their adverse sensory and tribological aspects and developing techniques to improve their

functionalities. These efforts contribute extensively to the body of research expanding on the ongoing surge of studies concentrated on plant proteins in recent years.

In addition to fundamental and sensory comprehension, this thesis presents a solution to enhance the effectiveness of plant proteins through novel “microgelation” approach. The transformation of these proteins into microgels with superior lubricating properties offers a new technological promise for enhancing sensory perception, application, and the potential for fat mimetic functionality in the future.

Thesis hypothesis: The overarching hypothesis in this thesis was that understanding tribological and adsorption characteristics of novel proteins will enable decoding sensorially-perceived astringency in plant proteins.

1.2 Food proteins in general

Proteins are hierarchical macromolecules consisting of a fundamental primary structure made up of a number of types of amino acids in varying ratios, differing in properties determined by the R group (Moutevelis and Woolfson, 2009). The hydrogen and disulphide bonds of these amino acids form specific secondary and tertiary three-dimensional structures which may link with other protein subunits to form quaternary structures, these are typically globular or fibrous in nature. The overall charge of protein molecules, which governs particle interactions and stability within a specific solution, is dictated by the proportion, sequence, and quantities of amino acids (Wada and Nakamura, 1981). Significant alterations to protein structure can also be induced by the disruption of hydrogen and covalent bonds among amino acids within the secondary to quaternary structure. For instance, variations in pH or temperature can trigger protein unfolding, thereby

exposing hydrophobic cores. This exposure leads to the aggregation of proteins, eventually culminating in the gelation of the protein dispersed solution.

From an origin point of view, food proteins are categorised into muscle proteins, dairy proteins and plant proteins. Muscle proteins, composed of actin and myosin, are fibrous in structure and form long filaments that make up muscle fibres, dairy proteins such as whey is globular whereas casein are flexible random coil (Sarkar and Singh, 2016), highly digestible and soluble with the specific purpose of providing nutrition to mammalian offspring. On the other hand, plant proteins exist as storage bodies in plant cells consisting of a number of subunit proteins forming highly compact water-resistant sources of amino acids that are a reserve for growing plant fruits and are essential for plant growth (Pernollet, 1978; Weber and Neumann, 1980).

The fundamental sequence of amino acid order of a protein, primarily determined by genetic code encoded in DNA, plays a vital role in defining a protein's inherent function but as macronutrients and ingredients in food influences the functional use along with sensory perceptions. Plant proteins, as storage bodies are uniquely conformed where their secondary double beta barrel structure provides heat and proteolysis resistance as well as generating other functional hurdles i.e. solubility (Heldt and Piechulla, 2021). These require specific optimisation strategies for their improved utilisation in food applications (Sarkar and Dickinson, 2020).

1.3 Rational behind the alternative proteins and solutions researched in this thesis

1.3.1 Whey protein

Whey protein and its subunits have benefited from decades of extensive study and was one of the first mass produced protein powder supplements extracted from whey as a by-product from cheese production (Smithers, 2008). Nonetheless, whey, originating from dairy cattle farming, is regarded as less sustainable when contrasted with plant protein. This assessment is supported with life cycle assessment (LCA), which reveal GHG emissions to be higher than pork (Xu et al., 2021) and over six times as much CO_2 emitted compared to soy (16 CO_2e/kg protein vs 2.4 kg CO_2e/kg protein for soy isolate) with a 8-80 times higher footprint (Braun et al., 2016). Additionally, increases in milk allergy and lactose intolerance have added to the need to replace whey powders with alternatives. Despite these challenges, whey protein remains popular as a protein fortifier due to its high solubility and functional performance in food. Whey protein comprises several subunit globular proteins, with beta lactoglobulin making up the majority, accounting for 50-75% by weight. Bovine beta lactoglobulin consists of 162 amino acids and has a molecular weight of 18.3 kDa (Stanislava Uhrı, 2000) containing a free thiol group and its tertiary structure stabilised by two disulphide bridges between cysteine residues (Aschaffenburg and Drewry, 1957)). Alpha lactalbumin is the next most prominent subunit protein making up ∼20% wt/wt of whey consisting of 123 amino acids. The secondary structure consists mainly of alpha helixes that similarly to beta lactoglobulin is stabilised by disulphide bonds but in this case four (Aschaffenburg and Drewry, 1957; Permyakov and Berliner, 2000). The remainder fraction of whey are immunoglobulins (∼10% wt/wt), serum albumin and other minor protein or peptides (Walstra and Jenness, 1984). From a nutritional perspective, it boasts high digestibility and a comprehensive amino acid profile. Furthermore, in contrast to plant proteins, whey maintains a heightened level of palatability and

excellent lubricity even when utilized at elevated concentrations (Zembyla et al., 2021). As such, whey protein was considered the gold standard in food proteins for palatability and used as an ideal comparison in research including this thesis in **Chapters 3** and **Chapter 4**.

1.3.2 Pea protein

Pea protein is a popular hypo-allergenic vegan alternative protein which has found somewhat of a place in high plant protein drinks, bars, powders and as functional food ingredient in recent years. Additionally, its low cost, lower water use and ability to grow in cooler temperatures has seen a steady growth in popularity and is the current most viable replacement of soya protein (Tulbek et al., 2017). Consistent with general plant improvements in sustainability, life cycle assessment has been performed on pea specifically when replacing meat incurring a 24-100% lower environmental impact across numerous categories (Saget et al., 2021; Xu et al., 2021). A major benefit is that legumes are nitrogen fixing crops, forming a symbiotic relationship with *Bradyrhizobium* soil bacteria converting atmospheric nitrogen that can be used by the plants which reduces the need for synthetic high carbon emission fertilizers (Fasolin et al., 2019). The protein, typically derived from yellow split peas contains 25-30% protein consisting of four sub-unit fractions: mostly globulins with albumins, prolamines and glutelins. The three globulins are vicilin (7S, 32-50kDa) that exists as a trimer, legumin (11S, 23, 41 kDa) comprises a hexamer and convicilin (72, 77kDa) similar to vicilin as a 7-8S trimer but with additional charged amino acid protein and cysteine residue where each are cleaved and linked by disulphide acidic and basic polypeptides. Each form similar secondary and tertiary structures, a beta barrel and three alpha helices with the beta barrel in a compact double stranded conformation where there exact amino acids vary depending on cultivation and

species. The unique conformation provides heat and proteolysis resistance and an important feature for storage proteins (Heldt and Piechulla, 2021). In general these protein fractions contain high levels of lysine but limiting in cysteine and methionine amino acids (Pownall et al., 2010; Lu et al., 2020). Pea protein concentrate is featured extensively throughout this thesis in **Chapters 3, 4 and 5**.

1.3.3 Lupin protein

Lupin protein is derived from a high protein yielding bean (35-40 wt% protein) which is also within the legume family. These beans are harvested from a crop acknowledged as one of the most ecologically sustainable plant options (Lucas et al., 2015). Although lupin is a known allergen their potential as a sustainable crop globally may be critical for many local communities. The crop is adaptable, thriving in both temperate and cooler climates while demanding minimal water requirements where the latter challenges become more prevalent with global warming. They are well-suited for cultivation across diverse soil types and are commonly farmed in regions encompassing Europe, Australia, and South America. Recent life cycle assessment of environmental impact profiles compared to milk protein show an 80% lower impact in general per kg of protein (Vogelsang-O'Dwyer et al., 2020) that supports general lower plant protein GHG impacts compared to animal protein (Xu et al., 2021). Lupin protein is composed of mostly globulins and albumins. The globulins are comprised of four subunit proteins these are an 11S α-conglutin hexamer (330-430 kDa) similar to legumin, a 7S β-conglutin trimer (143-260 kDa) akin to vicilin, constituting the bulk of lupin protein, along with smaller fractions of 2S δ-conglutin monomer and 7S tetramer (47 kDa) γ-conglutin (Nadal et al., 2011). The 7S and 11S vary from 400-600 amino acids similar to pea dependent on source of protein (Shrestha et al., 2021)

which is also limited in cysteine and methionine amino acids. Lupin protein isolate has been utilised and characterised in chapters 3 and 4. However due to its similarity to pea protein in general in terms of tribological and adsorption properties, their use was discontinued from **chapter 5** for microgelation.

1.3.4 Potato protein

Ranked as the third most significant crop globally, the potato offers substantial energy and protein yields per unit area (Waglay et al., 2014). Derived from potato juice, potato protein offers a resolution to the predicament of managing waste and pollution linked to the by-product generated during potato refining processes. Notably, significant juice sources of this protein include chip and crisp production, with starch manufacturing, in particular, yielding juice containing 30-41% protein content (Wojnowska et al., 1982). Consequently, the extraction process generates a valuable commodity, eliminating costs while further mitigating environmental harm. These proteins primarily consist of storage proteins, mainly patatins, accompanied by relatively lower quantities of protease inhibitors, lectins, and enzymes. Patatins are an O-linked glycoproteins consisting of 366 amino acids which is formed by covalent bond between an oligosaccharide and asparagine with a molecular weight of 42-44kDa (Racusen and Weller, 1984; Ralet and Guéguen, 2000; Welinder and Jørgensen, 2009; Waglay et al., 2014). The amino acid composition is excellent and stands out as one of the best among the plant proteins with a high protein digestibility score akin to that observed in animal proteins (Ariëns et al., 2021). On a global scale, the extensive scope of potato manufacturing holds considerable promise as a significant source of hypoallergenic vegetable protein. Potato proteins are prominently featured throughout this thesis, including in **Chapters 3, 4, and 5**.

1.3.5 Insect protein

Across more than 100 countries spanning Asia, Africa, and South America, the consumption of insects holds substantial importance providing nutrition and a sustainable source of high quality protein (Baiano, 2020). Insect farming is notably efficient, as it produces low emissions, uses minimal water and can be fed off waste side streams. Furthermore, insect farming can be done vertically, occupying less land use, which is a unique advantage. Insect proteins encompass an array of skeletal muscle proteins, encompassing haemolymph, proteinases, melanisation-engaging proteins, and β-glycosidase, collectively providing the complete set of nine essential amino acids. In this thesis the utilisation of Buffalo Beetle (*Alphitobius diaperinus)* protein concentrate was considered, the world's first commercial insect protein powder. However, as a novel ingredient many new insects are hindered by regulatory laws and unable to be used in food requiring a number of years in approval. Additionally there are also bacterial and heavy metal concerns and even more pertinent is in the western diet, food neo-phobia of insects drives a reluctance to consume the food. Extracting insect protein in the form of powder emerges as a more feasible approach to integrating insects as ingredients but due to the prevailing challenges as well as limited information on protein structure use was discontinued after **Chapter 3**.

1.3.6 Tannic acid

Tannic acid is a naturally occurring polyphenol found in various plant species. It is a molecule formed from esterification of glucose or other polyols with gallic acid with its structure varying depending on origin of extraction (Bajec and Pickering, 2008). In nature it is a pivotal compound by acting as a deterrent, inducing an astringency response where it has the ability to bind and crosslink proteins in saliva by hydrogen bonding and other molecular interactions that leads to protein

aggregate clusters, loss of lubrication and a sensation of dryness and roughening in the mouth (Bate-Smith, 1954; Guinard et al., 1986). Tannic acid was used in **chapters 4** as a control comparison to that of the astringent responses of plant proteins.

1.4 Rationale behind the selection of characterisation techniques

1.4.1 Dynamic light scattering (DLS)

DLS was used to characterise the hydrodynamic particle sizes of hydrated native (**Chapter 3**) and microgelled proteins (**Chapter 5**)**.** This imaging technique measures particle size distributions within a solvent continuous phase typically ranging from 1 nm to 1000 nm. A laser is directed at a dilute sample contained within a transparent cuvette where upon contact with particles, the laser scatters and diffracts. The intensity of the scattered light fluctuates over time due to the Brownian motion of the particles resulting from collisions with water molecules. The diffusion rate of smaller particles is faster than that of larger particles, leading to quicker or slower fluctuations in light intensity.

An auto correlator compares nanosecond time-dependant snapshots of the intensity where correlation decays with time, the larger the particle the longer the decay in correlation will take to decay and visa versa. Subsequently we obtain a translational diffusion coefficient, which is then used with the Stokes-Einstein equation to determine the hydrodynamic diameter of the particle:

$$d_H = \frac{k_B T}{3\pi\eta D} \tag{1.1}$$

Where $k_B$is the Boltzmann constant, T is the temperature (Kelvin), η is the viscosity of the medium at zero shear rate and D is the translational diffusion coefficient. The polydispersity is also obtained which indicates particle size distribution width where values less than 0.2 are taken as monodisperse

The hydrodynamic diameter refers to an equivalent hard sphere that diffuses at the same rate of the particle measured, thus, assumes particles are spherical and includes any protrusions that will contribute to diffusion, this is a notable observation considered for microgels when comparing sizes to that of atomic force microscopy in **Chapter 5**

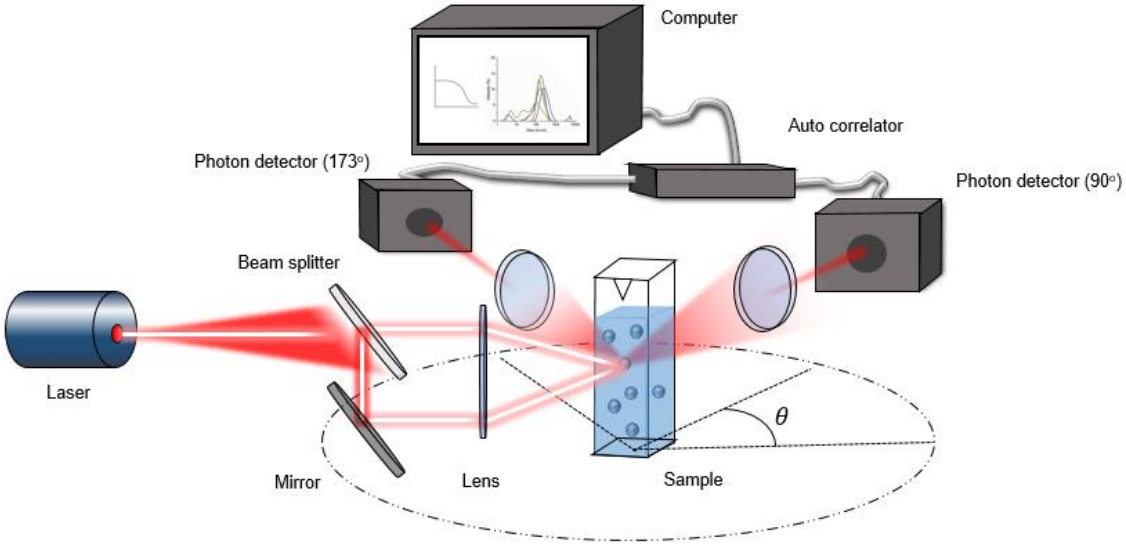

Figure 1.1. Schematic representation of dynamic light scattering

1.4.2 ζ-potential

The characteristic charges of different proteins were determined by zeta (ζ) potential. Proteins are charged at various pH dependant on amino acid type and ratio which give an overall charge to the protein. The charge is crucial for the stability, solubility, and functionality of proteins, as well as for surface interactions, such as those examined in **Chapter 3** and **Chapter 5** on QCM-D studies and protein-mucin interactions in **Chapter 4**. Throughout this thesis, proteins were

dispersed in a solution containing 20 mmol 4-(2-hydroxyethyl)-1-piperazineethanesulphonic acid (HEPPES) buffer, maintained at pH 7, where proteins typically exhibit a negative charge.

When proteins undergo ionization in water, they acquire an electrostatic charge that includes both the inner (stern layer) and outer (diffuse layer) regions **(Figure 1.2)**. Oppositely charged ions are attracted to the particle surface, while similarly charged ions are repelled (counter and co-ions, respectively). The counter ions adhere tightly to the surface of the particles, and a diffuse layer exists between the bound and bulk fluid. This diffuse layer moves along with the particle and mainly contains counter ions, with some co-ions balancing the charge. These two layers form the electrical double layer and between these is the boundary layer/slipping plane where the ζ-potential is determined **(Figure 1.2)**.

The ζ-potential is indirectly measured by evaluating the electrophoretic mobility of the protein under an applied electric field. A laser measures the velocity of the charged particles, with an increase in velocity indicating a higher charge. This can be calculated using Henry's equation:

$$\mu_e = \frac{2_{\varepsilon r \varepsilon o} \zeta f(ka)}{3\eta} \qquad (2.2)$$

Where εr is the relative permittivity or dielectric constant, ε0 is the permittivity of a vacuum, f(ka) is the Henry's function which takes into account particle radius (a), electrical double layer thickness (k) and the viscosity of the medium (η) at experimental temperature of 20^{o}C (η = 8.9x10^{-4} Pa s).

Typically charges between 10 and -10 are at risk of agglomeration, with 20 or -20 displaying enough electrostatic repulsion for stability with complete kinetic stabilisation at potentials over 30 or -30.

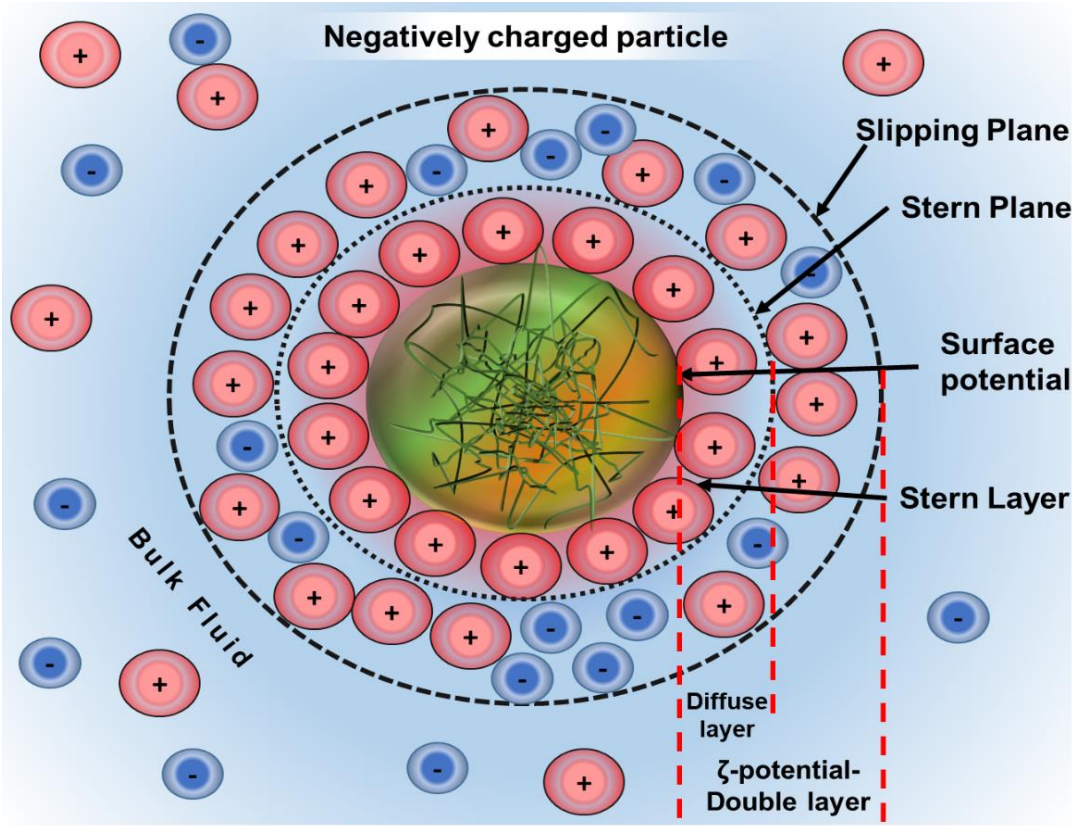

Figure 1.2 Schematic representation of zeta potential

1.4.3 Atomic force microscopy (AFM)

Chapter 5 utilised Atomic Force Microscopy to visualize the topographic surface behaviour of protein microgels. In comparison to other nanoscale imaging techniques AFM surpasses optical diffraction limit by utilising “touching” of particles. By measuring the probe's reaction to the force exerted by a particle, a precise 3D image can be created. A configuration of AFM is displayed below:

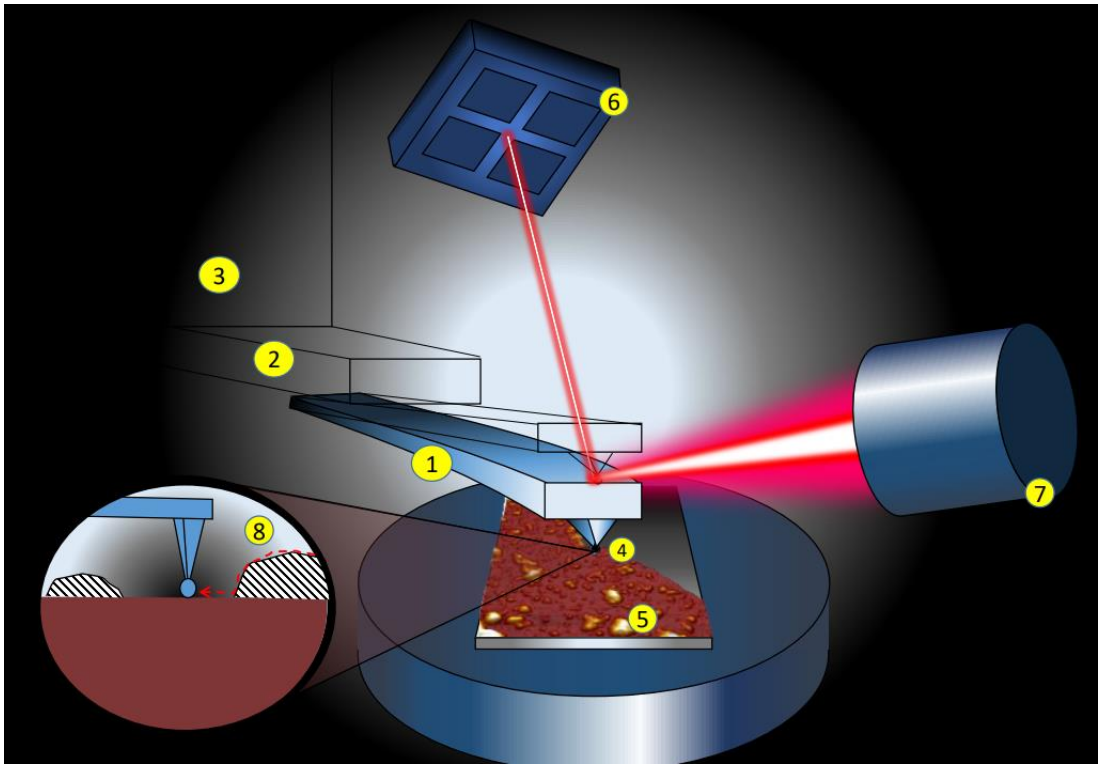

Figure 1.3 Schematic representation of atomic force microscopy

A cantilever (1) with a support (2) acts with spring like mechanics which allows for oscillation from the controller (3) depending on particle elastic properties and subsequent deformation. If wanting to measure specific surface-surface interactions, additional particles can be attached to the sample that comes in contact with the tip (4). The sample (5) is adhered onto a surface i.e. a silicon wafer on a stage that can move in x, y and z directions allowing 3D mapping of particles (8). Deflection of the cantilever occurs upon contact with the sample, which is dependent on Hooke's law.

$$F = -kx \tag{3.3}$$

Where F is the force, k the spring constant and x the cantilever deflection. To measure this cantilever deflection, a beam-deflection mechanism is commonly used where a laser (7) is reflected off the back of the cantilever into two closely

spaced photodiodes (6) whereby cantilever displacement results in one diode detecting more photons than the other which is compared to normalised signals.

1.4.4 Sodium dodecyl sulphate-polyacrylamide gel electrophoresis (SDS-Page)

Chapter 3 employed sodium dodecyl sulphate polyacrylamide gel electrophoresis (SDS-PAGE) to characterise the subunit fractions of native proteins as well determine their soluble and insoluble fractions. This technique separates the fractions based on their molecular weight.

As proteins are aggregates of a number of subunits these must be separated from the agglomerate, also as proteins vary in charge they also must be standardised with a uniformed negative charge before undergoing SDS-PAGE. To do this firstly, the proteins are denatured using SDS an amphipathic detergent and a reducing agent (i.e. Dithiothreitol). SDS binds non-covalently to two amino acids per molecule and the reducing agent causes a disassociation and cleaving of disulphide bonds into to linear subunit proteins of equalised charge and thus separation dependant on molecular weight.

Polyacrylamide gel serves as the separation medium for these proteins, which are loaded onto it. Upon applying an electric field, the proteins migrate towards the positively charged anode, with larger proteins moving through the medium more slowly and smaller proteins traveling through it at a faster rate. The gel then undergoes staining using a protein binding dye (i.e. Coomassie Blue) and resulting protein fraction bands are visualised which are compared to a standard molecular weight marker (**Figure 1.4**).

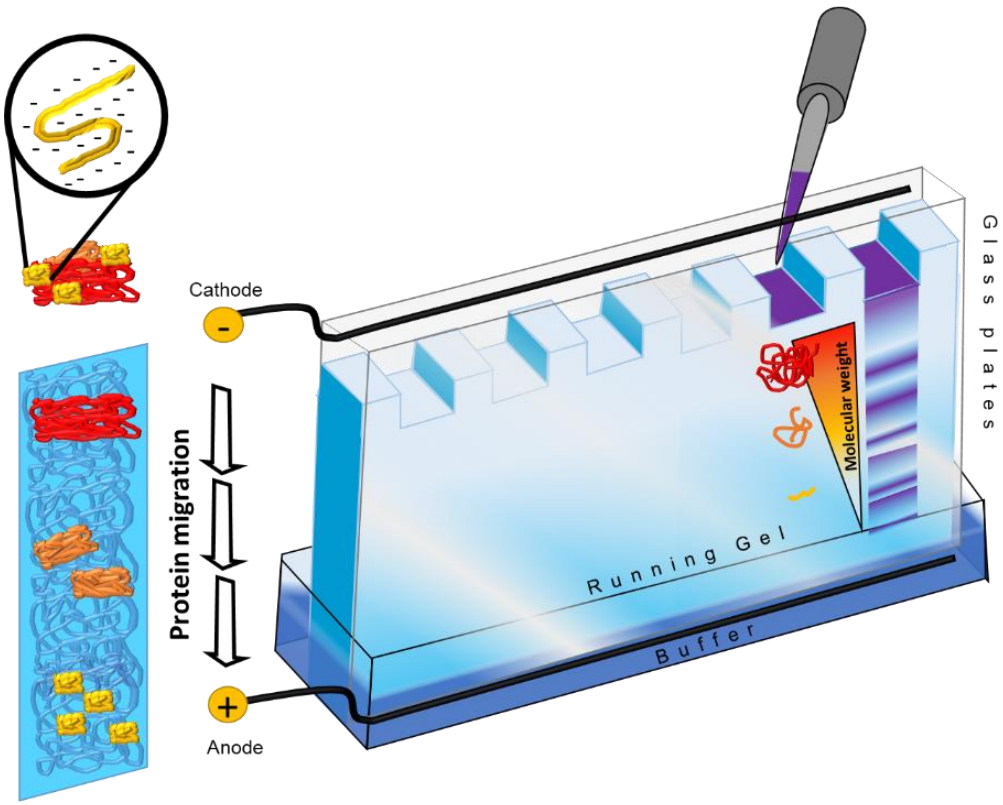

Figure 1.4 Visual representation of 1.4.4 Sodium dodecyl sulphate-polyacrylamide gel electrophoresis (SDS-Page) procedure and separation

1.4.5 Rheology

To define the flow and deformation properties of protein solutions and microgels, viscosity and oscillatory tests were conducted. The results from the data provides information in **Chapters 3** and **Chapter 5** on how protein particles behave under shear stresses, their original structure with any changes during microgelation, modulus changes with temperature and finally the modulus of parent protein gels of which microgel modulus may be assumed

When a force is applied to a material this material may flow or deform under a defined force where the rheological properties are established by measuring the shear stress (σ), shear strain (γ) and shear rate ($\dot{\gamma}$). Shear stress is the force (F) per unit area (A), shear strain is the displacement of the material due to the

stress and shear rate is the rate at which the strain occurs. These are related by the equations below:

Shear stress

$$\sigma = \frac{F}{A} \tag{4.4}$$

Shear strain

$$\gamma = \frac{\Delta l}{l} \tag{5.5}$$

Shear rate

$$\dot{\gamma} = \frac{v}{h} \tag{6.6}$$

Where F is the force, A is the area, l is the length with Δl corresponding to the change of length/deformation, v is the velocity (i.e. of moving plate) and h distance (i.e. between two plates)

Viscosity is defined as the materials resistance to flow and fundamentally the obstruction of water within a colloidal system. To conduct viscosity measurements there are three main measurement systems, concentric cylinder, parallel plate and cone plate. In this thesis the use of different geometries was required as proteins exhibited varying water holding capacities, particle sizes and used at 1-15 wt% protein creating samples of low to very high viscosity. Double gap concentric geometry was utilised for very low viscosity dilute solutions where the increased surface area provided higher torque resolutions. In contrast for viscous solutions it was necessary to use cone plate geometry with a serrated plate where the latter aimed to mitigate wall slip. This phenomenon is commonly

observed in proteins with limited aqueous solubility where proteins sediment due to gravitational forces during the time period of measurement. This was particularly relevant in the analysis of pea protein concentrate. By measuring torque the σ is determined, the deflection angle provides γ and speed the ˙γ where viscosity it calculated from the ratio between σ and ˙γ.

$$\eta = \frac{\sigma}{\dot{\gamma}} \tag{7.7}$$

Depending on particle organisation fluids typically fall into Newtonian or non-Newtonian fluids when under deformation. For ideal Newtonian fluids viscosity is independent to the shear rate at a given temperature. Examples of Newtonian materials would be dilute protein solutions of small molecular weight whilst more concentrated solutions and proteins of high molecular weight would exhibit a structure that is determined on ˙γ. Such materials are shear thinning or shear thickening, pseudoplastic or dilatants respectfully (**Figure 1.5**). The majority of food colloids demonstrate shear thinning characteristics, wherein particles deform and orient themselves to facilitate flow. This results in a reduction in viscosity as the shear rate increases, a trait commonly observed in protein solutions. On the other hand, only a small number of food systems display dilatant behaviour, showing a rise in viscosity as the shear rate increases. In these cases, the particles within the system interact and lead to a compacting of the systems structure and an example of this behaviour can be seen in corn starch solutions.

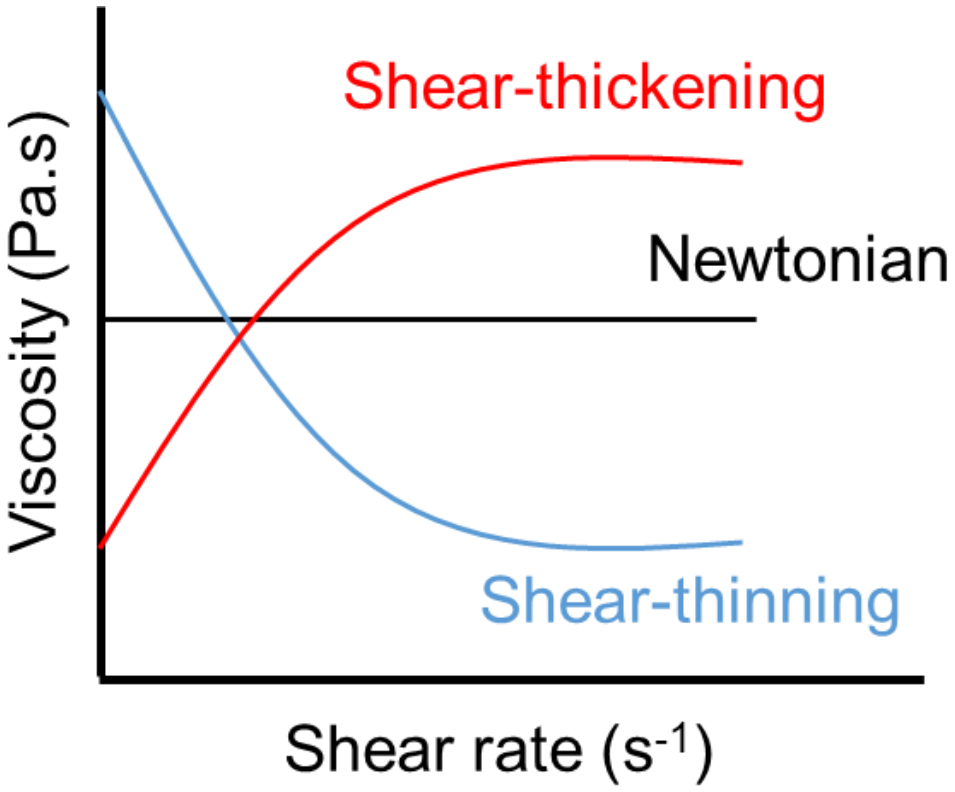

Figure 1.5 Material flow behaviour upon applied shear rate

1.4.6 Oscillatory rheology

For microgels the modulus of the parent gel has been related to lubrication properties in recent study (Andablo-Reyes et al., 2019) and was explored in this thesis. To understand the viscoelasticity of a material, measurements of storage modulus (G') and loss modulus (G'') are undertaken.

It is necessary to perform an amplitude sweep with controlled frequency and temperature with a variable strain to measure linear viscoelastic region which is the limit at which the material breaks down, this region is the identified strain for frequency and time sweeps to be conducted.

G' is the elastic solid state behaviour of the sample whilst G'' is the viscous liquid state behaviour of the sample. When deformed G' represents stored energy within the system whilst G'' is the energy lost through internal friction. Typically viscoelastic solids G' > G'' due to bonds within the system i.e. when proteins

crosslink and denature forming a gel, whilst G'' > G' for viscoelastic liquids containing no strong bonds within the sample.

1.4.7 Large deformation rheology

In **Chapter 5** it was necessary to characterise the structure of parent gels to apply such theoretical characteristics to microgel structure. As well as oscillatory shear, the large deformation was also characterised where an applied load at a constant force at a controlled speed compresses along a straight axis compresses a material until physical and chemical bonds throughout the material are weakened and eventually destroyed. Using these equations the true stress and strain is obtained:

True stress:

$$\frac{\boldsymbol{F_t}}{\boldsymbol{A_t}} \tag{8.8}$$

True strain

$$\left[\frac{\boldsymbol{H_t}}{\boldsymbol{A_t}}\right] \tag{9.9}$$

Where F_t is the applied force, A_t the cross sectional area of the sample and H_t the height of the sample at a given time. From this the Young's modulus can be calculated from the slope (stress/strain) of initial force displacement where the gels elasticity under tension was determined (Figure 1.6). This information was complimentary in understanding the elasticity and ability to withstand compression in parent gels that may be presumed for microgels.

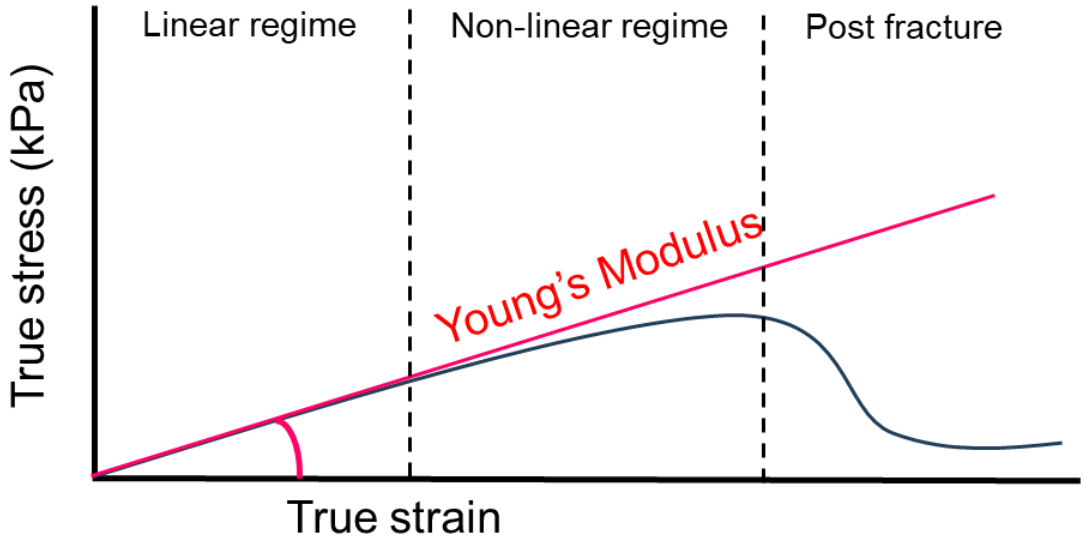

Figure 1.6 Example of stress strain curve of a typical solid material under large deformation which undergoes fracture

1.4.8 Frequency sweep

A frequency sweep is performed at a range of frequencies but at constant shear and temperature. High frequency simulates rapid motion and short term response whilst low frequency is slow motion and long term response, overall this allows understanding of crosslinking in the material. If highly cross-linked the elastic and storage modulus will remain constant over frequency G' >> G'' and remain parallel. With less crosslinking G' will increase until a plateau is met and G'' will increase till a maxima where a sudden drop will initiate, these values will remain closer to each other.

A temperature ramp combined with constant frequency and shear can also be undertaken to identify liquid to solid transition where G' will increase, remain equal to G'' then surpass G'' values indicating temperature of gelation. In proteins this is the point where molecular entanglement or denaturation of protein to expose groups for hydrogen or hydrophobic bonding takes place and an infinite cross-linked network is established.

1.4.9 Oral tribology

Tribology is the study of wear, lubrication and friction between two surfaces under an applied load. In oral tribology the surfaces are typically soft (i.e. PDMS) with roughness and elasticity similar to human oral cavity.

Such friction properties of food have been related to texture, mouthfeel and forms a key piece of surface related feelings within the mouth (i.e. fattiness, astringency, roughness) (Chen and Stokes, 2012; Krop et al., 2019).

Proteins are known to exhibit lubricating properties especially protein microgels which have been created into fat mimetics, however lubrication has only been measured with few proteins, namely whey protein and rarely with plant proteins.

Friction is defined as the ratio of the friction force (F) and normal load (W)

$$\mu = \frac{F}{W} \tag{10.10}$$

When a lubricant is entrained between two surfaces the friction is influenced by that materials flow behaviour, interactions with the surface (i.e. electrostatic, hydrophobic or van de Waals) and the speed of entrainment.

When friction is measured over increasing entrainment speeds a typical Stribeck curve is generated and is characterised by three lubrication regions, the boundary, mixed and hydrodynamic regimes.

When entrainment is low there is not sufficient pressure to entrain lubricant material and resides in the highest friction coefficient with friction being dominated by asperity properties and adsorption properties of lubricant. At a sufficient speed more lubricant material is entrained resulting in a decrease in friction as load is increasingly supported with fewer asperities contributing to friction, in this regime surface, fluid and fluid interaction contribute to friction. Eventually the

hydrodynamic regime is met resulting in full separation of contacts and of the lowest friction recorded, then it is the bulk properties (i.e. viscosity) that dominate the friction where with increasing speeds drag results in increasing friction once more (**Figure 1.7**).

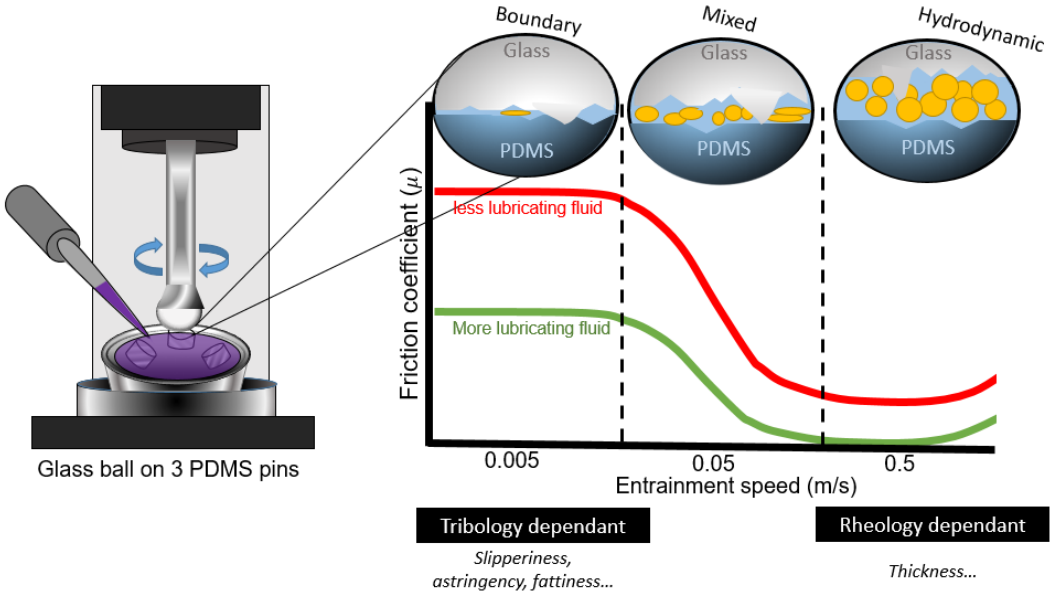

Figure 1.7 Schematic representation of a tribology system set up with a typical Stribeck curve shown. Boundary, mixed and hydrodynamic regimes are represented with corresponding images depicting particle/solution entrainment.

1.4.10 Biomimetic tongue tribology

The use of more realistic mouth surfaces for in-vitro tribology for sensory design was a major aspect of this thesis (**Chapter 5**). As a result friction coefficient was measured using a 3D printed moulded elastomer tongue with SPAN-80 which featured more realistic elasticity, wettability and papillae topography compared to traditionally used PDMS surfaces.

To measure friction the biomimetic tongue was attached to a 50.0 mm diameter steel plate-on-plate geometry using a rheometer. The force was fixed and shear

rate sweeps with the tongue attached contacting steel was created. Torque was measured and friction coefficient calculated from equation:

$$\mu = \frac{M}{RF_N} \tag{11.11}$$

Where R is the plate radius, F_N is the normal force and M is the torque. Friction coefficient is a function of the linear speed (V_R) and is calculated by $V_R = \Omega R$ which is the angular speed (Ω).

1.4.11 Adsorption

Throughout this thesis there are multiple comparisons between adsorption behaviour and on the influence on tribology to understand lubrication. To measure the film adsorption which hypothetically influences the boundary regimes in tribology we used QCM-D (Quartz crystal microbalance with dissipation monitoring).

This instrument measures mass and viscoelastic properties of thin films adsorbed on the surface of a quartz crystal resonator. When material is deposited on the surface a change in resonance frequency and the dissipation occurs, the former is proportional to mass change and the latter reflects the energy loss due to internal friction to determine viscoelastic properties. By comparing baseline and adsorbed mass resonance changes, mass, mechanical properties and dynamic behaviour can be understood.

Figure 1.8 depicts a typical set up. A crystal can be coated with a thin material layer (i.e. PDMS). This crystal is placed in the enclosed unit (1) where when initiated the crystal oscillates at resonance frequency (2). Using a peristaltic pump a buffer solution or the solutions continuous phase is pumped onto the crystal surface to obtain a baseline reading. Once stabilised the protein solution

is added, awaits for stabilisation, then buffer rinses loosely bound protein where information on the final deposited layer is obtained. A number of models are used to calculate mass of the layer.

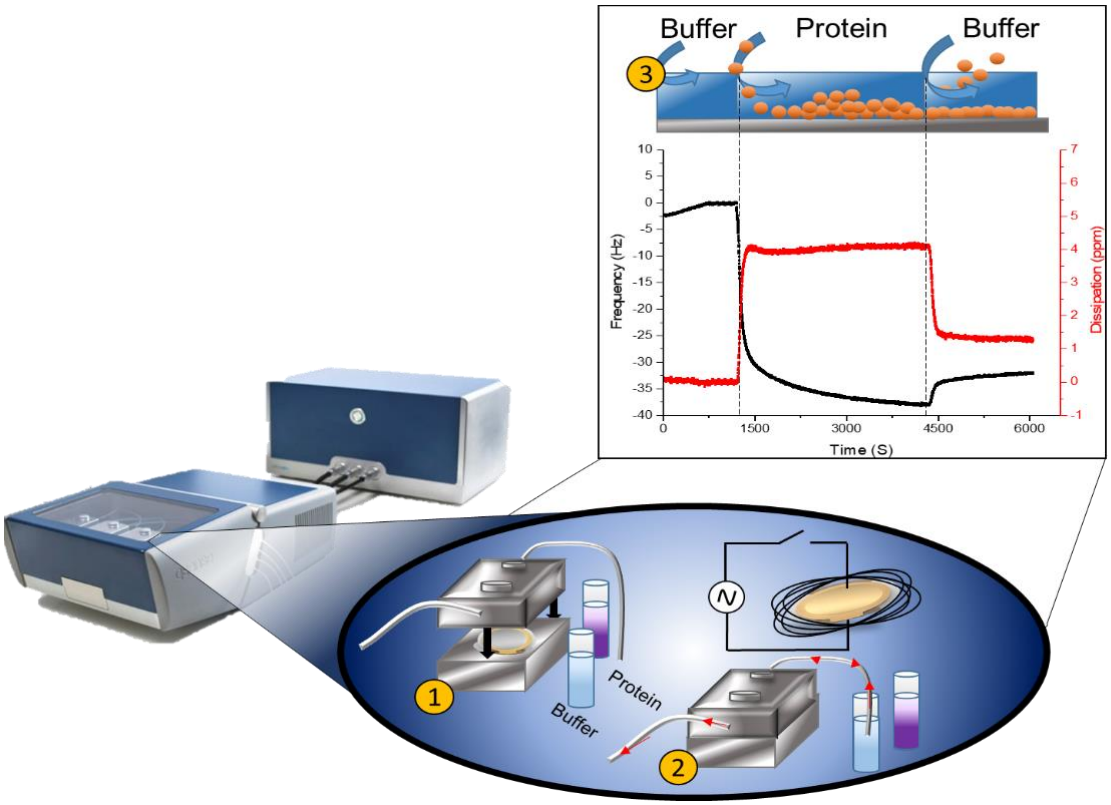

Figure 1.8 Schematic overview of quartz crystal balance with dissipation (QCM-D)

If the layer is rigid Saubrey equation is used:

$$\Delta m = -C\frac{\Delta f}{n} \tag{12.12}$$

Where n is the overtone number and C is mass sensitivity constant of the crystal sensor which is directly proportional to change in frequency (Δf). Saubrey is only valid if added mass is small compared to crystal mass, the mass is rigid and evenly distributed. However typically hydrated protein layers are not rigid, instead are viscoelastic and so dissipation, which is the energy loss from one period of oscillation, must be taken into account:

$$D \approx \frac{E_{dissipated}}{E_{stored}} \quad (13.13)$$

Where E is the energy either dissipated or stored. It was found when switched off quartz crystals decay exponentially (Spencer and Smith, 1966)

$$A(t) = AA_0 e^{t/T} \sin(2\pi f t + \varphi) \quad (14.14)$$

Where A is the amplitude, t is the time, T is decay time, f is the resonance frequency and φ is the phase angle. The decay time and resonance frequency can be calculated by QCM-D by switching off the voltage where dissipation is inversely proportional to decay time

$$D = \frac{1}{\pi f r} = \frac{2}{\omega T} \quad (15.15)$$

Where f is the resonance frequency, T, decay time where recording the amplitude decay and fitting data to the above equation frequency and dissipation can be calculated. The change of both these measurements at a number of different overtones, typically third (15 MHz), fifth (25 MHz) and seventh (35 MHz) are used to dictate viscoelastic properties of protein based on kevin-voigt viscoelastic model:

$$G* = G' + iG'' = \mu_1 + i2\pi f \eta_1 \quad (16.16)$$

Where G* is complex shear modulus, G is the storage modulus and G'' is the loss modulus. Q-Sense, Q-Tool (Goteborg, Sweden) utilises the Kevin-Voigt model to estimate viscoelasticity of the adsorbed protein layer as shown in **Figure 1.9**

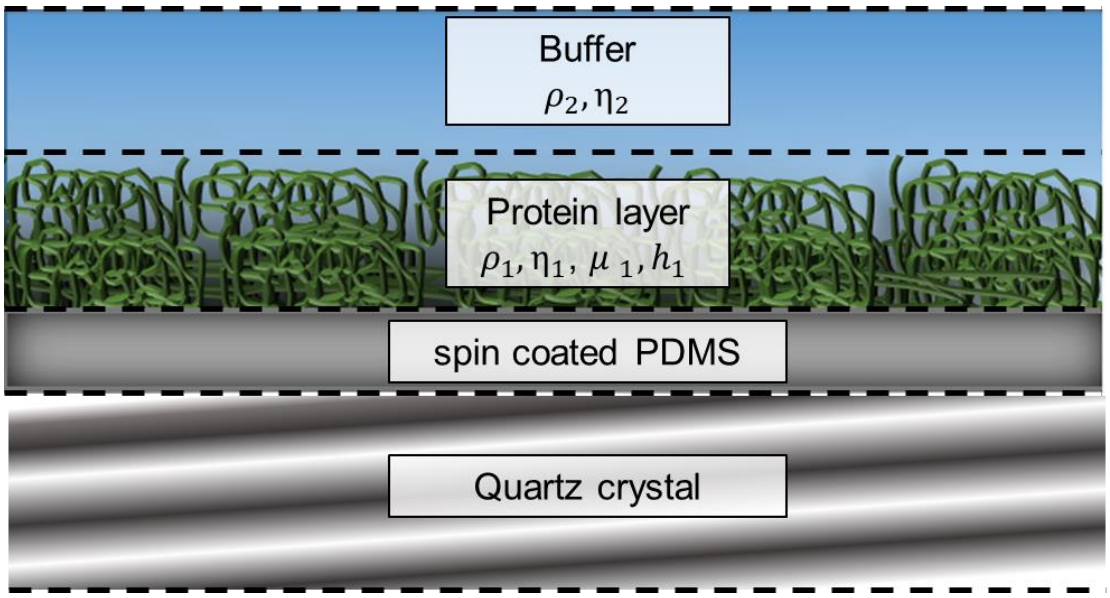

Figure 1.9 Typical representation of an adsorbed protein layer on quartz crystal microbalance dissipation (QCM-D).

Where the change in frequency (∆f) and dissipation (∆D) are related to the deposited materials thickness (h_1), density (ρ_1), viscosity (η_1) and shear modulus (μ_2) as well as the continuous phase's density (ρ_2) and viscosity (η_2).

$$\Delta f \approx \frac{1}{2\pi_{p_0 h_0}} \left\{ \frac{\eta_3}{\delta_3} + h_1 \rho_1 \omega - 2h_1 \left(\frac{\eta_3}{\delta_3} \right) 2 \frac{\eta_1 \omega^2}{\mu_1^2 + \omega^2 \eta_1^2} \right\} \tag{17.17}$$

$$\Delta D \approx \frac{1}{\pi f_{p_0 h_0}} \left\{ \frac{\eta_3}{\delta_3} + 2h_1 \left(\frac{\eta_3}{\delta_3} \right)^2 \frac{\eta_1 \omega}{\mu_1^2 + \omega^2 \eta_1^2} \right\} \tag{18.18}$$

Where p_0 is the density and h_0 thickness of the crystal. The bulk liquid viscosity and the viscous penetration depth of the shear wave is δ_3 and ω the frequency of oscillation. A number of harmonics are used throughout for modelling viscoelastic layers to obtain mass and rigidity of the film where the more spread out the dissipation is the thicker and softer the layer would suggest.

1.4.12 Rate-All-That-Apply (RATA)

Chapter 4 focused on exploring the sensory attributes of alternative proteins. To achieve this, a descriptive analysis known as Rate-All-That-Apply (RATA) was employed, involving a large sample of naïve participants. The necessary study participants have been estimated to range from 60 to 80 or potentially more, determined by the coefficients of the regression vector (Ares et al., 2014) with enhanced data stability achieved with a larger number of participants. Moreover, if intricate terms are employed, the sample size should be increased (Gacula Jr and Rutenbeck, 2006). Hence, for our study, we selected a cohort of 100 participants who received appropriate guidance on descriptions before the testing phase commenced.

RATA is an extension of traditional Check All That Apply (CATA) whereby RATA includes a weighted scale with attribute descriptors allowing for discrimination for similar samples (Meyners et al., 2016). RATA provides an extensive sensory profiling of samples where the use of model protein solutions are suggested to give general influence when utilised in food. RATA with sufficient untrained panel has shown to be as effective as a trained panel reducing time and expertise of such training (Oppermann et al., 2017). Moreover, when using an adequately sized untrained panel, this approach provides a more accurate representation of food perception from a consumer's perspective enabling greater diversity and allows for additional analysis of the influence of participant characteristics i.e. gender, age, ethnicity on scores (Ares and Varela, 2017).

1.4.13 Functional near-infrared spectroscopy (fNIRS)

To understand texture aspects of proteins, particularly astringency in plant proteins as well as quantify sensory assessment through neural response we utilised Functional Near-Infrared Spectroscopy (fNIRS) in **Chapter 4**. This

technique allows for non-invasive monitoring of neural activity which is highly mobile and offers flexibility in movement, thus easy consumption of food samples whilst measurements are taken.

A cap with source probes and detector probes are worn (**Figure 1.10**). The source probes shine infrared light into the brain, bypassing skin and bone which are optically transparent to near infrared (NIR) where blood haemoglobin acts as the chromophores thus strong absorbers of the light. Two wavelengths are typically utilised, one above and one below the isosbestic point of both haemoglobin (810nm~) where a modified beer lambert law can be utilised to measure concentration changes of oxyhaemoglobin (c_{HbO2}) and deoxyhaemoglobin (c_{Hb})

$$\Delta c_{HbO2} = \frac{\alpha_{Hb}^{\lambda 1}\frac{\Delta A^{\lambda 2}}{L^{\lambda 2}} - \alpha_{Hb}^{\lambda 2}\frac{\Delta A^{\lambda 1}}{L^{\lambda 1}}}{\alpha_{Hb}^{\lambda 1}\alpha_{Hb0_2}^{\lambda 2} - \alpha_{Hb}^{\lambda 2}\alpha_{Hb0_2}^{\lambda 1}} \tag{19.19}$$

$$\Delta c_{Hb} = \frac{\alpha_{Hb0_2}^{\lambda 1}\frac{\Delta A^{\lambda 2}}{L^{\lambda 2}} - \alpha_{Hb0_2}^{\lambda 2}\frac{\Delta A^{\lambda 1}}{L^{\lambda 1}}}{\alpha_{Hb0_2}^{\lambda 1}\alpha_{Hb}^{\lambda 2} - \alpha_{Hb0_2}^{\lambda 2}\alpha_{Hb}^{\lambda 1}} \tag{20.20}$$

Where α is the specific molar absorption coefficient of the chromosphores, λ_1, λ_2 are the two wavelengths whereby attenuation changes are measured and *L* is the path length of detected photons measured by detector probes where concentration is determined by least squares fitting (Kocsis et al., 2006).

Neural activation is determined by oxygen and glucose levels in the region. Following cortical activation a decrease in oxygenated haemoglobin and increase in deoxygenated haemoglobin occurs in area of activity which after processing

obtain a haemodynamic response function (HMF). When used vascular channels supply cortical regions rich in oxygen and glucose and blood flow increases from vasodilation. As concentration of HbO increases more light is absorbed by chromophores and less light detected by probes.

Artefacts are common when monitoring changes in neural activity and so it was necessary to strictly control surroundings and procedure to limit signal errors. A post processing software (HOMER3) is also used where a number of filters (i.e. high/low band pass) removes fluctuations from heart rate and other anomalies in activity (Dans et al., 2021).

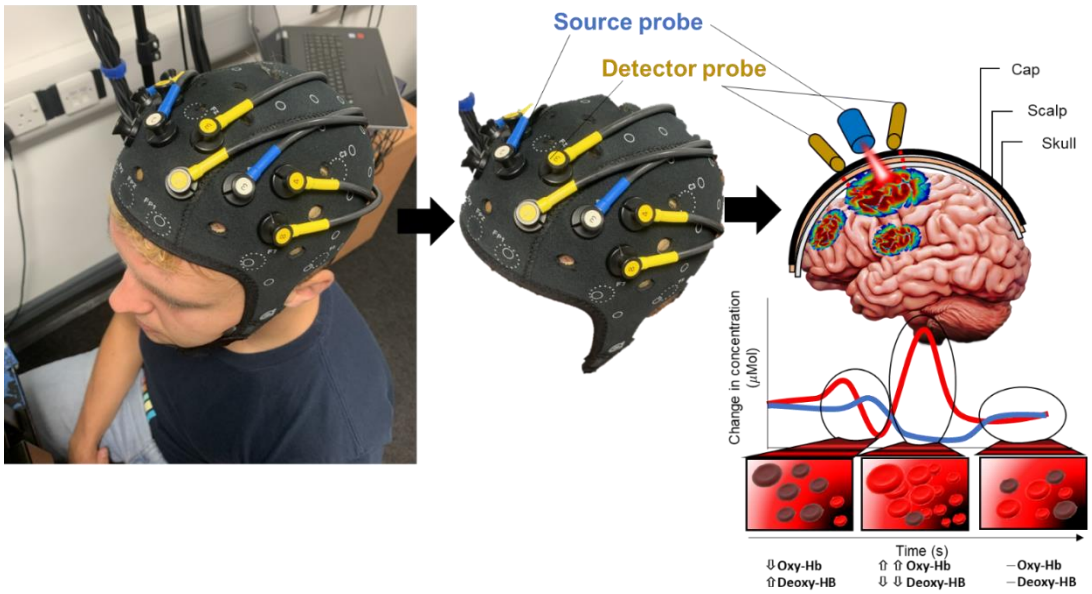

Figure 1.10 Schematic diagram and principles of functional near-infrared spectroscopy (fNIRS) in measuring haemodynamic response.

1.4.14 Cell culture

In **Chapter 4** the understanding of plant protein-mucin interactions was explored. An ex-vivo model using squamous cell carcinoma (TR146) cells derived from human buccal squamous cell carcinoma (Rupniak et al., 1985) that expressed MUC1 was followed using Ployon et al. (2016). This model was used as to measure protein binding ability of plant protein and tannic acid as hypothesised

in a trigeminal mechanism of activation (Schöbel et al., 2014; Soares et al., 2016; Brown et al., 2021; Vlădescu et al., 2023)

A neutral red cytotoxicity assay was carried out to determine cell viability after being exposed to astringent and non-astringent solutions at various concentrations. If cells were damaged by such solutions then the chromophore red dye uptake would not take place as intake is associated with non-ionic diffusion and accumulative staining of lysosomes in living cells. When under acid conditions dye is released and the light absorbance at 540nm is quantitatively measured.

To determine levels of specific mucin-solution binding an Alcian blue stain was utilised. This stain binds to anionic carboxylate and sulphate groups of mucin cells (TR146/ TR146-MUC1) and measured at 675nm. Where there were mucin binding these bound proteins are washed away leaving behind non-bound mucin and causes lower levels of absorption from staining (**Figure.11**).

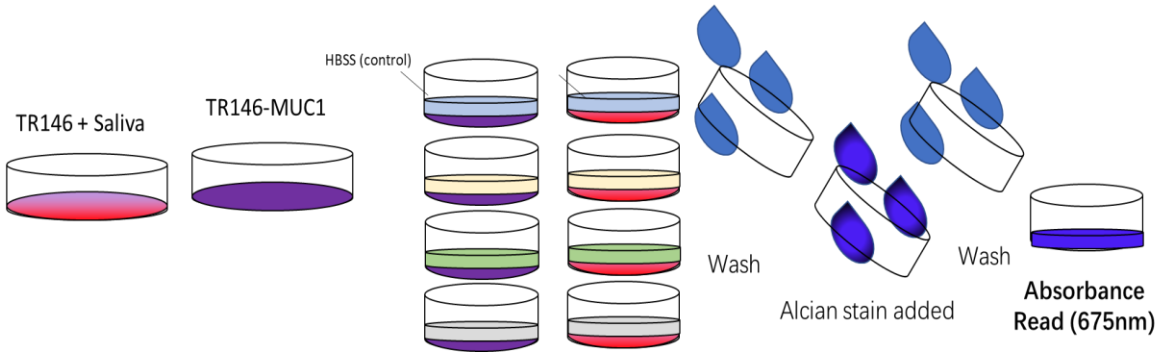

Figure 1.11 Schematic representation of the determination of salivary protein binding capacity of solutions

1.5 Outline of the thesis

This thesis begins with a literature review outlining the functional uses of proteins specifically focusing on gap on plant proteins. A range of alternative proteins were then characterised in their size, tribology, rheology and adsorption. Identified

plant proteins were also assessed in sensory trials combining, neural and cellular response giving both an *in vivo* and *in-vitro* perspectives. To conclude these proteins were transformed into lubricating microgels for optimal lubrication. The outline of this thesis is provided in **Figure 1.12**

1.5.1 Chapter 2: literature review

Includes a literature review of the latest research in the past 5 years of using proteins as fat replacers. Various protein powders, their characteristics, functions, and the results of a patent investigation are discussed including work on protein-based microparticles and microgels. A number of knowledge gaps were found which sets up the direction of the research in this thesis. The literature review that makes up this chapter was published in *Trends in Food Science and Technology*

1.5.2 Chapter 3: Characterisation of alternative proteins

In-vitro fundamental characterisation of a broad range of alternative proteins was conducted after extracting the purified fraction and compared in their size, protein composition, rheology and tribology in liquid dispersions at various concentrations. QCM-D, which has never before been used dually with such a broad range of proteins was used to characterise adsorption whereby relationships between lubrication and protein performance was understood using statistical approaches. The results of this chapter was published in *Food Hydrocolloids*.

1.5.3 Chapter 4: Sensory, neural and cellular response of plant proteins

In vivo characterisation of plant proteins was assessed here. The effects of type, concentration and mixing plant proteins were investigated using RATA spanning 17 attributes in taste, texture and after-feel (n=100). The study highlighted a significant challenge concerning astringency, which showed connections with the

in-vitro friction coefficient, and underscored a limited comprehension of the underlying causes of plant-based astringency. To address this, the research delved into a neural exploration of astringency using functional Near-Infrared Spectroscopy (fNIRS) (n = 35). The hemodynamic response of the pre frontal cortex was measured during consumption of a known astringent and plant protein dispersions. Additionally a mechanism for astringency was explored by applying plant protein solutions to saliva-coated TR146 mucin cells and measuring saliva-protein binding using tannic acid and non-astringent whey protein as control. The combination of sensory, neural and cellular in respect to understanding plant proteins is novel in methodology and this thorough understanding of sensory attributes of new proteins never been explored highlighting new application and challenges for food optimisation.

1.5.4 Chapter 5: Transforming sustainable plant proteins into ultra-lubricating microgels

In Chapter 5, we improve the negative frictional properties of plant proteins by processing them into hydrated and super-lubricating microgels. These microgels were characterised in size, shape and modulus using DLS, AFM, mathematically and in rheology. Additionally their viscosity, adsorption, tribology and stability were compared to non-microgelled native proteins of same protein concentration. The potential fat replacement application was also determined by measuring lubricity of 20:80 O/W on two tribological devices including optimised biomimetic surface supported by theoretical analyses. These newly developed particles were created with the ability to significantly enhance lubrication by orders of magnitude compared to native proteins and act like O/W emulsion despite being from plant origin with no lipidic addition. The use of new biomimetic surfaces were also used validating results and relates more to real life surface interactions.

1.5.5 Chapter 6: General discussion

Chapter 6 serves as the concluding section summarising the main outcomes. Subsequently, comprehensive implications of the findings and potential avenues for future research exploration are included.

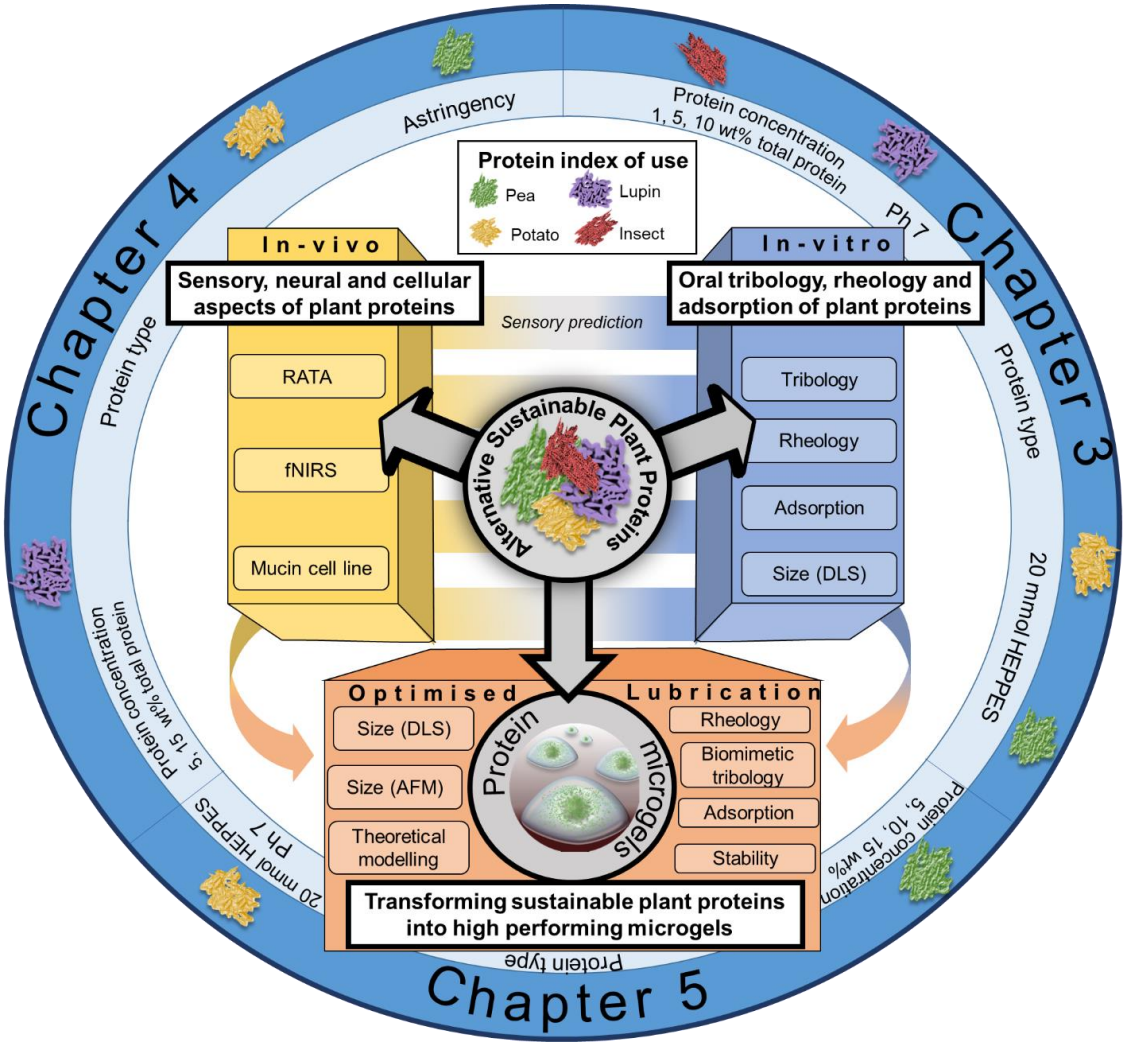

Figure 1.12 Schematical overview of thesis

1.6 References

Ares, G., Tárrega, A., Izquierdo, L. and Jaeger, S.R. 2014. Investigation of the number of consumers necessary to obtain stable sample and descriptor configurations from check-all-that-apply (cata) questions. *Food Quality and Preference.* 31, pp.135-141.

Ares, G. and Varela, P. 2017. Trained vs. Consumer panels for analytical testing: Fueling a long lasting debate in the field. *Food Quality and Preference.* 61, pp.79-86.

Ariëns, R.M.C., Bastiaan-Net, S., van de Berg-Somhorst, D.B.P.M., El Bachrioui, K., Boudewijn, A., van den Dool, R.T.M., de Jong, G.A.H., Wichers, H.J. and Mes, J.J. 2021. Comparing nutritional and digestibility aspects of sustainable proteins using the infogest digestion protocol. *Journal of Functional Foods.* 87, p104748.

Aschaffenburg, R. and Drewry, J. 1957. Improved method for the preparation of crystalline β-lactoglobulin and α-lactalbumin from cow's milk. *Biochemical Journal.* 65(2), p273.

Baiano, A. 2020. Edible insects: An overview on nutritional characteristics, safety, farming, production technologies, regulatory framework, and socio-economic and ethical implications. *Trends in food science & technology.* 100, pp.35-50.

Bajec, M.R. and Pickering, G.J. 2008. Astringency: Mechanisms and perception. *Critical Reviews in Food Science and Nutrition.* 48(9), pp.858-875.

Bate-Smith, E.C. 1954. Flavonoid compounds in foods. In: Mrak, E.M. and Stewart, G.F. eds. *Advances in food research.* Academic Press, pp.261-300.

Braun, M., Muñoz, I., Schmidt, J.H. and Thrane, M. 2016. Sustainability of soy protein from life cycle assessment. 30(S1), pp.894.895-894.895.

Brown, F.N., Mackie, A.R., He, Q., Branch, A. and Sarkar, A. 2021. Protein–saliva interactions: A systematic review. *Food & Function.* 12(8), pp.3324-3351.

Chen, J. and Stokes, J.R. 2012. Rheology and tribology: Two distinctive regimes of food texture sensation. *Trends in Food Science & Technology.* 25(1), pp.4-12.

Choudhury, D., Singh, S., Seah, J.S.H., Yeo, D.C.L. and Tan, L.P. 2020. Commercialization of plant-based meat alternatives. *Trends in Plant Science.* 25(11), pp.1055-1058.

Colonges, K., Seguine, E., Saltos, A., Davrieux, F., Minier, J., Jimenez, J.C., Lahon, M.C., Calderon, D., Subia, C., Sotomayor, I., Fernandez, F., Fouet, O., Rhone, B., Argout, X., Lebrun, M., Costet, P., Lanaud, C., Boulanger, R. and Solorzano, R.G.L. 2022. Diversity and determinants of bitterness, astringency, and fat content in cultivated nacional and native amazonian cocoa accessions from ecuador. *Plant Genome.* 15(4), article no: e20218 [no pagination].

Crippa, M., Solazzo, E., Guizzardi, D., Monforti-Ferrario, F., Tubiello, F.N. and Leip, A. 2021. Food systems are responsible for a third of global anthropogenic ghg emissions. *Nature Food.* 2(3), pp.198-209.

Dans, P.W., Foglia, S.D. and Nelson, A.J. 2021. Data processing in functional near-infrared spectroscopy (fnirs) motor control research. *Brain Sci* 11(5), p606.

Fasolin, L.H., Pereira, R.N., Pinheiro, A.C., Martins, J.T., Andrade, C.C.P., Ramos, O.L. and Vicente, A.A. 2019. Emergent food proteins – towards sustainability, health and innovation. *Food Research International.* 125, p108586.

Gacula Jr, M. and Rutenbeck, S. 2006. Sample size in consumer test and descriptive analysis. *Journal of Sensory Studies.* 21(2), pp.129-145.

Guinard, J.-X., Pangborn, R.M. and Lewis, M.J. 1986. The time-course of astringency in wine upon repeated ingestion. *American Journal of Enology and Viticulture.* 37(3), pp.184-189.

Heldt, H.-W. and Piechulla, B. 2021. Chapter 12 - products of nitrogen fixation and nitrate assimilation are deposited as storage proteins. In: Heldt, H.-W. and Piechulla, B. eds. *Plant biochemistry (fifth edition).* Academic Press, pp.299-305.

Kocsis, L., Herman, P. and Eke, A. 2006. The modified beer-lambert law revisited. *Phys Med Biol.* 51(5), pp.N91-98.

Krop, E.M., Hetherington, M.M., Holmes, M., Miquel, S. and Sarkar, A. 2019. On relating rheology and oral tribology to sensory properties in hydrogels. *Food Hydrocolloids.* 88, pp.101-113.

Lu, Z.X., He, J.F., Zhang, Y.C. and Bing, D.J. 2020. Composition, physicochemical properties of pea protein and its application in functional foods. *Critical Reviews in Food Science and Nutrition.* 60(15), pp.2593-2605.

Lucas, M.M., Stoddard, F., Annicchiarico, P., Frias, J., Martinez-Villaluenga, C., Sussmann, D., Duranti, M., Seger, A., Zander, P. and Pueyo, J. 2015. The future of lupin as a protein crop in europe. *Frontiers in plant science* 6.

Meyners, M., Jaeger, S.R. and Ares, G. 2016. On the analysis of rate-all-that-apply (rata) data. *Food Quality and Preference.* 49, pp.1-10.

Moutevelis, E. and Woolfson, D.N. 2009. A periodic table of coiled-coil protein structures. *Journal of Molecular Biology.* 385(3), pp.726-732.

Nadal, P., Canela, N., Katakis, I. and O'Sullivan, C.K. 2011. Extraction, isolation, and characterization of globulin proteins from lupinus albus. *Journal of Agricultural and Food Chemistry.* 59(6), pp.2752-2758.

Nehete, J.Y., Bhambar, R.S., Narkhede, M.R. and Gawali, S.R. 2013. Natural proteins: Sources, isolation, characterization and applications. *Pharmacognosy reviews.* 7(14), pp.107-116.

Oppermann, A.K.L., de Graaf, C., Scholten, E., Stieger, M. and Piqueras-Fiszman, B. 2017. Comparison of rate-all-that-apply (rata) and descriptive sensory analysis (da) of model double emulsions with subtle perceptual differences. *Food Quality and Preference.* 56, pp.55-68.

Permyakov, E.A. and Berliner, L.J. 2000. A-lactalbumin: Structure and function. *FEBS Letters.* 473(3), pp.269-274.

Pernollet, J.-C. 1978. Protein bodies of seeds: Ultrastructure, biochemistry, biosynthesis and degradation. *Phytochemistry.* 17(9), pp.1473-1480.

Ployon, S., Belloir, C., Bonnotte, A., Lherminier, J., Canon, F. and Morzel, M. 2016. The membrane-associated muc1 improves adhesion of salivary muc5b

on buccal cells. Application to development of an in-vitro cellular model of oral epithelium. *Archives of Oral Biology.* 61, pp.149-155.

Pownall, T.L., Udenigwe, C.C. and Aluko, R.E. 2010. Amino acid composition and antioxidant properties of pea seed (pisum sativum l.) enzymatic protein hydrolysate fractions. *Journal of Agricultural and Food Chemistry.* 58(8), pp.4712-4718.

Racusen, d. and Weller, d. 1984. Molecular weight of patatin, a major potato tuber protein. *Journal of Food Biochemistry.* 8(2), pp.103-107.

Ralet, M.-C. and Guéguen, J. 2000. Fractionation of potato proteins: Solubility, thermal coagulation and emulsifying properties. *LWT - Food Science and Technology.* 33(5), pp.380-387.

Rothstein, F. 1994. Differential precipitation of proteins. Protein purification process engineering. *Ed. RG Harrison.* pp.115-207.

Rupniak, H.T., Rowlatt, C., Lane, E.B., Steele, J.G., Trejdosiewicz, L.K., Hill, B.T., Laskiewicz, B. and Povey, S. 1985. Characteristics of four new human cell lines derived from squamous cell carcinomas of the head and neck. *Journal of the National Cancer Institute.* 75(4), pp.621-635.

Saget, S., Costa, M., Santos, C.S., Vasconcelos, M.W., Gibbons, J., Styles, D. and Williams, M. 2021. Substitution of beef with pea protein reduces the environmental footprint of meat balls whilst supporting health and climate stabilisation goals. *Journal of Cleaner Production.* 297, p126447.

Sarkar, A. and Dickinson, E. 2020. Sustainable food-grade pickering emulsions stabilized by plant-based particles. *Current Opinion in Colloid & Interface Science.* 49, pp.69-81.

Sarkar, A. and Singh, H. 2016. Emulsions and foams stabilised by milk proteins. In: McSweeney, P.L.H. and O'Mahony, J.A. eds. *Advanced dairy chemistry: Volume 1b: Proteins: Applied aspects.* New York, NY: Springer New York, pp.133-153.

Schöbel, N., Radtke, D., Kyereme, J., Wollmann, N., Cichy, A., Obst, K., Kallweit, K., Kletke, O., Minovi, A., Dazert, S., Wetzel, C.H., Vogt-Eisele, A., Gisselmann, G., Ley, J.P., Bartoshuk, L.M., Spehr, J., Hofmann, T. and Hatt, H. 2014. Astringency is a trigeminal sensation that involves the activation of g protein–coupled signaling by phenolic compounds. *Chemical Senses.* 39(6), pp.471-487.

Shrestha, S., Hag, L.v.t., Haritos, V.S. and Dhital, S. 2021. Lupin proteins: Structure, isolation and application. *Trends in Food Science & Technology.* 116, pp.928-939.

Smithers, G.W. 2008. Whey and whey proteins—from ‘gutter-to-gold’. *International Dairy Journal.* 18(7), pp.695-704.

Soares, S., Ferrer-Galego, R., Brandão, E., Silva, M., Mateus, N. and Freitas, V. 2016. Contribution of human oral cells to astringency by binding salivary protein/tannin complexes. *J Agric Food Chem.* 64(41), pp.7823-7828.

Spencer, W.J. and Smith, W.L. 1966. Defects in natural quartz. *J. Appl. Phys* 37(7), pp.2557-2563.

Stanislava Uhrı, n.N.B., Lindsay Sawyer, Mark H. Smith, Geoffrey B. Jameson, Dusan Uhrı, Paul N. Barlow. 2000. Structural changes accompanying ph-induced dissociation of the b -lactoglobulin dimer. *Biochemistry.* 39, pp.3565-3574.

Tanger, C., Utz, F., Spaccasassi, A., Kreissl, J., Dombrowski, J., Dawid, C. and Kulozik, U. 2022. Influence of pea and potato protein microparticles on texture and sensory properties in a fat-reduced model milk dessert. *ACS Food Science & Technology.* 2(1), pp.169-179.

Tulbek, M.C., Lam, R.S.H., Wang, Y., Asavajaru, P. and Lam, A. 2017. Chapter 9 - pea: A sustainable vegetable protein crop. In: Nadathur, S.R., et al. eds. *Sustainable protein sources.* San Diego: Academic Press, pp.145-164.

Vlădescu, S.-C., Agurto, M.G., Myant, C., Boehm, M.W., Baier, S.K., Yakubov, G.E., Carpenter, G. and Reddyhoff, T. 2023. Protein-induced delubrication: How plant-based and dairy proteins affect mouthfeel. *Food Hydrocolloids.* 134, p107975.

Vogelsang-O'Dwyer, M., Bez, J., Petersen, I.L., Joehnke, M.S., Detzel, A., Busch, M., Krueger, M., Ispiryan, L., O'Mahony, J.A., Arendt, E.K. and Zannini, E. 2020. Techno-functional, nutritional and environmental performance of protein isolates from blue lupin and white lupin. *Foods.* 9(2), p230.

Wada, A. and Nakamura, H. 1981. Nature of the charge distribution in proteins. *Nature.* 293(5835), pp.757-758.

Waglay, A., Karboune, S. and Alli, I. 2014. Potato protein isolates: Recovery and characterization of their properties. *Food Chemistry.* 142, pp.373-382.

Walstra, P. and Jenness, R. 1984. *Dairy chemistry & physics.* John Wiley & Sons.

Weber, E. and Neumann, D. 1980. Protein bodies, storage organelles in plant seeds. *Biochemie und Physiologie der Pflanzen.* 175(4), pp.279-306.

Welinder, K.G. and Jørgensen, M. 2009. Covalent structures of potato tuber lipases (patatins) and implications for vacuolar import*. *Journal of Biological Chemistry.* 284(15), pp.9764-9769.

Wojnowska, I., Poznanski, S. and Bednarski, W.J.J.o.F.S. 1982. Processing of potato protein concentrates and their properties. *Journal of Food Science* 47(1), pp.167-172.

Xu, X., Sharma, P., Shu, S., Lin, T.-S., Ciais, P., Tubiello, F.N., Smith, P., Campbell, N. and Jain, A.K. 2021. Global greenhouse gas emissions from animal-based foods are twice those of plant-based foods. *Nature Food.* 2(9), pp.724-732.

Yousseef, M., Lafarge, C., Valentin, D., Lubbers, S. and Husson, F. 2016. Fermentation of cow milk and/or pea milk mixtures by different starter cultures:

Physico-chemical and sensorial properties. *LWT - Food Science and Technology.* 69, pp.430-437.

Zembyla, M., Liamas, E., Andablo-Reyes, E., Gu, K., Krop, E.M., Kew, B. and Sarkar, A. 2021. Surface adsorption and lubrication properties of plant and dairy proteins: A comparative study. *Food Hydrocolloids.* 111, p106364.

Chapter 2 : Review on fat replacement using protein-based microparticulated powders or microgels: A textural perspective[1]

Abstract

Background: Due to the growing rise in obesity and food-linked diseases, the replacement of calorie dense fat has been a key focus of food industries in the last few decades with proteins being identified as promising fat replacers (FRs).

Scope and approach: This review aims to provide an overview of animal and plant protein-based FR studies that have been performed in the last 5 years. Protein isolates/concentrates, their microparticulated forms and protein microgels in model and real foods have been examined. Special emphasis has been given on the characterisation techniques that have been used to compare the full fat (FF) and low fat (LF) versions of the foods using FRs.

Key findings and conclusions: Microparticulated whey protein (MWP) has been the preferred choice FR with some success in replacing fat in model foods and dairy applications. Plant proteins on the other hand have attracted limited research attention as FRs, but show success similar to that of animal proteins.

[1] Published as: Kew B, Holmes M, Stieger M, Sarkar A. Review on fat replacement using protein-based microparticulated powders or microgels: A textural perspective. Trends Food Sci Technol. 2020 Dec;106:457-468

Key characterisation techniques used to compare full fat with low fat products containing FRs have been apparent viscosity, texture profile analysis, microscopy, particle size and sensory properties with oral tribology being a relatively recent undertaking. Coupling tribology with adsorption techniques (mucoadhesion) can be effective to bridge the instrumental-sensory property gap and might accelerate the development cycle of designing low/no fat products. From a formulation viewpoint, sub-micron sized microgels that show shear-thinning behaviour and have boundary lubrication properties offer promises with respect to exploiting their fat replacement potential in the future.

2.1 Introduction

Obesity is a growing health concern and socio-economic crisis globally (WHO, 2016). In the US, most adults are predicted to be overweight and 50% obese by 2030 consistently rising since 1999 (Wang et al., 2020). Obesity is related to a number of serious health issues such as cardiovascular diseases, cancer and type 2 diabetes with the latter accounting for nearly 9% of the overall National Health Service (NHS) budget in UK per year (Barron et al., 2018). Excessive consumption of calories particularly in the form of high fat western diets drive weight gain, with fat being the densest source of calories (9 kcal per gram) having more than double that of the carbohydrates and proteins. As a consequence, policy-makers and consumers are addressing dietary and associated health issues and, consequently food industries are attempting to accelerate their innovations in creating lower calorie food products (Bigliardi & Galati, 2013).

Reducing fat in foods is one of the potential strategies to decrease calorie intake significantly and consequently, LF versions of foods are gradually populating the supermarket shelves. However, many if not most, of these products are inferior in taste, texture and appearance as compared to their FF

counterparts and thus do not thrive in the marketplace. Hence, there has been motivation in the food industry and research community to design fat replacers that mimic the functional and sensory properties of fat. These include two classes of materials: fat substitute (FS) and fat mimetic (FM) ingredients, with an attempt to replicate the physicochemical and sensorial properties of fat in food products. Typically, FS involves direct replacement of fat with a substance that attempts to provide similar organoleptic properties to fat, these can be synthetic in nature or structured lipid moieties that provide little to no calories (O'Connor & O'Brien, 2016). A classic example is ‘Olestra’ , patented by Procter and Gamble Co (Jandacek & Letton, 1987). which is formed by esterification of sugars and long chain fatty acids which provides a Non-Newtonian pseudoplastic flow behaviour comparable to fats. Olestra behaves similar to those of conventional triglycerides but is resistant to lipolysis and, thus, serves as a non-calorific replacement for fats for designing LF foods. Other commercially formulated FS also include ‘Salatrim’ (Smith et al., 1994) and ‘Caprenin’ (William et al., 1993), latter being designed as a cocoa butter replacement for use in confectionary applications. These have also been utilised in LF baked and dairy products. However, the use of FS has been limited owing to possible associations with abdominal cramping and other side effects (Hunt et al., 1998), which has led to Caprenin being withdrawn and Olestra being prohibited for sale in the EU and other markets. FMs are substances that are used to mimic the specific microstructural, physicochemical and/or sensory properties of fat by using biocompatible and biodegradable carbohydrates and/or proteins either in their native form, in aggregated state or in the form of biopolymeric particles, physical complexes, either individually or in combination (Lucca & Tepper, 1994). In general, the FMs studied in literature can function by four potential mechanisms. These include 1)

thickening the food matrix to replicate the rheological properties of fat, 2) mimicking the microstructure of emulsified fat droplets, 3) match the fat droplet-matrix interaction using suitable processing aids and capitalising colloidal interactions (pH, temperature, ions etc.), and 4) replicating the oral tribological properties of fat i.e. fat-oral surface interactions.

Proteins are often considered as a suitable macronutrient to replace fat as they contribute to only 4 kcal per gram (Benelam, 2009; Veldhorst et al., 2009) with more satiation, per calorie, compared to other macronutrients (Benelam, 2009; Gerstein et al., 2004; Hoek, 2010; Westerterp-Plantenga, 2008). In fact, the protein content of foods correlates positively with Satiety Index scores (Holt et al., 1995). This benefit has been used by scientific community for considering protein based FRs. In addition, protein is also a highly tuneable structuring agent by virtue of its responsiveness to pH, ions, temperature and enzymes. **Figure 2.1** shows the reported bibliographic data for FRs and protein-based FRs showing the growth of scientific literature and citations with the highest number of publications being produced since 2017, highlighting the topical nature and importance of this field in the period (1998–2018). A substantial yearly increase can be observed from 2012 for both total FR and protein-based FRs, with the latter contributing to nearly one-third of the total FR publications to-date indicating this as a priority area in the food science community.

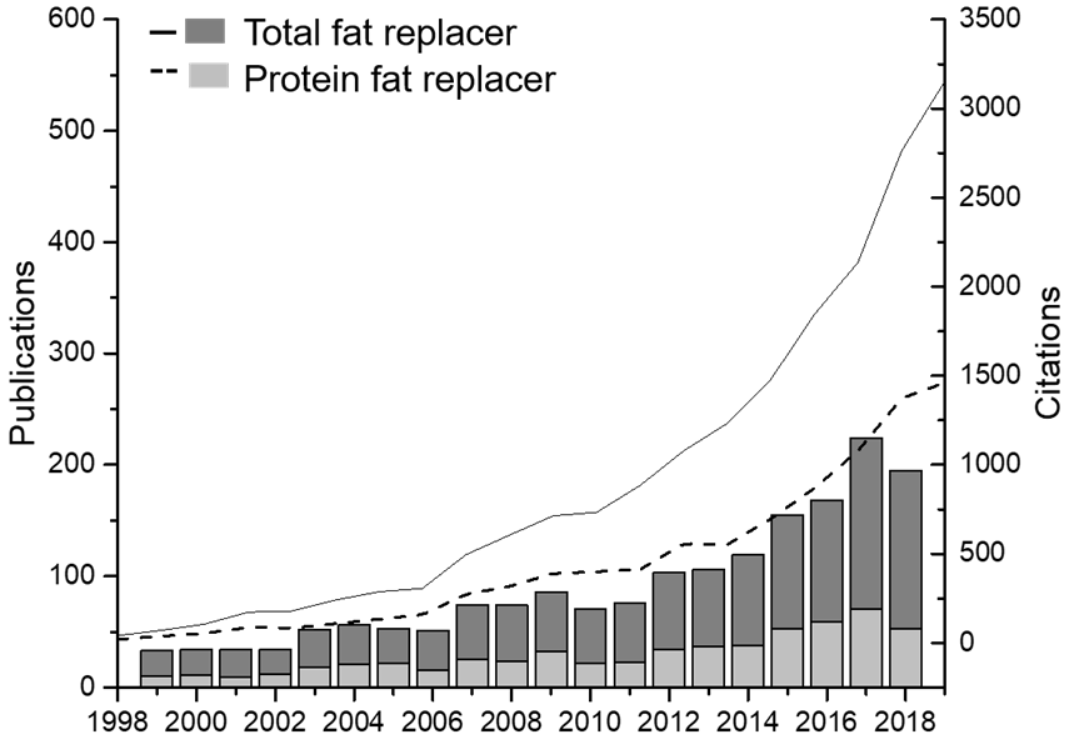

Figure 2.1 Number of publications (bars) and citations (lines) of fat replacers (black bar, solid line) and protein-based fat replacers (white bar, dashed line) using search engine, Web of science (ISI) from 1999-2018.

This review aims to assess the progress in the last 5 years in the design and application of protein-based fat replacement strategies in model and real food systems. We briefly discuss the protein concentrates of animal and plant origin followed by a strong emphasis on microparticulated forms of proteins that have been used as FRs. We have focussed on specific characteristics (e.g. size, viscosity (η), firmness, water holding capacity (WHC), colour, coefficient of friction (μ), sensory properties) that can be useful to compare FF and FR-containing LF versions of the product. We have subsequently examined applications of these FRs in some food products and discuss the degree of fat replacement that can be achieved without compromising sensorial properties. We highlight several

characterisation techniques that can be employed to bridge the gap between instrumental and sensory techniques to accelerate the development cycle of FR and possibly create FRs of just-right mouthfeel properties to mimic fat in real food products. Finally, we provide future perspectives on protein-based microgels that have been substantially characterised in literature in terms of physicochemical properties and which possess the potential to mimic fat but require further research attention with respect to fat replacement. Outside the scope of the present review are carbohydrate-related FRs that do not include protein as a component (Peng & Yao, 2017) as well as structured lipids as FSs (Marangoni et al., 2020) Also protein-polysaccharide based structures and their uses as fat replacers are outside the scope of this review (Goh et al., 2008; Weiss et al., 2019). Insights into product specific replacement of fat can be found in some recent elegant reviews, such as use of microparticulated whey protein in dairy texture improvement (Ipsen, 2017), or employment of FR in ice cream (Akbari et al., 2019), oil-based condiments (Ma & Boye, 2013), meat products (Varga-Visi & Toxanbayeva, 2016) and baked foods (Colla et al., 2018). Refer to **List of abbreviations** and **List of symbols** for nomenclature.

2.2 Protein isolates/concentrates as fat replacers

Protein-based powders fall into two main categories, those containing below 90 wt% protein are known as concentrates, whereas, above are protein isolates (Nehete et al., 2013). Protein concentrates and isolates possess a number of functional properties including gel forming, emulsifying, foaming, WHC etc. Among these, the WHC and viscosity of proteins are considered as key parameters for FR that affects colour, texture and other sensory properties, latter are relevant for FR purposes (Zhang et al., 2015).

Most recent FR studies using protein as concentrates or isolates have been performed on dairy products such as milk (Olivares et al., 2019; Protte et al., 2019), yoghurt (Fang et al., 2019), ice-cream (Liu et al., 2018b) and cheese (El Aidie., 2019; Urgu et al., 2019). As one might expect, whey protein has been seen to currently dominate the field of protein-based FRs (Protte et al., 2019). This is because whey protein, which is readily available as a by-product of cheese manufacturing process, has similar flavour profile and thus highly compatible with dairy applications (Lesme et al., 2020). More importantly, whey protein has been extensively characterised in literature in terms of its structural and functional properties allowing for fat replacement to be approached more mechanistically. For instance, in stirred goat milk yoghurt, removal of fat led to increased syneresis, a weaker body and a 50% reduction in the apparent viscosity (Costa et al., 2016). By increasing the levels of whey protein in the formulation up to 6.8 wt% total protein in the LF yoghurts, the syneresis was significantly reduced being comparable to those of the FF version with viscosity increased in the LF version by four times, latter containing no added whey protein (Costa et al., 2016). Whey has also been incorporated into low fat cheese which can mimic the breaking up of the casein network, often achieved with fat (Danesh et al., 2018). This is hypothesised due to the WHC and formation of microscopic free pools of water which reduce hardness and firmness (3–4% WPI g/L milk) although at concentrations of 4–6% g/L milk hardness returns as high levels of whey compacts the protein matrix.

Processing of proteins has been often used as a powerful tool to improve the functionalities of proteins for fat replacement purposes. Whey protein is comprised of two main proteins, β-lactoglobulin (β-lg) and α-lacalbumin (α-la) typically at 50% and 20% (Alves & Tavares, 2019). Native β-lg contains a single

thiol group capable of binding water. When denatured, at around 75 °C (Croguennec et al., 2017) more reactive thiol groups are exposed (Torres et al., 2017), which not only binds more water but also binds to adjacent protein thiol groups forming a continuous porous network and allow entrapment of water in food matrices resulting in higher WHC. By heating whey protein isolate (WPI) (85 °C for 30 min) at pH 8.5, lesser quantity of the protein (1.0 wt %) (Zhang et al., 2015) was needed to obtain similar viscosity (695 mPa.s) in LF goat milk yogurts as compared to those containing higher concentration (6.8 wt% total protein) of native whey protein (672 mPa.s) at the same shear rates (Costa et al., 2016).

Similarly, on addition of heat polymerised whey protein (PWP), fabricated using heat treatment of whey protein at varying temperature (70–90 °C/5–15 min) and pH conditions (pH 7.0–9.0) to no fat (NF) yoghurt, there was an increase in viscosity in NF yoghurt, similar to that of FF yoghurts (Fang et al., 2019). In other words, the viscosity of NF yoghurt containing PWP was significantly higher than those of NF yoghurts or yoghurts containing 1% fat. PWP also increased the firmness and improved WHC significantly as compared to NF yoghurt. The key mechanism proposed using confocal laser scanning microscopy imaging was that PWP acted as a ‘ water-immobiliser’ resulting in formation of yoghurt gel with smaller pore size, which was not achieved in NF yoghurt, latter having a loose network with large sized pores. Additionally, PWP was assessed as having an astringent aftertaste (Fang et al., 2019), highlighting one of the key sensorial issues associated with protein as a FR. Besides heat treatment, the ratio of whey protein to casein can also play an integral role on rheological properties of the LF products. For instance, in high protein (8 wt%) set yoghurt, increasing the ratios of heated whey protein (75 °C/5 min): casein ratio to 25:75 (w/w) and 35:65 (w/w) in comparison to the control (whey protein: casein ratio = 10:90 w/w),

respectively, resulted in less coarse, smoother, viscous, shinier product with desirable thickness (Jørgensen et al., 2015).

Besides conventional viscosity measurements, tribology measurements (measuring coefficients of friction) have also shown promising capability to distinguish iso-viscous commercial samples of FF and NF/LF yoghurts and cheeses, which were also discriminated based on their sensory properties. It was suggested that in these dairy products, FF products formed a continuous film of coalesced oil, which reduced the friction between polymeric surfaces in the tribological set up, this friction reduction was not achieved by the LF products (Laguna et al., 2017). In this light, WPI has recently demonstrated promising lubrication properties using tribology testing in model thermally treated protein-based solutions (Zhu et al., 2019). Increasing the ratio of whey protein to casein (0/100–100/0 w/w) in 3.4% w/v heat-treated milk protein solutions were found to increase viscosity by 32% and enhance lubrication with μ being around 10% lower at sliding speeds >10 mm/s. The lower μ of the solutions with replacement of casein by WPI was attributed to the smaller particle size (46–168 nm) and spherical shape of globular WPI that were postulated to act as nanometric ‘ball bearings’ mimicking that of fat droplet-associated lubrication. In addition, the denaturation of WPI at high temperature (95 °C for 10min) and possible formation of disulfide linkages with κ-casein at the surface of casein micelles was also cited as a possible reason for the decreasing of the μ by formation of a lubricant layer that prevented adhesive contacts between the tribological surfaces. However, gradual increase in whey protein resulted in transparency and loss in opaqueness, a key appearance trait of high fat dairy foods (Zhu et al., 2019).

With the increasing environmental sustainability, health, animal-welfare and allergy concerns as well as the rising popularity of vegan diets, there has

been burgeoning interests to shift towards use of alternative plant proteins in formulated food products. However, as far as FR is concerned, the impact of replacement of fat directly with plant protein concentrates/isolates alone is very limited. For example, soy protein isolate (SPI) has often been used to replace fat in sausages in the past, however, has been shown to be associated with off-flavour, texture alterations and reduction in overall acceptability (Nasonova & Tunieva, 2019). Nevertheless, successful studies have been conducted in combination of soy protein hydrolysate with xanthan gum (Liu et al., 2018b) to reduce ice cream fat by 50% and SPI with cellulose nanofibers (CNF) (Guo et al., 2018; Sun et al., 2015), where texture profile analysis (TPA) indicated no significant difference between SPI-CNF and control FF ice cream (Sun et al., 2015). Furthermore studies on understanding properties of dairy protein replacement by plant protein systems such as pea protein isolate (PPI), SPI and hemp protein concentrate (HPC) added at 1.4–2.8% have shown success to enhance the WHC by 1–8% leading to increased viscosities from 470 mPa s to 560 mPa s (Dabija et al., 2018), whether such properties can be used to replace fat remains elusive in literature to date.

In summary, most systems of fat replacement using protein concentrates/isolates have been conducted using a dairy medium as applications with the replacement of dairy fat as the sole purpose. Therefore, high fat plant-based products, such as hummus, vegetable patties, vegan cheese which contain similar aromatic and taste profiles to plant proteins may be more compatible for testing replacement of fat with plant protein isolates/concentrates. Plant protein isolate/concentrates that have fat mimicking potential or in combination with dairy proteins need more physical and physicochemical

characterisation, for testing their ability to act as FRs after suitable processing, which needs future research attention.

2.3 Protein-based microparticles as fat replacers

One of the most extensively investigated research areas for fat replacement has been the use of microparticulated proteins as FMs. Microparticulated proteins (**Figure. 2.2**) are mostly dried protein particles which are of smaller particle size compared to concentrate/isolate protein (0.1–20 μm diameter) that are created using thermal treatments and high shear processes at low pH (Ipsen, 2017). Such microparticulation processes came to existence through the first patent in 1988 on whey protein, which was launched with a commercial name of Simplesse® (Singer, Yamamoto, & Latella, 1988) by NutraSweet. The patented microparticulated protein by this thermo-mechanical process claimed to have " a substantially smooth, emulsion-like organoleptic character when hydrated". This was followed by a second patent two years later covering microparticulated bovine serum albumin (BSA), egg white protein (EWP) and plant proteins, such as soy protein (Singer et al., 1990). Once the patent expired, other commercially available microparticulated proteins surfaced with brand names such as APV LeanCreme™ (SPX technology) (Rajakari & Myllarinen, 2016) or other containing combinations of microparticulated protein with polysaccharides or carbohydrates, such as Dairy-Lo® (valentino & baughman, 2004) containing microparticulated protein + microparticulated cellulose). The key feature of microparticulated proteins is that they mimic the spherical shape and size of emulsified fat droplets (**Figure 2.2**) and are postulated to create a creamy mouthfeel by 'ball-bearing' mechanism (Cheftel & Dumay, 1993; Liu et al., 2016c). Few non-dairy microparticulated proteins such as egg and plant protein exist and have been used as FRs. Recently, microparticulated proteins from such alternative sources

have started populating the FR landscape with egg white protein (MEWP) being used in salad dressing (Liu et al., 2018a), microparticulated plant proteins in gluten-free bread (Beran et al., 2018), in yoghurt (Dabija et al., 2018) and model systems (Zhang et al., 2020b). Here, we discuss the applied research performed using microparticulated whey protein, microparticulated forms of egg and plant proteins in different model and real food applications that have been investigated in literature in the last 5 years using a range of rheological and tribological techniques (**Table 1**).

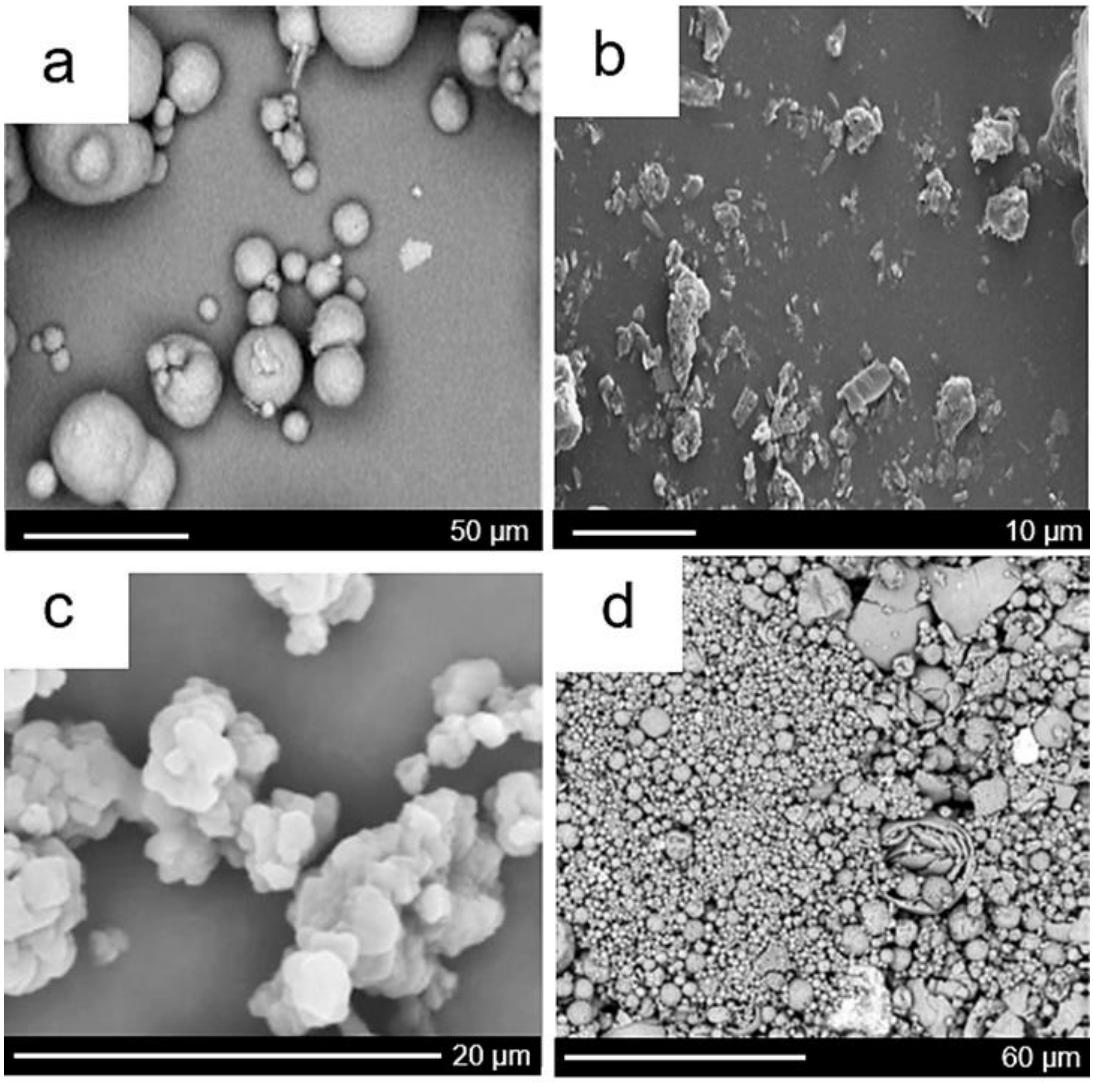

Figure 2.2 Scanning electron micrographs (SEM) of microparticulated proteins; (a) microparticulated whey protein (MWP), (Liu et al. 2016), (b) microparticulated egg white protein MEWP) (Liu et al. 2018a), (c) microparticulated soy protein (MSP) (Zhang et al.

2020a) and (d) microparticulated hemp protein (MHP) (Beran et al. 2018). Micrographs are reproduced with permission from Elsevier (a, c), J-STAGE (free access) (b) and Longdom Publishing SL (open access) (d).

Table. 1. A summary of micro-particulated proteins incorporated as fat replacer in a range of applications in the past 5 years of research. Arrows indicate improvement (up arrow) or reduction (down arrow) in characteristics of the product when protein type was increased in product if not mentioned otherwise.

Fat Replacers (FRs)	Application	Particle size (μm)	Production conditions	Key findings	References
Animal protein-based FRs					
Micro-particulated/ Nano-particulated whey protein	Model gels	0.1-1	- 0-8% w/w MWP - Measured at 20 ^{o}C	↑ η ↓ μ	(Liu et al., 2016b)
		0.2	- 0.6-4.4% w/w MWP -HTST treatment - pH 6.6 (milk gel pH 4.8) -Measured at 4 ^{o}C	↓ η ↓ G' ↓yield stress ↓tortuosity ~ Cohesiveness ↓ H_2O capacity ↓ firmness ↑ porosity	(Silva & O'Mahony, 2018)

	Skimmed milk	1.16	- 0.5-20.0% w/w MWP - Measured at 25 ^{o}C and 37 ^{o}C	↑ η ↓ μ ↓ n	(Olivares, et al., 2019)
	Stirred yoghurt	0.005 – 100	- 4.25% and 5.0% w/w (total protein) MWP, NWP, 10 variations - Pasteurised - Yoghurt pH 4.6 - Measured at 4 ^{o}C	↑ η (high N/D) ~ η (low N/D) ↑ Gel strength ↑ G' (high N/D) ↑ Elasticity ↑compaction ↑ H_2O capacity (high N/D) ↑ Mechanical resistance (high N/D)	(Torres, et al., 2018)
	Low fat Edam cheese	-	- 0.3-0.9% w/w MWP, 3 variations. - Pasteurised	↑ moisture, ↑ proteolysis, ↓ firmness, ↑ homogeneity ↑ texture sensory: ↓ texture (highest Simplesse®100, Prolo®11), ↑ flavour, ↑ appearance ↑	(El-Aidie, et al., 2019)

			- 4.5-5.3% salt (in moisture) - Measured at room temperature	OA ↑ bitterness (highest Simplesse®100, Prolo®11)	
	Low fat cheese emulsion	0.01–3	- 5-20% (of dry matter, 16-28%) MWP - Heated at 80 °C and sheared - pH 4.7-4.9 - 3% w/w salt Measured at: 45 °C	↑ followability ↓ η ↑↓ n ↓ shear stress ↑ porosity ↑ Whiteness; Sensory: ↑ flowability ↑ Glossiness ↓ Mouth-coating	(Urgu, et al., 2019)
	LF Pickled cheese	-	- 1% w/w MWP - Pasteurised	↑ moisture ↓ hardness ↑ springiness ↓ cohesiveness ↓ gumminess ↓	(Akin & Kirmaci, 2015)

			- pH 5.1-5.2 - 2.5-3.5% w/w salt - Measured at 4 ^{o}C	chewiness, Sensory: ↑ whiteness ↑ appearance ↑ OA ↑ odour ↑ flavour	
	Processed cheese	0.01-3	- 3-7% w/w MWP - Heated 90 ^{o}C 5 min - pH 5.6 - Measured at 5 ^{o}C	↑ G′ ↑ G″ ↓ Max tan δ ↑ Gel-sol transition temp ~ firmness ~ hardness ~ colour	(Schädle, et al., 2020)
	Kefir	-	- 2% w/w MWP, 2 variations - Heated 93^{o}C 15 min - pH 4.3-4.4. - Measured at 20 ^{o}C	↑ η, Sensory: ↑OA	(Temiz & Kezer, 2015)

	Multi grain cookies	-	- 7% w/w MWP - 0.2% w/w salt - Heated 165 ^{o}C 16 min - Measured at room temperature	~ colour ~ flavour ↓ OA ↓ Tenderness	(Aggarwal, et al., 2016)
Egg white protein	Salad dressings	9.42	- 9-11 g/mL MEWP sample vs commercial salad cream - Heating 13 min, sheared - pH 3.6	↑ η ↑ ↓ n ↑ G' ↑ G'' ↑ tan(δ) ↓ thixotropy; Sensory: cohesiveness ~ appearance ↓ flavour ~ OA	(Liu et al., 2018a)
Plant protein-based FRs					

Micro-particulated plant proteins	Microparticulated soy protein + egg white protein	Model liquid	5.0 – 20.0	- 6-15% wt/wt MSPI, MSPI+EWP - Heated 95 ^{o}C 30 min - pH 7 - Measured at 25 ^{o}C	↓ μ (MSPI), ↓↓ μ (EWP+MSPI) ↑ η↓ off-flavour volatiles	(Zhang, et al., 2020b)

2.4 Microparticulated whey protein

Simplesse®, the first microparticulated whey protein (MWP) available commercially was created by thermal aggregation and intense shearing at low pH (pH 4.0–5.5) resulting in the thermal denaturation of β-lg, α-la and BSA, whereby the thiol groups of β-lg are exposed for covalent disulphide interaction. Lower electrostatic repulsive forces using relevant pH enabled hydrophobic interactions in the proteins to take place resulting in aggregation and finally forming particles via shearing process with particle size of <5 μm (Beran et al., 2018; Liu et al., 2018a; Toro-Sierra et al., 2013). As can be seen from micrographs, MWP is spherical and smooth with particles having no sharp facets (**Figure 2.2a**), however, there are also reports of development of large coarse aggregated particles of >30 μm size during the spray drying process. Spray drying has been shown to affect particle size and native/denatured (N/D) ratio in whey proteins. Torres et al. (2011) investigated ten MWP types produced using different processing methods and found that a high N/D whey protein ratio (0.94–1.33) in the MWPs generated LF yoghurt with enhanced viscosity, yield stress, storage modulus (G') and creaminess perception (Table **1**). In contrast, another study (Toro-Sierra et al., 2013) found that 90% of protein was found to be of the same size before and after drying with little significance of inlet and outlet temperature, suggesting controlling temperature alone was not sufficient to attain a certain particle size.

In LF dairy foods, MWP has shown ability to improve organoleptic (creaminess, lubrication) and functional (viscosity, flow) properties (Ipsen, 2017; Liu et al., 2016a). In addition to dairy matrices, MWP has also been successfully used in mayonnaise (Sun et al., 2018) and glazes (Meza et al., 2016). However,

use of MWP as FRs in baked foods such as cookies (Aggarwal et al., 2016) and fried products (Pokorny, 1998) was not promising owing to the high temperature conditions used in these processed food, leading to thermal interaction of MWP with other ingredients resulting in loss of fat like texture (Lucca & Tepper, 1994; O'Connor & O'Brien, 2016). Furthermore, MWP has not shown success in ice cream when used as a sole FR as it lowered viscosity, smoothness and mouth coating and increased generation of undesirable volatiles (Welty et al., 2001). However, in combination with polysaccharides, MWP has shown synergistic effects to replace fat in ice cream (Ipsen, 2017). Considering a detailed review already exists on applications of MWP in dairy applications (Ipsen, 2017), we have only focussed on research carried out after 2017 in this application area unless there is a mechanistic information that applies to other applications.

Model systems. Liu et al. (2016c) postulated for a ball bearing type mechanism of lubrication whereby small spherical MWP particles (less than 5 μm in diameter (see **Figure 2.2a**) are able to roll across the surfaces, reducing friction, proposing to mimic emulsified-fat droplet inducing a creaminess like sensation in the mouth. In the presence of small quantities of MWP, μ was greatly reduced but at ≥3 wt% MWP, the lubrication effect was significantly reduced with plateau between 5 and 8%, likely because of saturation of these particles between the tribo-pair surfaces preventing the rolling mechanism to persist (**Table 1**). This ball bearing effect was also observed to be better in liquids than in semi solids. In a recent study, friction behaviours similar to FF emulsions (0.5–20.0% w/w fat) were again demonstrated using various concentrations of MWP (Simplesse®) at sliding speeds (10–50 mm s−1) typical of oral processing (Olivares et al., 2019). Size is known to be vital where small particles of MWP were associated with body and richness but sizes above 10 μm diameter were

detected with roughness, and increase in μ values. However, the viscosity and perceived thickness of the medium was found to be effective in masking the larger particulates (Liu et al., 2016b; Liu et al., 2016c). From this study it was concluded, MWP can help to reduce rather than replace fat in food as MWP did not replicate the fattiness in sensory, due to lack of any oily film formation, thus, limiting usage of MWP for FF replacement.

Milk gels. In high protein acid milk gels, MWP has been shown to interact with casein, forming a more open structure creating a softer product compared to control i.e. milk gels containing no added MWP (Silva & O'Mahony, 2018). MWP gels were characterised as softer, lower firmness, consistency and cohesiveness with significantly increased porosity as well as a decrease in tortuosity as a result of the open structure. Addition of nanoparticulated whey protein (NWP) (particle size of <1 μm) resulted in higher firmness of the acidified gels through both covalent and non-covalent interactions (**Table 1**).

Yoghurt. . In yoghurt, removal of fat leads to increased syneresis, weaker body and unsatisfying texture. Addition of MWP (Torres et al., 2018) has been shown to reduce such detrimental characteristics. For instance, in LF yoghurt containing MWP having higher ratios of native β-lg/α-la in the MWP resulted in higher elastic modulus, better flow behaviour (n), lower syneresis, dense aggregates and low serum pores (observed using scanning electron microscopy, SEM) in LF yoghurt closely resembling FF yoghurt (Torres et al., 2018). The small particle size of MWP, such as the use of NWP in yoghurt, might have behaved as ‘ active fillers’ , which might have further increased the viscosity and G’ (Torres, Murray, & Sarkar, 2016) of LF yoghurt. Nevertheless, MWP has also been reported to act instead as ‘inactive fillers’ not associating with the gel network (Sandoval-Castilla et al., 2004). In such cases, electron micrographs have shown

LF yoghurt with a more open network with localised dense areas of protein, which may result in a lower WHC. Furthermore, where MWP are larger than that of fat globules, it creates a higher level of serum separation, increased graininess and lower firmness as compared to whey protein concentrate (**Table 1**).

Cheese. In case of cheese, fat is integral to structure, making up approximately 20–30% of the product. Although, commercially available LF cheeses can be distinguishable from FF cheeses based on tribological and sensory properties (Laguna et al., 2017), the incorporation of MWP in cheese can be beneficial in terms of sensory attributes. In LF Edam cheese, the addition of three types of commercially available microparticulated whey protein (Simplesse® , DairyLo® and Protelo®) at 0.3–0.9% was demonstrated to reduce firmness, restore proteolysis, opaqueness and improve sensory acceptability (El-Aidie et al., 2019). The MWP was shown to act as an ‘inactive fillers’ , as opposed to active ones as seen in yoghurt (Torres et al., 2018). Addition of Simplesse® at 0.9% level significantly opened up the microstructure resulting in the lowest firmness, this effect was also seen with another study of LF pickled cheese with Simplesse® at 1% (Akin & Kirmaci, 2015) however a study using higher concentrations (3–7% w/w) found that hardness and firmness increased which limits the effective use of MWP in cheese to small concentrations (Schädle et al., 2020) (**Table 1**). In terms of sensory properties, the water retention properties of the MWP that is proportional to firmness of the cheese correlated directly to sensory appreciation of optimum body and texture. It was found that all three MWP at 0.6% resulted in optimum body and texture with DairyLo® and Protelo® with better flavour than Simplesse® (El-Aidie et al., 2019) (**Table 1**). In the case of pickled cheese, LF cheese with Simplesse® achieved better sensory results in all aspects as compared to the FF cheese.

In case of spray-dried cheese powders, removal of fat from the liquid pre-emulsified cheese leads to an 14 × increase in viscosity, resulting in severe issues with atomisation as well as detrimental sensory changes in the finished cheese powder (Urgu et al., 2019). Addition of 3% MWP (in dry matter of 20%) has shown to create similar open porous structures as that of FF cheese powders restoring the original viscosity and increased lubrication, improving flow rate in piped systems. Furthermore, MWP enhanced glossiness and were able to replicate mouth coating scores of FF cheese powders at 3% with no off flavours detected even at highest concentration of MWP (4%) (Urgu et al., 2019). However, interestingly increasing MWP in the LF cheese lead to proportional decreases in mouth coating and at high dry matter (the optimum 25% in FF cheese emulsion), MWP was not able to replicate instrumental viscosity or sensory thickness suggesting that a change in processing and formulation design might be required when using MWP as FR.

Non-dairy foods. Most applied research on MWP has been conducted in dairy applications with rare attention being given to non-dairy systems. For instance, in multigrain cookies MWP failed to significantly perform as a FR, the cookies received the lowest sensory, texture, colour and overall acceptability score (Aggarwal et al., 2016) (**Table 1**). The cookies became tender in texture and darker in colour due to the Maillard reaction of excess amino acids from the MWP with the reducing sugars. However, MWP showed promising effects in replacement of fat in glazes (Meza et al., 2016). Flow properties of glazes made of high sugar were replicated with replacement of sunflower oil with Simplesse®. Both 6% fat (in FF glazes) and 9% MWP (in NF glazes) increased yield stress, viscosity, consistency coefficient (K), viscoelasticity and film thickness with no significant differences between the FF and LF glazes (Meza et al., 2016). MWP

was able to bind excess water and restricted metastable sugar transformation into larger and harder crystals. It was revealed microscopically that NF glazes with 6% MWP and FF glazes with 9% fat had similar sized sugar crystals and no discontinuities in the crystal matrix, in contrast with no fat, no MWP glazes.

Ultimately MWP has an extensive history of use as a FR and it has dominated the FR domain with application to foods, however the limitations of the level of fat being replaced vary depending upon the size of MWP used and viscosity of the continuous medium. In addition, emerging research attention is now paid to alternative proteins and new methodologies to advance the understanding of fat replacement which is discussed later.

2.5 Microparticulated egg white protein

Besides microparticulation of whey protein, microparticulated egg white protein (MEWP) has also been reported in literature where applied research may have been driven by growing consumer demands for LF mayonnaises, salad dressing etc., where egg is a key ingredient. As can be observed using the SEM image in **Figure 2.2b**, MEWP is non spherical in shape with mean size of 9.42 μm (Liu et al., 2018a) and with sharp facets unlike the smooth spherical structures of MWP (**Figure 2.2b**). Therefore, it remains uncertain if MEWP could roll and lubricate via the ‘ball bearing mechanism’ as proposed for MWP. Nevertheless, in this study the overall acceptability of MEWP salad dressings was demonstrated to be comparable to that of commercial salad dressing at 35% fat (**Table 1**). MEWP has been scarcely investigated in literature and so further research using MEWP in various food applications and exploring rheological and especially tribological properties of non-spherical MEWP/other proteins, could be a topic of future consideration.

2.6 Microparticulated plant protein

Plant protein-based microparticles have only recently been considered as FRs with very limited studies to date. Soy protein isolate has very recently been microparticulated (MSP) by heating a 15% dispersion at 95 °C (5–15 min), homogenising and spray drying (Zhang et al., 2020b). As shown in **Figure 2.2c**, MSP displays highly irregular non-spherical particle clusters with a mean size of 2–20 μm. Interestingly, MSP (10% w/w protein dispersion) showed an effective reduction in friction coefficient (μ ~ 0.1) at orally relevant speeds of 50 mm/s (Zhang et al., 2020b) similar to what was obtained with 20% MWP in milk (Olivares et al., 2019). The high rigid particles enhanced by increased disulphide bonds were thought to be reasons for lower friction, although irregular in shape, which may suggest as with MEWP surface topography may not be vital for lubrication. Recently, hemp and canola protein extracted from filter cakes have also been microparticulated to create microparticulated hemp protein (MHP) and microparticulated canola protein (MCP) (Beran et al., 2018). Microparticulation was performed using carbon-dioxide nebulisation, combining drying and micronisation at lower temperatures (25–65 °C) with saturation of carbon-dioxide at 4–8 MPa, the resulting powder was then separated using a cyclone to produce nanosized particles with enhanced solubility and functionality. In comparison to MWP, MHP had an open hollow spheretype of architecture, with surface cracks and had high degree of polydispersity as can be seen in **Figure 2.2d**. Interestingly, MHP has an average size of 0.6 μm, smaller than that of Simplesse® (1 μm). This unique production of plant microparticles offer potential for fat replacement and needs further research attention in application for other food. However, one should not overlook that MHP and MCP suffered from

astringency issues when applied in baked goods (Beran et al., 2018), which might be associated with lubrication failure phenomena limiting FR use.

Dual protein microparticulation is a relatively recent endeavour for improving the functionalities of plant protein-based microparticles. In this direction, recently SPI and EWP were elegantly co-microparticulated (4:1 SPI/EWP) by Zhang et al., 2020b (**Table 1**), where EWP acted as a thiol group donor. Such combination with EWP led to better protein-protein gelation due to disulphide crosslinking resulting in final microparticles (M (SPI + EWP)) with much smoother surface as compared to the MSP shown in **Figure 2.2c**. The remarkable feature of this new microparticulated co-protein was that it enabled friction coefficient reduction by an order of magnitude from 0.1 to 0.01 at orally relevant speeds of 50 mm/s (Zhang et al., 2020b) highlighting synergy of using these two proteins for lubrication performance. However, authors reported that the viscosity of this co-protein was greatly reduced by over 75% compared to standard MSPI (12–15 wt%) and hence, may have a softening effect in final food application.

Overall there has been little research in plant/alternative proteins and needs much focused attention. It is unclear how much fat can be replaced using plants protein/co-proteins, but tribological evidence offers early promises that it may promote fatty like behaviours in LF foods. Furthermore the unique structural, physiochemical and mechanical properties of plant proteins as well as such vast varieties of plant sources offer strong future development for a number of fat replacement uses using plants in our food.

2.7 New protein-based microgels – as future fat replacers

In recent years there has been much interest in the development of protein-based microgels, which shows strong potential to act as future FRs. These protein-

based microgels are soft colloidal particles that are produced by preparing physically cross-linked heat-set hydrogel (90–95 °C, 10–30 min) using highly concentrated protein solutions, followed by breaking them down to micrometer- or nanometric-sized gel particles under high shear forces. A combination of steric and electrostatic repulsions confer good colloidal stability to these particles in aqueous dispersions (Dickinson, 2017). In our laboratory, protein microgels have been synthesized using the above-mentioned top down approach from highly concentrated whey protein (Araiza-Calahorra & Sarkar, 2019; Sarkar et al., 2016), pea protein (Zhang et al., 2020a), egg white protein (Li et al., 2020) or lactoferrin (Sarkar et al., 2018) that is gelled via thermal aggregation and subsequently homogenized to create microgels or even sub-micron sized nanogels ranging in size from 80 to 90 nm (see Figure 3a) (Andablo-Reyes et al., 2019; Araiza Calahorra & Sarkar, 2019) to 300–400 nm (Sarkar et al., 2017).

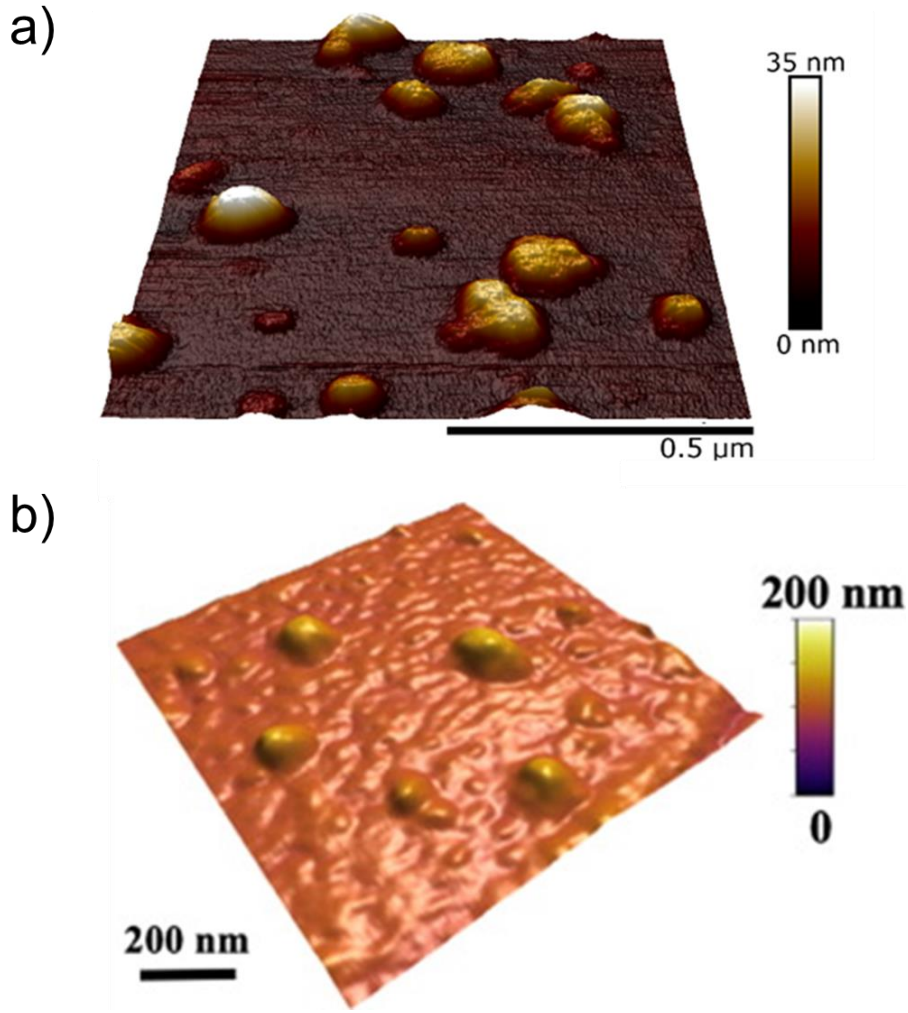

Figure 2.3. Atomic force microscopy (AFM) images of whey protein microgel particles obtained by (a) a top down (Andablo-Reyes et al., 2019), reproduced with permission from RSC (open access) or (b) bottom up approach (Bahri, et al., 2019), reproduced with permission from Elsevier.

Protein microgels can also be made by cold gelation of denatured proteins using calcium ions followed by shearing process (Ni et al., 2015; Torres et al., 2017), gelation via enzymatic approaches followed by shearing (Jiao, Shi, Wang, & Binks, 2018) or by bottom up approaches involving pH- and temperature-induced aggregation of proteins into microgels (see **Figure 2.3b**). Microgels fundamentally differ from microparticulated proteins as the former is swollen and saturated with water providing unique rheological capabilities that lie in between the protein and the gel. Processing techniques have been well-documented in

literature to control vital characteristic such as particle size and elastic modulus of the microgels. For instance, it was found that a ten-fold decrease in particle size can be obtained by using lower concentration of calcium ions and lower turbulent mixing time in case of cold gelation technique (Torres et al., 2017). Protein microgels also undergo pH-dependant alternation in their microstructure and deformability. For instance, a 15-fold increase in stiffness was reported at pH 5.5 and 3.0 in whey protein microgels as compared to being at neutral pH (Bahri et al., 2019).

Generally, microgels have a shear-thinning character depending upon the volume fractions of the microgels and have been recently proven to act as excellent bio-lubricants. They tend to reduce friction either acting as physical surface separators between tribo-contact surfaces or the gel particles roll via ‘ball bearing mechanisms’ , latter is often postulated owing to the smooth, spherical nature of these swollen soft particles as can be observed in the atomic force microscopy images (**Figure 2.3**) (Andablo-Reyes et al., 2019; Bahri et al., 2019). Of the few reports available on tribology in whey protein microgels (WPM), increasing volume fractions 10–80% has been demonstrated to lead to decrease μ by a factor of 10 in hydrophobic tribological surfaces (Sarkar et al., 2017). Interestingly, ‘ soft’ WPM (G’ ~ 100 Pa, prepared with 10 wt% WPI) was found to be less lubricating than ‘hard’ WPM (G’ ~10 kPa prepared with 15 wt% WPI) (AndabloReyes et al., 2019). For example, a two fold increase in viscosity was recorded with hard microgels with enhanced lubricating capabilities. Such reduction in μ was also seen when the WPM was dispersed in a continuum ranging from buffer to other Newtonian (corn syrup) and non-Newtonian mediums (xanthan gum) depending upon the stiffness of the WPM (hard versus soft) as

well as viscosity and rheological behaviour of the continuum (Andablo-Reyes et al., 2019), which may have beneficial application when designing LF products.

Currently, microgels are still being physicochemically characterised in literature and in present times, there exist a number of hindrances for its commercial use as a food ingredient. One is the control of microgels swelling/deswelling ability in response to environmental pH, ions and temperature. Changes to the environment as well as interaction with other ingredients may create stability issues in the microgel during storage and processing. The processing of microgels is complex and particles are often irregular in morphology, conditions would need to be strictly controlled and further clarification of unwanted polymer by-products (i.e. non-microgelled protein in the continuous phase) would make it an overall expensive processing technology. Microgels contain >90 wt% water and economically should be transported in a dry state, commonly cost-effective drying techniques (i.e. spray drying) may impact the morphology and functionality of the microgels. Literature has shown evidence that freeze drying is effective with little physicochemical changes upon rehydration, however, such data is limited to non-food grade poly(N-isopropylacrylamide) microgels (Agbugba et al., 1998) and food grade application is limited to soy protein microgels (Benetti et al., 2019).

In summary a paucity of tribology data in microgels other than WPI and no sensory data in microgels to date suggests further research is required in this domain. Considering the viscosity modifying properties and high lubricating ability, microgels offer strong candidacy as FRs, which needs to be investigated particularly from sensory viewpoint in model foods primarily, followed by its application in real food systems and cost-effective upscaling of microgels needs to be explored. One should also consider investigating the properties of these

swollen microgels versus hydrated versions of dried microgels to really understand whether the microgels get swollen to the optimized state after drying.

2.8 Summary of design features for protein-based fat replacers

To summarize the overall landscape of FRs in last 5 year and clearly identify the knowledge gap, **Figure 2.4** illustrates the characterisation techniques, number of studies, the systems and forms of the proteins used in model and real food systems that have appeared in literature in the last half a decade. In model systems, there are relatively few studies using protein concentrates/isolates and microparticulated proteins as FRs with a more saturated research effort in case of protein microgels. It is well recognized that model systems are ideal for fundamental understanding and generating mechanistic insights on how proteins can act as FRs. Therefore, the limited research in understanding the role of proteins and microparticulated proteins in model foods in last 5 years might be attributed to the extensive work already done in the past (Lucca & Tepper, 1994; Nateghi et al., 2012) with the level of research slowing down. This is in close agreement with significant levels of research done in real foods with proteins and microparticulated proteins. This suggests that research in use of proteins and microparticulated proteins have progressed well over the last few decades where the paradigm has been shifted towards research in real food applications. In stark contrast, microgels have been employed only with model systems to gain fundamental understanding as they have been synthesized at laboratory scale. To our knowledge, no paper has reported using microgels as FRs in real food application microgels. Nevertheless, a patent search shown in **Table 2** shows examples of proteinaceous microgels or microgel-like particles that have been applied in fat replacement restricted to mostly diary with some condiment and confectionary applications. Advancements in microgel preparation, appropriate

scale up, characterisation of their lubrication capabilities and sensorial properties may offer wider application of microgels in real food use and consequently will advance the field. This clearly highlights an untapped opportunity space for exploration by researchers and food industries in the future. In regards to protein type, there are only few studies using proteins from plant sources in all areas of fat replacement presenting further opportunity considering the global rise of sustainability demands and rapid rise in microparticulated plant proteins as discussed previously.

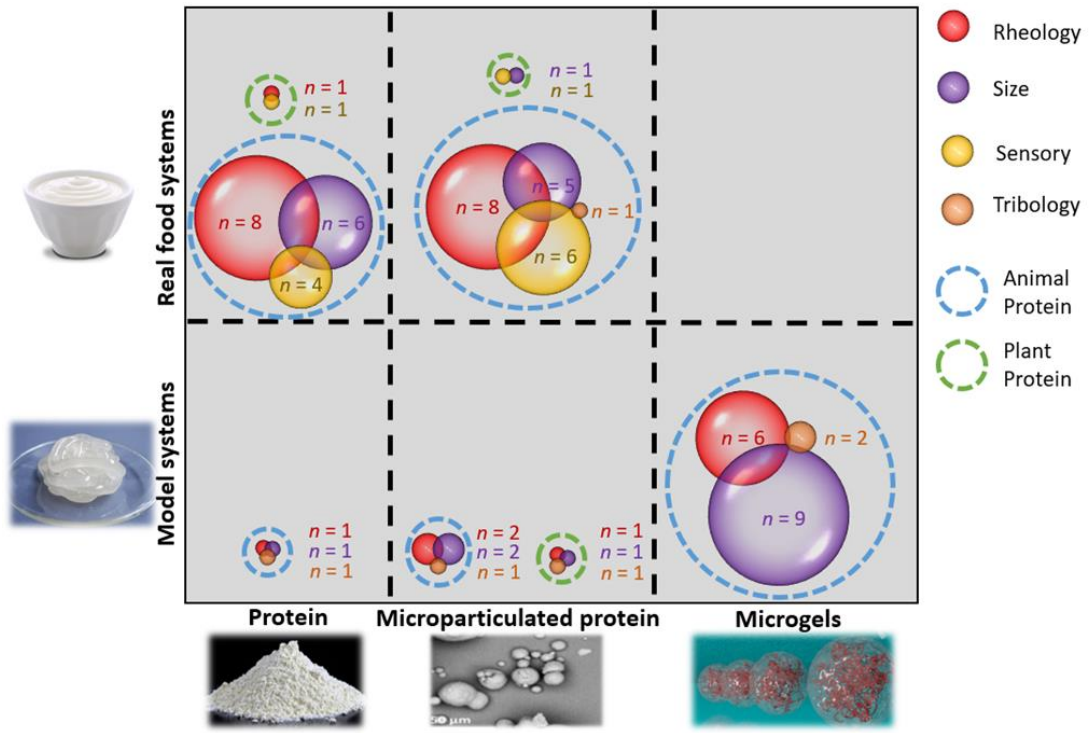

Figure 2.4 Bubble plot illustrating the characterisation techniques, protein types used as fat replacers including microgels with applications in real or model systems discussed in the review, where n = number of studies (see Appendix A Table A1) for raw data.

Table 2. List (non-exhaustive) of patents using microgels or microgel-like particles for fat replacement applications.

Patent name	Reference	Filing date	Current Assignee	Size	Examples of fat replacement applications
Protein product	EP0323529B1 (Singer et al., 1987)	1987	Labatt Breving Co Ltd	0.1-2.0 μm	Ice cream, mayonnaise, salad dressing
Insoluble protein particles	EP1292196B1 (Villagran et al., 2001)	2001	The Folgers Coffee Company	< 2 μm (preferentially 0.1-3.0 μm)	Ready to drink beverages
Low fat creamer compositions	EP1589821B1 (Villagran and Baughman, 2003)	2003	Procter and Gamble Co	0.1-10.0 μm (preferentially 0.1-5.0 μm)	Coffee and tea creamer
Satiety enhancing food product and a method for manufacturing such	EP1833309A1 (Adams et al., 2005)	2005	Unilever PLC Unilever NV	< 300 μm	Meal replacer
Whey protein micelles	EP1839492B1 (Schmitt et al., 2006)	2006	Nestec SA	< 1 μm (preferentially 0.2 - 0.4 μm)	Dairy desserts, coffee creamers, fat based condiments, chocolate, spreads
Creamer composition comprising plant protein microparticles	EP2991498A1 (Schmitt and Rade-Kukic, 2014)	2014	Nestec SA	100-4000 μm	Coffee and tea creamer

In both real food and model food systems (**Figure 2.4**), rheology and particle size measurement appear to dominate the characterisation space for fat replacement as these have been postulated to have strong mechanistic and empirical association to some of the sensory attributes (Foegeding, 2007). In contrast to model food systems, sensory characterisation is very popular in real food systems, which is definitely the most important test to identify whether or not the NF/LF products using the FRs can replicate the sensory perception of FF products. It is notable that sensory analyses are limited in model foods, this is largely associated with difficulty in training participants with model food systems as compared to trained panellists recruited in food industries for real food systems. Oral tribology is now acknowledged as a promising tool to relate to mouthfeel perception that occur in the later stages of oral processing and cannot be explained by rheological analysis alone (Pradal and Stokes, 2016; Sarkar et al., 2019; Sarkar and Krop, 2019). A lack of appreciation of tribology in real food systems is apparent (**Figure 2.4**) as no studies have yet been performed. Recent studies on model proteins, microparticulated proteins and microgels have incorporated tribology given its importance in understanding the role of fat and protein-based FRs in lubrication. Especially with advancements of fundamental tribological studies and tribology-sensory correlations, it should be a key area of characterisation in future research when designing FRs or testing FRs in model and real foods for designing NF/LF products. It is also important to highlight that recent advancement of promising adsorption techniques such as quartz crystal microbalance with dissipation (QCM-D) using saliva-coated surfaces may complement the tribology analysis (Xu et al., 2020). Such combination of tribology with muco-adhesion experiments may be a powerful approach in the understanding of the interactions of FRs with saliva and thus help to reduce the

development cycle of food product development by reducing the number of sensory trials.

We postulate in the following some key take-home messages on physiochemical and structural properties for designing protein-based FRs in order to be functionally viable for designing LF/NF products with appropriate sensory perception:

Particle size, shape and rigidity. Particle sizes in protein-based FRs range from aggregated protein isolates at 46– 168 μm, microparticluation proteins (0.2–9 μm) to sub-micron sized (0.04–0.3 μm) particles in case of microgels. It is evident from literature that small particle size is important for boundary lubrication to allow entrainment of the particles in the narrow gap between the tongue and palate surfaces during oral processing (or tribopairs in oral tribology experiments), with particle sizes greater than 10 μm often being perceived as gritty and with increased friction. Particle shape may be important, where irregular-shaped particles with sharp facets could cause reduced creaminess perception where-by spherical particles offer 'ball-bearing' lubrication mechanism, but needs further investigation. Besides size and shape of the microparticulated proteins and microgels, rigidity of particles are very important and can influence the mouthfeel perception by virtue of their tribological properties (Andablo-Reyes et al., 2019; Araiza-Calahorra & Sarkar, 2019). Therefore, modifying size and shape of FRs with appropriate deformability to closely resemble fat-based emulsion droplets might be an appropriate approach to generate mouthfeel in LF/NF products similar to that of FF products.

Rheology. All FRs have shown the ability to greatly modify the bulk viscosity in both model and real food systems. Fat has viscosity enhancing properties, as such, LF foods tend to suffer from 25 to 50% decrease in this

attribute both measured using instrumental and sensory techniques. Most FRs are therefore designed so that they can contribute to water binding ability. Another important feature is that many, if not, most fat-based emulsions have a shear-thinning behaviour. Of course such properties are difficult to achieve using proteins on its own as aqueous dispersions of protein tend to have a Newtonian behaviour. Hence, proteins combined with polysaccharides (xanthan gum, cellulose) are often used to improve the viscosity of the food matrix. In addition, microgels can be particularly interesting as FRs as they possess excellent shear thinning behaviour in orally relevant shear-rates (Andablo-Reyes et al., 2019; Araiza Calahorra & Sarkar, 2019), however such rheological behaviour might change depending upon the food matrix as well as rigidity of the particles (Andablo-Reyes et al., 2019; Araiza-Calahorra & Sarkar, 2019), which needs to be investigated in the future.

Tribology. Fat acts as a lubricant film and thus has the ability to reduce the friction coefficient between the tongue and oral palate in the later stages of oral processing where the thickness of those fatty films range from few molecules to hundreds of nanometres of thickness. Recent work with proteins, microparticulated proteins and microgels have shown lubrication attribute with specific attention to ball bearing mechanism. However, often, there is lack of direct evidence for the proposed underlying mechanism. Hence, it is crucial to understand the in situ flow-induced structural alterations of microparticulated proteins and microgels under shear. For instance, it might be interesting to combine tribological set up with small angle neutron-scattering facility to reveal the structure of the lubricating film between the tribo-pair while it is sliding. Also, lubrication behaviour of microgels and microparticulated systems is also dictated by size, shape, rigidity and viscosity, which needs focused attention. In general,

the FRs that can reduce boundary friction to a large extent and when introduced in LF/NF products provide comparable friction coefficient to that of FF products should be a useful tool to screen FRs. In general, creaminess is a highly complex mouthfeel perception that is mostly present in FF products and not in LF/NF products. Generally, creaminess is correlated to smoothness, fatty mouth feel and creamy flavour (Frøst & Janhøj, 2007), which can be predicted using combination of complementary assessment of particle size, shape, rheology, tribology and QCM-D.

Protein-ingredient interactions. Proteins are highly responsive to other ingredients and environments (i.e. heat, pH, ions) which may cause challenges when used as a FM. Proteins vary in charge across pH ranges and the net charge is influenced by the ionic conditions leading to variations in protein-protein and protein-ingredient interactions, which may result in macroscopic physical and chemical changes. Fundamentally the water binding ability of proteins may limit availability of water for other components, leading to rheological and microstructural implications. It is well known proteins interact with various thickeners used in food applications such as carrageenan (Drohan, Tziboula, McNulty, & Horne, 1997). Such interactions may be repulsive or attractive which may govern phase macroscopic separation (Goh et al., 2008). Heated foods presents an additional degree of challenge for proteins as FR. At prolonged high temperatures, typical of baked foods, aggregation and loss of water binding is expected resulting in macrostructural changes. Above 140 °C, the available amino acids in protein-based FRs and reactive carbonyl from reducing sugar in the food i.e. monosaccharides, lactose, maltose may react causing browning and generation of complex flavour compounds, known as the Maillard reaction, which might hinder applications of protein-based FRs in baked foods.

2.9 Conclusions

In order to design low fat/no fat products that mimic the behaviour of full fat products, there has been extensive research in last few decades using proteins and microparticulated proteins. Whey protein appears to dominate the field with most usage in dairy fat replacement. There has been recent interests in the use of plant proteins, however characterisation, understanding and application is highly limited to date. Besides particle size, rheology and sensory evaluation, tribology appears to be a new tool that is being applied to understand the lubrication properties of fat replacers mostly in model food systems. Combination of tribology with muco-adhesion techniques can be powerful screening tools for identifying fat replacers with just-right mouth feel properties in the future for sensory testing. Besides proteins and commercially available microparticulated proteins, microgels that are designed in laboratory setting have recently demonstrated superior rheological and lubrication performance with ability to act as potential fat replacers. However, information lacking in sensory perception of microgels in literature and the challenges of tailored commercial scale microgel production appear to be the bottlenecks to find its usage in real food applications.

With key gaps identified, the thesis has shifted its attention towards emphasising plant proteins as a primary focus. Furthermore, **Chapter 3** delves into the comprehension of their lubrication characteristics, while **Chapter 4** investigates their sensory attributes. These investigations ultimately culminate in the development of plant protein microgels, as detailed in **Chapter 5**.

2.10 References

Agbugba, C.B., Hendriksen, B.A., Chowdhry, B.Z., & Snowden, M.J. (1998). The redispersibility and physico chemical properties of freeze-dried colloidal

microgels. *Colloids and Surfaces A: Physicochemical and Engineering Aspects*, 137, 155–164.

Aggarwal, D., Sabikhi, L., & Sathish Kumar, M.H. (2016). Formulation of reduced-calorie biscuits using artificial sweeteners and fat replacer with dairy–multigrain approach. NFS Journal, 2, 1–7. Akbari, M., Eskandari, M.H., & Davoudi, Z. (2019). Application and functions of fat replacers in low-fat ice cream: A review. *Trends in Food Science & Technology*, 86, 34–40.

Akin, M.S., & Kirmaci, Z. (2015). Influence of fat replacers on the chemical, textural and sensory properties of low-fat Beyaz pickled cheese produced from Ewe's milk: Vol. 68 (pp. 127–134).

Alves, A.C., & Tavares, G.M. (2019). Mixing animal and plant proteins: Is this a way to improve protein techno-functionalities? *Food Hydrocolloids*, 97, 105171.

Andablo-Reyes, E., Yerani, D., Fu, M., Liamas, E., Connell, S., & Torres, O., et al. (2019). Microgels as viscosity modifiers influence lubrication performance of continuum. *Soft Matter*, 15, 9614–9624.

Araiza-Calahorra, A., & Sarkar, A. (2019). Pickering emulsion stabilized by protein nanogel particles for delivery of curcumin: Effects of pH and ionic strength on curcumin retention. *Food Structure*, 21, 100113.

Bahri, A., Chevalier-Lucia, D., Marchesseau, S., Schmitt, C., Gergely, C., & Martin, M. (2019). Effect of pH change on size and nanomechanical behavior of whey protein microgels. *Journal of Colloid and Interface Science*, 555, 558–568.

Barron, E., Clark, R., Hewings, R., Smith, J., & Valabhji, J. (2018). Progress of the healthier you: NHS diabetes prevention programme: Referrals, uptake and participant characteristics: Vol. 35 (pp. 513–518).

Benelam, B. (2009). Satiation, satiety and their effects on eating behaviour. *Nutrition Bulletin*, 34, 126–173. Benetti, J.V.M., Silva, J.T.D., & Nicoletti, V.R. (2019).

SPI microgels applied to pickering stabilization of O/W emulsions by ultrasound and high-pressure homogenization: Rheology and spray drying. *Food Research International,* 122, 383–391.

Beran, M., Drahorád, J., Vltavsky, O., Urban, M., Laknerova, I., & Fronek, M., et al. (2018). Pilot-scale production and application of microparticulated plant proteins. *Journal of Nutrition & Food Sciences*, 8.

Bigliardi, B., & Galati, F. (2013). Innovation trends in the food industry: The case of functional foods. *Trends in Food Science & Technology*, 31, 118–129.

Cheftel, J.C., & Dumay, E. (1993). Microcoagulation of proteins for development of “creaminess”. *Food Reviews International*, 9, 473–502.

Colla, K., Costanzo, A., & Gamlath, S. (2018). Fat replacers in baked food products. *Foods*, 7, 12.

Costa, M.P., Frasao, B.S., Rodrigues, B.L., Silva, A.C.O., & Conte-Junior, C.A. (2016). Effect of different fat replacers on the physicochemical and instrumental analysis of low-fat cupuassu goat milk yogurts. *Journal of Dairy Research*, 83, 493–496.

Croguennec, T., Tavares, G.M., & Bouhallab, S. (2017). Heteroprotein complex coacervation: A generic process*. Advances in Colloid and Interface Science*, 239, 115–126.

Dabija, A., Codina, G., Anca, G., Sanduleac, E., & Lacramioara, R. (2018). Effects of some vegetable proteins addition on yogurt quality. *Scientific Study and*

Research: Chemistry and Chemical Engineering, Biotechnology, Food Industry, 19, 181–192.

Danesh, E., Goudarzi, M., & Jooyandeh, H. (2018). Transglutaminase-mediated incorporation of whey protein as fat replacer into the formulation of reduced-fat Iranian white cheese: Physicochemical, rheological and microstructural characterization. *Journal of Food Measurement and Characterization*, 12, 2416–2425.

Dickinson, E. (2017). Biopolymer-based particles as stabilizing agents for emulsions and foams. *Food Hydrocolloids*, 68, 219–231.

Drohan, D.D., Tziboula, A., McNulty, D., & Horne, D.S. (1997). Milk protein-carrageenan interactions. *Food Hydrocolloids*, 11, 101–107.

El-Aidie, S., I Ghita, E., M El-Dieb, S., & Elgarhi, H. (2019). Physicochemical, microstructural and sensory impact of fat replacers on low-fat edam cheese manufactured from buffalo's milk. I*nternational Journal of Advancement in Life Sciences Research*, 2. 2581-4877.

Fang, T., Shen, X., Hou, J., & Guo, M. (2019). Effects of polymerized whey protein prepared directly from cheese whey as fat replacer on physiochemical, texture, microstructure and sensory properties of low-fat set yogurt. *Lebensmittel-Wissenschaft & Technologie*, 115, 108268.

Foegeding, E.A. (2007). Rheology and sensory texture of biopolymer gels. *Current Opinion in Colloid & Interface Science*, 12, 242–250.

Frøst, M.B., & Janhøj, T. (2007). Understanding creaminess. *International Dairy Journal*, 17, 1298–1311.

Goh, K.K.T., Sarkar, A., & Singh, H. (2008). Chapter 12 - milk protein–polysaccharide interactions. In Thompson, A., Boland, M., & Singh, H. (Eds.), Milk proteins (pp. 347–376). San Diego: Academic Press.

Guo, Y., Zhang, X., Hao, W., Xie, Y., Chen, L., & Li, Z., et al. (2018). Nano-bacterial cellulose/soy protein isolate complex gel as fat substitutes in ice cream model. *Carbohydrate Polymers*, 198, 620–630.

Hunt, R., Zorich, N.L., & Thomson, A.B.R. (1998). Overview of olestra: A new fat substitute. *Canadian Journal of Gastroenterology*, 12, 193–197.

Ipsen, R. (2017). Microparticulated whey proteins for improving dairy product texture. International Dairy Journal, 67, 73–79.

Jandacek, R.J., & Letton, J.C. (1987). In U. S. P. a. T. Office (Ed.), Compostions containing novel solid, nondigestible, fat-like compounds - US4797300a.

Jiao, B., Shi, A., Wang, Q., & Binks, B.P. (2018). High-internal-phase pickering emulsions stabilized solely by peanut-protein-isolate microgel particles with multiple potential applications: Vol. 57 (pp. 9274–9278).

Jørgensen, C.E., Abrahamsen, R.K., Rukke, E.-O., Johansen, A.-G., Schüller, R.B., & Skeie, S.B. (2015). Improving the structure and rheology of high protein, low fat yoghurt with undenatured whey proteins. *International Dairy Journal*, 47, 6–18.

Laguna, L., Farrell, G., Bryant, M., Morina, A., & Sarkar, A. (2017). Relating rheology and tribology of commercial dairy colloids to sensory perception. *Food & Function*, 8, 563–573.

Lesme, H., Rannou, C., Famelart, M.-H., Bouhallab, S., & Prost, C. (2020). Yogurts enriched with milk proteins: Texture properties, aroma release and sensory perception. *Trends in Food Science & Technology*, 98, 140–149.

Li, X., Murray, B.S., Yang, Y., & Sarkar, A. (2020). Egg white protein microgels as aqueous pickering foam stabilizers: Bubble stability and interfacial properties. *Food Hydrocolloids*, 98, 105292.

Liu, G., Jæger, T.C., Lund, M.N., Nielsen, S.B., Ray, C.A., & Ipsen, R. (2016a). Effects of disulphide bonds between added whey protein aggregates and other milk components on the rheological properties of acidified milk model systems. *International Dairy Journal*, 59, 1–9.

Liu, K., Stieger, M., van der Linden, E., & van de Velde, F. (2016b). Effect of microparticulated whey protein on sensory properties of liquid and semi-solid model foods. *Food Hydrocolloids*, 60, 186–198.

Liu, K., Tian, Y., Stieger, M., van der Linden, E., & van de Velde, F. (2016c) Evidence for ball-bearing mechanism of microparticulated whey protein as fat replacer in liquid and semi-solid multi-component model foods. *Food Hydrocolloids*, 52, 403–414.

Liu, R., Tian, Z.J., Song, Y.S., Wu, T., Sui, W.J., & Zhang, M. (2018a) Optimization of the production of microparticulated egg white proteins as fat mimetic in salad dressings using uniform design. *Food Science and Technology Research*, 24, 817–827.

Liu, R., Wang, L., Liu, Y., Wu, T., & Zhang, M. (2018b) Fabricating soy protein hydrolysate/xanthan gum as fat replacer in ice cream by combined enzymatic and heat-shearing treatment. *Food Hydrocolloids*, 81, 39–47.

Lucca, P.A., & Tepper, B.J. (1994). Fat replacers and the functionality of fat in foods. *Trends in Food Science & Technology*, 5, 12–19.

Ma, Z., & Boye, J.I. (2013). Advances in the design and production of reduced-fat and reduced-cholesterol salad dressing and mayonnaise: A review. *Food and Bioprocess Technology*, 6, 648–670.

Marangoni, A.G., van Duynhoven, J.P.M., Acevedo, N.C., Nicholson, R.A., & Patel, A.R. (2020). Advances in our understanding of the structure and functionality of edible fats and fat mimetics. *Soft Matter*, 16, 289–306. Meza, B.E., Peralta, J.M., & Zorrilla, S.E. (2016).

Rheological characterization of full-fat and low-fat glaze materials for foods. *Journal of Food Engineering*, 171, 57–66.

Nasonova, V.V., & Tunieva, E.K. (2019). A comparative study of fat replacers in cooked sausages. IOP Conference Series: Earth and Environmental Science, 333, 012085.

Nateghi, L., Roohinejad, S., Totosaus, A., Mirhosseini, H., Shuhaimi, M., & Meimandipour, A., et al. (2012). Optimization of textural properties and formulation of reduced fat Cheddar cheeses containing fat replacers. *Journal of Food Agriculture and Environment*, 10, 46–54.

Nehete, J.Y., Bhambar, R.S., Narkhede, M.R., & Gawali, S.R. (2013). Natural proteins: Sources, isolation, characterization and applications. *Pharmacognosy Reviews*, 7, 107–116.

Ni, Y., Wen, L., Wang, L., Dang, Y., Zhou, P., & Liang, L. (2015). Effect of temperature, calcium and protein concentration on aggregation of whey protein isolate: Formation of gel-like micro-particles. *International Dairy Journal*, 51, 8–15.

O'Connor, T.P., & O'Brien, N.M. (2016). Fat replacers. Reference Module in food science. Elsevier.

Olivares, M.L., Shahrivar, K., & de Vicente, J. (2019). Soft lubrication characteristics of microparticulated whey proteins used as fat replacers in dairy systems. *Journal of Food Engineering*, 245, 157–165.

Peng, X., & Yao, Y. (2017). Carbohydrates as Fat Replacers, *Annu Rev Food Sci Technol* 8, 331–351.

Pokorny, J. (1998). Substrate influence on the frying process. J Grasas y Aceites, 49, 265–270.

Protte, K., Weiss, J., Hinrichs, J., & Knaapila, A. (2019). Thermally stabilised whey protein-pectin complexes modulate the thermodynamic incompatibility in hydrocolloid matrixes: A feasibility-study on sensory and rheological characteristics in dairy desserts. *Lebensmittel-Wissenschaft & Technologie*, 105, 336–343.

Rajakari, K., & Myllarinen, P. (2016). In WIPO/PCT (Ed.), Whey preparation obtained by cavitation and uses thereof.

Sandoval-Castilla, O., Lobato-Calleros, C., Aguirre-Mandujano, E., & Vernon-Carter, E.J. (2004). Microstructure and texture of yogurt as influenced by fat replacers. *International Dairy Journal*, 14, 151–159.

Sarkar, A., Ademuyiwa, V., Stubley, S., Esa, N.H., Goycoolea, F.M., & Qin, X., et al. (2018). Pickering emulsions co-stabilized by composite protein/polysaccharide particle-particle interfaces: Impact on in-vitro gastric stability. *Food Hydrocolloids*, 84, 282–291.

Sarkar, A., Kanti, F., Gulotta, A., Murray, B.S., & Zhang, S. (2017). Aqueous lubrication, structure and rheological properties of whey protein microgel particles. *Langmuir*, 33, 14699–14708.

Sarkar, A., Murray, B., Holmes, M., Ettelaie, R., Abdalla, A., & Yang, X. (2016). In-vitro digestion of pickering emulsions stabilized by soft whey protein microgel particles: Influence of thermal treatment. *Soft Matter*, 12, 3558–3569.

Schädle, C.N., Eisner, P., & Bader-Mittermaier, S. (2020). The combined effects of different fat replacers and rennet casein on the properties of reduced-fat processed cheese. *Journal of Dairy Science*, 103, 3980–3993.

Schmitt, C.J.E., Bovetto, L., Robin, F., & Pouzot, M. (2006). In E. P. Office (Ed.), Whey protein micelles - EP1839492B1.

Schmitt, C.J.E., & Rade-Kukic, K. (2014). In E. P. Office (Ed.), Creamer composition comprising plant protein microparticles - EP2991498A1.

Silva, J.V.C., & O'Mahony, J.A. (2018). Microparticulated whey protein addition modulates rheological and microstructural properties of high-protein acid milk gels. *International Dairy Journal*, 78, 145–151.

Singer, N.S., Latella, J., & Shoji, Y. (1990). In U. S. Patent (Ed.), Fat emulating protein products and process - US4961953A.

Singer, N.S., Latella, J., & Yamamoto, S. (1987). In E. P. Office (Ed.), Protein product - EP0323529B1. Singer, N.S., Yamamoto, S., & Latella, J. (1988). In U. S. Patent (Ed.), Protein product base - US4734287A.

Smith, R.E., Finley, J.W., & Leveille, G.A. (1994). Overview of SALATRIM: A family of low-calorie fats. *Journal of Agricultural and Food Chemistry*, 42, 432–434.

Sun, L., Chen, W., Liu, Y., Li, J., & Yu, H. (2015). Soy protein isolate/cellulose nanofiber complex gels as fat substitutes: Rheological and textural properties and extent of cream imitation. *Cellulose*, 22, 2619–2627.

Sun, C., Liu, R., Liang, B., Wu, T., Sui, W., & Zhang, M. (2018). Microparticulated whey protein-pectin complex: A texture-controllable gel for low-fat mayonnaise. *Food Research International*, 108, 151–160.

Temiz, H., & Kezer, G. (2015). Effects of fat replacers on physicochemical, microbial and sensorial properties of kefir made using mixture of cow and goat's milk: Vol. 39 (pp. 1421–1430).

Toro-Sierra, J., Schumann, J., & Kulozik, U. (2013). Impact of spray-drying conditions on the particle size of microparticulated whey protein fractions. *Dairy Science & Technology*, 93, 487–503.

Torres, I.C., Amigo, J.M., Knudsen, J.C., Tolkach, A., Mikkelsen, B.Ø., & Ipsen, R. (2018). Rheology and microstructure of low-fat yoghurt produced with whey protein microparticles as fat replacer. *International Dairy Journal*, 81, 62–71.

Torres, I.C., Janhøj, T., Mikkelsen, B.Ø., & Ipsen, R. (2011). Effect of microparticulated whey protein with varying content of denatured protein on the rheological and sensory characteristics of low-fat yoghurt. *International Dairy Journal,* 21, 645–655.

Torres, O., Murray, B., & Sarkar, A. (2016). Emulsion microgel particles: Novel encapsulation strategy for lipophilic molecules. *Trends in Food Science & Technology*, 55, 98–108.

Torres, O., Murray, B., & Sarkar, A. (2017). Design of novel emulsion microgel particles of tuneable size. *Food Hydrocolloids*, 71, 47–59.

Urgu, M., Türk, A., Ünlütürk, S., Kaymak-Ertekin, F., & Koca, N. (2019). Milk fat substitution by microparticulated protein in reduced-fat cheese emulsion: The effects on stability, microstructure, rheological and sensory properties. *Food science of animal resources*, 39, 23–34.

Valentino, F., & baughman, V.j. m. (2004). In WIPO/PCT (Ed.), Low fat creamer compositions - WO2004071203A1. Adams, S., Butler, M.F., & Clark, A.H. (2005). In E. P. Office (Ed.), Satiety enhancing food product and a method for manufacturing such - EP1833309A1.

Varga-Visi, E., & Toxanbayeva, B. (2016). Application of fat replacers and their effect on quality of comminuted meat products with low lipid content: A review. *Acta Alimentaria*, 46, 1–6.

Veldhorst, M.A.B., Nieuwenhuizen, A.G., Hochstenbach-Waelen, A., Westerterp, K.R., Engelen, M.P.K.J., & Brummer, R.-J.M., et al. (2009). Effects of high and normal soyprotein breakfasts on satiety and subsequent energy intake, including amino acid and “satiety” hormone responses. *European Journal of Nutrition*, 48, 92.

Villagran, F.V., & Baughman, J.M. (2003). In E. P. Office (Ed.), Low fat creamer compositions - EP1589821B1.

Villagran, F.V., Dria, G.J., Young, H.T., Baughman, J.M., & Chen, J. (2001). In E. P. Office (Ed.), Insoluble protein particles - EP1292196B1.

Wang, Y., Beydoun, M.A., Min, J., Xue, H., Kaminsky, L.A., & Cheskin, L.J. (2020). Has the prevalence of overweight, obesity and central obesity levelled off in the United States? Trends, patterns, disparities, and future projections for the obesity epidemic. *International Journal of Epidemiology*.

Weiss, J., Salminen, H., Moll, P., & Schmitt, C. (2019). Use of molecular interactions and mesoscopic scale transitions to modulate protein-polysaccharide structures. *Advances in Colloid and Interface Science*, 271, 101987.

Welty, W.M., Marshall, R.T., Grün, I.U., & Ellersieck, M.R. (2001). Effects of milk fat, cocoa butter, or selected fat replacers on flavor volatiles of chocolate ice cream. *Journal of Dairy Science*, 84, 21–30

William, C.F., Josef, C.D., & Joke, D.F.N. (1993). In WIPO/PCT (Ed.), Reduced calorie fats - WO9315612A1.

Zhang, S., Holmes, M., Ettelaie, R., & Sarkar, A.(2020a) Pea protein microgel particles as Pickering stabilisers of oil-in-water emulsions: Responsiveness to pH and ionic strength. *Food Hydrocolloids*, 102, 105583.

Zhang, T., Guo, J., Chen, J.-F., Wang, J.-M., Wan, Z.-L., & Yang, X.-Q. (2020b) Heat stability and rheological properties of concentrated soy protein/egg white protein composite microparticle dispersions. *Food Hydrocolloids*, 100, 105449.

Zhang, T., McCarthy, J., Wang, G., Liu, Y., & Guo, M. (2015). Physiochemical properties, microstructure, and probiotic survivability of nonfat goats' milk yogurt using heat-treated whey protein concentrate as fat replacer. *Journal of Food Science*, 80, M788–M794.

Zhu, Y., Bhandari, B., & Prakash, S. (2019). Tribo-rheology characteristics and microstructure of a protein solution with varying casein to whey protein ratios and addition of hydrocolloids. *Food Hydrocolloids*, 89, 874– 884.

Chapter 3 : Oral tribology, rheology and adsorption of alternative food proteins[2]

Abstract

Mechanistic knowledge using tribology and adsorption may help to screen various proteins with better lubrication; aiding the fast tracking of new ingredient formulations for use in low-fat/high protein food development. The aim of this study was to compare the lubrication, adsorption and physicochemical properties of alternative proteins (pea, potato, lupin and insect proteins) with whey protein isolate (WPI) as the control. Soluble fractions (1–10 wt%) of pea protein concentrate (PPC_{sol}), insect protein concentrate (IPC_{sol}), potato protein isolate ($PoPI_{sol}$) and lupin protein isolate (LPI_{sol}) were chosen as the alternative proteins. All proteins were negatively-charged at neutral pH and showed various degrees of aggregation (hydrodynamic diameters ranging from 25 nm for $PoPI_{sol}$ to 244 nm for PPC_{sol}). The boundary friction coefficient (μ) at 5 wt% protein followed the trend as $PPC_{sol} > LPI_{sol} > IPC_{sol} > PoPI_{sol} > WPI_{sol}$, highlighting excellent lubrication performances of $PoPI_{sol}$, IPC_{sol} and WPI_{sol}. At higher protein concentrations (10 wt%), μ significantly increased for LPI_{sol}, $PoPI_{sol}$ and IPC_{sol}, while decreasing for WPI_{sol}. Quartz crystal microbalance with dissipation monitoring (QCM-D) results revealed formation of rigid elastic films on hydrophobic surfaces by $PoPI_{sol}$ and WPI_{sol} giving rise to low μ while more viscous films by PPC_{sol} led to high μ. PPC_{sol} had the highest hydrated mass (11.0 mg m^{-2}) as compared to WPI_{sol} (8.0 mg m^{-2}) with lower values reported for other proteins (5.0–5.4 mg m^{-2}). Strong correlations existed between μ scaled to

[2] Published as Kew, B., Holmes, M., Stieger, M. and Sarkar, A. 2021. Oral tribology, adsorption and rheology of alternative food proteins. Food Hydrocolloids. 116, p106636.

viscosity, size and hydrated mass and viscoelasticity of films in alternative proteins, validating the surface-linked phenomena in frictional response.

3.1 Introducton

There exists a significant potential for proteins to act as a fat replacers in food formulation; providing less than half the calories of fat (4 kcal per gram), having the highest satiety-providing ability of the macronutrients (Veldhorst et al., 2008) with some of them having the ability to act functionally as fat mimetic after suitable modifications (Kew, Holmes, Stieger, & Sarkar, 2020). Although there have been several recent studies and industrial developments in this direction using proteins either alone (Nastaj et al., 2020), in combination with thickeners (Graf et al., 2020), or in advanced microstructural forms (*e.g.* microparticulated proteins) (Sánchez-Obando et al., 2020), often such fat replacement strategies fail in mimicking the lubricating mouthfeel of fat leading to the rejection of the product by consumers.

Rheological analyses such as viscosity, water holding capacity, compression tests and particle size have typically aided macro-formulation with proteins (Laiho et al., 2017). However, rheology and particle size do not paint a complete picture on predicting mouthfeel attributes that are lubrication-dominant such as creaminess, smoothness *etc.* (Chen & Stokes, 2012; Kokini et al., 1977; Pradal & Stokes, 2016; Prakash et al., 2013; Sarkar & Krop, 2019b)

Tribology, the study of lubrication and friction has therefore gained much interest recently for its ability to characterise and enhance our understanding of fat-related and more broadly surface-induced mouthfeel perception. A tribometer is utilised to measure such lubrication in which friction coefficients at a range of entrainment speeds are measured. Consequently, a distinct Stribeck curve is generated where friction coefficient is plotted against film thickness with

identification of three defined lubrication regimes; boundary, mixed and hydrodynamic regime (Sarkar et al., 2019; Stokes et al., 2013). It is generally in the boundary and mixed regimes, where friction tends to correlate with a range of friction-related sensory properties *i.e.* smoothness, slipperiness, pastiness, melting *etc.* (Chen et al., 2012; Kokini et al., 1977; Pradal et al., 2016; Prakash et al., 2013; Sarkar & Krop, 2019). Although biopolymers in general have attracted significant research attention for tribological analysis, systematic tribological characterisation of proteins is fairly limited in literature to date (Chojnicka et al., 2008; Kew et al., 2020).

To advance our fundamental understanding of lubrication in tribological analysis, adsorption techniques such as quartz crystal-microbalance with dissipation (QCM-D) has been utilised recently. Such techniques have been elegantly employed by Stokes et al., (2011) using hydrophobically modified sensors to mimic the surfaces used in tribotesting. Such modification of surfaces in QCM-D offers advanced insights into real-time adsorption of proteins onto hydrophobic surfaces providing information about the viscoelasticity and thickness of the lubricating film indirectly providing information about the frictional phenomenon (Glumac et al., 2019). Therefore, tribology coupled with QCM-D may provide in-depth fundamental understanding of the adsorbed layers of proteins. Such mechanistic knowledge will not only help to understand lubrication properties of proteins, but may provide an opportunity to screen various proteins with better lubrication properties and help in accelerating the design of new ingredient formulations for use in low-fat/high protein food development.

Whey protein isolate (WPI) has been extensively used in literature for fat replacement owing to its neutral taste and the ability to enhance fatty mouthfeel (Guzmán-González et al., 2019) with the ability to reduce friction in tribology by

hydration lubrication (Zembyla et al., 2021) or in the case of microparticulated whey proteins/microgels, a proposed ball-bearing phenomenon (Liu et al., 2016). Protein powders, especially WPI, are also popular in high protein snacks and drinks consumed after exercise or in body building to promote muscle recovery and hypertrophy (Hulmi et al., 2010). With sustainability now at the forefront of product development, requiring lower usage of environmental resources and producing lower emissions, alternative plant- or insect-based proteins are gaining increasing momentum in product development. Alternative proteins although interesting from a sustainability viewpoint often suffer from limited solubility, aggregation, sensorial off taste and unpleasant textural perception, such as sandiness, astringency, dryness *etc.*, which needs attention in literature.

Soy protein has historically been the alternate plant protein of choice (Dabija et al., 2018) because of its ability to increase viscosity and mimic melting properties of fat in various dairy applications (Liu et al., 2018) and in meat replacement (Belloque et al., 2002). Nevertheless, it has often been negatively perceived being an allergen and associated with off-flavours (Damodaran & Arora, 2013). Soy proteins have also shown interesting lubrication ability, with friction coefficients reduced to 0.1 when micro-particulated with further reduction by an order of magnitude when combined with egg white protein (Zhang et al., 2020). Besides soy protein, pea protein has recently gained considerable interests in product formulation since it is hypoallergenic. Recent work by Zembyla et al. (2021) has shown that pea protein has lubrication ability at low concentrations (1–10 mg/mL). However, pea protein tends to aggregate at higher concentrations (>100 mg/mL) and such transition from dissolved polymer-to aggregated particle-like behaviour results in lubrication failure. In contrast, whey protein shows increased lubrication at higher concentrations. With the ever expanding research

of food proteins, their diversity, application and sourcing, new commercially available proteins are appearing every year. Promising proteins include tolerably grown legumes like lupin protein and vegetable waste protein such as potato protein. Furthermore with the growing importance of efficient protein yields, although currently limited by food-neophobia, even insects are being made into protein powders, in all of which, lubrication and adsorption properties have never been investigated, which can help in designing products with optimized mouthfeel.

To summarise, tribological, adsorption and rheological analyses of alternative plant and insect proteins are essential to give a useful reference on how these proteins could be used to replace whey proteins. Hence, the objective of this study was to systematically characterise the lubrication and physiochemical properties of alternative proteins using whey protein as a control, at various protein concentrations. Vegetable protein (potato protein isolate), legumin-rich proteins (pea protein concentrate, lupin protein isolate) and insect protein concentrate (*Alphitobius diaperinus*) were selected to cover a broad range of sustainable alternative proteins. Insolubility is known to increase friction and so only soluble fractions were characterise to observe lubrication behaviour. Overall these solutions were characterised in their material properties for the first time utilising tribology, rheology, electrophoresis, dynamic light scattering and adsorption techniques using quartz crystal microbalance with dissipation (QCM-D). Pearson's correlation was employed to correlate frictional data and other measured instrumental parameters. The fundamental insights generated in this work aims to influence future product development with alternative proteins focussing on bulk and surface properties.

3.2 Materials and methods

3.2.1 Materials

Whey protein isolate (WPI) was obtained from Fonterra (Auckland, New Zealand) containing ≥ 96% protein. Pea protein concentrate (PPC, Nutralys S85 XF) containing 85% protein was kindly gifted by Roquette (Lestrem, France). Potato protein isolate (PoPI) was purchased from Guzmán Gastronomía (Barcelona, Spain) containing 91% protein. Insect protein concentrate (IPC, *Alphitobius diaperinus*) with a protein content of 58% was kindly donated by Protifarm (Ermelo, The Netherlands). Lupin protein isolate (LPI) containing 91% protein was purchased from Prolupin GmbH (Grimmen, Germany). Sodium dodecyl sulphate polyacrylamide gel electrophoresis (SDS-PAGE) reagents including Bolt™ 4–12% Bis-Tris Plus gels, 20 × Bolt™ sodium dodecyl sulphate (SDS) running buffer, 4 × Bolt™ lithium dodecyl sulphate (LDS) sample buffer and PageRuler™ Plus Pre-stained protein ladder were purchased from Thermo Fisher Scientific (Loughborough, UK). All solutions were prepared from analytical grade chemicals unless otherwise mentioned. The solvent used was Milli-Q water (purified using Milli-Q apparatus, Millipore Corp., Bedford, MA, USA).

3.2.2 Preparation of protein samples

Aqueous solutions of the proteins *i.e.* WPI, LPI, PoPI, PPC and IPC (1–10 wt% protein) were prepared by dispersing and mixing the protein powders in 20 mM HEPES (4-(2-hydroxyethyl)-1-piperazineethanesulfonic acid) buffer at pH 7.0 for 2 h. These aqueous dispersions were then centrifuged at 20, 000 *g* for 30 min and the supernatant was used as the soluble fraction with subscript ‘sol’ for further characterisation (see Table 1 for nomenclature). Note that soluble protein concentrations were used to prepare 1-10 wt% protein by considering raw protein content in the powder and the %solubility measured which is discussed later. Due to the low solubility for PPC and inability to mix at high concentrations, the

centrifuged supernatant was extracted, freeze dried and then the soluble PPC powder was used to make protein solution of 10 wt% using 20 mM HEPES buffer at pH 7.0, which was further diluted to 1 or 5 wt%.

Table 3. Physicochemical characteristics of centrifuged and filtered protein solutions at pH 7.0. Error bars indicate standard deviation for triplicate samples (n = 3 × 3 for solubility, $d_{H,}$ PDI and 5 × 3 for ζ-potential). Parameters denoted with the same lower case subscripts do not differ statistically at the confidence of $p \geq 0.05$.

Soluble fractions of protein samples	Nomenclature	Isoelectric point (pI)	Solubility	Hydrodynamic diameter (d_H) (nm)	Polydispersity index (PDI)	ζ-potential (mV)
Whey protein isolate	WPI_{sol}	5.2[a] (Weinbreck et al., 2003)	100% ± 4.6%^{d}	220.0 ± 30.9^{d}	0.35 ± 0.12^{bc}	-18.5 ± 0.9^{a}
Potato protein isolate	$PoPI_{sol}$	4.5 – 5.0 (Schmidt, et al., 2019)	100% ± 1.0%^{d}	24.7 ± 1.0^{a}	0.7 ± 0.35^{c}	-22.4 ± 1.1^{bc}
Pea protein concentrate	PPC_{sol}	4.0 (Adal, et al., 2017)	32% ± 4.5%^{a}	244 ± 23.6^{d}	0.4 ± 0.005^{bc}	-20.6 ± 1.3^{ab}
Lupin protein isolate	LPI_{sol}	4.5 (Jayasena, et al., 2011)	75% ± 4.0%^{b}	116.0 ± 4.8^{b}	0.3 ± 0.003^{b}	-23.0 ± 0.5^{c}
Insect protein concentrate	IPC_{sol}	4.0 – 4.5 (Bußler et al., 2016; Lacroix et al., 2019)	88% ± 7.8%^{c}	160 ± 3.7^{c}	0.2 ± 0.04^{a}	-20.7 ± 0.9^{b}

[a] Isoelectric point of β-lactoglobulin.

3.2.3 Protein solubility

The solubility of proteins was estimated following Bio-Rad *DC* Protein assay using Coomassie blue at an absorbance of 750 nm. A calibration curve was

created using bovine serum albumin (BSA) at 0.2–1.2 mg/mL concentrations and the solubility of each protein was determined as a percentage of protein remaining in supernatant compared to the non-centrifuged initial sample.

3.2.4 Particle size

Protein solutions were diluted to 0.1 wt% and filtered using a 0.22 μm syringe filter (PTFE Syringe filters, PerkinElmer, USA) for particle size measurement using dynamic light scattering (DLS) experiments. The mean hydrodynamic diameters (d_H) of the proteins were measured using a Zetasizer Ultra, Malvern Instruments Ltd, Worcestershire, UK. The samples in DTS0012 disposable cuvettes (PMMA, Brand Gmbh, Wertheim, Germany) were introduced in the Zetasizer. The refractive index (RI) of the protein solution was set at 1.5 with an absorption of 0.001. The viscosity of water i.e. 1 mPa s was used and the samples were equilibrated for 120 s at 25 °C, which were then analysed using backscattering technology at a detection angle of 173° in triplicate.

3.2.5 Sodium dodecyl sulphate polyacrylamide gel electrophoresis (SDS-PAGE)

Each of the protein solutions (32.5 μL) at a concentration of 1 mg/mL were added to 5.0 μL of pre-prepared solution containing 0.078 g of Dithiothreitol (DTT) in 1 mL of Milli-Q and 12.5 μL of Bolt™ LDS sample buffer. The solution was heated at 95 °C for 5 min and 10 μL of the sample + buffer mixture was loaded onto the precast gels placed on an In-vitrogen™ Mini Gel Tank system (Thermo Fisher Scientific, Loughborough, UK) submerged in a solution of running buffer: Milli-Q (1:20 v/v). Protein molecular weight marker (5 μL) was added in the first lane of the gels. After running the gel at 200 V for 22 min, the gel was fixed using Milli-Q: Methanol: Acetic acid (5:4:1 v/v) solution for 1 h and stained for 2 h with Coomassie Brilliant Blue R-250 solution in 20 vol% isopropanol. The gels were

destained overnight in Milli-Q water and scanned using a ChemiDoc™ XRS + System with image LabTM Software (Bio-Rad Laboratories, Richmond, CA, USA). The intensities of the protein bands were quantified using Image Lab Software Version 6.0.

3.2.6 ζ-potential

The electrophoretic mobilities of the protein samples were measured in the Malvern Zetasizer Ultra, Malvern instruments Ltd, Worcestershire, UK at 25 °C. Diluted samples (0.01 wt% protein) were prepared and measured in a DTS1070 folded capillary electrophoresis cells. The electrophoretic mobility was determined considering the dielectric constant (ε) of the medium, the viscosity of HEPES buffer which is equivalent to water (1 mPa.s) and Henry's function ($F(k_a)$) using the Smoluchowski approximation, which was taken as 1.5.

3.2.7 Apparent viscosity

Flow curves of protein solutions (10 wt% soluble protein) were recorded at 37 °C using a stress-controlled rheometer (Paar Physica MCR 302, Anton Paar, Austria) equipped with a concentric cylinder geometry (inner diameter of the cup is 24.5 mm and diameter of the bob is 23 mm). Shear rates from 1 s^{-1} to 1000 s^{-1} were measured and a minimum of three replicates were measured for each protein sample.

3.2.8 Tribology

The friction coefficient (μ) was obtained using a tribology-cell attachment to the rheometer *i.e.* a glass ball (R = 7.35 mm) on three polydimethylsiloxane (PDMS) pins (6 mm pin height), latter inclined at 45° to the base. Samples were added in an enclosed chamber with an applied glass ball on top of PDMS plates with samples covering all of the PDMS pins with an evenly distributed 2 N load. The

sliding speeds were measured upwards and varied from 0.001 to 1 m/s whilst the plates remained stationary generating three-sliding point contact. All measurements were performed at 37 °C with the μ of the HEPES buffer measured as a control.

Normal force is related to the total normal load acting on the plates as described in equation (1). Furthermore, the torque sensed by the glass ball is related to total frictional force (FF) denoted by equation (3.1, 3.2).

$$\boldsymbol{F_L = \sqrt{2F_N}} \tag{3.1}$$

$$\boldsymbol{F_F = \frac{\sqrt{2T}}{R}} \tag{3.2}$$

Therefore, μ can be expressed as:

$$\boldsymbol{\mu = \frac{F_F}{F_N} = \frac{T}{F_N R}} \tag{3.3}$$

The PDMS pins were cleaned using ethanol with subsequent ultra-sonication in detergent solution for 10 min. Careful attention was given to signs of surface wear before each experiment, which subsequently followed replacement. A minimum of three replicates were measured for each protein sample whereby a running in period of 30 seconds was performed before measuring the first friction measurements.

3.2.9 Quartz crystal microbalance with dissipation (QCM-D)

For QCM-D experiments, PDMS-coated quartz sensors were prepared by spin-coating silica sensors (QSX-303, Q-Sense, Biolin Scientific, Sweden) with a solution of 0.5 wt% PDMS in toluene at 5000 rpm for 30 s with an acceleration of 2500 rpm/s, before leaving overnight in a vacuum oven at 80 °C (for details, see Zembyla et al., 2021). Prior to use, the PDMS-coated crystals were further cleaned by immersing in toluene for 1 min, then 1 min in isopropanol and a final immersion in Milli-Q for 5 min before being dried using nitrogen gas.

Adsorption of protein on PDMS-coated sensors was measured using quartz crystal microbalance with dissipation monitoring (QCM-D, E4 system, Q-Sense, Biolin Scientific, Sweden) (Xu et al., 2020a). Protein solutions were made at a concentration of 1 wt% and were equilibrated in buffer at (25 °C) before measurement. The flow rate was controlled using peristaltic pump at a rate of 100 µL/min at 25 °C. For initial measurements, buffer solution was initially injected to obtain a stable baseline reading and then the prepared protein solutions were injected until equilibrium adsorption *i.e.* no change in frequency (*f*) or dissipation (*D*) was recorded. Finally, the buffer was used once more to remove the non-adsorbed protein. Hydrated mass was calculated from the frequency data using viscoelastic Voigt's model (Voigt, 1889), using “Smartfit Model” by Dfind (Q-Sense, Biolin Scientific, Sweden) software. The 3rd, 5th, 7th and 11th overtones was taken into account for data analysis and only 5th overtone is shown in the results. A minimum of three replicates were measured for each protein sample.

3.2.10 Statistical analysis

All results are reported as means and standard deviations on at least three repeats. Statistical analysis on the significance between data sets was calculated using analysis of variance (ANOVA) with Tukey post hoc test. Pearson's

correlation (r) were used to assess relationships between hydrodynamic diameter, hydrated mass, ratio of dissipation to frequency ($-\Delta D/\Delta f$) and coefficient of friction scaled at high shear rate viscosity ($U\eta_{\infty}$) in the boundary (at 0.01 Pa m), mixed (at 0.1 Pa m and 0.3 Pa m) and hydrodynamic regimes (at 1.0 Pa m) at 10 wt% protein. Only alternative proteins were included in the Pearson's correlation analyses. Statistical significance of Pearson's correlation was also conducted using Spearman's rank to obtain the *p-values*. All statistical analyses were done using R version 3.5 (R Core Team, 2018, p. 2012).

3.3 Results and discussion

3.3.1 Protein solubility and composition

Plant proteins are well known to encounter solubility problems even though pH can typically be far from pI (Zhang et al., 2020). This insolubility can arise due to complex quaternary structures, processing, a strong tendency to self-aggregate and association with other metabolites such as polyphenols in the natural state (Sarkar & Dickinson, 2020). Hence in this study, we first investigated the solubility of the alternative proteins at pH 7.0 and used the supernatant after centrifugation *i.e.* the soluble-fraction of the protein solutions for further creating different concentrations of proteins (1–10 wt%) for further characterisation.

As shown in Table 3, previous studies have reported similar pI for all protein (pH 4–5.2) and in our results found protein solubility spanned from 32% to 100%, the lowest soluble fractions being PPC and the highest being WPI and PoPI. Simply by observing the changes in the turbidity of the protein solutions, one can predict their solubility. Visual images in **Figure 3.1** reveal that WPI is highly translucent, in other words soluble, this was also true for PoPI, latter has a slight amber hue owing to the presence of brown aromatic compounds (Akyol et al., 2016). This excellent solubility of PoPI has been reported previously with

protein subunits, such as patatins and protease inhibitors showing solubility of >95% and ~85%, respectively (Ralet et al., 2000). On the other hand, IPC shows somewhat unusual behaviour in that even after centrifugation, the supernatant remained as a somewhat cloudy dispersion but with a relatively high degree of solubility of 88%. This turbidity in IPC might have been due to the presence of some protein nanoaggregates that could not be removed by centrifugation. LPI had a solubility of 75% and initially demonstrated a cloudy appearance which may have been a result of the large proportion of low Mw proteins. These small proteins which were not centrifuged out may be responsible for the slight turbidity of the soluble protein fraction along with the slight yellow colouration which is likely due to carotenoid-induced pigmentation (Wang et al., 2008, pp. 198–202).

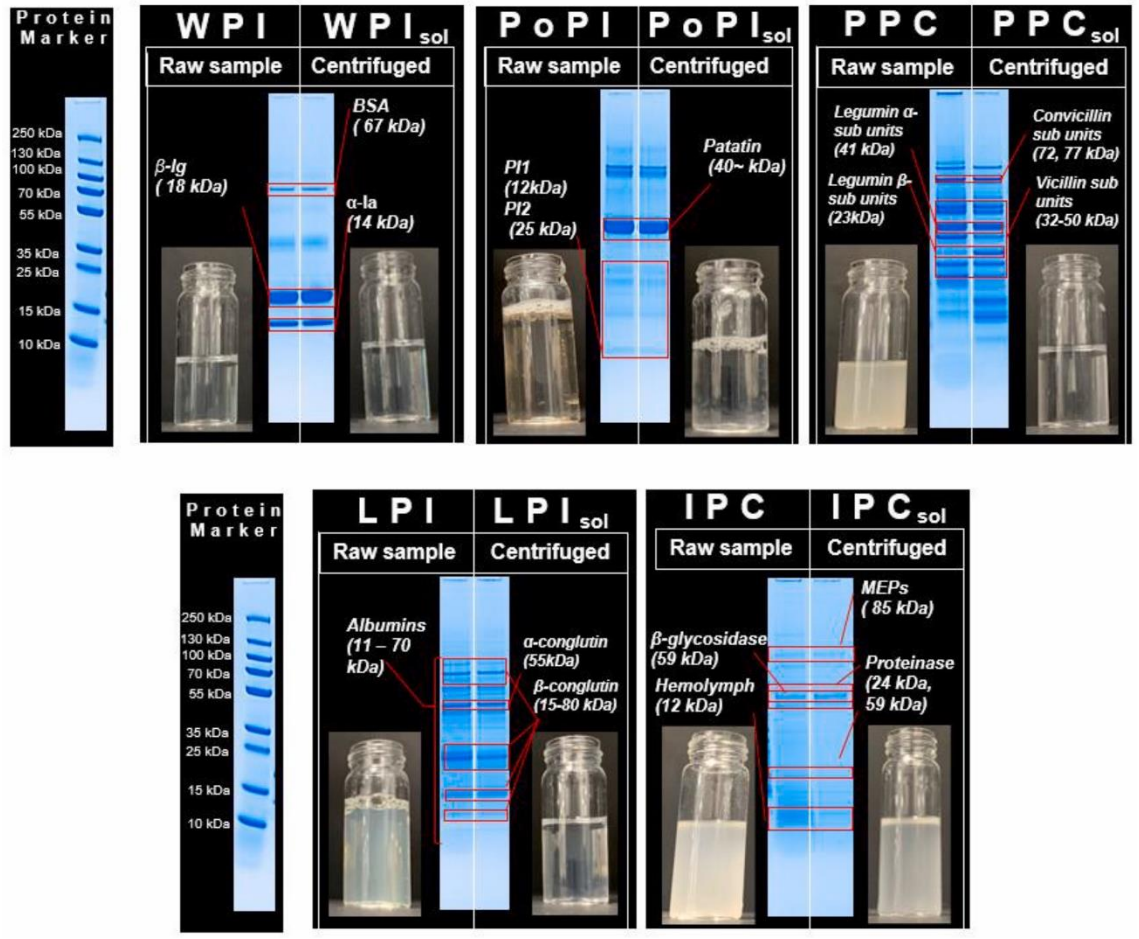

Figure 3.1 Sodium dodecyl sulphate polyacrylamide gel electrophoresis (SDS-PAGE) of protein solutions and their % solubility at pH 7.0. Protein fractions are as follows, beta-

lactoglobulin (*β*-lg), bovine serum albumin (BSA), alpha-lactalbumin (*α*-la), protease inhibitor 1 and 2 (PI1, PI2), melanization engaging proteins (MEPs).

PPC shows the most notable change, from highly cloudy to nearly colourless in appearance as a large fraction of insoluble protein was precipitated out upon centrifugation, which confirms the lowest solubility of 32% of the original concentrate (**Figure 3.1**). Solubility of around 30% has also been observed in a range of pea protein types in previous studies (Chao et al., 2018; Lam et al., 2018).

To understand whether centrifugation removes any particular subunits of proteins, protein composition of the raw samples and the soluble protein fraction *i.e.* supernatant collected after centrifugation was characterised using SDS-PAGE (**Figure 3.1**, see Appendix Figure B1 for the original electrophoresis gels). As expected the centrifugation step did not influence the protein composition of WPI. In both the un-centrifuged and centrifuged fractions, three main bands were visible in the SDS-PAGE of WPI (**Figure 3.1**) reflecting *β*-lactoglobulin (*β*-lg) (18 kDa), which is the most abundant protein typically present at 50–60%, *α*-lactalbumin (*α*-la) (14 kDa) at ~15% and bovine serum albumin (BSA) (67 kDa) at ~5–10%. These constituent protein fractions of WPI are extensively evidenced in literature (Adal et al., 2017; Chihi et al., 2016; Edwards & Jameson, 2014; Kilara & Vaghela, 2004).

In case of PoPI, the proteins segmented into three main groups (**Figure 3.1**)). Patatins (~40 kDa), which are glycoproteins and act as protein storage, made up just under half the proteins of the PoPI existing naturally as 88 kDa dimers (Ralet et al., 2000), followed by the lowest molecular weight (MW) bands making up the protease inhibitors (4–25 kDa) and finally enzymes such as lipoxygenases that are present as faint bands. SDS-PAGE reveals the

distinctions very well similar to other studies (Schmidt et al., 2019; Waglay, Achouri, Karboune, Zareifard, & L'Hocine, 2019) with little to no changes in protein after centrifugation, which is concurrent with the solubility data of PoPI (**Figure 3.1**).

In case of PPC, SDS-PAGE reveals the three globulin proteins, vicilin (7 S, 32–50 kDa), legumin (11 S, 23, 41 kDa) and convicilin (72, 77 kDa) (**Figure 3.1**), which is in agreement with previous reports (Adal et al., 2017; Lam et al., 2018; Oliete Bonastre, 2018). In the PPC supernatant, there was an increase in vicilin and low MW fractions (10–25 kDa) with subsequent loss of ~100 kDa proteins as compared to the un-centrifuged sample. It should be noted the ratio of 11 S:7 S composition in pea can vary from 0.2 to 2.0 depending upon the environmental conditions (Lam et al., 2018) and may present physicochemical differences that need further investigation.

LPI displayed multiple bands with centrifugation having a negligible effect on the intensity levels of the bands (**Figure 3.1**). Lupin proteins are made up of two main groups, the albumins (11–70 kDa) and the conglutins, latter being the main storage protein for lupin. As seen in the electrogram, conglutins comprised of *α*-conglutins (11 S, 55 kDa) and *β*-conglutins (7 S, 15–80 kDa), which accounts for approximately 33% and 45% of the total protein (Nadal, Canela, Katakis, & O'Sullivan, 2011).

The IPC displayed a rather complex mixture of faint bands in comparison to the other proteins, which might suggest that the protein bands were not effectively separated in the resolving gel (**Figure 3.1**)). There was a small loss in ~10 kDa and ~130 kDa fractions in the supernatant corroborating the solubility data of IPC. The band observed most likely corresponds to the skeletal muscle proteins, which include four main protein fractions, haemolymph (12 kDa),

proteinases (24 kDa, 59 kDa), melanization-engaging proteins (85 kDa) and *β*-glycosidase (59 kDa) (Lacroix et al., 2019; Yi et al., 2013). In summary, PPC showed the largest influence of centrifugation on solubility and composition of the proteins followed by IPC with WPI, PoPI and LPI showing negligible influence. Hereafter, only soluble fractions of proteins have been used for characterisation of physicochemical properties, tribology and adsorption properties with these soluble fractions of protein being named as WPI_{sol}, PPC_{sol}, $PoPI_{sol}$, IPC_{sol} and LPI_{sol}.

3.3.2 Physicochemical properties of the soluble protein fractions

Hydrodynamic diameter (d_H) of the protein solutions was measured using DLS. All the proteins showed certain degree of aggregation with d_H ranging from 25 nm to 244 nm, with $PoPI_{sol}$ and PPC_{sol} representing the lowest and highest d_H, respectively (**Table 3**). Often smaller d_H can be associated with higher degree of solubility and lower levels of turbidity. However, this is not that clear with one of the largest (WPI_{sol}) and smallest d_H sized protein ($PoPI_{sol}$) both having 100% solubility (**Figure 2.5**). For WPI_{sol}, the mean d_H was averaged out of three size distribution peaks at 5 nm, 300 nm and a peak in the order of few thousands of nanometres (**Figure 3.2**), which is reflected in its polydispersity index (PDI) (**Table 3**). A high proportion of WPI is *β*-lg, which might correspond to the 5 nm sized peak (Chihi et al., 2016) and observed as the lowest band in the SDS-PAGE (**Figure 3.1**). Multiple peaks in DLS of WPI have been also observed previously in studies where these distributions have ranged in sizes from 144 to 3000 nm (Nishanthi et al., 2017; Sats et al., 2014) showing high degree of aggregation (Bouaouina, Desrumaux, Loisel, & Legrand, 2006). On the other hand, $PoPI_{sol}$ has the lowest reported d_H (**Table 3**), which may be due to high levels of phenol that promote protein-polyphenol interactions rather than protein-protein

aggregation (Ralet et al., 2000). Also similar to WPI_{sol}, many size distribution peaks ranging from 5 nm to a few hundreds of nanometres are seen in the DLS graph (**Figure 3.2**) for $PoPI_{sol}$, with highest PDI (0.7) among all the proteins studied (**Table 3**). This might be attributed to a range of low Mw sub units that were aggregated/non-aggregated as can be observed from the SDS-PAGE (**Figure 3.1**).

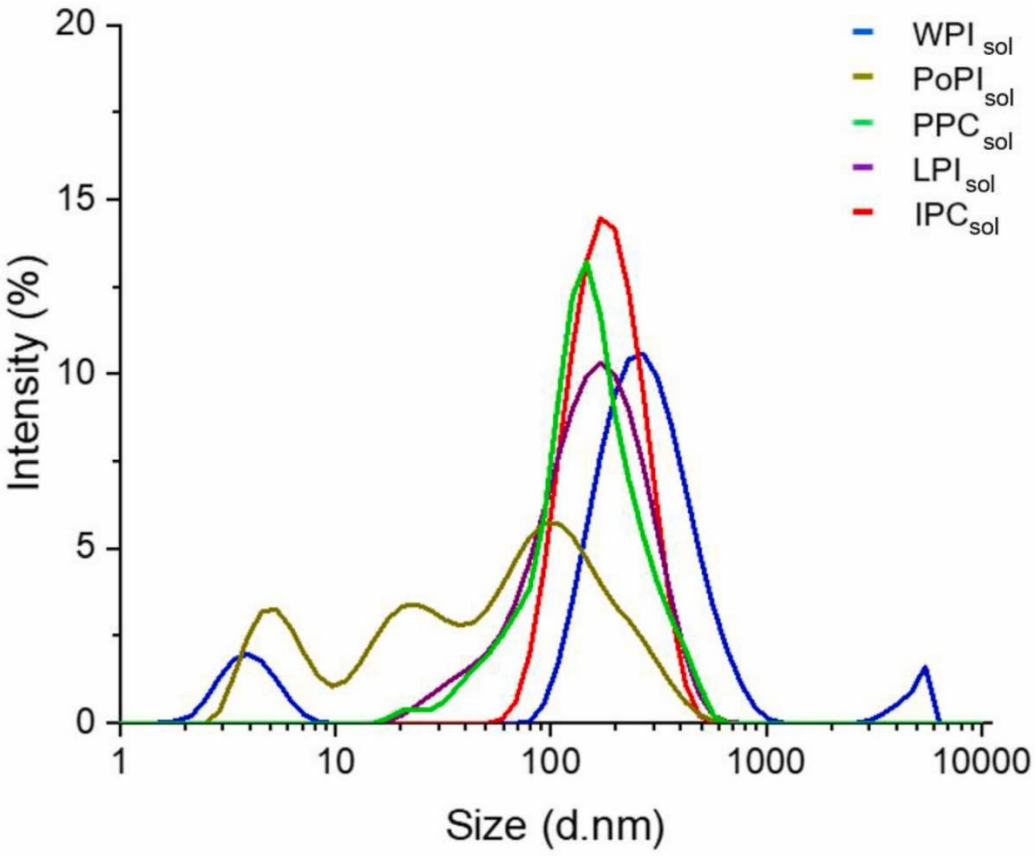

Figure 3.2 Particle size distribution of protein samples (0.1 wt% protein) at pH 7.0 after centrifugation and filtration using 0.22 µm syringe filter (n = 3 × 3).

The d_H of 244 nm was recorded for PPC_{sol} (Table 3) with a single peak on the DLS graph shown in **Figure 3.2**, this is in agreement with previous study by Adal et al. (2017). Small angle X-ray scattering (SAXS) studies have demonstrated that the radius of individual legumin and vicilin are 4.45 and 4.40 nm, respectively. These individual nanometric-sized proteins form the larger secondary aggregate structures as shown in our study (Table 3) and is in

agreement with previous reports on size obtained using transmission electron micrographs (TEM) (Oliete et al., 2019) with secondary aggregation ranging from 100 to 1000 nm. Nevertheless, it is worth noting that in the previous study (Oliete et al., 2019), PPC was prepared in the lab from flour different to our commercially available PPC, it is likely the processing involving conversion of pea to pea protein powder might have induced different mechanical and thermal processing as compared to our study, increasing protein interaction thus aggregation in the former. Interestingly, $PPC_{sol,}$ LPI_{sol} and IPC_{sol} had single peaks in DLS (**Figure 3.2**). However, the mean d_H of >100 nm (Table 3) in all three suggests that there were protein aggregates rather than monomeric proteins, but the protein-protein aggregates in LPI_{sol} and IPC_{sol} were relatively smaller and evenly sized as compared to WPI_{sol}. Noteworthy that comparison of SDS-PAGE (**Figure 3.1**) and DLS peaks (**Figure 3.2**) is not straightforward as all the proteins studied are composed of a large array of a number of proteins/protein sub-units, existing naturally as complex aggregates.

All proteins studied had isoelectric points ranging from pH 4.0–5.2 as shown in Table 1 (Adal et al., 2017; Buβler et al., 2016; Guimarães & Gasparetto, 2005; Jayasena et l., 2011; Lacroix et al., 2019; Schmidt et al., 2019; Weinbreck, de Vries, Schrooyen, & de Kruif, 2003). Therefore, at pH 7.0, it is not surprising that all the proteins studied here displayed negative ζ-potential values ranging from −18.5 to −23.0 mV, and thus the electrostatic repulsion enabled stable protein dispersions in each case as shown in **Figure 3.1** in the soluble protein fractions.

3.3.3 Tribology

To understand the tribological behaviour, we measured the friction coefficients of glass-PDMS tribopairs in the presence of soluble proteins at various

concentrations (1–10 wt%) to understand the difference between the types of proteins as well as to identify the role of protein concentration dependence on frictional parameters (**Figure 3.3**).

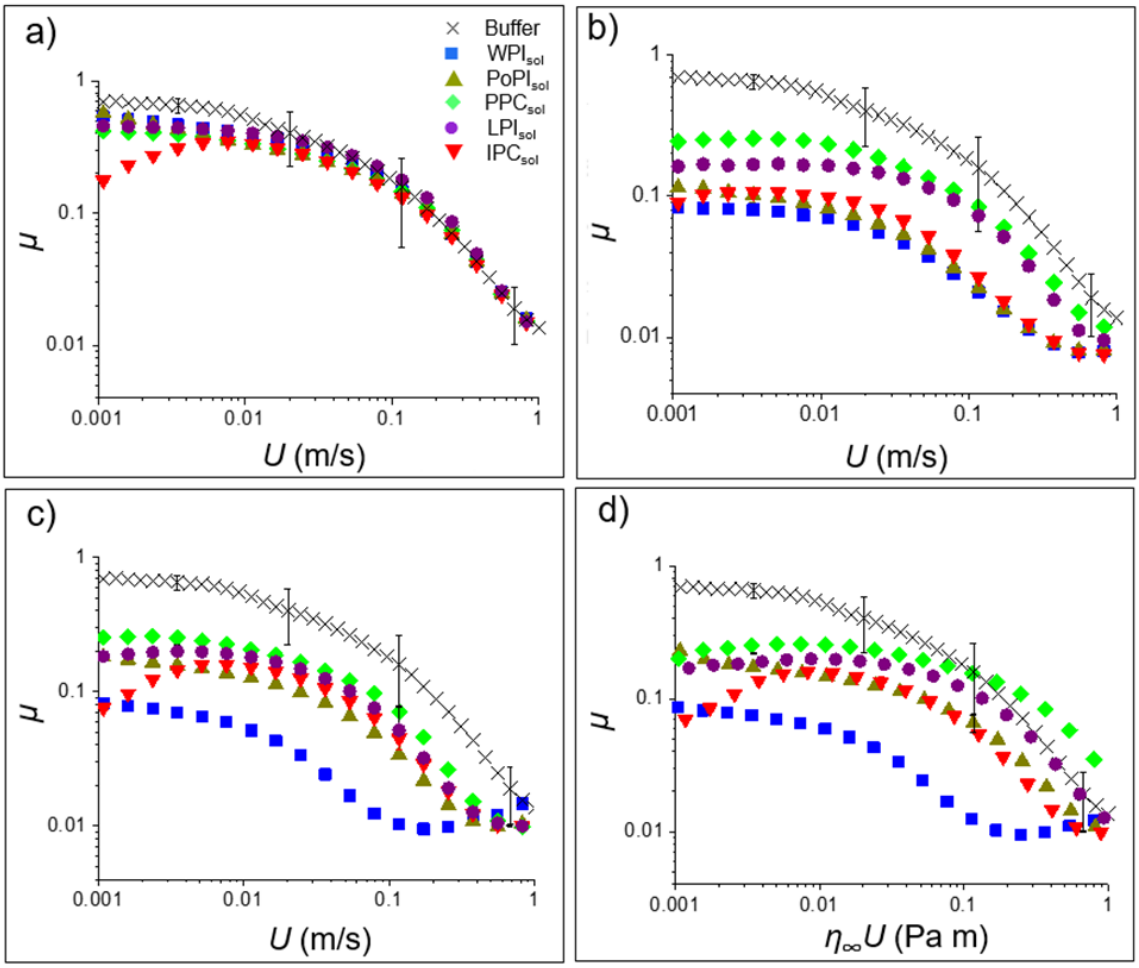

Figure 3.3 Mean friction coefficients (μ) as a function of entrainment speed (U) determined between glass ball and PDMS surface at 2 N load in presence of protein solutions at 1.0 wt% (a), 5.0 wt% (b), and 10 wt% (c) protein, respectively and scaling of friction curves (d) of 10 wt% proteins to high shear rate viscosity (η_∞ = 1000 s^{-1}). Friction curves of HEPES buffer are shown in all the graphs. Error bars indicate standard deviation for triplicate experiments (n = 3 × 3).

Figure 3.3a–d displays that the buffer showed only boundary (U = 0.001–0.01 m/s) and mixed regimes (U = 0.01–0.3 m/s), which is in line with previous report (**Sarkar et al.,** 2017). However, the onset of mixed regime was at one order

of magnitude lower in speed as compared to that of the previous study (U = 0.1 m/s) (Sarkar et al., 2017). One might expect this discrepancy owing to the hydrophilic-hydrophobic contact (glass-PDMS) used in this study allowing easy entrainment of the buffer to enable the onset of mixed lubrication regime as opposed to being squeezed out of the contact in the case of the hydrophobic-hydrophobic contact (PDMS-PDMS) used in the previous study (Sarkar et al., 2017).

All the proteins showed a decrease in friction coefficient with an increase in entrainment speed, with protein solutions gradually transferring from the boundary to the mixed lubrication regimes separating the tribopair surfaces. Firstly focussing on low concentration levels (1 wt%) (**Figure 3.3a**, see Appendix B Table B1a for statistical significance), $PoPI_{sol}$, PPC_{sol}, IPC_{sol} show significant decrease in boundary friction compared to the buffer (~35% decrease, $p < 0.05$) with WPI_{sol} and LPI_{sol} showing some decrease but of non-significance compared to the buffer. Upon entering the mixed regime – U_{max} all solutions showed similar friction with no significant differences observed with buffer. Although significantly different verses buffer $PoPI_{sol}$, PPC_{sol}, IPC_{sol} friction remains high at 0.35–0.40 reflecting little surface separation between glass ball and PDMS contact thus insufficient protein for good lubricating properties. It is interesting to note IPC_{sol} at very low entrainment speeds (0.001–0.01 m/s) recorded much lower friction. Although, at this point, it is just a speculation, this behaviour of IPC_{sol} might be associated with some stabilization issue and not necessarily boundary lubrication.

At 5 wt% protein concentration (**Figure 3.3b**), all proteins exhibited lubrication ability with distinct reduction in friction coefficients irrespective of the lubrication regimes in comparison to the buffer. This is due to a substantial level

of protein that is able to form a hydration layer separating the contact surfaces and allowing for increased mobility for the sliding contacts. Interestingly, the most soluble proteins (WPI_{sol}, $PoPI_{sol}$ and IPC_{sol}) showed similar friction coefficient decreases by an order of magnitude in both the boundary ($\mu_{0.01}$) and mixed regimes ($\mu_{0.3}$) as compared to the buffer in equivalent regimes. Both the legumin-rich proteins *i.e.* PPC_{sol} and LPI_{sol} which displayed lower solubility showed similar trends being more lubricating than the buffer but less as compared to WPI_{sol}, $PoPI_{sol}$ and IPC_{sol} ($p < 0.05$) (see Appendix B Table B1b for statistical significance). Solubility may be important for tribology in terms of the ability to bind water and form a lubricating layer upon entrainment.

At the highest concentration used in this study (10 wt%) (**Figure 3.3**c), protein entrained between contact can be expected to be the maximum, leading to enhancement in lubricity effectiveness, which has been seen in a number of protein-based tribology studies (**Liu et al.,** 2016; Zhang, Guo, et al., 2020). In general from most to least lubricating protein followed pattern of $WPI_{sol} > PoPI_{sol} > IPC_{sol} > LPI_{sol} > PPC_{sol}$ ($p < 0.01$). An interesting feature was that WPI_{sol} showed an onset of hydrodynamic regime unlike the alternative proteins (**Figure 3.3c**). WPI_{sol} also retained extensive lubrication property at higher concentrations of 10 wt% (**Figure 3.3**c) with a further decrease in friction coefficient as compared to 5 wt% concentration levels (**Figure 3.3**b) in complete contrast to the other proteins (see Appendix B Table B1c for statistical significance). For instance, $PoPI_{sol}$ had one of the lowest friction coefficients in the boundary regime and showed decrease in boundary friction coefficients by 75% when concentration was raised from 1 to 5 wt% concentration (**Figure 3.3**a–b), however $PoPI_{sol}$ suffered from a substantial increase of friction coefficient (~50%) when concentration was raised from 5 to 10 wt% (**Figure 3.3**b–c). Similar

percentage decreases and increases in friction coefficients were also observed for $PoPI_{sol}$ in the mixed regime from 1 to 5 wt % (**Figure 3.3**a–b) and evidently higher when concentration was raised from 5 wt% to 10 wt% (**Figure 3.3b–c**). The latter behaviour was also found for IPC_{sol}, where the boundary friction coefficient shows a decrease when concentration was raised from 1 to 5 wt% ($\mu_{0.01}$ = 0.34 and 0.10) in **Figure 3.3a** and **b**, respectively following an increase of friction at 10 wt% ($\mu_{0.01}$ = 0.15, see **Figure 3.3c**). LPI_{sol} was also similar in pattern but with only a marginal increase in boundary friction at 10 wt%.

PPC_{sol} at 5 wt% and 10 wt% was the least lubricating protein when compared to all proteins at boundary (0.01 m/s) and mixed regimes (0.1 m/s) and in some speeds even showed overlapping friction to buffer (see Appendix B Table B1b and B1c for statistical significance). Even still, at boundary regime a 30% reduction in friction was produced by increasing the concentration from 1 wt% ($\mu_{0.01}$ = 0.33) (**Figure 3.3a**) to 5 wt% ($\mu_{0.01}$ = 0.23) (**Figure 3.3b**), with little further reduction in boundary friction when the concentration was raised to 10 wt% ($\mu_{0.01}$ = 0.21) (**Figure 3.3c**), in line with previous report using different tribopairs (Zembyla et al., 2021). Similar levels of reduction in PPC_{sol} was also seen for the mixed regime between 1 and 5 wt% ($\mu_{0.1}$ = 0.16 and 0.1) (**Figure 3.3a** and **b**) with a slight decrease in 10 wt% concentration ($\mu_{0.1}$ = 0.08) (**Figure 3.3c**).

In summary (see schematic in **Figure 3.4**), whey protein shows a concentration dependent lubrication performance with lower concentration of WPI acting as a poor lubricant (1 wt%) and higher concentration (10 wt%) resulting in lower μ. Unlike WPI, until 5 wt% protein concentration, $PoPI_{sol}$ and IPC_{sol} show excellent lubricating properties. However, at higher concentrations (10 wt%), $PoPI_{sol}$ and IPC_{sol} might have undergone protein-protein aggregation

in the contact zone. This most likely creates a particle-like behaviour rather than a continuous polymer-like behaviour, which potentially jams the contact region, resulting in limited sliding and thus leads to increased μ unlike WPI_{sol}. This jamming effect is a relatively new phenomenon, which was firstly observed with higher volume fractions of whey protein microgels (Sarkar et al., 2017) and more recently with pea protein at high concentration (Zembyla et al., 2021).

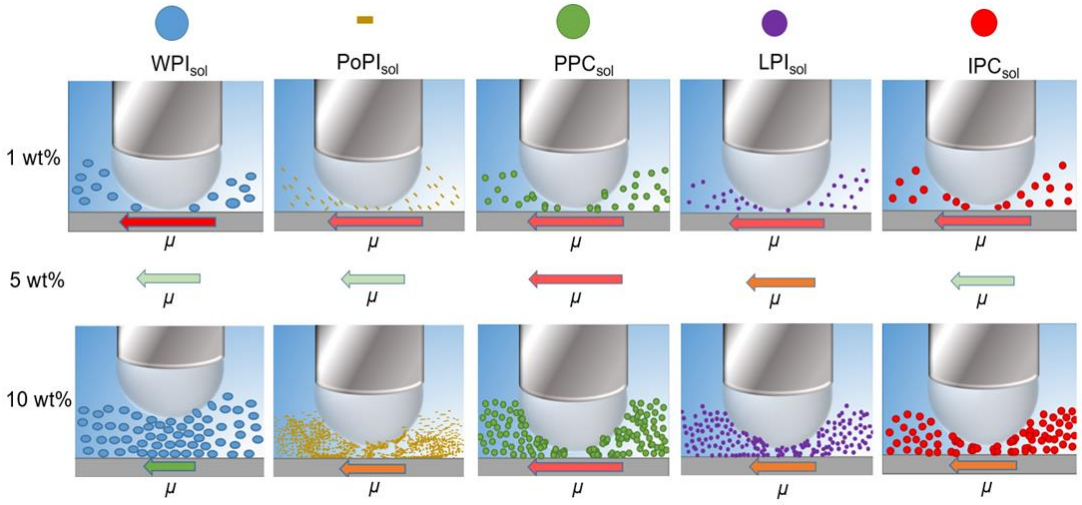

Figure 3.4 Schematic representation (not to scale) of the lubrication behaviour of WPI_{sol} $PoPI_{sol}$ PPC_{sol} LPI_{sol} and IPC_{sol} on glass ball on PDMS surface illustrating the effect of concentration and protein type on friction coefficient (μ) (depicted as green, orange and red friction arrows showing lowest friction to highest friction induced by proteins, respectively). (For interpretation of the references to colour in this figure legend, the reader is referred to the Web version of this article.)

It should also be noted that better lubricating proteins ($PoPI_{sol}$, WPI_{sol}) also displayed DLS particle size peaks in the range of 1–10 nm (**Figure 3.2**) as opposed to the aggregated proteins of around a few hundred nanometres for PPC_{sol}, LPI_{sol} and IPC_{sol}. One possible explanation is that proteins made up of more aggregates (detected by higher Mw bands in SDS-PAGE, **Figure 3.1**) could result in a *particle-like* rather than *polymer-like* film behaviour. In other words smaller sized protein particles may be better entrained, contributing to improved

lubrication as seen previously (Liu, Stieger, et al., 2016). It should be noted that larger whey protein aggregates have also been reported to enhance lubrication (Chojnicka et al., 2008) therefore discrepancy in literature as well as a difficulty in measuring hydrodynamic size with accuracy in case of alternative proteins due to aggregation suggest that direct correlation of particle size of protein with tribology might not be straightforward, which is discussed later.

Finally, a key aspect of frictional behaviour is the rheological property of lubricant. Particularly, the high shear rate viscosity (η_∞) of the lubricant becomes a highly relevant parameter to understand the frictional behaviour in the mixed and hydrodynamic lubrication regimes (Andablo-Reyes et al., 2019). It is worth noting that elastohydrodynamic lubrication (EHL) theory (de Vicente, Stokes, & Spikes, 2005) confirms that a very high shear rate exists in the tribological regime and even at very low entrainment speeds, shear rates can be well above 1000 s^{-1}. In addition, the entrainment speed is scaled to remove any viscous contributions delaying the onset of boundary lubrication ensuring comparability amongst sample. Appendix B Figure B2 shows the flow curves of all the proteins at 10 wt% concentration level. At shear rates of 1–1000 s^{-1}, the buffer, IPC_{sol}, and LPI_{sol} displayed Newtonian behaviour where viscosity was independent of the shear rate. WPI_{sol}, PPC_{sol} and $PoPI_{sol}$ on the other hand showed shear thinning behaviour, however, they showed plateau region above 10 s^{-1}. The η_∞ at 1000 s^{-1} was used to scale the tribology data (**Figure 3.3d**) to understand the influence of viscosity on frictional behaviour. It can be seen that alternative proteins, $PoPI_{sol}$, LPI_{sol} and IPC_{sol} overlapped with the buffer in the mixed lubrication regime (0.3 m/s) with PPC_{sol} being significantly higher in friction ($p < 0.05$) and WPI_{sol} significantly lower ($p < 0.05$) (Appendix B Table B1d). The boundary lubrication behaviour could not be explained by the viscosity data and

indeed adsorption measurements are crucial to explain those differences in the tribological behaviour, which is discussed in the following section.

.

3.3.4 Surface adsorption characteristics

To understand protein-surface interaction and to explain the tribological features particularly in the boundary regime where adsorption can be an important contributing factor, QCM-D was used to measure the adsorbed hydrated mass and the mechanical properties of the protein films. Since PDMS pins were used in tribological experiments, PDMS-coated crystals in QCM-D replicated the hydrophobic character for the adsorption experiments. Buffer was used to obtain a stable baseline reading, and then protein solutions were applied, all of which resulted in substantial decrease in frequency (f) suggesting that proteins were being adsorbed and formed a viscoelastic layer as supported with an increase in dissipation (D) (**Figure 3.5a**). After the proteins had formed a stable layer (i.e. no further change in f), the buffer was again used to wash the residual protein that was not effectively adsorbed to the surface. In all the cases, the f increased upon the addition of the subsequent buffer, which suggests that a significant proportion of the proteins were loosely attached to the surface, which were then removed by the washing phase (**Figure 3.5a**). Hydrated mass was calculated using Voigt's model as dissipation of the adsorbed proteins increased rapidly as a function of time rendering the Sauerbrey's model invalid.

a)

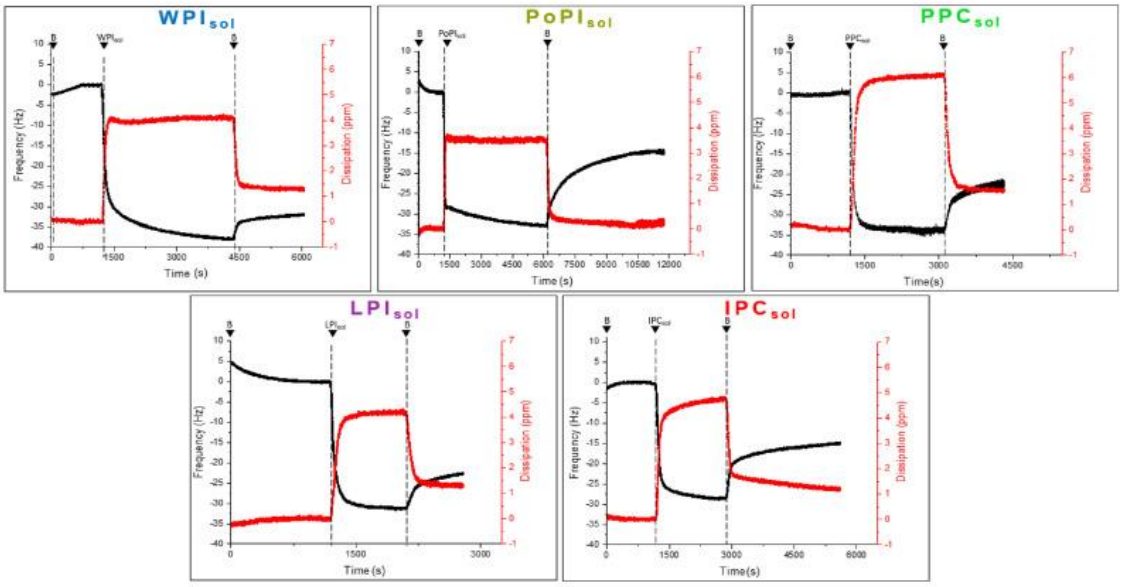

b)

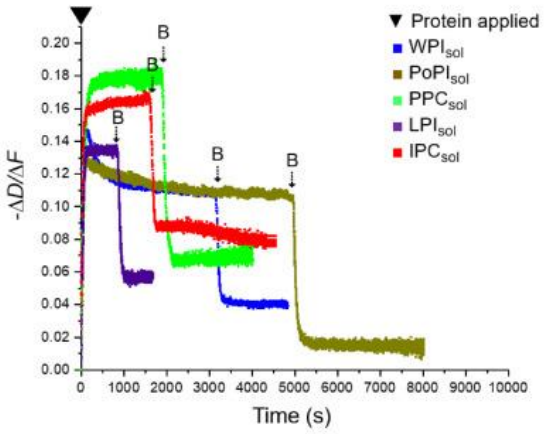

c)

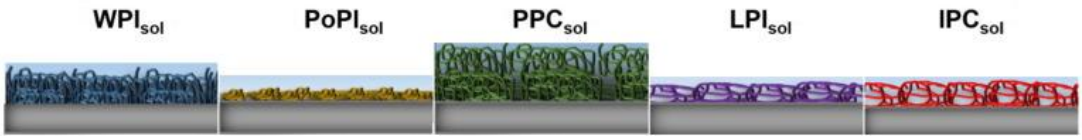

Figure 3.5 Mean frequency and dissipation (5th overtone shown) (a) of 1.0 wt% WPIsol, PoPIsol, PPCsol, LPIsol and IPCsol on PDMS-coated hydrophobic sensors, respectively with B implying the HEPES buffer. Dissipation shift (ΔD)/frequency shift (Δf) ratio i.e. -ΔD/Δf (b) of the protein solutions with step B representing the final buffer rinsing stage to understand the final characteristics of the film. Schematic representation (c) of the hydrated layer of protein films on PDMS surface.

To understand better the viscoelastic property of the protein films, the ratio of dissipation and frequency *i.e. -ΔD/Δf* is shown in **Figure 3.5b** and a schematic illustration is shown in **Figure 3.5c**. This schematic takes into account *-ΔD/Δf* as well as hydrated mass which is discussed later. A higher *–ΔD/Δf* indicates a more viscous and less elastic film, one where time to dissipate energy is increased, whilst a lower *–ΔD/Δf* implies a more rigid quicker dissipating film (Xu et al., 2020). For all proteins, the initial layer formed was a viscoelastic one, *i.e.* a loosely packed hydrated film with *-ΔD/Δf* values ranging from 0.11 to 0.18 (**Figure 3.5b**). However, when washed with buffer, the unabsorbed proteins appeared to be removed with rigidity increasing. Results show that final film viscoelasticity followed the following pattern *i.e.* IPC_{sol} > PPC_{sol} > LPI_{sol} > WPI_{sol} > $PoPI_{sol}$. In other words, $PoPI_{sol}$ and WPI_{sol} formed the most rigid layers as schematically shown in **Figure 3.5c**, which may be due to the size and mobility of the proteins to pack efficiently. The relative rigidity of $PoPI_{sol}$ as compared to other alternative proteins might be attributed to it low d_H (Table 3) and large proportion of single subunit proteins **(Figure 3.1** and **Figure 3.2**) that allowed to form a more ordered, compact and rigid hydrated film on the surface (**Figure 3.5c**). It is also interesting to note that both WPI_{sol} and $PoPI_{sol}$ were the most soluble (Table 3) thus hydrated more uniformly as a continuous film, which promoted higher lubrication (**Figure 3.3b**). Hence, it can be inferred that a rigid continuous layer of hydrated film (**Figure 3.5**) might be beneficial in reducing boundary friction.

On the other hand, with more complex numbers of subunit proteins **(Figure 3.1**) and higher aggregation observed in the case of IPC_{sol} and PPC_{sol} (**Table 3**) a rather unordered viscous layer of protein-protein particles adsorbed with trapped water increasing the *–ΔD/Δf* value (**Figure 3.5b**). In other

words, PPC_{sol} resulted in a film with more viscosity and less rigidity (**Figure 3.5c**) and thus might have been easily depleted from the boundary region under tribological stress resulting in higher boundary μ (**Figure 3.3b**).

Figure 3.6 shows the final hydrated adsorbed mass of the protein. Not surprisingly, PPC_{sol} (11 mg m^{-2}) resulted in significantly higher adsorbed mass as compared to all the remaining proteins, followed by WPI_{sol} (8 mg m^{-2}) with no significant differences being found between $PoPI_{sol}$, LPI_{sol} and IPC_{sol} ($p > 0.05$) representing similar masses of around 5 mg m^{-2}. Reasons as to why PPC_{sol} adsorbs so heavily may be associated with its high degree of aggregation, as discussed previously (Zembyla et al., 2021).

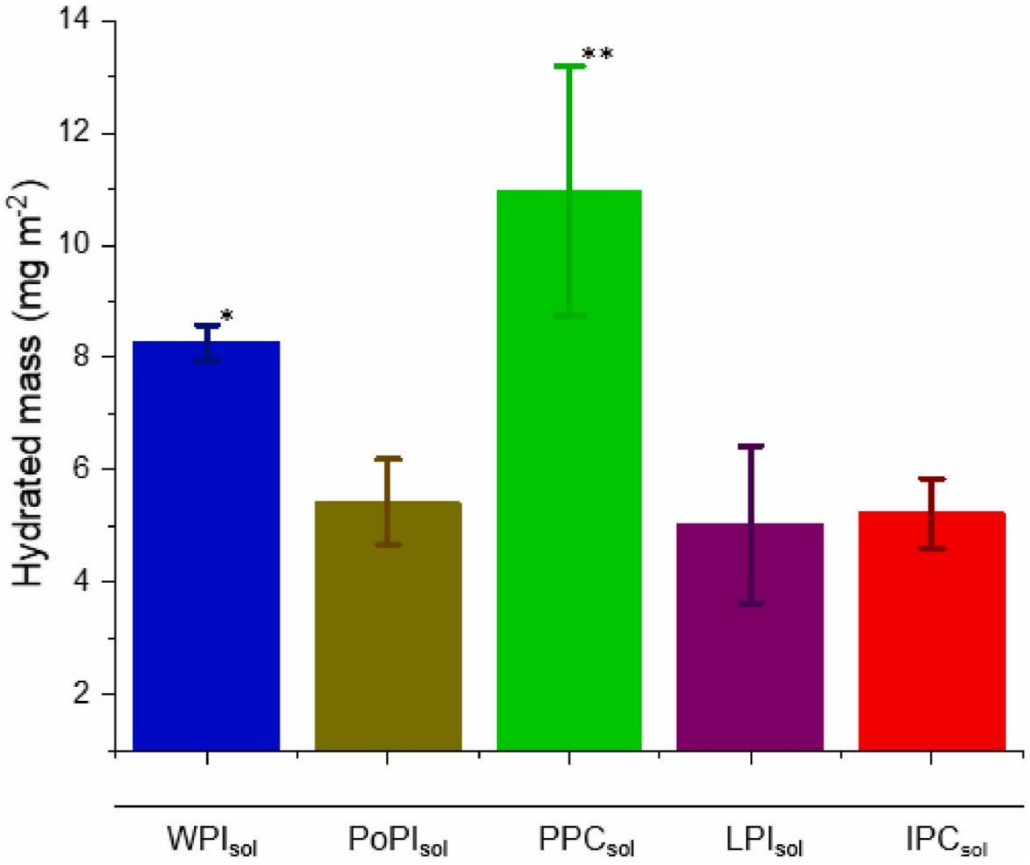

Figure 3.6 Hydrated mass of protein solutions at pH 7.0 (1.0% w/v) on PDMS-coated hydrophobic sensors using QCM-D. Error bars indicate standard deviation for triplicate experiments (n = 3 × 3). The asterisk represents significant difference ($p < 0.05$).

3.4 Correlations between various instrumental characteristics

Correlating frictional properties with physical attributes will help to provide mechanistic insights and thus potentially help fast-tracking desirable proteins/ingredients to act as fat mimetics or replicate the low friction coefficients as found in fats. Therefore, we evaluated the various instrumental data used in this study for alternative proteins with an aim to identify relationships between hydrodynamic diameter, hydrated mass, viscoelasticity (–ΔD/Δf) and μ in different regimes scaled to viscosity and the transition point (Uηmin) i.e. the transition from mixed to hydrodynamic regime where lowest friction coefficient (at μmin) is obtained. Since WPI_{sol} was used as a control in this study and distinctly different in lubrication properties as compared to the alternative proteins, only alternative protein data was used for evaluating the relationships.

Figure 3.7 shows that μ in boundary (Uη0.01), mixed (Uη0.3) and hydrodynamic lubrication (Uη1.0) regimes are strongly positively correlated ($r = 0.96–0.99$, $p < 0.001$) which is unsurprising as onset friction coefficient in the hydrodynamic regime is related to the mixed regime and in turn likely to be influenced from the reduction in friction in the boundary regime. When observing the relationship between hydrodynamic diameter and μ in all regimes, there is a positive correlation of $r = 0.76–0.81$ (**Figure 3.7**), with correlation with μ particularly in the boundary regime being highly significant ($p < 0.01$), to our knowledge this is not reported in literature to date. Increased hydrodynamic size of alternative proteins might result in exclusion of the proteins from the contact zone resulting in increased μ in the boundary regime. So, particle sizing can be an interesting starting point to predict boundary lubrication performance.

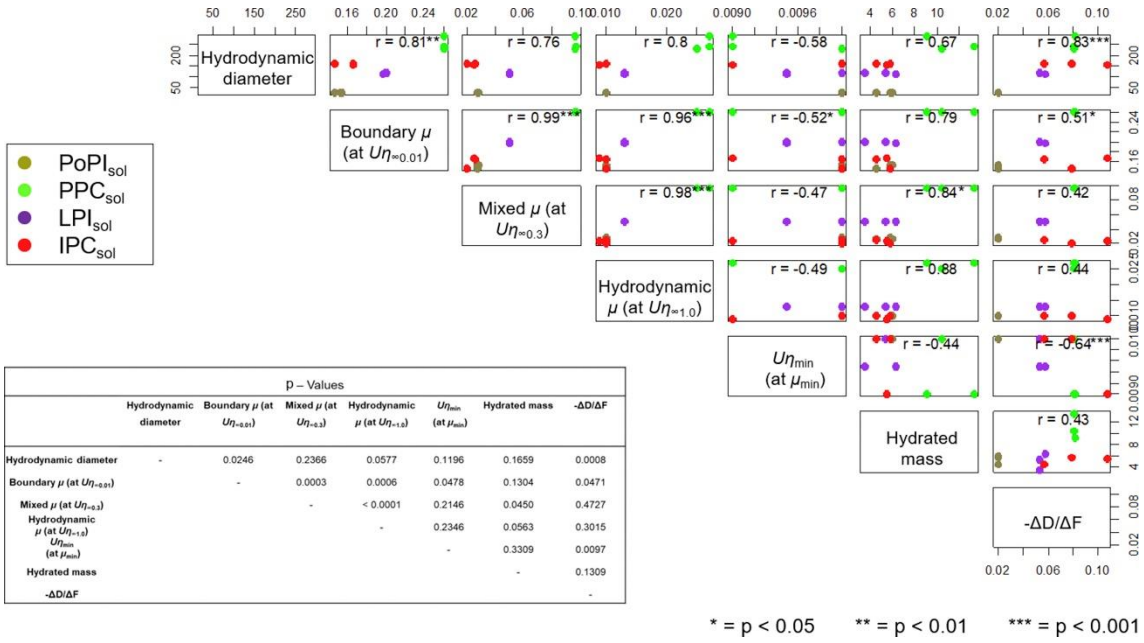

p – Values

	Hydrodynamic diameter	Boundary μ (at $U\eta_{\infty 0.01}$)	Mixed μ (at $U\eta_{\infty 0.3}$)	Hydrodynamic μ (at $U\eta_{\infty 1.0}$)	$U\eta_{min}$ (at μ_{min})	Hydrated mass	-ΔD/ΔF
Hydrodynamic diameter	-	0.0246	0.2366	0.0577	0.1196	0.1659	0.0008
Boundary μ (at $U\eta_{\infty 0.01}$)		-	0.0003	0.0006	0.0478	0.1304	0.0471
Mixed μ (at $U\eta_{\infty 0.3}$)			-	< 0.0001	0.2146	0.0450	0.4727
Hydrodynamic μ (at $U\eta_{\infty 1.0}$)				-	0.2346	0.0563	0.3015
$U\eta_{min}$ (at μ_{min})					-	0.3309	0.0097
Hydrated mass						-	0.1309
-ΔD/ΔF							-

Figure 3.7 Pearson correlation (r) of instrumental data for 10 wt% protein solutions where n = 3 for each protein data sets. *–ΔD/ΔF* is the dissipation shift (*ΔD*)/frequency shift (*Δf*) ratio. Spearman's rank was used to obtain the *p-values* as an inset table and translated into *, **, *** indicating 0.05–0.001 in order of significance.

Hydrated mass determined by QCM-D also positively correlates with *μ* in all regimes (r = 0.79–0.88). In this respect hydrodynamic diameter and hydrated mass also correlate (r = 0.67) and so a larger sized particle with higher hydrated mass may point towards a particle-like behaviour that induces a physical jamming and friction increasing effect. It should be pointed out that the correlation with *μ* was only significant in the mixed regime ($U\eta_{\infty 0.3}$) with hydrated mass ($p < 0.05$) and also PoPI $_{sol,}$ LPI $_{sol}$ and IPC $_{sol}$ had non-significant differences in hydrated mass yet different tribological responses. Static measurement of QCM-D adsorption may not accurately portray the film behaviour that is under dynamic conditions during the high shear experienced during tribology, so it might not be straightforward to find a relationship between hydrated mass and *μ*. Hydrodynamic diameter and *–ΔD/Δf* are also positively correlated with high significance (p < 0.001) suggesting smaller d_H proteins are more likely to form a

rigid and packed layer as opposed to larger ones forming a more viscoelastic layer.

A weak positive correlation was found between $-\Delta D/\Delta f$ and lubrication although this is likely due to the large deviations of measurements from $IPC_{sol.}$ We conducted a correlation removing IPC_{sol} focussing just on plant proteins as shown in Appendix B Figure B3. With the removal of IPC_{sol}, we observed highly positive correlation (r = 0.9–0.99) with significance ($p < 0.001$) between $-\Delta D/\Delta f$ values suggesting a rigid layer improves lubrication irrespective of the regimes. This can be explained as the highly viscoelastic layer might be easily removed from the contact region, as opposed to a rigid layer which might remain creating a gap between the contact surfaces reducing μ.

Next when observing $U\eta_{min}$ (at μ_{min}), we can see this is the only parameter producing a negative correlation with all other parameters and further increases in negative correlation in Appendix B Figure B3 when excluding IPC_{sol}. This negative correlation found between the entrainment speed where the friction coefficient is a minimum, corresponding to the transition between the hydrodynamic and mixed regime $U\eta_{min}$ (at μ_{min}), and the wet mass as well as $-\Delta D/\Delta f$ values is in line with the findings previously reported by Stokes et al. (2011). In other words, we can say that although a rigid layer with lower hydrated mass might be efficient in providing optimal boundary lubrication, presence of a viscoelastic layer might help in accelerating the transition from mixed to boundary lubrication regimes.

To sum everything up with respect to correlations for alternative proteins, it can be inferred that proteins with highest lubrication performance investigated within this study have the lowest hydrodynamic diameter, are more rigid and of lower hydrated mass (*i.e.* $PoPI_{sol}$) and the opposite holds true for proteins

showing lowest lubrication performance (*i.e.* PPC_{sol}). While statistically speaking, these correlation coefficients appear reasonable, with only four alternative protein types, it is difficult to prove whether such relationships are just empirical or truly causal at this stage.

Bartlett tests show that there is significantly correlated data however upon conducting a Kaiser-Meyer-Olkin test the value is less than 0.5 due to the limited number of sample data and ultimately a trend can be predicted but not causative and so these parameters should undergo further investigation. It should be emphasised that more data points would establish stronger evidence and greater confidence in the observed correlations, nonetheless there are clearly strong associations of high statistical significance, which for the first time have been established in such a range of alternative proteins that may serve as a reference to fast track the development of food with optimally lubricating alternative proteins.

3.5 Conclusions

Lubrication and adsorption properties of alternative proteins sourced from potato, pea, lupin and insects were compared with whey protein. Soluble fractions of these concentrates/isolates were characterised by means of hydrodynamic size, charge, rheology, tribology and adsorption (hydrated mass, film viscoelasticity). The lowest solubility was reported with PPC_{sol}, all other proteins displayed good solubility with complete dissolution being observed for $PoPI_{sol}$ and WPI_{sol}. Proteins were all negatively-charged and showed various degrees of aggregation with hydrodynamic sizes ranging from PoPIsol at tens of nanometres to WPIsol and PPCsol at a couple hundred of nanometres.

Strikingly, all alternative proteins showed effective lubrication at 5 wt% concentration following a distinct reduction in friction. PPCsol showed the lowest

effective lubrication in comparison to all other proteins with highest friction coefficient amongst the tested proteins at both 5 wt% and 10 wt% concentration. Interestingly, for LPI_{sol}, particularly $PoPI_{sol}$, and IPC_{sol}, friction coefficients were increased when concentration was raised from 5 wt% to 10 wt%, most possibly due to aggregation and jamming of the proteins in the contact region behaving like particle aggregates than a lubricating polymeric film. WPIsol was superior in lubrication with lowest boundary friction coefficient even when the concentration was increased to 10 wt%. Results from QCM-D reveal rigid film formation may result in a reduction in boundary lubrication and visa versa for viscoelastic films. Pearson's correlation between alternative protein data plots revealed relationship of lubrication as well as transition between lubrication regimes to hydrated mass, hydrodynamic size and viscoelasticity.

It is worth noting that whey proteins showed substantial lubrication performance as compared to alternative proteins particularly at higher concentrations. Nevertheless, alternative proteins may still be utilised to lubricate at lower concentrations. Among the tested proteins, potato protein seems to stand out in its lubrication performance because of its smaller size and ability to form a rigid layer at the surface. Finally, sensory tests are key to understand whether such increased lubrication, hydrated mass and viscoelasticity are associated with positive mouthfeel perception such as smoothness in alternative proteins. Herein a focus is shifted to sensory characterisation of these plant proteins in **chapter 4.**

3.6 References

Adal, E., Sadeghpour, A., Connell, S., Rappolt, M., Ibanoglu, E., & Sarkar, A. (2017). Heteroprotein complex formation of bovine lactoferrin and pea protein isolate: A multiscale structural analysis. *Biomacromolecules*, 18(2), 625–635.

Akyol, H., Riciputi, Y., Capanoglu, E., Caboni, M. F., & Verardo, V. (2016). Phenolic compounds in the potato and its byproducts: An overview. *International Journal of Molecular Sciences*, 17(6), 835.

Andablo-Reyes, E., Yerani, D., Fu, M., Liamas, E., Connell, S., Torres, O., et al. (2019). Microgels as viscosity modifiers influence lubrication performance of continuum. *Soft Matter*, 15(47), 9614–9624.

Belloque, J., García, M., Torre, M., & Marina, M. (2002). Analysis of soyabean proteins in meat products: A review. *Critical Reviews in Food Science and Nutrition*, 42, 507–532.

Bouaouina, H., Desrumaux, A., Loisel, C., & Legrand, J. (2006). Functional properties of whey proteins as affected by dynamic high-pressure treatment. *International Dairy Journal*, 16(4), 275–284.

Bußler, S., Rumpold, B. A., Jander, E., Rawel, H. M., & Schlüter, O. K. (2016). Recovery and techno-functionality of flours and proteins from two edible insect species: Meal worm (Tenebrio molitor) and black soldier fly (Hermetia illucens) larvae. *Heliyon, 2* (12). e00218-e00218.

Chao, D., Jung, S., & Aluko, R. E. (2018). Physicochemical and functional properties of high pressure-treated isolated pea protein. *Innovative Food Science & Emerging Technologies*, 45, 179–185.

Chen, J., & Stokes, J. R. (2012). Rheology and tribology: Two distinctive regimes of food texture sensation. *Trends in Food Science & Technology*, 25(1), 4–12.

Chihi, M.-L., Mession, J.-l., Sok, N., & Saurel, R. (2016). Heat-induced soluble protein aggregates from mixed pea globulins and β-lactoglobulin. *Journal of Agricultural and Food Chemistry*, 64(13), 2780–2791.

Chojnicka, A., de Jong, S., de Kruif, C. G., & Visschers, R. W. (2008). Lubrication properties of protein aggregate dispersions in a soft contact. *Journal of Agricultural and Food Chemistry*, 56(4), 1274–1282.

Dabija, A., Codina, G., Anca, G., Sanduleac, E., & Lacramioara, R. (2018). Effects of some vegetable proteins addition on yogurt quality. *Scientific Study and Research: Chemistry and Chemical Engineering, Biotechnology, Food Industry*, 19, 181–192.

Damodaran, S., & Arora, A. (2013). Off-flavor precursors in soy protein isolate and novel strategies for their removal. *Annual Review of Food Science and Technology*, 4(1), 327–346.

Edwards, P. J. B., & Jameson, G. B. (2014). Chapter 7 - structure and stability of whey proteins. In H. Singh, M. Boland, & A. Thompson (Eds.), Milk proteins (2nd ed., pp. 201–242). San Diego: Academic Press.

Glumac, M., Ritzoulis, C., & Chen, J. (2019). Surface properties of adsorbed salivary components at a solid hydrophobic surface using a quartz crystal microbalance with dissipation (QCM–D). *Food Hydrocolloids*, 97, 105195.

Graf, B., Protte, K., Weiss, J., & Hinrichs, J. (2020). Concentrated whey as protein source for thermally stabilized whey protein-pectin complexes. *Journal of Food Engineering*, 269, 109760.

Guimaraes, D., & Gasparetto, C. (2005). Whey proteins solubility as function of temperature and pH. Lebensmittel-Wissenschaft und -Technologie- *Food Science and Technology,* 38, 77–80.

Guzm´ an-Gonz´ alez, M., Morais, F., Ramos, M., & Amigo, L. (1999). Influence of skimmed milk concentrate replacement by dry dairy products in a low fat set-type yoghurt model system. Use of whey protein concentrates, milk protein

concentrates and skimmed milk powder. *Journal of the Science of Food and Agriculture,* 79(8), 1117–1122.

Hulmi, J. J., Lockwood, C. M., & Stout, J. R. (2010). Effect of protein/essential amino acids and resistance training on skeletal muscle hypertrophy: A case for whey protein. *Nutrition and Metabolism*, 7(1), 51.

Jayasena, V., Chih, H., & Abbas, S. (2011). Efficient isolation of lupin protein. *Food Australia*, 63, 306–309.

Kew, B., Holmes, M., Stieger, M., & Sarkar, A. (2020). Review on fat replacement using protein-based microparticulated powders or microgels: A textural perspective*. Trends in Food Science & Technology*, 106, 457–468.

Kilara, A., & Vaghela, M. N. (2004). 4 - whey proteins. In R. Y. Yada (Ed.), Proteins in food processing (pp. 72–99). Woodhead Publishing.

Kokini, J. L., Kadane, J. B., & Cussler, E. L. (1977). Liquid texture perceived in the mouth. *Journal of Texture Studies*, 8(2), 195–218.

Lacroix, I. M. E., Davalos ´ Teran, ´ I., Fogliano, V., & Wichers, H. J. (2019). Investigation into the potential of commercially available lesser mealworm (A. diaperinus) protein to serve as sources of peptides with DPP-IV inhibitory activity (Vol. 54, pp. 696–704), 3.

Laiho, S., Williams, R. P. W., Poelman, A., Appelqvist, I., & Logan, A. (2017). Effect of whey protein phase volume on the tribology, rheology and sensory properties of fat free stirred yoghurts*. Food Hydrocolloids*, 67, 166–177.

Lam, A. C. Y., Can Karaca, A., Tyler, R. T., & Nickerson, M. T. (2018). Pea protein isolates: Structure, extraction, and functionality. *Food Reviews International*, 34(2), 126–147.

Lesme, H., Rannou, C., Loisel, C., Famelart, M.-H., Bouhallab, S., & Prost, C. (2019). Controlled whey protein aggregates to modulate the texture of fat-free set-type yoghurts. *International Dairy Journal*, 92, 28–36.

Liu, K., Stieger, M., van der Linden, E., & van de Velde, F. (2016). Effect of microparticulated whey protein on sensory properties of liquid and semi-solid model foods. *Food Hydrocolloids*, 60, 186–198.

Liu, K., Tian, Y., Stieger, M., van der Linden, E., & van de Velde, F. (2016). Evidence for ball-bearing mechanism of microparticulated whey protein as fat replacer in liquid and semi-solid multi-component model foods. *Food Hydrocolloids*, 52, 403–414.

Liu, R., Wang, L., Liu, Y., Wu, T., & Zhang, M. (2018). Fabricating soy protein hydrolysate/xanthan gum as fat replacer in ice cream by combined enzymatic and heat-shearing treatment. *Food Hydrocolloids*, 81, 39–47.

Nadal, P., Canela, N., Katakis, I., & O'Sullivan, C. K. (2011). Extraction, isolation, and characterization of globulin proteins from Lupinus albus. *Journal of Agricultural and Food Chemistry*, 59(6), 2752–2758.

Nastaj, M., Terpiłowski, K., & Sołowiej, B. G. (2020). The effect of native and polymerised whey protein isolate addition on surface and microstructural properties of processed cheeses and their meltability determined by Turbiscan. *International Journal of Food Science and Technology*, 55(5), 2179–2187.

Nishanthi, M., Chandrapala, J., & Vasiljevic, T. (2017). Compositional and structural properties of whey proteins of sweet, acid and salty whey concentrates and their respective spray dried powders. *International Dairy Journal*, 74, 49–56.

Oliete Bonastre, P. F., Eliane, C., & R´emi, S. (2018). Modulation of the emulsifying properties of pea globulin soluble aggregates by dynamic high-

pressure fluidization. *Innovative Food Science & Emerging Technologies*, 47, 292–300.

Oliete, B., Yassine, S. A., Cases, E., & Saurel, R. (2019). Drying method determines the structure and the solubility of microfluidized pea globulin aggregates*. Food Research International*, 119, 444–454.

Pradal, C., & Stokes, J. R. (2016). Oral tribology: Bridging the gap between physical measurements and sensory experience. *Current Opinion in Food Science*, 9, 34–41.

Prakash, S., Tan, D. D. Y., & Chen, J. (2013). Applications of tribology in studying food oral processing and texture perception. *Food Research International*, 54(2), 1627–1635.

Ralet, M.-C., & Gu´eguen, J. (2000). Fractionation of potato proteins: Solubility, thermal coagulation and emulsifying properties*. Lebensmittel-Wissenschaft und –Technologie Food Science and Technology*, 33(5), 380–387.

Sanchez-Obando, J.-D., Cabrera-Trujillo, M. A., Olivares-Tenorio, M.-L., & Klotz, B. (2020). Use of optimized microparticulated whey protein in the process of reduced fat spread and petit-suisse cheeses*. Lebensmittel-Wissenschaft und -Technologie*, 120, 108933.

Sarkar, A., Andablo-Reyes, E., Bryant, M., Dowson, D., & Neville, A. (2019). Lubrication of soft oral surfaces. *Current Opinion in Colloid & Interface Science*, 39, 61–75.

Sarkar, A., & Dickinson, E. (2020). Sustainable food-grade Pickering emulsions stabilized by plant-based particles. *Current Opinion in Colloid & Interface Science*, 49, 69-81

Sarkar, A., Kanti, F., Gulotta, A., Murray, B. S., & Zhang, S. (2017). Aqueous lubrication, structure and rheological properties of whey protein microgel particles. *Langmuir*, 33 (51), 14699–14708.

Sarkar, A., & Krop, E. M. (2019). Marrying oral tribology to sensory perception: A systematic review. *Current Opinion in Food Science*, 27, 64–73.

Sats, A., Mootse, H., Pajum agi, S., Pisponen, A., Tatar, V., & Poikalainen, V. (2014). Estimation of Particle size distribution in bovine colostrum whey by dynamic light scattering (DLS) Method. *Agronomy Research*, 12.

Schmidt, J. M., Damgaard, H., Greve-Poulsen, M., Sunds, A. V., Larsen, L. B., & Hammershøj, M. (2019). Gel properties of potato protein and the isolated fractions of patatins and protease inhibitors – impact of drying method, protein concentration, pH and ionic strength. *Food Hydrocolloids*, 96, 246–258.

Stokes, J. R., Boehm, M. W., & Baier, S. K. (2013). Oral processing, texture and mouthfeel: From rheology to tribology and beyond. *Current Opinion in Colloid & Interface Science*, 18(4), 349–359.

Stokes, J. R., Macakova, L., Chojnicka-Paszun, A., de Kruif, C. G., & de Jongh, H. H. J. (2011). Lubrication, adsorption, and rheology of aqueous polysaccharide solutions. *Langmuir*, 27(7), 3474–3484.

Veldhorst, M., Smeets, A., Soenen, S., Hochstenbach-Waelen, A., Hursel, R., Diepvens, K., et al. (2008). Protein-induced satiety: Effects and mechanisms of different proteins. *Physiology & Behavior*, 94(2), 300–307.

Voigt, W. U. (1889). The relationship between the two elasticity constants isotropic body. *Wiedemann's Annalen der Physik und Chemie*, 38, 573–587.

Waglay, A., Achouri, A., Karboune, S., Zareifard, M. R., & L'Hocine, L. (2019). Pilot plant extraction of potato proteins and their structural and functional properties*. Lebensmittel-Wissenschaft und -Technologie*, 113, 108275.

Wang, S., Errington, S., & Yap, H. (2008). Studies on carotenoids from lupin seeds. Canterbury: International Lupin Association.

Weinbreck, F., de Vries, R., Schrooyen, P., & de Kruif, C. G. (2003). Complex coacervation of whey proteins and gum Arabic. *Biomacromolecules,* 4(2), 293–303.

Xu, F., Liamas, E., Bryant, M., Adedeji, A. F., Andablo-Reyes, E., Castronovo, M., et al. (2020). A self-assembled binary protein model explains high-performance salivary lubrication from macro to nanoscale, *Adv. Mater. Interfaces* 7(1), 1901549.

Yi, L., Lakemond, C. M. M., Sagis, L. M. C., Eisner-Schadler, V., van Huis, A., & van Boekel, M. A. J. S. (2013). Extraction and characterisation of protein fractions from five insect species. *Food Chemistry*, 141(4), 3341–3348.

Zembyla, M., Liamas, E., Andablo-Reyes, E., Gu, K., Krop, E. M., Kew, B., et al. (2021). Surface adsorption and lubrication properties of plant and dairy proteins: A comparative study*. Food Hydrocolloids*, 111, 106364.

Zhang, T., Guo, J., Chen, J.-F., Wang, J.-M., Wan, Z.-L., & Yang, X.-Q. (2020). Heat stability and rheological properties of concentrated soy protein/egg white protein composite microparticle dispersions. *Food Hydrocolloids*, 100, 105449.

Zhang, S., Holmes, M., Ettelaie, R., & Sarkar, A. (2020). Pea protein microgel particles as Pickering stabilisers of oil-in-water emulsions: Responsiveness to pH and ionic strength. *Food Hydrocolloids*, 102, 105583.

Chapter 4 : Sensory, neural and cellular response of plant proteins

Abstract

Plant proteins are of critical importance to sustainable, lower carbon footprint food systems a problem exacerbated by recent environmental disasters and demand to feed a population of 10 billion by 2050. Despite paramount importance, plant proteins face significant sensory challenges, lack of plant protein diversity with struggled product placement necessitating the addition of additives, fat, sugar and salt but compromising healthier design. Astringency is a persistent challenge and continues to perplex in its origin, mechanism and detrimental output for plant protein food. Herin the aim of this work is to elucidate the sensory, neural and cellular intricacies of plant proteins and their astringency. Pea, potato and lupin proteins spanning a range of concentrations and combinations were extensively profiled in 17 sensory attributes using Rate-All-That-Apply. Specific attention was then given to astringency combining neural and cellular methodology to discern any parallels to trigeminal and tannins response. Findings highlight plant protein textural application but also detrimental sensory implications to consider when integrating into food design. Neural insights uncovered similar prefrontal cortex responses to both astringent pea protein and tannic acid with cellular application identifying prominent salivary precipitation in both cases. Overall the study brings to attention the significant impact of astringency in plant proteins, its need to be addressed and assessment of plant proteins role in texture and taste within food.

4.1 Introduction

Our preference for food is a deeply primeval instinct developed over millions of years once vital in our survival of obtaining calories and avoiding anti nutritional food sources. One prime example is the pleasure of sweetness or the creamy

mouthfeel, driving our likening to calorie-rich high energy foods or conversely avoiding unpleasant, bitter and/or astringent foods that may be lower in energy density. However, owing to recent advances in farming practices, innovation in manufacturing and the ability to concentrate nutrients into highly processed sensory-driven foods, calories are no longer scarce to obtain and in forms that cause overindulgence and overconsumption of preferred foods containing more sugar, fat and salt (Hall et al., 2019).

Recently, there has been increasing importance to think about planetary health and using plant protein-rich foods have been considered to be vital in reducing our greenhouse gas (GHG) emissions, transitioning away from animal proteins (Xu et al., 2021). However, often these plant proteins suffer from astringency, dry mouthfeel (Cheynier, 2012; Brown et al., 2021; Tanger et al., 2022; Vlădescu et al., 2023) and these sensory challenges making it difficult to replace the animal proteins in food product development.

Astringency is a complex multisensory phenomenon where it is defined by the American Society for Testing Materials as “the complex of sensations due to shrinking, drawing or puckering of the epithelium as a result of exposure to substances such as alums or tannins” (Testing and Materials, 1983). Astringency is often associated with plant material originating from the production of phytonutrients as part of an evolutionary chemical defence mechanism, deterring consumption of vital plant structures, unripe fruits and seeds (War et al., 2012). Despite decades of research, the astringency mechanism remains elusive, however a number of theories exist, firstly an oral somatosensation where proteins in saliva bind to astringent inducing compounds. This was first investigated in 1954 by Bate-Smith (1954) who proposed such salivary proteins bind with tannins particularly to proline-rich proteins which then precipitate.

Tannins also have shown to bind to other salivary proteins such as peptides and statherins (Soares et al., 2011; Soares et al., 2012) where such precipitation leads to increased oral friction and lubrication failure (Canon et al., 2013). Secondly, a taste receptor mechanism has been proposed where astringent compounds bind to specific receptors (Schiffman et al., 1992) where such gustatory regions in the brain also indicate stimulation with astringency (Kishi et al., 2017). Conversely, a third mechanism has been evidenced with astringency being not a taste but a trigeminal neural response (Payne et al., 2009; Kurogi et al., 2014). In fact Schöbel et al. (2014) found that astringency did not involve taste but a trigeminal response by performing anaesthesia of lingual and trigeminal nerves in humans and also with the trigeminal ganglion neurons of mice. Additionally new conjecture has been recently proposed such as aggregation of tethered MUC1 proteins by astringent compounds leading to subsequent rupture and intracellular signal release to neurotransmitters (Canon et al., 2021). In general the topic of astringency holds significant fascination and likely to be a complex combination of receptor-based activation of trigeminal or taste nerves (Schöbel et al., 2014) or/and in combination down to the loss of salivary lubrication upon the formation of polyphenol-peptide complexes in salivary proteins (Charlton et al., 2002; Bajec and Pickering, 2008; Upadhyay et al., 2016).

Although these aforementioned hypotheses exist for astringency of polyphenols, the mechanism of astringency of macromolecular plant proteins that have inherently complex quaternary structures remain principally unexplored. Given the diverse range of mechanisms involved, it becomes imperative to adopt a comprehensive, multiscale approach to understand the underlying cause of astringency of plant proteins. Whist astringency is frequently observed in various actual food products containing plant proteins where sensory data with trained or

untrained panel is available (Cosson et al., 2020; García Arteaga et al., 2021; Liu et al., 2021; Tanger et al., 2022; Zheng et al., 2023), there is a scarcity of studies that specifically investigate the sensorially perceived astringent effects of isolated plant proteins (**Figure 4.1a**) To study this complexity of plant protein response, the neural effects should be considered (**Figure 4.1b**) Such neural imaging techniques allow for real-time quantitative data collection without subjects' post consumption psychological bias where there is a growing interest to use these devices to complement sensory or utilised in sensory prediction (Laves et al., 2022).

Previous neural study has often utilised functional magnetic resonance imaging (fMRI) where both texture and taste including, viscosity (De Araujo and Rolls, 2004; De celius alonso et al., 2007), umami (McCabe and Rolls, 2007), oral fat (De Araujo and Rolls, 2004) sweetness, pungency and astringency (Kishi et al., 2017; Zhu et al., 2023) has been conducted. fMRI allows for precise measuring throughout the brain particularly deeper regions such as the primary gustatory regions (operculum, insula), secondary gustatory regions (orbitofrontal cortex), anterior cingulate cortex, amygdala and hypothalamus. fMRI however requires that the participant is immobile which makes capturing normal eating behaviour in a practical sensory environment challenging. An alternative neural technique, functional near-infrared spectroscopy (fNIRS), could serve as a more suitable device that measures haemoglobin changes via absorbed infrared light where both oxyhaemoglobin (HbO) and deoxyhaemoglobin (HbR) changes are measured whilst offering flexibility and mobility by simply requiring the user to wear a cap. However fNIRS is limited in its ability to only measure cortical surface and an aerial neuron response rather than individual neuronal responses. Despite these drawbacks there has been success in quantifying sensory

preference and prefrontal cortex (PFC) stimulation to taste (Okamoto et al., 2009; Bembich et al., 2010; Minematsu et al., 2018). Only one study has paired fNIRS and PFC stimulation with a real food system where preference and taste aspects were compared between two plant based milks (Laves et al., 2022). This study found unique haemodynamic responses in different parts of the PFC where in particular the dorsolateral prefrontal cortex, involved in secondary gustatory responses (Iannilli et al., 2014; Rolls, Edmund T., 2015), was stimulated by both samples however could not distinguish milk samples from one another. This dorsolateral region has also recently been shown to be stimulated by sucrose as well (Zhu et al., 2023) and may provide a complimentary insight into general sensory response. In respect to astringency neural imaging may provide an new insight into this sense, how its perceived, processed and origin of response. More importantly, it can give indication whether the astringency of plant proteins has a similar neural basis as phenolic compounds. In addition, comprehending whether the response to plant proteins resembles that of animal protein or that of polyphenols needs validation at a cellular level (**Figure 4.1c**).

Herein, we have designed a unique sensory, neural and cellular combinatorial approach in decoding the astringency mechanism of isolated plant proteins (**Figure 4.1a**). Our hypothesis was that plant proteins are astringent and have a cellular and neural basis of astringency resembling those of polyphenol-mediated mucin interaction. Pea, lupin and potato proteins were selected as a range of sustainable protein candidates representing two legume and one tuber proteins with low greenhouse gas emissions that have gained recent interests in use in food and the scientific community (Lucas et al., 2015; Tulbek et al., 2017; Schmidt et al., 2019; Sim et al., 2021). Sensory study was conducted using Rate

All That Apply (RATA) to profile 17 taste, texture and afterfeel attributes at low and high concentrations. Potato proteins retained desirable textural attributes at high concentrations conversely compared to lupin and pea proteins that were more rough and astringent. Mixing proteins was shown to synergistically detriment sensory profile when combing with pea protein but ultimately astringency was prevalent in all plant protein and show further deterioration of texture under repeat consumption. The neural response of astringency was next performed using fNIRS brain imaging in the PFC where a significant level of activity occurred with both astringent polyphenol (tannic acid) and pea protein at a high concentration. This observation implies that astringency does impact the PFC, and it suggests that fNIRS serves as a valuable complementary tool for sensory investigation. Lastly, we explored the cellular effects of astringent plant proteins exposing a model human buccal mucosa cell line, derived from squamous cell carcinoma cells (TR146), to plant and animal protein solutions after incubation with saliva. We found mucin binding to be significant in astringency-inducing tannic acid and pea protein that was concentration-dependent and where conversely no significant binding was found with non-astringent animal (whey) protein counterpart. In summary, this study offers insights into sensory outcomes of plant proteins. Moreover, we delve into the astringency mechanism of plant proteins, which appears to be resembling that of polyphenol in both cellular and neural responses, mostly associated with mucin binding.

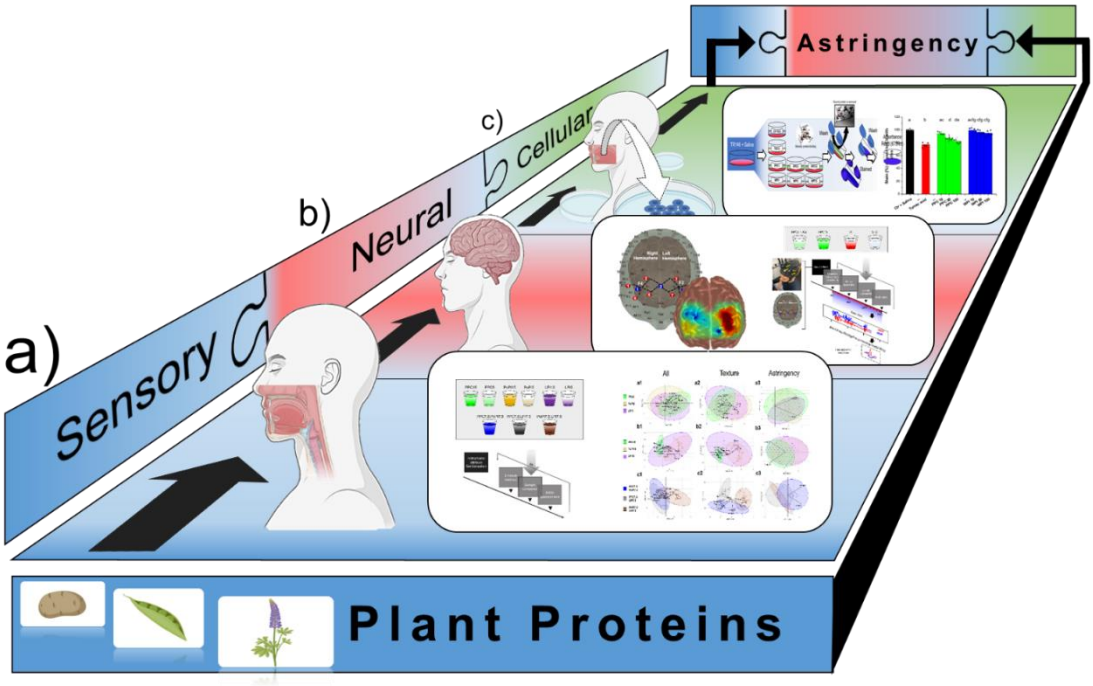

Figure 4.1 Illustrative overview of sensory, neural and cellular design in elucidating the sensory and astringency effect of plant proteins. Pea, potato and lupin proteins were characterised in (a) sensory evaluation using Rata-All-That-Apply (RATA). Focus was given on astringency where astringent plant proteins were characterised (b) neurally using functional near-infrared spectroscopy (fNIRS) compared to tannic acid. Astringency mechanism was then characterised (c) cellularly applying plant, animal protein and tannic acid solutions to squamous cell carcinoma cells (TR146) cell lines to measure salivary protein binding. Overall this methodology provides insights into the texture and taste profile of plant proteins and their induced astringency.

4.2 Methods

Materials Pea protein concentrate (PPC, Nutralys S85 XF) containing 85 wt% protein was kindly gifted by Roquette (Lestrem, France). Potato protein isolate (PoPI) was purchased from Guzmán Gastronomía (Barcelona, Spain) containing 91 wt% soluble protein (Kew et al., 2021). Whey protein isolate was kindly gifted from (Fonterra, New Zealand) containing at least 95 wt% protein. Lupin protein

isolate was purchased from Prolupin (GmbH, Grimmen, Germany) containing 90 wt% protein. Food grade Tannic acid was purchased from APC pure (UK) and xanthan gum purchased from Special ingredients (UK). Madagascan vanilla extract and sucralose sweetener (maltodextrin, sucralose (1%)) were purchased from a local supermarket (Morrisons, UK). Refer to **Table 4** for all solutions used in this study.

For the cell culture, the squamous cell carcinoma cells (TR146) cell line (wild type) was kindly provided by Prof F.M. Goycoolea (Leeds), and mucin-expressing TR146 cell line (TR146/MUC1) was gifted by Dr F. Canon (INRAE, France) (Ployon et al., 2016). Reagents for cell culture were purchased from Gibco ThermoFisher Scientific (Loughborough, UK), including Dulbecco's Modified Eagle Medium (DMEM), Dulbecco's Phosphate-Buffered Saline (DPBS), Hanks' balanced salt solution (HBSS), penicillin/streptomycin (P/S), and trypsin/Ethylenediaminetetraacetic (EDTA) whereas fetal bovine serum (FBS) was obtained from Sigma-Aldrich (Dorset, UK). Alcian blue stain was purchased from Epredia (Runcorn, UK), and neutral red dye was purchased from Sigma-Aldrich. The glacial acetic acid and ethanol were obtained from ThermoFisher, UK and dimethyl sulfoxide (DMSO) were obtained from Santa Cruz Biotechnology (Heidelberg, Germany). Milli-Q water was purified using Milli-Q apparatus, Millipore Corp., Bedford, MA, USA).

Table 4 Summary of all solutions, their nomenclature, formulation and the characterisation methodology tested. Friction coefficient values are presented as means and standard deviation of three repeats on triplicate samples (n = 3 x 3)

Nomenclature	Pea protein concentrate (Total protein wt%)	Potato protein isolate (Total protein wt%)	Lupin protein isolate (Total protein wt%)	Whey protein isolate (Total protein wt%)	Tannic Acid (wt%)	Sensory (RATA)	Neural (fNIRS)	(Cellular) TR146 cell line
PPC1	1	-	-	-	-	✓		✓
PPC5*	5	-	-	-	-	✓		✓
PPC15*	15	-	-	-	-	✓	✓	✓
PoPI1	-	1	-	-	-	✓		
PoPI5*	-	5	-	-	-	✓		
PoPI15*	-	15	-	-	-	✓		
LPI1	-	-	1	-	-	✓		
LPI5*	-	-	5	-	-	✓		
LPI15*	-	-	15	-	-	✓		
PPC7.5:PoPI7.5*	7.5	7.5		-	-	✓		
PPC7.5:LPI7.5*	7.5		7.5	-	-	✓		
PoPI7.5:LPI7.5*	-	7.7	7.5	-	-	✓		
WPI1	1	-	-	1	-			✓
WPI5	5	-	-	5	-			✓
WPI15	15	-	-	15	-			✓
PPC5+XG*	5	-	-	-	-		✓	✓
TA0.8*	-	-	-	-	0.8		✓	✓
STD*	-	-	-	-	-	-	✓	✓

*contained 1.2 wt% vanilla and 1 wt% sweetener for sensory and neural methodology

4.2.1 Subjects

Healthy male and female volunteers (n=135 for both RATA tasting and brain imaging study) between 18 and 55 years old were recruited using advertisement posters to students and staff at the University of Leeds, UK. Participants were excluded if they were underweight (BMI <18.5 kg/m^2), overweight or obese (BMI ≥ 25 kg/m^2), were smokers, had suffered from long-term effects of COVID-19, had oral problems or were using medication that would affect ability to eat/sense/digest food, were pregnant/lactating, had a food allergy/intolerance and free of neurological and psychiatric disorders. Participants were informed not to eat, and only drink water 2 hours before sensory procedure. Participants were informed on the purpose and safety of experiments with written consent forms collected before participation and received financial reimbursement for compensation after study. The study was approved by University of Leeds Faculty Ethics Committee (MEEC 16-046) and School of Psychology Research Ethics Committee (PSYC-475)

4.2.2 Rate-All-That-Apply (RATA)

A total of 100 volunteers were recruited, 40 male and 60 female between age of 18-40 with a mean age of 24 ± 4.2. Participants were screened beforehand using an online health questionnaire and each participant came in once. Nine protein samples were presented, refer to **Table 4** for formulations.

These samples were mixed in distilled water and flavoured using 1.2 wt% vanilla extract and 1 wt% sucralose sweeter. Exactly 20 mL of each sample was provided in black opaque cups with a lid and straw to prevent appearance discrepancies affecting scoring. The samples were randomly labelled with a 3 digit code and provided one at a time in random order generated using

compusense (v5.0, Ontario, Canada). Prior to attending, participants were familiarised with definitions and examples of the chosen 17 RATA sensory attributes divided over three categories: Taste (5) , texture (9) and afterfeel (3) (refer to Appendix C Table C1 for definitions). Definitions were also explained before commencing the session and provided throughout the assessment. Participants rated the attributes on a 1-9 scale (anchored low to high) and were allowed multiple tastings. A 3 minute washout period between samples was provided with crackers and water to wash out and neutralise the palate between the samples.

4.2.3 Functional near-infrared spectroscopy (fNIRS)

Oxyhaemoglobin (HbO) and deoxyhaemoglobin (HbR) blood (µmol/L) was measured using OxyMon MkII functional near-infared spectroscopy (fNIRS) system (Artinis Medical Systems, B.V., The Netherlands). To monitor such changes, we utilised infrared light of 765 nm and 855 nm wavelengths relating to the absorption spectrum of haemoglobin (700nm-900 nm). Using this wavelength of light, we detect the differential absorption of HbO and HbR reflecting increase in arteriolar vasodilation and cerebral blood flow corresponding to prefrontal cortex stimulation. Differential path length factor (DPF) was calculated from participants' age using formula: DPF = 4.99 + 0.067*(age^0.814). Detector optodes were embedded onto a black cap secured with elastic to optimise signal to noise ratio by removing ambient light. Placement of the cap was done by identifying fiducial points of the naison, inion and left/right preauricular joints. A drip stand was used to suspend cables to reduce artefacts associated with likelihood of movement. 3 x detector optodes (Blue dots D1-3 **Figure 4.4a**) and 8 source optodes (Yellow dots S1-8 **Figure 4.4a**). This optode configuration resulted in 12 channels (8 split, 4 unsplit) sampling at a rate of 10 Hz. This

arrangement spanned the left, midline and right prefrontal cortex region of the brain with D1 and D3 corresponding to the 10-20 EEG standardised MNI coordinate system F4 (right dorsolateral prefrontal cortex, DLPFC), F3 (left DLPFC), F2,F1 and Fz (DMPFC) respectively. Each of the 12 channels were 3.5cm long with a recording depth of 2-3mm from the surface of the cortex.

4.2.4 Functional near-infrared spectroscopy (fNIRS) procedure

.A total of 35 healthy volunteers were recruited, 14 male and 21 female between age of 18 and 55 with a mean age of 23.3 ± 3.9 , 1 participant was excluded due to poor signal feedback detected during data analysis.

Brain responses during the consumption of four samples were collected. Viscosity was standardised between control non-astringent and astringent samples (Refer to viscosity flow curves in Appendix C Figure C1) with xanthan gum added to PPC5 to exclude viscosity-associated brain response effects.

Participants sat on a chair and laptop facing a wall and dim white lighting to reduce any outside distraction resulting in noise. The study procedure was created using Gorilla™ (www.gorilla.sc) where the participant filled out an information sheet, consent form and were provided with written and verbal instructions. The fNIRS cap with optodes (see **Figure 4.3**) was fitted on the scalp and participants were asked to limit unnecessary movement and to complete tasks in silence to reduce data artifacts. Participants firstly had 40 s to consume a small cracker and water, the 60 s baseline waiting period commenced followed by 40 s to consume 20ml of the 4 samples (**Figure 4.3**). Finally, the subjects rated sample texture and taste attributes and these steps were repeated 3 more times to obtain brain response to all 4 samples with samples being randomized between participants. Strict timing and markers allowed baseline and brain responses to be accurately located for the analysis stage. Astringency,

roughness, creaminess, sweetness and thickness texture attributes were rated similarly to RATA procedure described previously whereby definitions were familiarised before starting procedure.

Data files were converted into matlab format using oxysoft2matlab function (R2017a, Mathworks Ltd). Pre-processing was performed to remove biological and technical artefacts using Homer3 (V1.31.2) ((Huppert et al., 2009)) converting haemodynamic intensity raw data into optical density applying the following protocol: a PCA filter was used to remove first principal components of noise, motion artefacts were removed using an auxiliary high pass filter (HPF, -0.020 Hz) and low pass filter (LPF, 1.00 Hz) and converted to optical density. Finally, the modified Beer-Lambert law (MBLL) was applied to obtain HbO and HbR concentrations. We used a General Linear Model to generate block averages for each of the 12 channels during the first 30s of sample consumption for each participant to the each of the samples. Individual subject data was then subjected to a group analysis resulting in a group level Δ HbO for each sample, that was subsequently mapped onto a template brain using AtlasViewer (Aasted et al., 2015). NIRS Brain AnalyzIR (Santosa et al., 2018) toolbox via MatLab (2022b, Mathworks) was used to generate statistical differences between samples. The heatmaps show T-stats of increases (warm colours) and decreasing (cool colours) in HbO compared to baseline.

4.2.5 Cell culture and maintenance

TR146 and TR146-S cells were cultivated in Dulbecco's Modified Eagle Medium (DMEM) (4.5 g L^{-1} *D*-glucose with pyruvate) supplemented with 10% (Fetal Bovine Serum) FBS and 1% Penicillin-Streptomycin (P/S) under standard conditions (5% CO_2, 37 °C) with medium replacement every other day. After reaching 80-90% confluence, the cells were rinsed with DPBS (1×) and detached

with trypsin/EDTA (1×). Cells were used for experiments up to 15 inhouse passages.

4.2.6 Cytotoxicity assay

Toxicity of pea protein, whey protein and tannic acid towards the cells was determined by neutral red assay, which is based on the lysosomal accumulation of dye in viable cells. To this end, cells were seeded in 24-well plates at a density of 8 $\times 10^4$ cells cm^{-2}. Upon reaching 95% confluence, the medium was replaced by pea and whey protein (10-150 mg mL^{-1}), and tannic acid (2-8 mg mL^{-1}) dissolved in medium and incubated for 1-24 h, meanwhile the medium control and positive control (5% DMSO), *v/v*) were performed in parallel to each replicate. Cytotoxicity of saliva (1-400 µL mL^{-1}) towards TR146 cells (wild type) was also examined at 1 h duration. After incubation, the treatments were removed and replaced by the FBS-free medium containing neutral red (40 µg mL^{-1}) followed by 3 h incubation. After washing with DPBS, the cells were destained in water/ ethanol/ glacial acid (49:50:1, *v/v/v*) and shaken horizontally for 5 min in the dark. Absorbance readings were recorded on a Tecan Spark 10M™ at 540 nm. The relative cell viability was calculated in percentage of the medium control.

4.2.7 Saliva collection.

Human saliva was collected at the same time from healthy non-smoker subjects (n=10, 6 female, 4 male aged between 23-31) who were refrained from eating/drinking for at least 2 h before saliva collection. The volunteers spat saliva into a collection tube after accumulation for 10 minutes under unstimulated conditions. Unstimulated was chosen as it is the saliva that first interacts when consuming a substance and a pooled sample better represents the average saliva composition as saliva variation is large between individuals. Immediately after collection, the saliva was pooled and centrifuged at 4,000 g for 5 minutes.

The supernatant was applied straight away to TR146 cells. Ethics approved from the University of Leeds (MEEC 16-046 ethics approved by the Faculty Ethics Committee, University of Leeds).

4.2.8 Alcian blue staining

The amount of mucin bound to the epithelial cell layer was estimated by the alcian blue method when alcian blue interacts with the anionic carboxylate and sulphate groups of mucin. The TR146-MUC1 cells, grown in 24-well plates to 95 % confluence were equilibrated in HBSS for 1 h before adding pea and whey protein (10-150 mg mL^{-1}) and tannic acid (2-8 mg mL^{-1}) dissolved in HBSS. The duration of treatment was determined to be 1 h on account of the cell viability and oral administration conditions. TR146 wild type cells were incubated in 30 % saliva in HBSS solution (*v/v*) for 1 h prior to the treatments of proteins and tannic acid. After incubation, solutions with additions were removed, cells were washed twice with DPBS, and 1% alcian blue dye (*w/v*) in 3% acetic acid (*v/v*) was subsequently applied on the cell surface followed by 15 min incubation at room temperature in the dark. After removing the dye, cells were rinsed in DPBS for 3-4 times prior to the destaining procedure in DMSO. The plate was shaken horizontally for 5 min under light shielding, then absorbance was measured at 675 nm using Tecan Spark reader. The proportion of mucin was calculated in percentage respect to the control of saliva + HBSS.

4.2.9 Statistical analysis

Unless specified else where all results are reported as means and standard deviations on at least three repeats on three independent experiments. Statistical analysis was performed using R where the significance between data sets was calculated using analysis of variance (ANOVA) with Tukey post hoc test, significance level $p<0.05$. With respect to sensory results Bonferroni correction

was applied and data normalised before subjected to statistical tests. PCA was used as an initial step in the multivariate analysis and dimensionality reduction by calculation of principal components and reduces the contribution of less significant variables. Percentage contribution of principal components are presented along with biplots of scores and loadings. These represent relationships between samples and factors respectively.

4.3 Results

4.3.1 Sensory response of plant proteins

Firstly, RATA was utilised in this study that serves as an adaptation to Check-All-That-Apply (CATA) that allows for scaled quantitative data of plant protein solutions to be collected. Sensory analysis was conducted on low and high concentrations of pea, potato and lupin proteins dispersed in water with sucralose sweetener and vanilla flavouring to generate a standard taste and flavour profile. (refer to **Table 4** in methods for formulations). The concentrations were chosen as to represent current levels or high protein concentration levels in foods. The proteins were also mixed in a 1:1 ratio to understand any sensory changes that may occur when employing a protein complementation strategy to enhance amino acid profile of the food. Of the essential amino acids the legume family lacks methionine, cysteine and tryptophan whilst cereal families lack lysine and so mixtures of plant proteins are sought for to balance amino acid profile which should be considered in future plant protein food design (Young and Pellett, 1994; Pownall et al., 2010; Galili and Amir, 2013)

Before RATA, a preliminary CATA sensory test was performed for all solutions to finalise sensory attributes used. These 17 attributes are listed along with descriptors in Appendix C Table C1. In this study 9 texture, 3 after feel and 5 taste attributes were chosen. An emphasis was given on texture, given that

taste can be manipulated and vastly altered through product formulation, whilst the significance of texture in relation to plant protein implications might be underestimated (Kew et al., 2020; Stribiţcaia et al., 2020; Paul et al., 2022). We also report on afterfeel to capture any enduring or cumulative textural responses which is a significant aspect due to the consumption of food over a period of time, especially concerning astringency. Mean intensities from the nine samples obtained by RATA (n = 100) are shown in **Table 5**. To summarise the results of the sensory evaluation, **Figure 4.2** represents the Principle Component Analysis bi-plot of the 9 samples where protein type and concentration where compared to all, tactile and astringency attributes.

4.3.2 Sensory analysis of low protein-content solutions

Firstly we analyse the taste, flavour and texture ratings of samples containing 5 wt% total protein. When including taste and flavours, differences between low protein-content solutions were indistinct (**Figure 4.2 a1**) where all were rated similarly and in particular rated on average highest in comparisons to high protein- and mixed protein-containing solutions in sweetness (5.2-5.8) and vanilla flavour (3.5-5.1) (**Table 5**). However, when focusing on texture (**Figure 4.2 a2)**, we see distinct textural separation from PPC5 to PoPI5 and LPI5 where in the latter two samples compared to PPC5 significant differences were observed with higher ratings of smooth ($p < 0.05$), slippery ($P < 0.01$) and thin ($P < 0.01$) and lower ratings of graininess (LPI5 $P < 0.05$), and roughness were found (PoPI5 $P < 0.05$) (**Table 5**). Nonetheless, astringency was detected by 59% - 69% of participants even at these low concentrations where some individuals show extreme astringency towards legume protein solutions with ratings of above 6 for pea (n = 20) and lupin (n = 13) (data not shown). At low concentrations, little changes in afterfeel was observed showing a monotonous response (**Figure 4.2**

a3). Overall we show that despite taste/flavours remaining similar, plant proteins can individually influence texture with astringency detected even at low concentrations especially with PPC5 and LPI5.

4.3.3 Sensory analysis of high protein-content solutions

Upon increasing concentration to 15 wt% protein, the sensory profile of protein solutions dramatically changed with PPC15 and PoPI15 distinctly separated in PCA (**Figure 4.2 a1**). In taste and flavour there are undesirable reductions in vanilla and sweetness with more off, cereal and beany flavours appearing with higher protein concentration being introduced. As well as off flavour, beany is regarded as an unpleasant flavour commonly associated with plant proteins (Jiang et al., 2016), in particular, PPC15 in particularly ranked the highest of all proteins (6.1) (**Table 5**). Proteins are well known as flavour carriers particularly through covalent bonding, especially with cysteine, lysine and arginine amino acids (Arora and Damodaran, 2010; Wang et al., 2022). Additionally proteins can form non-covalently bonds with volatile and non-volatile compounds generating a multitude of flavour (Guichard, 2002). It is therefore not surprising for such beany and off-flavour increase with high protein concentration. Interestingly, PoPI15 did not change significantly in sweetness or off flavour despite a threefold increase in protein concentration (**Table 5**). This is likely as viscosity influences sweetness for a range of sweetening compounds (Pangborn et al., 1973; Cook et al., 2003) and are able to diffuse quicker to taste receptors of the tongue in thin solutions which synergistically improves flavour perception whilst in thicker solutions flavour and volatiles may govern sensory perception leading to an off flavour generation. of more importance, potato protein was ranked highly as beany (4.7) and significantly higher than that of lupin ($P = 0.04$) (**Table 5**). A cause

of the similar flavours may be fundamentally be a profile for plant proteins with similar evolutionary effect to astringency to reduce consumption (Cheynier, 2012). Additionally the origins of flavour development could be due to plant powder processing where chemical extraction, precipitation and drying could generate flavours from Maillard and oxidation reactions (Arora and Damodaran, 2010).

In tactile context, there are also distinctive changes upon increasing the protein concentration (**Figure 4.2 b2**). Proteins have a high water holding capacity and so increasing viscosity at higher concentrations lead to greater thickness perception and conversely for thinness. In general PCA is separated by PPC15 as thick, grainy, rough, mouthcoating and astringent whilst PoPI15 is thin, smooth, slippery with LPI15 sharing characteristics from each of these proteins (**Figure 4.2 b2**). As an alternative legume, LPI15 retains creamy (5.7) and mouthcoating characteristics (4.0) with significantly higher smooth (6.1, $p < 0.05$) and significantly lower astringency (2.8, $p < 0.01$), rough (1.6, $p < 0.05$ and grainy qualities (1.4, $p < 0.05$) which in comparison to PPC15 provides better textural properties (**Table 5**). Despite an increase in concentration PoPI15 retains non-significant differences ($p > 0.05$) in grainy, smooth, rough and astringent attributes compared to PoPI5 presenting as a favourable protein with less issues in its use at higher concentrations (**Table 5**).

Graininess is associated with the formation of large particles in the mouth, which might result from an oral interaction with saliva that leads onto roughness and loss of slipperiness and smoothness (Sarkar and Krop, 2019). Pea protein at higher concentrations was the most significant contributor of graininess that was four-six times higher than with lupin and potato proteins ($p < 0.05$) (**Table 5**). Creaminess, which was related to mouthcoating is a complex textural attribute

combining both rheological and surface textural responses which is long known to be a desired attribute (Kokini et al., 1977; Elmore et al., 1999). It is no surprise that thickness can be related to the creaminess and so pea and lupin proteins at high concentration show highest ratings creaminess (5.7-5.9, $p < 0.05$). Despite such a creamy response PPC15 is also grainy (6.0) and rough (5.4) where PoPI15, which is thin (0.4) and very slippery (4.0) is not rated as creamy so it appears thickness governs such response (**Table 5**).

When focusing solely on astringency aspects (**Figure 4.2 b3**) all proteins remained indistinct. Asides from PoPI15, there were additional significant increases in astringency from 5 wt% protein in both LPI15 ($p < 0.05$) and especially PPC15 ($P < 0.01$) the later doubling in intensity and the highest rated of all proteins (**Table 5**). Despite this, for PoPI15, 25% of participants rated astringency highly between 6-9 similarly to LPI15 (27%), however also, 36% of participants did not rank PoPI15 and 32% for LPI15 as astringent at all suggesting a large variation in how astringency is perceived by participants (Nuvoli et al., 2023). PPC15 stands out in astringency with 67% rating 6-9 and 0% as undetectable(data not shown).

Lastly, we asses afterfeel where astringency increased in small amounts for PoPI15 and LPI15 with a larger increase from 5.1 to 6.1 in PPC15. As one might expect, subsequently, creaminess decreased for all samples and roughness increased in PoPI15 and LPI15 (**Table 5**). These textural attribute changes could suggest a loss of lubricity in the mouth related to the binding and increased binding of saliva over time which has been observed in repeat consumption for known astringent solutions (Guinard et al., 1986). At high concentrations we suggest plant proteins may inflict an increasingly unpleasant astringency and oral mouthfeel phenomenon that would hinder pleasant long

term consumption of a food and lead to oral dryness and increase rejection of product.

In summary we observe participants to understand sensory terms with similarities of response recording from similar attributes observed in RATA data. At high concentrations of plant legume proteins can provide thickness and creaminess with LPI15 showing more desirable attributes in regards to texture, taste and flavour to PPC15. Overall, PoPI15 shows potential to be used at high concentrations with a number of non-significant differences in sensory attributes from low to high protein concentration.. However, an underlying issue proves to be astringency, especially for PPC15, where upon repeat consumption astringency further increases along with loss of creaminess and increases in roughness responses in the mouth. Hence, PPC was chosen as a key protein to consider further for testing its neural and cellular response.

Table 5 Rata-All-That-Apply (RATA) scores of 5 wt% total protein pea protein concentrate (PPC5), potato protein isolate (PoPI5), lupin protein isolate (LPI5), 15 wt% total protein pea protein concentrate (PPC15), potato protein isolate (PoPI15), lupin protein isolate (LPI15) and 1:1 mixtures of 15 wt% total protein of pea protein concentrate with potato protein isolate (PPC7.5:PoPI7.5), Pea protein concentrate with lupin protein isolate (PPC7.5:LPI7.5) and potato protein isolate with lupin protein isolate (PoPI7.5:LPI7.5). Results are presented as means with standard deviation from 100 participants. Subscripted lowercase letters in the same row with the same letters do not differ statistically at the confidence of $p > 0.05$.

	PPC5	PoPI5	LPI5	PPC15	PoPI15	LPI15	PPC7.5:PoPI 7.5	PPC7.5:LPI7.5	PoPI7.5:LPI7.5
Taste									
Sweetness	5.2 ± 2.1^{a}	5.5 ± 2.0 ^{a}	5.8 ± 2.0 ^{a}	2.6 ± 2.5 ^{c}	5.2 ± 2.4^{a}	3.4 ± 2.7 ^{bc}	3.6 ± 2.7 ^{b}	3.2 ± 2.7^{bc}	3.5 ± 2.7^{bc}
Vanilla flavour	4.7 ± 1.9^{a}	3.5 ± 1.7^{b}	5.1 ± 2.1^{a}	1.6 ± 2.3^{c}	1.9 ± 2.4^{b}	1.7 ± 2.2^{b}	1.7 ± 2.3^{c}	1.4 ± 2.2^{c}	1.5 ± 2.0^{c}
Cereal flavour	3.4± 2.7^{a}	2.4 ± 2.8^{a}	3.2 ± 2.5^{a}	3.6 ± 3.0^{b}	3.0 ± 3.0^{ab}	4.0 ± 3.1^{ab}	3.6 ± 3.3^{ab}	3.8 ± 3.1^{ab}	3.4 ± 2.9^{ab}
Off flavour	1.7± 2.4^{b}	3.1 ± 3.2^{a}	1.6 ± 2.1^{a}	2.8 ± 3.1^{d}	3.5 ± 3.3^{b}	4.2 ± 3.3^{cd}	5.7 ± 2.8^{bc}	3.4 ± 3.2^{d}	6.2 ± 2.5^{bc}
Beany flavour	3.6 ± 2.7^{cde}	3.9 ± 3.1^{bcd}	2.6 ± 2.6^{e}	6.1 ± 2.2^{a}	4.7 ± 3.0^{bc}	3.3 ± 3.2^{de}	4.7 ± 3.0^{bc}	5.0 ± 3.1^{bc}	4.6 ± 3.1^{bcd}
Texture									
Creamy	2.3 ± 2.4^{cde}	1.6 ± 2.4^{e}	2.0 ± 2.4^{de}	5.9 ± 2.4^{a}	2.7 ± 2.5^{cde}	5.7 ± 2.2^{a}	3.0 ± 2.9^{cd}	4.4 ± 2.9^{b}	3.1 ± 2.6^{c}
Slippery	3.7 ± 2.5^{c}	6.7 ± 2.0^{a}	6.6 ± 1.9^{a}	1.0 ± 1.5^{f}	4.0 ± 3.3^{c}	3.3 ± 3.0^{cd}	2.5 ± 3.0^{de}	1.9 ± 2.4^{ef}	5.2 ± 2.3^{b}
Grainy	1.7 ± 2.2^{c}	0.9 ± 1.6^{cd}	0.8 ± 1.5^{d}	6.0 ± 2.6^{a}	1.0 ± 1.6^{cd}	1.4 ± 2.3^{cd}	5.4 ± 2.3^{a}	3.1 ± 3.0^{b}	1.5c ± 2.2^{cd}
Smooth	6.0 ± 1.6^{b}	7.0 ± 2.0^{ab}	7.3 ± 1.9^{a}	2.2 ± 2.8^{c}	6.8 ± 1.6^{ab}	6.1 ± 2.1^{b}	3.9 ± 3.0^{c}	3.0 ± 3.1^{c}	6.0 ± 2.3^{b}
Rough	1.6 ± 2.3^{bc}	0.6 ± 1.1^{d}	1.0 ± 1.7^{cd}	5.4 ± 2.0^{a}	1.3 ± 2.3^{bcd}	1.6 ± 2.5^{bc}	4.8 ± 2.2^{a}	5.2 ± 2.0^{a}	2.0 ± 2.7^{b}
Thick	1.4 ± 1.8^{f}	0.7 ± 1.3^{f}	1.0 ± 1.7^{f}	7.7 ± 1.9^{a}	1.6e ± 2.2^{f}	4.0 ± 2.9^{c}	3.0 ± 2.7^{d}	5.1 ± 2.8^{b}	2.4 ± 2.5^{de}
Thin	5.2 ± 3.0^{b}	7.6 ± 1.8^{a}	6.8 ± 2.5^{a}	5.6 ± 3.0^{a}	0.4 ± 0.9^{e}	2.3 ± 2.9^{d}	3.0 ± 3.1^{cd}	1.0 ± 1.8^{e}	3.8 ± 3.2^{c}

Mouthcoating	3.0 ± 3.0^{cd}	2.0 ± 2.5^{d}	2.5 ± 2.6^{d}	6.1 ± 1.9^{a}	3.1 ± 3.0^{cd}	4.0 ± 2.9^{bc}	5.1 ± 2.0^{ab}	5.6 ± 1.8^{a}	3.0 ± 2.7^{cd}
Astringent	2.3 ± 2.6^{de}	2.0 ± 2.5^{de}	1.6 ± 2.0^{e}	5.1 ± 2.7^{b}	2.4 ± 2.8^{de}	2.8 ± 2.9^{cd}	5.4 ± 2.6^{a}	4.8 ± 3.0^{bc}	5.6 ± 2.1^{a}
After-feel									
Creamy	2.1 ± 2.1^{bc}	1.3 ± 1.8^{c}	1.8 ± 2.4^{bc}	5.0 ± 2.1^{a}	2.0 ± 2.4^{bc}	4.7 ± 1.9^{a}	1.7 ± 2.3^{bc}	2.5 ± 2.6^{b}	2.0 ± 2.4^{bc}
Rough	1.9 ± 1.9^{c}	1.7 ± 2.4^{c}	1.6 ± 2.2^{c}	5.2 ± 2.1^{a}	2.2 ± 2.6^{bc}	2.3 ± 2.8^{bc}	5.5 ± 2.0^{a}	5.5 ± 2.1^{a}	2.8 ± 2.9^{b}
Astringent	2.7 ± 2.7^{bc}	2.2 ± 2.4^{cd}	1.5 ± 1.5^{d}	6.1 ± 1.9^{a}	2.9 ± 2.8^{cd}	3.2 ± 2.9^{bc}	6.0 ± 2.4^{a}	3.6 ± 2.7^{b}	5.6 ± 2.0^{a}

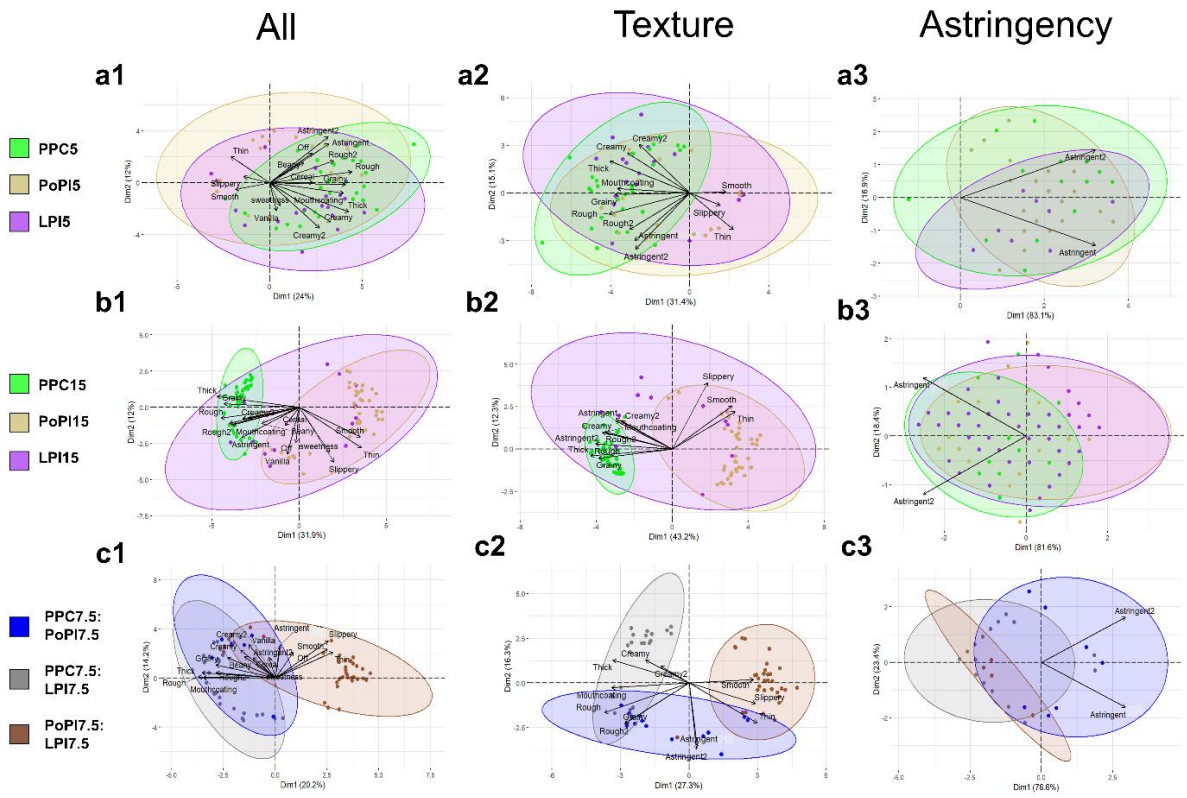

Figure 4.2 Principle component analysis biplots separated by all attributes (a1-c1), texture attributes (a2-c2) and astringency attributes (a3-c3) of (a1-3) 5 wt% total protein pea protein concentrate (PPC5), potato protein isolate (PoPI5), lupin protein isolate (LPI5), (b1-3) 15 wt% total protein pea protein concentrate (PPC15), potato protein isolate (PoPI15), lupin protein isolate (LPI15) and (c1-3) 1:1 mixtures of 15 wt% total protein of pea protein concentrate with potato protein isolate (PPC7.5:PoPI7.5), Pea protein concentrate with lupin protein isolate (PPC7.5:LPI7.5) and potato protein isolate with lupin protein isolate (PoPI7.5:LPI7.5). Bigger points represent the centroid of the distribution for each attribute type.

4.3.4 Neural response of plant proteins

There is considerable curiosity to understand and comprehend neural consequences of astringency. This reaction directly assessed in the brain could

unveil the mechanism or how astringency is experienced as well as introduce a novel means of quantifying sensory perception, an area that has been minimally explored so far in literature.

To assess neural activity, we utilised fNIRS to measure hemodynamic changes in the PFC spanning dorsomedial and dorsolateral areas. In general, the PFC is a higher-order functioning region of the brain responsible for thoughts, actions and emotions (Wood and Grafman, 2003). The dorsolateral PFC (DLPFC) area is responsible for connections in sensory processing, regulating thought and action whilst dorsomedial PFC (DMPRC) responds to more anxiety, fear based responses that in turn regulates activity to amygdala and hypothalamus responsible for emotional habit and response ((Petrides, 2005)).

To our knowledge, no fNIRS study in the PFC been used to date when consuming plant proteins nor in the understanding of texture or astringency. To investigate this technique and the astringent neural response of plant proteins we used PPC15 which was selected as the highest single plant protein in astringency during RATA. A lower astringency pea protein sample was also chosen with a matched viscosity using xanthan gum (PPC5+XG) to standardise taste and viscosity effects (refer to Appendix C Figure C1 for viscosity flow curve). Water was also consumed as a control standard (STD) where tannic acid at 0.8 wt% (TA0.8) was used as a known astringent comparison used as a standard throughout neural astringency study (Schöbel et al., 2014; Kishi et al., 2017; Zhu et al., 2023). Overall samples were controlled in astringency, viscosity and taste, with the latter we added sweetener and vanilla as standardised flavours. A schematic overview of the neural procedure is shown in **Figure 4.3**. After consumption of the sample, a RATA questionnaire was taken from the participants subjected to fNIRS tests where ratings of astringency, creaminess,

sweetness, thickness and smoothness were used as a measurement to correlate neural and sensory responses (ratings are provided in Appendix C Table C1)**.** RATA was found to also be comparable to the prior sensory experimentation with relevant samples.

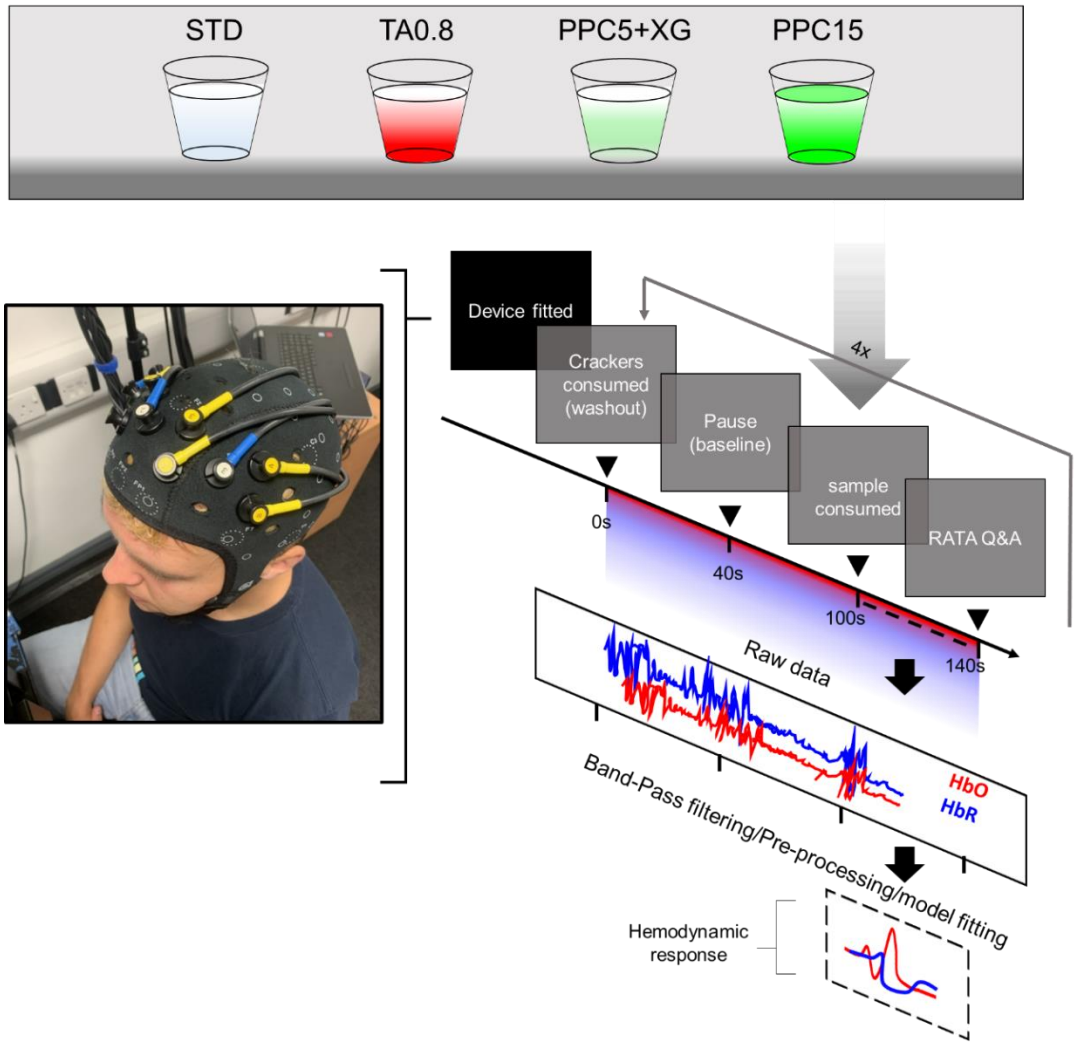

Figure 4.3 Schematical overview in the measuring and processing of oxyhaemoglobin (HbO) and deoxyhaemoglobin (HbR) changes using functional near-infrared spectroscopy (fNIRS) when consuming water (STD), 0.8 wt% tannic acid (TA0.8), 5 wt% total protein pea protein concentrate with xanthan gum (PPC+XG) and 15 wt% pea protein concentrate (PPC15).

Figure 4.4a displays the positioning of the detector (1-3, blue) and source (1-8) nodes. Source nodes emit near-infrared light, with blood haemoglobin serving as a chromophore. Detector nodes then capture the intensifying reflected

and refracted light, a phenomenon that becomes more pronounced as blood flow to the brain region rises. T-stat results were used to compare overall effect between solutions (Refer to Appendix C Table C2 for values).

Overall each sample initiated a PFC response leading to increases or decreases in oxyhaemoglobin HbO (**Figure 4.4b-e**). When analysing STD (**Figure 4.4a**), a significant increase of HbO in the left hemisphere of the brain relating to the DLPFC with stimulation between D2-S3 ($p = 0.03$) and a lower increase in HbO from D3-S3 (P = 0.008). As this was a low viscosity solution this sample would have more pronounced levels of flavour and taste which was indicated by sweetness level in RATA (Appendix C Figure C3), it may be presumed sweetness and vanilla flavours stimulate these areas as was found previously for sweetness with Zhu et al. (2023).

The most prominent activation was seen for TA0.8 (**Figure 4.4c**) where significant increases of HbO were measured in twelve of the thirteen detector and source nodes of which ten had highly significant responses ($P < 0.001$). When performing a contrast to remove the effects of STD and the taste/flavour effect astringency is shown to be significantly detected between 9 detectors and source nodes, in particular in the left hemisphere (Appendix C Figure C2a)

In fMRI tannic acid astringency has only been reported to activate primary gustatory regions of the brain as a possible taste association. We show a clear prefrontal stimulation towards TA0.8 including the DMPFC that is related to trigeminal responses, where such an intense response has not been recorded before in neural study. It is interesting that PPC15 (**Figure 4.4e**), despite being rated similarly in astringency, did not initiate a similar response. This may be due to viscosity where astringency would be initiated slowly over longer durations and dampen immediate HbO without such intense effect especially as RATA was

conducted 40 seconds after consumption, this has been reported with increasingly viscous solutions by Smith et al. (1996). However a response was captured in **Figure 4.5d** with HbR that is a pre-neural response before the upregulation of HbO and so both HbR and HbO was considered in this study.

In comparing samples of pea protein, in PPC5+XG (**Figure 4.4c**) there is a significant decrease in HbO from both D1-S6 ($p > 0.02$) and D3-S4 ($p > 0.001$), which is also detected in PPC15 (**Figure 4.4e**). This suggests that both share neural response similarities between solutions that is related to viscosity and thickness perception where a contrast is presented in Appendix C Figure C2b.

With PPC15 there are additional significant decreases in HbO in D1-S2 ($p < 0.001$) as well as D2-S6 ($p = 0.05$) signalling a movement of oxygenated blood away in the right hemisphere, this may be due to other neural induced textural sensations as recorded in RATA or the start of a reaction to plant astringency and blood movement to another area of the brain, such regions may be the primary gustatory insula where flavours or taste may dominate overall neural response.

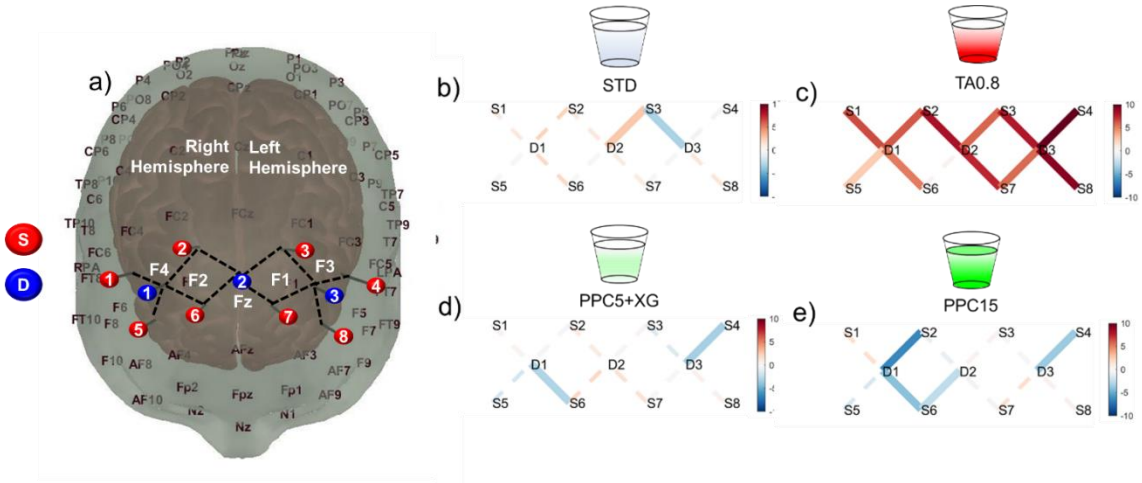

Figure 4.4 (a) Schematical diagram of the placement of detector (blue, D1-3) and source nodes (red, S1-8) spanning the right and left dorsolateral areas (F3, F4) and dorsomedial areas (F1, Fz, F2) of the prefrontal cortex. Block averaged overall oxygenated haemoglobin (HbO) effect (T-stat) from 35 participants of (b) water (STD), (c) 0.8 wt%

tannic acid (TA0.8), (d) 5 wt% total protein pea protein concentrate (PPC5+XG), (e) 15 wt% total protein pea protein concentrate. Solid connecting lines represent statistically significant response ($p < 0.05$) with their colour legend indicating magnitude of difference. A positive value (warm colours) reflects increase in HbO whilst a negative value (cool colours) reflects decreased HbO.

To explore an alternative PFC visualisation approach haemoglobin response the deoxygenated blood flow (HbR) was also represented using AtlasViewer (Aasted et al., 2015). **Figure 4.5** displays a heat map of neural activation. Similarly to HbO differences in **Figure 4.4** we observe unique responses from all samples. For STD (**Figure 4.5a**) we see stimulation from the left hemisphere with increases of HbR whilst on the right hemisphere there is a decrease in HbR consistent with increasing HbO in **figure 4.4b**.

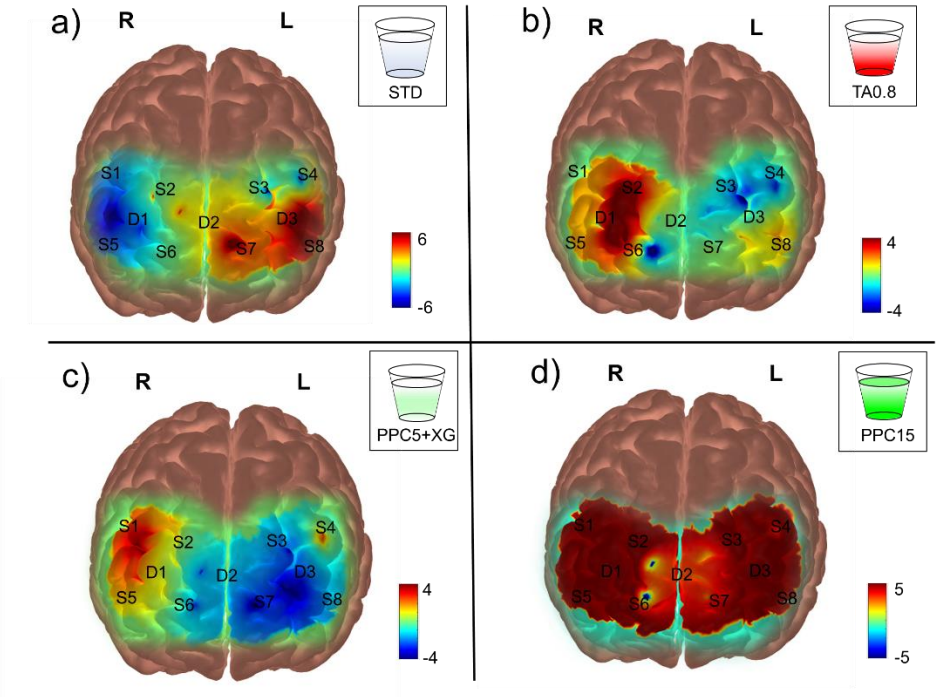

Figure 4.5 Block averaged overall deoxygenated haemoglobin (HbR) effect (T-stat) from 35 participants of (a) water (STD), (b) 0.8 wt% tannic acid (TA0.8), (c) 5 wt% total protein pea protein concentrate (PPC5+XG), (d) 15 wt% total protein pea protein concentrate. Solid connecting lines represent statistically significant response ($p < 0.05$) with their

colour legend indicating magnitude of difference. A positive value (warm colours) reflects increase in HbR whilst a negative value (cool colours) reflects decreased HbO.

For TA0.8 we observe less of a pronounced reaction (**Figure 4.5b**) compared to **Figure 4.4c** with a more focused area of HbR increase on the right side for astringency. This right side HbR increased response was also observed for all samples where astringency was detected (TA0.8, PPC5+XG and PPC15 (**Figure 4.5b-d)**) which conversely do not observe for the STD (**Figure 4.5a**) that may specifically coincide with astringency. This left DLPFC region may specifically be astringent sensitive as is the only factor associating between the three solutions. For PPC15 there is additional pronounced HbR increase detected across the whole of the PFC (**Figure 5.5d**) similar to the HbO response of tannic acid in **Figure 4.4c** and may be a precursor to a later HbO increase not detected due to a viscosity delaying intensity effect. Despite this, it is clear from **Figure 4.4** and **Figure 4.5** the most astringent samples (TA0.8 and PPC15) leads to pronounced increases throughout the PFC in either HbO or HbR dependant on viscosity. This potential time-dependant capturing of astringency in the neural response should be analysed in future study by comparing at multiple time points.

Such intense stimulation of the PFC of both TA0.8 and PPC15 may initiate a multitude of cascades of activation throughout the brain including amygdala which has been reported previously (Rolls, E. T., 2015; Rolls, 2020). In particular the activation in the DMPFC may be related to an evolutionary response mediated to protect the individual and cause a heightened level of response after consumption of astringent compounds. Additionally the DMPFC is stimulated by a pain response and may generate similar cascade of activation upon astringent exposure proving as to why astringency sensitivity is perceived (Apkarian et al., 2005). Overall the neural effect of astringent plant proteins were comparable to

responses of tannic acid where fNIRS provides a prominent insight into astringency response as a future tool for sensory assessment.

4.3.5 Cellular response of plant protein induced astringency

To further confirm if plant protein generated astringency is similar to that of tannic acid observed in neural responses, the saliva binding properties were measured as per the astringency-mechanosensation theory (Schöbel et al., 2014; Shuanhong et al., 2016). To do this we created an in-vitro cellular environment formed of saliva inoculated TR146 mucin cells (TR146+S) which were exposed to astringent and non-astringent solutions.

TA0.8 interaction was measured as a known astringent compound that is known to aggregate with salivary proteins (Payne et al., 2009; Kurogi et al., 2014; Schöbel et al., 2014) providing the effect comparison. Tannins bind via a hydrophobic interaction between aromatic ring structures and hydroxyl groups with hydrogen acceptor sites of peptide bonds, which the complex is then stabilised by hydrogen bonding. The peptide is collectively coated with these phenolics which initiates crosslinking between adjacent peptides resulting in large complex precipitation with stability dependent on tannin dimension, number of phenolics and nature of protein (Charlton et al., 2002; Frazier et al., 2003). Pea protein was chosen as the most astringent protein where three concentrations were tested (1-15 wt% total protein) as a dependency existed for astringent ratings during RATA.

For comparable non-astringent solutions a control with water was used and for non-astringent protein, whey protein (WPI) was introduced. Whey protein is a highly palatable protein that is successful in high protein food fortification namely for its neutral taste, texture (Kew et al., 2020) and excellent lubrication properties in contrast to plant proteins (Campbell et al., 2017; Sarkar et al., 2017;

Sánchez-Obando et al., 2020; Kew et al., 2021). Additionally pea protein is often viewed as the whey replacement with a number of alternative pea replacement products available, however pea is often faulted with the astringency and sensory aspects greatly hinders its use and fails to replace whey. Therefore whey protein was chosen as an ideal comparison to pea that also allows for general protein and salivary binding to be understood.

Before exposing solutions to the TR146+S toxicity tests were conducted to determine cell viability (Appendix C Figure C3). To measure binding ability an Alcian blue stain methodology was used where mucopolysacharides and glycoproteins are stained within the salivary mucins and absorbance measured. **Figure 4.6** offers a schematic summary in which the mechanosensation response would be correlated to the capacity of solutions to aggregate salivary proteins, subsequently leading to their removal, yielding a reduced absorbance reading.

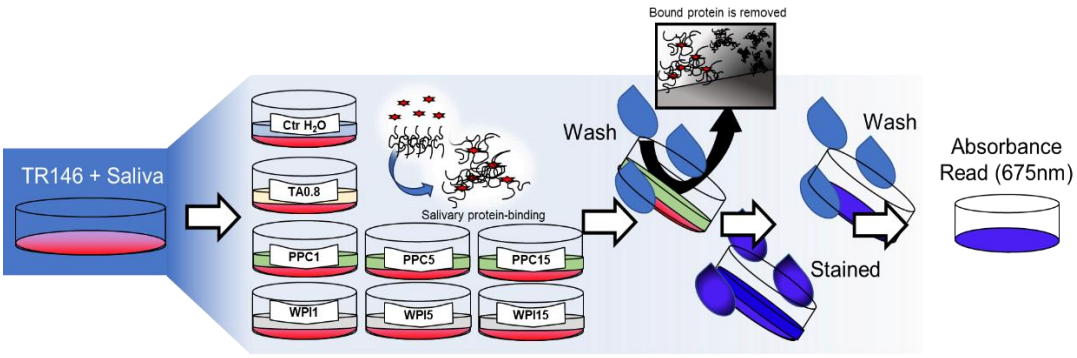

Figure 4.6 Schematical overview of cellular methodology to determine salivary binding properties of plant proteins. squamous cell carcinoma cells with inoculated saliva (TR146+S) model cell lines were created where solutions of a water control (Ctr), 0.8 wt% tannic acid (TA0.8), pea protein concentrate at a total protein concentration of 1 wt% (PPC1), 5 wt% (PPC5) and 15 wt% (PPC15), and whey protein isolate at a total protein concentration of 1 wt% (WPI1), 5 wt% (WPI5) and 15 wt% (WPI15) were applied. Alcian blue staining method was then used where the measure absorbance that was used to quantify amount of bound protein loss in all solutions compared to Ctr.

The results are shown in **Figure 5.7**. Tannic acid observed the greatest difference in absorbance compared to control with over a 20% significant decrease in absorbance ($p > 0.001$) owing to the precipitation of salivary mucins.

We also observe a significant decrease in % absorbance with pea proteins (PPC5, PPC15) compared to control ($p < 0.05$) proving that a similar mucin binding mechanism to that of tannic acid can be confirmed in pea proteins. Interestingly at low concentrations, a non-significant decrease is observed ($p > 0.05$) (**Figure 4.7**) which suggests sufficient quantities of pea protein may be needed in order to aggregate and disrupt the salivary film and may not induce astringency at low protein concentrations.

Upon comparing to whey protein, remarkably even at concentrations of 15% a non-significant level binding to mucin occurred compared to control which proves that there is a disruption to salivary film induced by pea protein but not seen with whey protein.

Overall we present strong evidence that the binding of saliva from pea generates an astringent response governed by the binding of mucin.

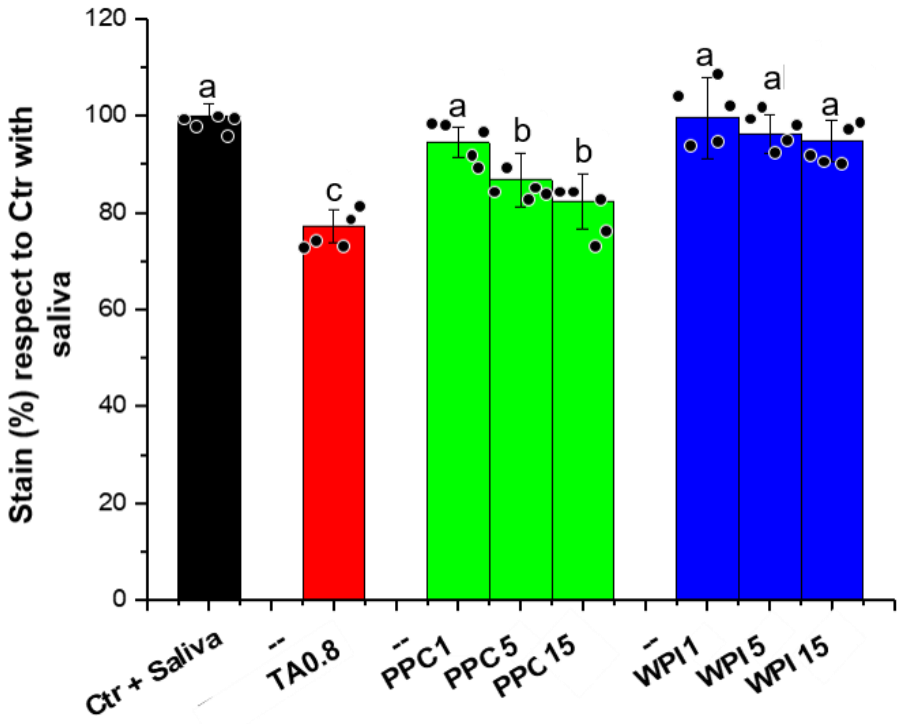

Figure 4.7 Saliva protein binding capacity of solutions. Absorbance of Alcian blue stained squamous cell carcinoma cells with saliva (TR146+S) after application and washed with water control (Ctr), 0.8 wt% tannic acid (TA0.8), pea protein concentrate at a total protein concentration of 1 wt% (PPC1), 5 wt% (PPC5) and 15 wt% (PPC15), and whey protein isolate at a total protein concentration of 1 wt% (WPI1), 5 wt% (WPI5) and 15 wt% (WPI15). The stain (%) is calculated in comparison to TR146+S absorbance with water. Means and standard deviations of 5 measurements on triplicate samples ($n = 5 \times 3$) are presented where statistical analysis was performed using two tailed unpaired Student's t-test with differing lower-case letters in the same bar chart indicate a statistically significant difference ($p < 0.05$) (Refer to Appendix C Table C3 for solution comparable P-vales).

4.4 Discussion

A comprehensive methodological approach encompassing sensory, neural and cellular characterisation was employed that explores alternative plant protein's sensorial influence and astringency caused by plant proteins. This approach provides a detailed grasp of the sensory influence and difficulties plant protein

incorporation faces that could shed light on strategies for better utilisation whilst addressing their astringency perception in future study

Firstly, using RATA we examine the sensory profile and changes in 17 sensory attributes of pea, potato and lupin proteins when presented at 5-15 wt% total protein concentration along with high protein blended combinations. Overall, pea protein was perceived as having a thick, grainy, and rough texture, accompanied by pronounced levels of off-flavour and a distinct beany note. In contrast, potato protein displayed a thin, slippery, and smooth texture. However, it also received relatively high ratings for the beany characteristic. Lupin protein showcased an enhanced sensory profile when contrasted with pea protein, while still maintaining attributes of creaminess and thickness which makes it a promising legume-derived protein option. Overall we showcase a diverse sensory profile for each plant protein providing insights into individual taste and textural properties. However, despite such properties in taste and texture, all proteins suffered with an underlying astringency. This challenge was further complicated by the presence of groups that underwent either imperceptible or notably intense astringent reactions where astringency further escalated at the 15 wt% protein level, except in the case of potato. Considering the variability observed in participant responses, it is essential to explore this further in future research. This variability could potentially be attributed to habitual diet or other participant-related factors (Nuvoli et al., 2023). It was also found after repeated consumption this astringency response heightened showing adverse impacts for other attributes like creaminess and roughness. Combining different proteins did not alleviate the issues related to texture, taste, or astringency and resulted in further inferior sensory qualities. Despite potato protein receiving favourable attribute ratings at elevated concentrations, a synergistic astringency phenomenon

emerged when it was mixed with legume proteins. Mixtures containing potato protein obtained the highest scores for astringency and off flavours implying unpredictable interactions when influenced by other proteins that may extend to other ingredients reducing adoptability.

With astringency prevalent we next investigated the neural impacts of plant proteins compared to tannic acid. Additionally, we examined the role of viscosity in influencing these neural responses. For both PPC15 and TA0.8 there existed a significant neural response on the PFC spanning both dorsolateral and dorsomedial area where such a response has not been reported in neural study to date. Additionally with lower concentrations of pea similar responses were found for HbR concentration that even at low levels astringency is detected and experienced in the brain. Such response may suggest why some participants were particularly sensitised to astringency underscoring the distinct challenge posed by astringency in plant-based applications for food. As a complimentary tool we also demonstrate neural activation of taste perception and a distinct region related to viscosity. This offers an initial glimpse into how fNIRS can be harnessed in sensory analysis. Furthermore, fNIRS holds potential as a rapid and predictive tool for sensory assessment, warranting exploration in conjunction with machine learning in future study.

Finally, we illustrate a mechanism underlying this astringency phenomenon. Through the use of saliva-inoculated TR146 cell lines, we reveal that both plant proteins and tannic acid prompt significant salivary binding. This outcome could result in diminished salivary lubrication and increased oral friction, triggering a trigeminal response associated with astringency. We also show how concentration influences binding revealing that lower levels of PPC result in minimal binding, while higher levels exhibit a substantial binding. More strikingly

we also compare WPI, a milk protein often used in high protein beverages. Even at 15 wt% protein there was no binding measured demonstrating this as a unique issues for plant proteins.

As the landscape of plant-based protein foods continues to expand, promoting sustainable and healthier food systems, it becomes imperative to shift our attention towards adopting alternative plant proteins that offer more favourable sensory attributes. However astringency is a prominent issue for all plant proteins, evidenced in this study and widely amongst others. Overall with comprehensive taste and texture assessment we highlight the unique astringency as a foremost challenge, one that leaves a strong neural impact and is influenced, at least in part, by salivary binding. This study brings to attention the significance of addressing astringency in the context of food, as well as the critical role of assess individual plant proteins in texture and taste. In **Chapter 5** we focus on how to possibly mitigate astringency in plant proteins as well as improve the lubrication found to be problematic in **Chapter 3** using a novel colloidal strategy *i.e.* microgelation.

4.5 References

Aasted, C.M., Yücel, M.A., Cooper, R.J., Dubb, J., Tsuzuki, D., Becerra, L., Petkov, M.P., Borsook, D., Dan, I. and Boas, D.A. 2015. Anatomical guidance for functional near-infrared spectroscopy: Atlasviewer tutorial. *Neurophotonics*. 2(2), pp.020801-020801.

Apkarian, A.V., Bushnell, M.C., Treede, R.-D. and Zubieta, J.-K. 2005. Human brain mechanisms of pain perception and regulation in health and disease. *European Journal of Pain* (4), pp.463-463.

Arora, A. and Damodaran, S. 2010. Competitive binding of off-flavor compounds with soy protein and β-cyclodextrin in a ternary system: A model study. *Journal of the American Oil Chemists' Society*. 87(6), pp.673-679.

Bajec, M.R. and Pickering, G.J. 2008. Astringency: Mechanisms and perception. *Critical Reviews in Food Science and Nutrition*. 48(9), pp.858-875.

Bate-Smith, E.C. 1954. Flavonoid compounds in foods. In: Mrak, E.M. and Stewart, G.F. eds. Advances in food research. Academic Press, pp.261-300.

Bembich, S., Lanzara, C., Clarici, A., Demarini, S., Tepper, B.J., Gasparini, P. and Grasso, D.L. 2010. Individual differences in prefrontal cortex activity during perception of bitter taste using fnirs methodology. *Chemical Senses*. 35(9), pp.801-812.

Brown, F.N., Mackie, A.R., He, Q., Branch, A. and Sarkar, A. 2021. Protein–saliva interactions: A systematic review. *Food & Function*. 12(8), pp.3324-3351.

Campbell, C.L., Foegeding, E.A. and van de Velde, F. 2017. A comparison of the lubrication behavior of whey protein model foods using tribology in linear and elliptical movement. *Journal of Texture Studies* 48(4), pp.335-341.

Canon, F., Belloir, C., Bourillot, E., Brignot, H., Briand, L., Feron, G., Lesniewska, E., Nivet, C., Septier, C., Schwartz, M., Tournier, C., Vargiolu, R., Wang, M., Zahouani, H. and Neiers, F. 2021. Perspectives on astringency sensation: An alternative hypothesis on the molecular origin of astringency. *Journal of Agricultural and Food Chemistry*. 69(13), pp.3822-3826.

Canon, F., Paté, F., Cheynier, V., Sarni-Manchado, P., Giuliani, A., Pérez, J., Durand, D., Li, J. and Cabane, B. 2013. Aggregation of the salivary proline-rich protein ib5 in the presence of the tannin egcg. *Langmuir*. 29(6), pp.1926-1937.

Charlton, A.J., Baxter, N.J., Khan, M.L., Moir, A.J.G., Haslam, E., Davies, A.P. and Williamson, M.P. 2002. Polyphenol/peptide binding and precipitation. *Journal of Agricultural and Food Chemistry*. 50(6), pp.1593-1601.

Cheynier, V. 2012. Phenolic compounds: From plants to foods. *Phytochemistry Reviews.* 11(2), pp.153-177.

Cook, D.J., Hollowood, T.A., Linforth, R.S.T. and Taylor, A.J. 2003. Oral shear stress predicts flavour perception in viscous solutions. *Chemical Senses*. 28(1), pp.11-23.

Cosson, A., Souchon, I., Richard, J., Descamps, N. and Saint-Eve, A. 2020. Using multiple sensory profiling methods to gain insight into temporal perceptions of pea protein-based formulated foods. *Foods*. 9(8), p969.

De Araujo, I.E. and Rolls, E.T. 2004. Representation in the human brain of food texture and oral fat. *Journal of Neuroscience.* 24(12), pp.3086-3093.

De celius alonso, B., Marcina, L., Head, K., Clark, P., Spiller, R.C., Rayment, P., Ablett, S., Francis, S. and Gowland, P.A. 2007. Functional magnetic resonance imaging assessment of the cortical representation of oral viscosity. *J Neurotrauma* 38(6), pp.725-737.

Elmore, J.R., Heymann, H., Johnson, J. and Hewett, J.E. 1999. Preference mapping: Relating acceptance of "creaminess" to a descriptive sensory map of a semi-solid. *Food Quality and Preference*. 10(6), pp.465-475.

Frazier, R.A., Papadopoulou, A., Mueller-Harvey, I., Kissoon, D. and Green, R.J. 2003. Probing protein−tannin interactions by isothermal titration microcalorimetry. *Journal of Agricultural and Food Chemistry*. 51(18), pp.5189-5195.

Galili, G. and Amir, R. 2013. Fortifying plants with the essential amino acids lysine and methionine to improve nutritional quality. *Plant Biotechnology Journal*. 11(2), pp.211-222.

García Arteaga, V., Kraus, S., Schott, M., Muranyi, I., Schweiggert-Weisz, U. and Eisner, P. 2021. Screening of twelve pea (pisum sativum l.) cultivars and their isolates focusing on the protein characterization, functionality, and sensory profiles. *Foods*. 10(4), p758.

Guichard, E. 2002. Interactions between flavor compounds and food ingredients and their influence on flavor perception. *Food Reviews International*. 18(1), pp.49-70.

Guinard, J.-X., Pangborn, R.M. and Lewis, M.J. 1986. The time-course of astringency in wine upon repeated ingestion. *Am J Enol Vitic* 37(3), pp.184-189.

Hall, K.D., Ayuketah, A., Brychta, R., Cai, H., Cassimatis, T., Chen, K.Y., Chung, S.T., Costa, E., Courville, A., Darcey, V., Fletcher, L.A., Forde, C.G., Gharib, A.M., Guo, J., Howard, R., Joseph, P.V., McGehee, S., Ouwerkerk, R., Raisinger, K., Rozga, I., Stagliano, M., Walter, M., Walter, P.J., Yang, S. and Zhou, M. 2019. Ultra-processed diets cause excess calorie intake and weight gain: An inpatient randomized controlled trial of ad libitum food intake. *Cell Metabolism*. 30(1), pp.67-77.e63.

Huppert, T.J., Diamond, S.G., Franceschini, M.A. and Boas, D.A. 2009. Homer: A review of time-series analysis methods for near-infrared spectroscopy of the brain. *Applied Optics*. 48(10), pp.D280-D298.

Iannilli, E., Noennig, N., Hummel, T. and Schoenfeld, A.M. 2014. Spatio-temporal correlates of taste processing in the human primary gustatory cortex. *Neuroscience*. 273, pp.92-99.

Jiang, Z.Q., Pulkkinen, M., Wang, Y.J., Lampi, A.M., Stoddard, F.L., Salovaara, H., Piironen, V. and Sontag-Strohm, T. 2016. Faba bean flavour and technological property improvement by thermal pre-treatments. *LWT*. 68, pp.295-305.

Kew, B., Holmes, M., Stieger, M. and Sarkar, A. 2020. Review on fat replacement using protein-based microparticulated powders or microgels: A textural perspective. *Trends in Food Science & Technology*. 106, pp.457-468.

Kew, B., Holmes, M., Stieger, M. and Sarkar, A. 2021. Oral tribology, adsorption and rheology of alternative food proteins. *Food Hydrocolloids*. 116, p106636.

Kishi, M., Sadachi, H., Nakamura, J. and Tonoike, M. 2017. Functional magnetic resonance imaging investigation of brain regions associated with astringency. *Neuroscience Research*. 122, pp.9-16.

Kokini, J.L., Kadane, J.B. and Cussler, E.L. 1977. Liquid texture perceived in the mouth. Journal of Texture Studies. 8(2), pp.195-218.

Krefting, J. 2017. The appeal of pea protein. *Journal of Renal Nutrition*. 27(5), pp.e31-e33.

Kurogi, M., Kawai, Y., Nagatomo, K., Tateyama, M., Kubo, Y. and Saitoh, O. 2014. Auto-oxidation products of epigallocatechin gallate activate trpa1 and trpv1 in sensory neurons. *Chemical Senses*. 40(1), pp.27-46.

Lam, A.C.Y., Karaca, A.C., Tyler, R.T. and Nickerson, M.T. 2018. Pea protein isolates: Structure, extraction, and functionality. *Food Reviews International*. 34(2), pp.126-147.

Laves, K., Mehlhose, C. and Risius, A. 2022. Sensory measurements of taste: Aiming to visualize sensory differences in taste perception by consumers—an

experiential fnirs approach. *Journal of International Food & Agribusiness Marketing*. pp.1-21.

Liu, Y., Toro-Gipson, R.S.D. and Drake, M. 2021. Sensory properties and consumer acceptance of ready-to-drink vanilla protein beverages. *Journal of Sensory Studies*. 36(6), pe12704.

Lucas, M.M., Stoddard, F., Annicchiarico, P., Frias, J., Martinez-Villaluenga, C., Sussmann, D., Duranti, M., Seger, A., Zander, P. and Pueyo, J. 2015. The future of lupin as a protein crop in europe. *Frontiers in plant science* 6.

McCabe, C. and Rolls, E.T. 2007. Umami: A delicious flavor formed by convergence of taste and olfactory pathways in the human brain. *European Journal of Neuroscience* 25(6), pp.1855-1864.

Minematsu, Y., Ueji, K. and Yamamoto, T. 2018. Activity of frontal pole cortex reflecting hedonic tone of food and drink: Fnirs study in humans. *Scientific Reports*. 8(1), p16197.

Nuvoli, C., Fillion, L., Lacoste Gregorutti, C. and Labbe, D. 2023. Comparison of sensitivity to taste and astringency stimuli among vegans and omnivores. *Physiology & Behavior.* 262, p114092.

Okamoto, M., Dan, H., Clowney, L., Yamaguchi, Y. and Dan, I. 2009. Activation in ventro-lateral prefrontal cortex during the act of tasting: An fnirs study. *Neuroscience Letters.* 451(2), pp.129-133.

Pangborn, R.m., Trabue, I.M. and Szczesniak, A.S. 1973. Effect of hydrocolloids on oral viscosity and basic taste intensities *Food Hydrocolloids*. 4(2), pp.224-241.

Paul, V., Tripathi, A.D., Agarwal, A., Kumar, P. and Rai, D.C. 2022. Tribology – novel oral processing tool for sensory evaluation of food. *LWT*. 160, p113270.

Payne, C., Bowyer, P.K., Herderich, M. and Bastian, S.E.P. 2009. Interaction of astringent grape seed procyanidins with oral epithelial cells. *Food Chemistry*. 115(2), pp.551-557.

Petrides, M. 2005. Lateral prefrontal cortex: Architectonic and functional organization. *Phil. Trans. R. Soc.*360(1456), pp.781-795.

Pownall, T.L., Udenigwe, C.C. and Aluko, R.E. 2010. Amino acid composition and antioxidant properties of pea seed (pisum sativum l.) enzymatic protein hydrolysate fractions. *Journal of Agricultural and Food Chemistry*. 58(8), pp.4712-4718.

Rolls, E.T. 2015. Taste, olfactory, and food reward value processing in the brain. *Prog Neurobiol*. 127-128, pp.64-90.

Rolls, E.T. 2015. Taste, olfactory, and food reward value processing in the brain. *Progress in Neurobiology*. 127-128, pp.64-90.

Rolls, E.T. 2020. The texture and taste of food in the brain. *Journal of Texture Studies*. 51(1), pp.23-44.

Sánchez-Obando, J.-D., Cabrera-Trujillo, M.A., Olivares-Tenorio, M.-L. and Klotz, B. 2020. Use of optimized microparticulated whey protein in the process of reduced-fat spread and petit-suisse cheeses. *LWT*. 120, p108933.

Santosa, H., Zhai, X., Fishburn, F. and Huppert, T. 2018. The nirs brain analyzir toolbox*. Algorithms.* 11(5), p73.

Sarkar, A., Kanti, F., Gulotta, A., Murray, B.S. and Zhang, S. 2017. Aqueous lubrication, structure and rheological properties of whey protein microgel particles. *Langmuir.* 33(51), pp.14699-14708.

Sarkar, A. and Krop, E.M. 2019. Marrying oral tribology to sensory perception: A systematic review. *Current Opinion in Food Science*. 27, pp.64-73.

Schiffman, S.S., Suggs, M.S., Sostman, L. and Simon, S.A. 1992. Chorda tympani and lingual nerve responses to astringent compounds in rodents. *Physiology & Behavior.* 51(1), pp.55-63.

Schmidt, J.M., Damgaard, H., Greve-Poulsen, M., Sunds, A.V., Larsen, L.B. and Hammershøj, M. 2019. Gel properties of potato protein and the isolated fractions of patatins and protease inhibitors – impact of drying method, protein concentration, ph and ionic strength. *Food Hydrocolloids*. 96, pp.246-258.

Schöbel, N., Radtke, D., Kyereme, J., Wollmann, N., Cichy, A., Obst, K., Kallweit, K., Kletke, O., Minovi, A., Dazert, S., Wetzel, C.H., Vogt-Eisele, A., Gisselmann, G., Ley, J.P., Bartoshuk, L.M., Spehr, J., Hofmann, T. and Hatt, H. 2014. Astringency is a trigeminal sensation that involves the activation of g protein–coupled signaling by phenolic compounds. *Chemical Senses.* 39(6), pp.471-487.

Sim, S.Y.J., SRV, A., Chiang, J.H. and Henry, C.J. 2021. Plant proteins for future foods: A roadmap. *Foods*. 10(8), p1967.

Smith, A.K., June, H. and Noble, A.C. 1996. Effects of viscosity on the bitterness and astringency of grape seed tannin. *Food Quality and Preference*. 7(3), pp.161-166.

Soares, S., Mateus, N. and de Freitas, V. 2012. Interaction of different classes of salivary proteins with food tannins. *Food Research International*. 49(2), pp.807-813.

Soares, S., Vitorino, R., Osório, H., Fernandes, A., Venâncio, A., Mateus, N., Amado, F. and de Freitas, V. 2011. Reactivity of human salivary proteins families

toward food polyphenols. *Journal of Agricultural and Food Chemistry*. 59(10), pp.5535-5547.

Stribiţcaia, E., Evans, C.E.L., Gibbons, C., Blundell, J. and Sarkar, A. 2020. Food texture influences on satiety: Systematic review and meta-analysis*. Scientific Reports.* 10(1), p12929.

Tanger, C., Utz, F., Spaccasassi, A., Kreissl, J., Dombrowski, J., Dawid, C. and Kulozik, U. 2022. Influence of pea and potato protein microparticles on texture and sensory properties in a fat-reduced model milk dessert. *ACS Food Science & Technology*. 2(1), pp.169-179.

Testing, A.S.f. and Materials. 1983. Annual book of astm standards: Nonferrous metal products. Die-cast metals; aluminum and magnesium alloys. In: Astm.

Tulbek, M.C., Lam, R.S.H., Wang, Y., Asavajaru, P. and Lam, A. 2017. Chapter 9 - pea: A sustainable vegetable protein crop. In: Nadathur, S.R., et al. eds. Sustainable protein sources. San Diego: Academic Press, pp.145-164.

Upadhyay, R., Brossard, N. and Chen, J. 2016. Mechanisms underlying astringency: Introduction to an oral tribology approach. *Journal of Physics* D: *Applied Physics*. 49(10), p104003.

Vlădescu, S.-C., Agurto, M.G., Myant, C., Boehm, M.W., Baier, S.K., Yakubov, G.E., Carpenter, G. and Reddyhoff, T. 2023. Protein-induced delubrication: How plant-based and dairy proteins affect mouthfeel. *Food Hydrocolloids*. 134, p107975.

Wang, Y., Tuccillo, F., Lampi, A.-M., Knaapila, A., Pulkkinen, M., Kariluoto, S., Coda, R., Edelmann, M., Jouppila, K., Sandell, M., Piironen, V. and Katina, K. 2022. Flavor challenges in extruded plant-based meat alternatives: A review. *Advances in food and nutrition research.* 21(3), pp.2898-2929.

War, A.R., Paulraj, M.G., Ahmad, T., Buhroo, A.A., Hussain, B., Ignacimuthu, S. and Sharma, H.C. 2012. Mechanisms of plant defense against insect herbivores. *Plant Signal Behav*. 7(10), pp.1306-1320.

Wood, J.N. and Grafman, J. 2003. Human prefrontal cortex: Processing and representational perspectives. *Nature Reviews Neuroscience*. 4(2), pp.139-147.

Xu, X., Sharma, P., Shu, S., Lin, T.-S., Ciais, P., Tubiello, F.N., Smith, P., Campbell, N. and Jain, A.K. 2021. Global greenhouse gas emissions from animal-based foods are twice those of plant-based foods. *Nature Food.* 2(9), pp.724-732.

Young, V.R. and Pellett, P.L. 1994. Plant-proteins in relation to human protein and amino-acid nutrition. *American Journal of Clinical Nutrition*. 59(5), pp.1203S-1212S.

Zheng, Y.X., Gao, Y.X., Sun, C.X., Zhao, Y.G., Cao, Y.P., Lu, W., Guo, Z.B. and Fang, Y.P. 2023. Amyloid fibrils-regulated high-moisture extruded soy proteins: Texture, structure, and taste. *Food Hydrocolloids*. 144, article no: 109026 [no pagination].

Zhu, Y., Thaploo, D., Han, P. and Hummel, T. 2023. Processing of sweet, astringent and pungent oral stimuli in the human brain. *Neuroscience*. 520, pp.144-155.

Chapter 5 : Transforming sustainable plant proteins into high performance lubricating microgels[3]

Abstract

With the resource-intense meat industry accounting for over 50% of food-linked emissions, plant protein consumption is an inevitable need of the hour. Despite its significance, the key barrier to adoption of plant proteins is their astringent off-sensation, typically associated with high friction and consequently poor lubrication performance. Herein, we demonstrate that by transforming plant proteins into physically cross-linked microgels, it is possible to improve their lubricity remarkably dependent on their volume fractions as evidenced by combining tribology using biomimetic tongue-like surface with atomic force microscopy, dynamic light scattering, rheology and adsorption measurements. Experimental findings which are fully supported by numerical modelling reveal that these non-lipidic microgels not only decrease boundary friction by an order of magnitude as compared to native protein but also replicate the lubrication performance of a 20:80 oil/water emulsion. These plant protein microgels offer a much-needed platform to design the next-generation of healthy, palatable and sustainable foods.

5.1 Introduction

There is arguably no bigger existential challenge to food scientists than ensuring the security of safe, affordable, palatable, healthy and environmentally-sustainable nutrients to feed the growing human population, achieving the United

---

[3] Published as: Kew, B., Holmes, M., Liamas, E. et al. Transforming sustainable plant proteins into high performance lubricating microgels. Nat Communications 14, 4743 (2023).

Nations' Sustainable Development Goals (SDGs) to help alleviate the perils of hunger while respecting the planet's environmental boundaries. Global greenhouse gas (GHG) emissions from the production of food has been estimated to be >18 Gt CO2eq yr−1 (one-third of the total human-caused GHG emissions (Crippa et al., 2021)), of which those produced by animal-based foods (57%) have been calculated to be nearly twice as those of plant-based foods (29%) (Xu et al., 2021). To ensure continued supply of safe, pleasurable and healthy food, while reducing net GHG emissions, the transition from animal to plant-based foods is a much-needed endeavour. As a result, food manufacturers have reacted by incorporating and increasing plant proteins in their food products. However, adoption of plant proteins at a population scale is restricted and require vast time-scales in product development due to their sensorial-functionality issues (Kew et al., 2020; Cosson et al., 2021; Liu, Y. et al., 2021). It is now well-evidenced that one of the primary barriers to adoption of plant protein is their negative "astringent" i.e. dry, puckering, non-juicy perception. Oral lubrication has shown to be crucial to understand, and serves as a well-acknowledged in-vitro proxy for quantifying friction-related mouthfeel characteristics (Sarkar and Krop, 2019). Multiscale tribology measurements across laboratories supported by sensory trials have revealed that plant proteins increased oral friction due to particle-like protein-protein aggregation and jamming as well as interaction with saliva, in contrast to dairy proteins (Kew et al., 2021; Zembyla et al., 2021; Liamas et al., 2023; Pang et al., 2023; Vlădescu et al., 2023). Such lubrication failure or "delubrication" (Vlădescu et al., 2023) highlights a major issue if plant proteins are to be used instead of conventional animal proteins, incurring adverse textural modifications and development of these astringent, drying characteristics would reduce consumer acceptability of plant protein-rich foods. For instance, it is the

boundary lubrication behaviour governed by coalescence of fat, which generates desirable low-friction creamy mouthfeel (Dresselhuis et al., 2007) whilst in non-lipidic, fat mimetics, hydration lubrication and molecular ball-bearing mechanisms (Liu, K. et al., 2016b) are often cited to be the key mechanisms to achieve optimal lubrication performance (Kew et al., 2021).

Proteins themselves have also been attempted as a fat mimetic for producing greater satiety, lower calorie foods. With less than half the calories of fat per gram (4 kcal vs 9 kcal) offering highest satiety per calorie (Veldhorst et al., 2008), as well as viscosity enhancing properties, proteins are ideal macronutrients to substitute fat, however, the lack of understanding and maximising in lubrication performance has become the major limitation. Of recent considerable interest for fat mimetics and the improved texture of proteins are the creation of protein microgel structures. Protein microgels, are crosslinked, swollen, percolating protein networks which are sheared down to discrete micron- or nanometric-sized soft colloidal particles. These microgels mostly consist of water (85-95%) by weight with moduli ranging from 0.1 – 10 kPa (Sarkar et al., 2017). Animal protein-based, polysaccharide as well as synthetic microgels such as whey protein-based, polyacrylic acid-based and carrageenan-based microgels have demonstrated varying degree of lubricity (de Vicente et al., 2006; Garrec and Norton, 2013; Andablo-Reyes et al., 2019) depending upon volume fraction and elasticity of particles entrained in the contact. Often such lubrication mechanism has been governed by viscosity modification with microgels acting as physical surface separators (Garrec and Norton, 2013; Andablo-Reyes et al., 2019) or by so-called (often debated) ball bearing mechanisms (Liu, K. et al., 2016a; Liu, K. et al., 2016b). Nevertheless, protein-based fat mimetic research has been largely restricted to dairy proteins, with rare attention being given to plant proteins (Kew

et al., 2020). With the intense pressure to replace animal proteins with more sustainable, ethical, hypoallergenic proteins, plant proteins are occupying the research landscape rapidly and methods to improve performance in food is needed to avoid unacceptability and associated food wastage. Additionally, plant proteins also face intra-variability within the protein type, where both natural climate conditions and industrial processing can result in non-standardised proteins with a range of poor solubility, limited functionality and poor hydrating ability (Lam et al., 2018; Ma et al., 2022) resulting in oral dryness. These present major challenges for plant proteins to be used as a food ingredient where microgelation can be a much-needed structuring platform to standardize and overcome these oral frictional hurdles, which is the key question this study answers. Therefore, lubrication evidences on microgelation of plant proteins are imperative before such microgels can be applied as a highly functional, pleasurable ingredient for designing next generated plant protein-reformulated foods (Sim et al., 2021).

Herein, we demonstrate using a combination of experimental and theoretical approaches that engineering physically cross-linked, soft, sub-micron sized plant-based microgels offers higher lubrication performance as compared to their parent native protein counterparts. Remarkably, these fabricated microgels allow an order of magnitude reduction in boundary frictional forces as compared to the proteins. Using a complementary suite of techniques such as rheology, tribology, adsorption using quartz crystal microbalance with dissipation monitoring (QCM-D), dynamic light scattering (DLS), atomic force microscopy (AFM) and mathematical modelling, we show that such microgelation of plant proteins renders lubricity similar to that of an oil/water (O/W) emulsion without using any additional lipidic substance. To aid a more accurate *in vivo* prediction of oral

surface induced frictional behaviour, a biomimetic 3D tongue-like surface with similar deformability, topography and surface wettability to that of real human tongue was utilised for tribological measurements. These designed plant-based microgels provide a platform of food ingredients to enhance palatability and functionality, thus, the improved design of next generation protein-based, healthy, tasty and sustainable diets in order to accelerate the transition to plant-based foods.

5.2 Methods

5.2.1 Materials

Pea protein concentrate (PPC, Nutralys S85 XF) containing 85% protein was kindly gifted by Roquette (Lestrem, France). Potato protein isolate (PoPI) was purchased from Guzmán Gastronomía (Barcelona, Spain) containing 91% protein. Sunflower oil was purchased from a local supermarket (Morrison's) and used without further purification. HEPES (4-(2-hydroxyethyl)-1-piperazineethanesulfonic acid) were purchased from Fisher Scientific, UK. The solvent used was Milli-Q water (purified using Milli-Q apparatus, Millipore Corp., Bedford, MA, USA). Atomic force microscopy (AFM) cantilevers (HQ:CSC37/tipless/Cr–Au) were purchased from Windsor Scientific Ltd, UK. For creating the 3D-tongue like biomimetic surface with human tongue-like deformability, wettability and spatial distribution, size and shape of filiform and fungiform papillae, a similar procedure to that of Andablo-Reyes et al. (2020) was followed where Ecoflex 00-30 kit was purchased from Smooth-on Inc (Pennsylvania, U.S.A.) and the two components mixed in 1:1 w/w ratio with the wettability modified by adding 0.5 wt% Span 80, purchased from Sigma-Aldrich (Dorset, U.K.). Mixing and degassing was performed using Thinky Planetary mixer system ARE-250, intertronics (Kidlington, U.K.) using a mixing cycle of 2

min at 2,000 rpm followed by 1 min degassing at 2,200 rpm. 3D printed tongue moulds were created from a Perfactory P3 mini 3D printer model (EnvisionTEC, Dearborn, U.S.A.) and used to cast a 2 cm × 2 cm 3D biomimetic tongue-like surface. All solutions were prepared from analytical grade chemicals unless otherwise mentioned.

5.2.2 Preparation of plant protein microgels

Aqueous dispersions of plant protein microgels were prepared based on a similar procedure as described previously (Sarkar et al., 2016). By thermal processing-induced disulphide crosslinking of proteins to form gels followed by shearing. Aqueous solutions of PPC (15.0 wt% total protein), PoPI (5.0 wt% total protein or 10.0 wt% total protein) and mixed PPC and PoPI (7.5 wt% and 5.0 wt% total protein, respectively) were prepared by dissolving the protein powders in 20 mM HEPES buffer at pH 7.0 for 2 h to ensure complete solubilisation. For samples undergoing microgelation, the aqueous protein dispersions were subsequently heated at 80 ^{o}C for 30 min and cooled in a cold water bath followed by storage at 4 ^{o}C overnight to form the thermally-crosslinked protein gels. These protein hydrogels were broken down using a hand blender (HB711M, Kenwood, UK) dispersed in HEPES buffer (70 vol%) for 5 min. These macrogel particle dispersions were degassed using Thinky Planetary mixer at 2,200 rpm for 1 min. Protein dispersions were then passed through the PANDA homogeniser (Panda Plus 2000, GEA Niro Soavi Homogeneizador Parma, Italy) three times through a two-stage valve homogeniser operating at first/ second stage pressures of 250/ 50 bars. The resultant protein microgels are termed as PPM15, PoPM5, PoPM10, PPM7.5:PoPM5. Microgels were prepared multiple times to obtain at least three repeat measurement in analysis.

Volume fraction of microgels were calculated using equation (5.1):

$$\boldsymbol{vol}\% = \frac{\boldsymbol{wt}\%}{\boldsymbol{\rho}} = \frac{\boldsymbol{x}}{(\boldsymbol{x}+\boldsymbol{y})\,\boldsymbol{\rho}}\ \mathbf{x\ 100}\% \tag{5.1}$$

where, ρ is the density of the gel, x is the weight of the gel and y is the weight of the buffer. To obtain solutions of lower volume fractions (10–60 vol %), 70 vol% of the protein microgels were diluted with HEPES buffer at pH 7.0.

5.2.3 Preparation of 20:80 oil in water emulsion

Potato protein (1.5 wt%) was dissolved in Milli-Q water with continuous mixing for 2 h. Subsequently, sunflower oil was added in a ratio of 20:80 w/w oil to aqueous phase containing protein. The mixture was subjected to mixing in the Ultra Turrax (Janke & Kunkel, IKA-Labortechnik) at 9,400 rpm for 2 min, and then immediately passed (2 passes) through a two-stage valve homogenizer (Panda Plus 2000; GEA Niro Soavi Homogeneizador Parma, Italy) operating at pressures of 300 bars, respectively, droplet size distribution of the emulsion is provided in Appendix D Figure D10. O/W emulsion were prepared multiple times to obtain at least three repeat measurement in analysis.

5.2.4 Particle and droplet size and stability measurements

The mean hydrodynamic size (d_H) of the protein microgels were measured utilising dynamic light scattering (DLS) (Zetasizer Ultra, Malvern Instruments Ltd, Worcestershire, UK). The protein microgels were introduced into the Zetasizer in DTS0012 disposable cuvettes (PMMA, Brand Gmbh, Wertheim, Germany). The refractive index (RI) was set at 1.5 with an absorption of 0.001. The samples were equilibrated for 120 s and measured at 25 ^{o}C using non-invasive backscattering technology at a detection angle of 173 ^{o}. The particle size of the microgels were also measured as a function of storage time every week for several months (data shown until 28 days) when stored at 22 ^{o}C and also when subjected to food

processing (90 ^{o}C for 30 min). Droplet size distributions of emulsions were measured using static light scattering at 25 ^{o}C using Malvern Mastersizer 3000 (Malvern Instruments Ltd, Malvern, Worcestershire, UK). The mean particle size was reported as volume mean diameter (d_{43}). Means were calculated from six measurements on three independent samples.

5.2.5 Atomic force microscopy

Dispersions of pea protein microgel (PPM15), potato protein microgel (PoPM5), potato protein microgel (PoPM10), and mixed pea and potato protein microgel (PPM7.5:PoPM5) were diluted by a factor of 1:50 v/v using 20 mM HEPES buffer solution at pH 7.0, deposited (100 µL) onto new, clean but untreated silicon wafers, and were allowed to adsorb for 10 min. Subsequently, to remove non-adsorbed microgels that could adhere onto the AFM tip, the solution was exchanged 5 times with 100 µl 20 mM HEPES buffer using a pipette while ensuring that the sample was kept constantly hydrated. Finally, the samples were transferred to an AFM for imaging. Topographic images were acquired using a Bruker Multimode 8 AFM equipped with a Bruker Nanoscope V controller. The plant protein microgels were imaged in contact mode, using silicon nitride AFM cantilevers (model MLCT-BIO-DC, Cantilever C) with a nominal spring constant of 0.01 N/m, purchased from Bruker AFM probes (Camarillo, CA). AC modes such as 8 kHz liquid tapping or 110 kHz FastScan-D tapping, or Peak Force tapping at 1-8kHz that would preferably be used on delicate samples fail, probably due to instability and induced oscillations of the soft microgel material. The microgels are hugely sensitive to setpoint, with only a 50 pN window between lifting away from the surface, and disturbing/sweeping the microgels from the surface, necessitating use of the thermally stablilised MLCT-BIO-DC probe. Slow line rates of 0.5-0.8 Hz and gains at the very upper limits of stability were

necessary to track the microgels with minimum disturbance. The measurements were performed at room temperature, using a fluid cell loaded with 20 mM HEPES buffer at pH 7.0. Images were acquired at 1024-1560 pixel resolution and processed using Bruker Nanoscope Analysis v3.0. Particle sizes from AFM images were measured using ImageJ-FIJI (NIH). After 2nd order flattening using masking, the images were 3x3 median filtered in Nanscope Analysis, then thresholded and converted to binary in ImageJ, and the binary image cleaned using the 'OPEN' function, which performs a dilate and erode operation. Finally, the particles were measured for area, position and length of the major and minor axis from a fitted ellipse. Particle diameters were calculated from the area, $d = 2\sqrt{(A/\pi)}$. Diameters were also calculated from the average of major and minor axes, and the values found were virtually identical to the first method. Several thousand microgels were analysed for each sample to obtain robust statistical analysis of size and shape.

5.2.6 Small deformation rheology

Viscoelasticity of the protein hydrogels was investigated by oscillatory shear rheology using modular compact rheometer (MCR-302 Anton paar, Austria) with a cone-and-plate geometry (CP50-1, diameter: 50 mm, cone angle: 1^{o}) at 37 ^{o}C. The setup was initialized with a 0.208 mm gap between cone and plate with use of silicon oil around the cone geometry to prevent evaporation of the sample. Elastic (*G'*) and viscous (*G''*) moduli were measured by applying 0.01-10% strain at 1.0 Hz on the systems to determine linear viscoelastic region. A temperature ramp was performed to understand gelation characteristics and to gel the protein samples for frequency sweep, samples were heated (25-80 ^{o}C, rate of 0.08 ^{o}C/ s) at a constant strain of 0.1% at 1 Hz and held at 80 ^{o}C for 30 min, the temperature was reduced to 37 ^{o}C and frequency sweep of 1 – 100 Hz

at a strain of 0.1% initiated. Means were calculated from six repeat measurements. Flow curves of sheared protein hydrogels after passing through homogenizer i.e. the aqueous dispersions of the resultant protein microgels at a volume fraction of 10-70 vol% were measured at 37 ^{o}C using a stress-controlled rheometer (Paar Physica MCR 302, Anton Paar, Austria) equipped with a concentric cylinder geometry (inner diameter of the cup is 24.5 mm and diameter of the bob is 23 mm). Mean shear rates of 1 s^{-1} to 1000 s^{-1} were measured six times from three replicates of each sample.

5.2.7 Large deformation rheology

Force distance curves of parent protein gels were measured using Texture Analyzer (TA-TX2, Table Micro Systems Ltd., Surrey, UK) attached with a 50 kg load cell. Samples were compressed using cylindrical probe (59 mm) at room temperature (22 ^{o}C) at a constant speed of 1 mm/s and deformation level set at 80% strain. A minimum of three replicates were measured for each parent plant protein gel sample in duplicate.

5.2.8 Tribology

Tribological experiments were carried out using a tribology-cell attachment to the rheometer utilising steel ball (R = 7.35 mm) on three polydimethylsiloxane (PDMS) pins (6 mm height) inclined at 45^{o} forming a steel ball-PDMS (hard-soft) contact. Samples were added in an enclosed chamber covering PDMS pins with steel ball geometry applying an evenly distributed load of 2.0 N. Upwards sliding speeds of 0.001-1.0 m/s were measured with pins remaining stationary generating three-sliding point contact. Measurements were performed at 37 ^{o}C with μ of HEPES measured as control. PDMS pins were cleaned using isopropanol then sonication in detergent for 10 min. Pins were replaced following signs of surface wear. A minimum of 6 measurements were carried out for

triplicate samples. Load dependency experiments were performed on pea protein microgels (volume fraction = 70 vol%), native pea protein and O/W emulsion using same protocol using increasing loads ranging from 2.0 to 10.0 N.

In addition to the conventional tribology using hard-soft contacts surface, tribology was also performed using 3D biomimetic tongue-like similar to previous methodology (Andablo-Reyes et al., 2020) using a Kinexus Ultra+ rotational rheometer (Malvern Instruments, Malvern U.K.) equipped with 50 mm diameter stainless steel plate-on-plate geometry. The tongue-like soft, rough and hydrophilic surface was glued at the rim of the top plate forming a steel-elastomer contact. Experiments were performed in normal force (F_N) control and shear rate control mode. Normal force was 1.0 N with shear rates ranging from 0.005 to 1.0 s^{-1}. Friction coefficient μ was calculated using torque values following equation (5.2):

$$\boldsymbol{\mu = \frac{M}{RF_N}} \tag{5.2}$$

where, R is the plate radius (R = 0.025 m). Friction coefficient (μ) is presented as a function of the linear speed V_R at the rim of the plate and is calculated by $V_R = \Omega R$, where Ω is the angular speed.

5.2.9 Adsorption

Adsorption behaviour of plant protein microgel were measured using quartz crystal microbalance with dissipation monitoring (QCM-D, E4 system, Q-Sense, Biolin Scientific, Sweden). Using a similar procedure to (Zembyla et al., 2021), silicon sensors coated with PDMS were prepared by spin-coating (QSX-303, Q-Sense, Biolin Scientific, Sweden) with a solution of 0.5 wt% PDMS in toluene at 5000 rpm for 30 s with an acceleration of 2500 rpm/s, before leaving overnight in a vacuum oven at 80 °C. Before use, PDMS-coated crystals were further cleaned

by immersing in toluene for 1 min, then 1 min in isopropanol and a final immersion in Milli-Q for 5 min before being dried using nitrogen gas.

Protein solutions were made at a volume fraction of 1 vol% and were equilibrated in buffer at (25 °C) before measurement. The flow rate was controlled using peristaltic pump at a rate of 100 µL/min at 25 °C. HEPES buffer solution was initially injected to obtain a stable baseline reading and then the prepared protein solutions were injected until equilibrium adsorption *i.e.* no change in frequency (*f*) or dissipation (*D*) was recorded. Finally, the buffer was used once more to remove any non-adsorbed protein microgels. Hydrated mass was calculated from the frequency data using viscoelastic Voigt's model (Voigt, 1889) using “Smartfit Model” by Dfind (Q-Sense, Biolin Scientific, Sweden) software. The 3^{rd}, 5^{th}, 7^{th} and 11^{th} overtones was taken into account for data analysis and only 5^{th} overtone is shown in the results. A minimum of three replicates were measured for each protein sample in duplicate.

5.2.10 Statistical analysis

All results are reported as means and standard deviations on at least three measurements carried out on three independent samples prepared on separate days. Statistical analysis on the significance between data sets was calculated using analysis of variance (ANOVA) with Tukey post hoc test, significance level $p<0.05$. All model calculations were performed using R version 4.1.0 (2021-05-18), model parameters were estimated using non-linear solvers in the packages nlstools, nls2 and minpack.

5.3 Results

5.3.1 Structure of microgels across scales.

Initially the size, morphology and stability of the plant protein microgels were investigated. This study utilised pea protein and potato protein as typical exemplar plant proteins which take the form of globular multimer storage proteins. Pea proteins are composed mostly of 11S and 7S globulins (S. Tomoskozi, 2001) and frequently reported for being of limited aqueous solubility (S. Tomoskozi, 2001; Lam et al., 2018; Kew et al., 2021) result in high friction and sensorial astringency (Tanger et al., 2022; Vlădescu et al., 2023). On the other hand, potato proteins are composed of globular, glycoprotein *i.e.* patatins (Waglay et al., 2014), with comparatively higher fractions of soluble protein (Waglay et al., 2014; Schmidt et al., 2019; Kew et al., 2021) but still suffer from astringency issues(Kew et al., 2021; Tanger et al., 2022) due to high surface hydrophobicity (Mao et al., 2020). A blend of the proteins were also investigated to determine any synergistic or detrimental effect on lubricity. The latter approach also provides a way to enhance the amino acid profile of possible formulations through protein complementation, a crucial consideration in non-animal protein diets (Dimina et al., 2022). Four types of microgels were fabricated utilising a top-down methodology involving thermal gelation-induced physical crosslinking of these otherwise sedimenting (Appendix D Figure D1) plant proteins resulting in a percolating, viscoelastic protein-based hydrogels followed by controlled shearing into microgels (**Figure 5.1**, see detailed preparation in method section). In order to attain different elasticities of these microgels, which are known to be important in lubrication (Andablo-Reyes et al., 2019), and the high protein concentrations typically found in tribology studies involving high levels of friction (Kew et al., 2021), the concentration of the solutions was adjusted to promote gel formation with varying properties which offer an opportunity to study the microgelation

process and its effectiveness for lubrication in plant proteins (see details in method section).

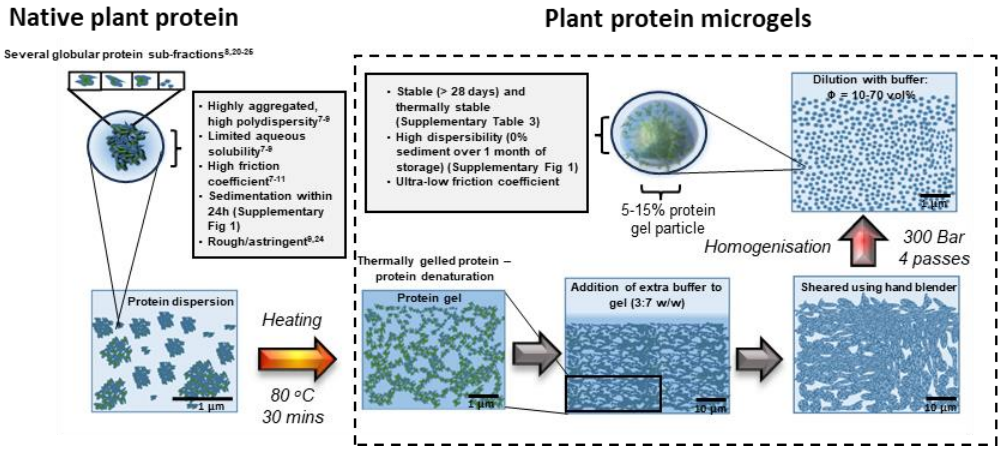

Figure 5.1 Visual representation of microgelation procedure. Native plant proteins are highly aggregated causing functional and sensory problems in food design. By hydrating them with water and thermally gelling using hydrophobic interactions, hydrogen bonding and disulphide-based covalent crosslinking occurring without any added crosslinking agents, the native plant proteins act as connecting particulate points in a highly percolating hydrogel network, which is then converted into gel-like particles via controlled homogenisation consisting of 5–15 wt% protein and 85–95 wt% water. These microgels remove functional issues associated with native protein allowing for improved functional application of plant proteins in food.

Microgels fabricated using pea protein concentrate (15.0 wt% total protein, PPM15), potato protein isolate at two concentrations (5.0 and 10.0 wt% total protein PoPM5, PoPM10) and a mixed plant protein (pea protein concentrate 7.5 wt% total protein, potato protein isolate 5.0 wt% total protein , PPM7.5:PoPM5) at volume fractions (Φ) 10-70 vol% are shown in **Figure 5.2a**. We find, as expected, an increase in opacity with higher Φ (**Figure 5.2a**), especially true for microgels able to scatter more light thanks to their larger hydrodynamic diameter (d_H), as obtained using dynamic light scattering (DLS) (**Figure 5.2b**). The brown pigmentation from potato aromatics (Akyol et al., 2016) and orange hue from pea

is not surprising and results from the presence of natural carotenoids (Ashokkumar et al., 2014a). At the nanoscale, microgels can be described as soft, gel-bead like particles 100-1000 nm in size with an ability to swell or deswell in altered solvent conditions. These gelled particles are likely to consist of a hydrated protein core with an hydrated “water-reservoir” like shell as a result of a concentration gradient of protein-water from the core to the outer surface of the microgel that displaying diffuse brush topography with protrusions from the core(Sarkar et al., 2017) (**Figure 5.1**).

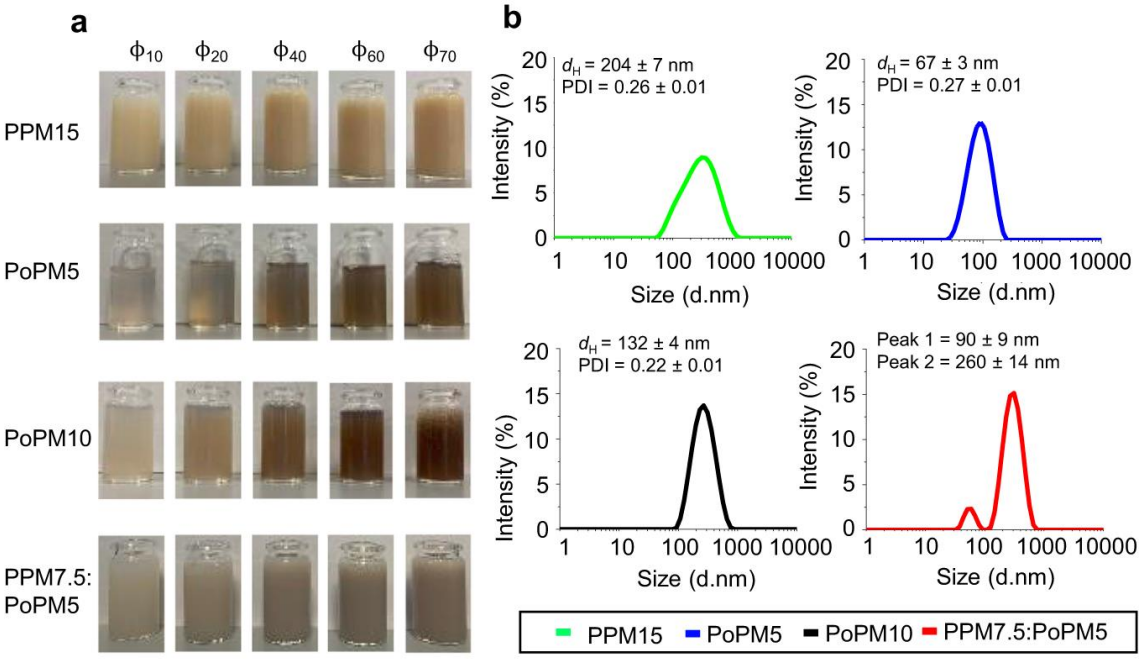

Figure 5.2 Visual images (a) showing various degrees of opacity and size distribution obtained using dynamic light scattering (DLS) (b) using pea protein concentrate to form a 15.0 wt% total protein microgel, (PPM15), potato protein isolate to form a 5.0 wt% total protein microgel (PoPM5), potato protein isolate to form a 10.0 wt% total protein microgel, (PoPM10), and using a mixture of pea protein concentrate at 7.5 wt% total protein and potato protein isolate at 5.0 wt% total protein microgel (PPM7.5:PoPM5) at volume fractions (ϕ) 10–70 vol%, at 25.0 °C. Insets in (b) shows the mean hydrodynamic diameter (dH) and polydispersity index (PDI) values. Results are plotted as average of six measurements on triplicate samples ($n = 6 \times 3$).

Individual microgels (PPM15, PoPM5, PoPM10) display d_H ranging from 67 to 204 nm possessing low polydispersity index (PDI) in contrast with the mixed microgels (**Figure 5.2b**), PPM7.5:PoPM5 which show two distinct peaks where the peak < 100 nm likely represents the potato protein system. This is likely due to the different denaturation temperatures with potato protein gelling at 60 °C (Schmidt et al., 2019) and pea at > 85 °C (Liang and Tang, 2013) the proteins do not complex into one microgel remaining as separate microgel entities perhaps with minor sub-unit complexation as d_H remain similar to individual microgels. Such d_H values are typical to other reported microgels from both animal and plant protein-based sources (Andablo-Reyes et al., 2019; Araiza-Calahorra and Sarkar, 2019; Zhang et al., 2020; Aery et al., 2023) with their differences in size dependant on protein size, solubility and water holding capacity. When comparing to native proteins *i.e.* non-microgelled plant protein isolates/ concentrates, these often produce more variation in size as they are highly polydisperse, aggregated and may need filtering due to sedimentation (Kew et al., 2021; Liamas et al., 2021). For instance, microgels even after a month of storage show no sedimentation in comparison to the non-microgelled counterparts that sediment within few hours (Appendix D Figure D1) where there is little change in particle size (Appendix D Table D1). Even when the microgels were further processed such as those simulating food processing (*e.g.* thermally treated at 90 °C for 30 min), no marked change was observed in hydrodynamic diameter or polydispersity index (Appendix D Figure D2) highlighting the excellent thermodynamic stability of these microgels.

To investigate microgel morphology in more detail, atomic force microscopy (AFM) was employed to image fully hydrated microgels, shown in Fig

3 with corresponding particle size distributions. All microgels are in the same general size range of 50-200 nm as found by DLS. (**Figure 5.2b**).

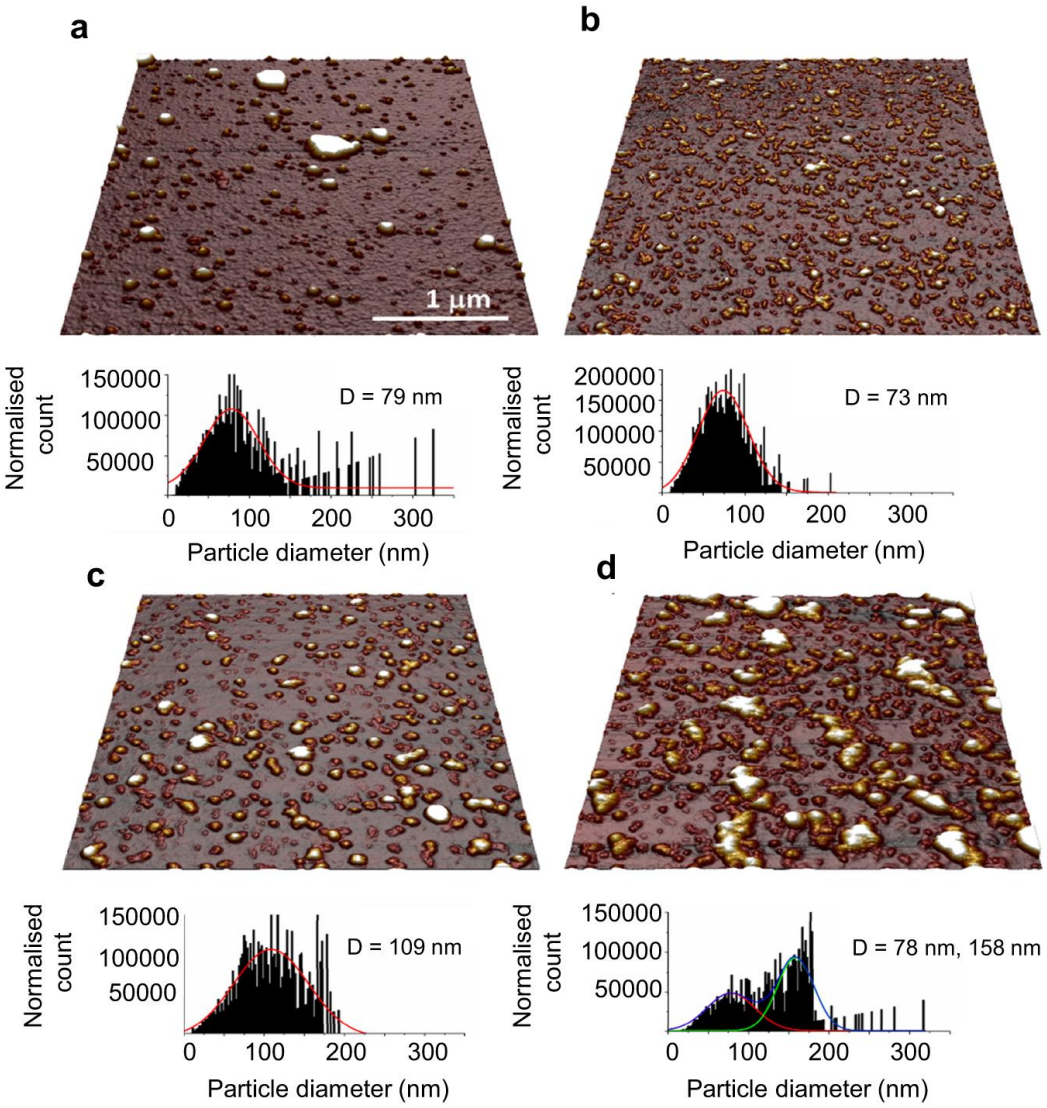

Figure 5.3 Topographic images and respective histograms showing diameters of aqueous dispersions of protein microgels prepared using (a) pea protein concentrate to form a 15.0 wt% total protein microgel, (PPM15), (b) potato protein isolate to form a 5.0 wt% total protein microgel (PoPM5), (c) potato protein isolate to form a 10.0 wt% total protein microgel, (PoPM10), and (d) a mixture of pea protein concentrate at 7.5 wt% total protein and potato protein isolate at 5.0 wt% total protein to form microgel (PPM7.5:PoPM5).

The mixed PPM:PoPM (**Figure 5.3d**) system displays two distinctly sized population of microgels which could be the result of sub-unit protein complexes forming from pea and potato protein as discussed previously in DLS. PoPM5 (**Figure 5.3b**) is remarkably similar in size in both techniques, 67 nm (DLS) vs 73 nm (AFM). In the other samples the AFM size was slightly smaller than DLS; for PoPM10 (**Figure 5.3c**) the diameters DLS:AFM were 132 nm:109 nm, and for the mixed PPM:PoPM were 90 nm: 78 nm for the first peak, and 260 nm: 158 nm for the second. This reduction in size can be explained by noting that the loosely structured brush-like features extends from the surface of microgels and occupies a larger hydrodynamic volume, we speculate the increased overestimation from DLS could be related to the hydration shell whilst force microscopy measures the protein core, this explains the similar size of PoPM5 and larger size of PoPM10 as more protein have an extended influence on hydrodynamic diameter. PPM15 (**Figure 5.3a**) showed a larger discrepancy, 204 nm (DLS) vs 79 nm (AFM). This could be explained by the presence of a small number of polydisperse large particles or aggregates in this sample which could skew the DLS measurement to a higher value (these aggregates were not seen in the distributions of PoPM5 and PoPM10) or show the presence of a highly hydrated shell spanning far from the core. Shape analysis (Appendix D Figure D2) showed the majority of particles were spherical or near spherical with an aspect ratio < 2:1, although with increasing aspect ratio with size, which is probably explained by the larger particles being aggregates. Overall microgels take on a smooth and spherical shape showing convexed spreading on the surface (**Figure 5.3a-d**) which has also been observed for synthetic and whey protein microgels in previous studies (Aufderhorst-Roberts et al., 2018; Andablo-Reyes et al., 2019).

5.3.2 Viscosity of microgels.

Microgels are cited in literature as viscosity modifiers with range of thinning/ thickening behaviour (Shewan and Stokes, 2013) with the ability to influence lubrication performance particularly in the fluid film regimes by altering viscosity as perceived at the macroscale (Andablo-Reyes et al., 2019). Before characterising viscosity, it is nevertheless important to understand the stiffness of the microgels which may influence their viscous dissipation such that higher storage modulus (G') of microgels corresponding to higher viscosities of the microgel dispersion (Andablo-Reyes et al., 2019). We assume microgels are sub-micrometric units of the parent hydrogels and thus possess the same elasticity. To quantify this, oscillatory shear rheology (see temperature ramp and frequency sweeps in Appendix D Figure D3 and D4, respectively) was performed on the parent protein hydrogels prior to shearing to obtain G' and loss (G'') modulus (**Figure 5.4a**) and large scale deformation tests were performed (Appendix D Figure D5) to calculate the Young's modulus (**Figure 5.4b**). Typically, the higher the protein content of the microgel, the higher the G'. For instance, G' of the parent gels for PoPI5 (~800 Pa), was an order of magnitude lower than that of PoPI10 (~8500 Pa), explaining the value of PoPM10 viscosity observed in **Figure 5.4c,d** compared to the softer, easily compressible microgels contributing to lower viscosity, which is true of PoPM5.

Most plant-based microgels in this study display Newtonian behaviour (**Figure 5.4c**) as viscosity is independent of increasing shear rates suggesting a non-interactive network of microgels from of the protein systems with the exception at Φ = 60-70% where there is a clear shear thinning nature. Particularly, in the case of PoPM10 Φ = 60-70% when compared to native protein of same protein concentration, in which a strong pseudoplastic behaviour is

observed, where particle interactions dominate and sharp increases of viscosity with increased Φ is evident (Appendix D Figure D6c). In general, such rheological behaviour of microgels is in sharp contrast to those of the native proteins where especially PoPI5.5, PoPI7.0 and PPC5.2.5:PoPI3.5 show shear thinning behaviour and an initial aggregated particle network (Appendix D Figure D6b-d). This leads us to propose an interesting conjecture, microgelation in plant proteins offer a desirable structural route to make the system much less aggregated, create a better control of size as compared to the parent protein, irrespective of their type.

The change in solution viscosity as a function of volume fraction (Φ =10-70%) is shown at low shear (**Figure 5.4c**) and orally relevant shear rates (**Figure 5.4d**). Although as expected the magnitude differs, the microgel viscosity show similar dependency on volume fraction, irrespective of shear rates (**Figure 5.4c, d**). We find in line with our expectation that as Φ increases, an increase in viscosity is observed for all microgels with PoPM10 displaying more pronounced increases at a low Φ = 40% compared to all other microgels with PoPM5 show little viscosity changes throughout.

An interesting anomaly is observed with PPM15 which despite containing the highest protein content has a low viscosity. This is explained by the modulus of PPC15 (Figs. 4a, 4b) which provides further evidence of the pea protein inability to gel effectively due to low solubility (~30%) (Kew et al., 2021)) which renders it inability to form high solvent volume microgels, a factor to be considered in protein microgel formulation. Additionally viscosity flow curves of the microgels at each volume fraction (Appendix D Figure D6) reveals further

discrepancies where PPM15 has less than half of G' of PoPM5 (**Figure 5.4a**), yet viscosity is higher in Φ =10-20 vol% and similar for other Φ. When analysing mixtures of these proteins (PPC7.5:PoPI5) both proteins are able to synergistically contribute to the structure as moduli increases vastly compared to PoPM5 and PPM15 which are both ranked as the second strongest hydrogels (**Figure 5.4a**). Strikingly, PPM15 displays close resemblance to the viscous behaviour of PPM7.5:PoPM5 (see **Figure 5.4c,d** and Appendix D Figure D6) despite having a markedly lower modulus (**Figure 5.4a,b**) ($p < 0.05$). This shows the gel structure is held primarily by the gelling of PoPM5 (**Figure 5.4b**) but when microgelled, the parent gels breaks down into two separate particles with viscosity influenced by pea protein moieties as PoPM5 has little viscosity influence (**Figure 5.4c-d**). Overall the evidence suggests that when homogenised separation of the two protein microgels from the gelled matrix occurs, which is also evident from the size distribution (**Figure 5.2b, Figure 5.3d**), therein it is clear that PPM7.5:PoPM5 result in two disparate populations of microgels.

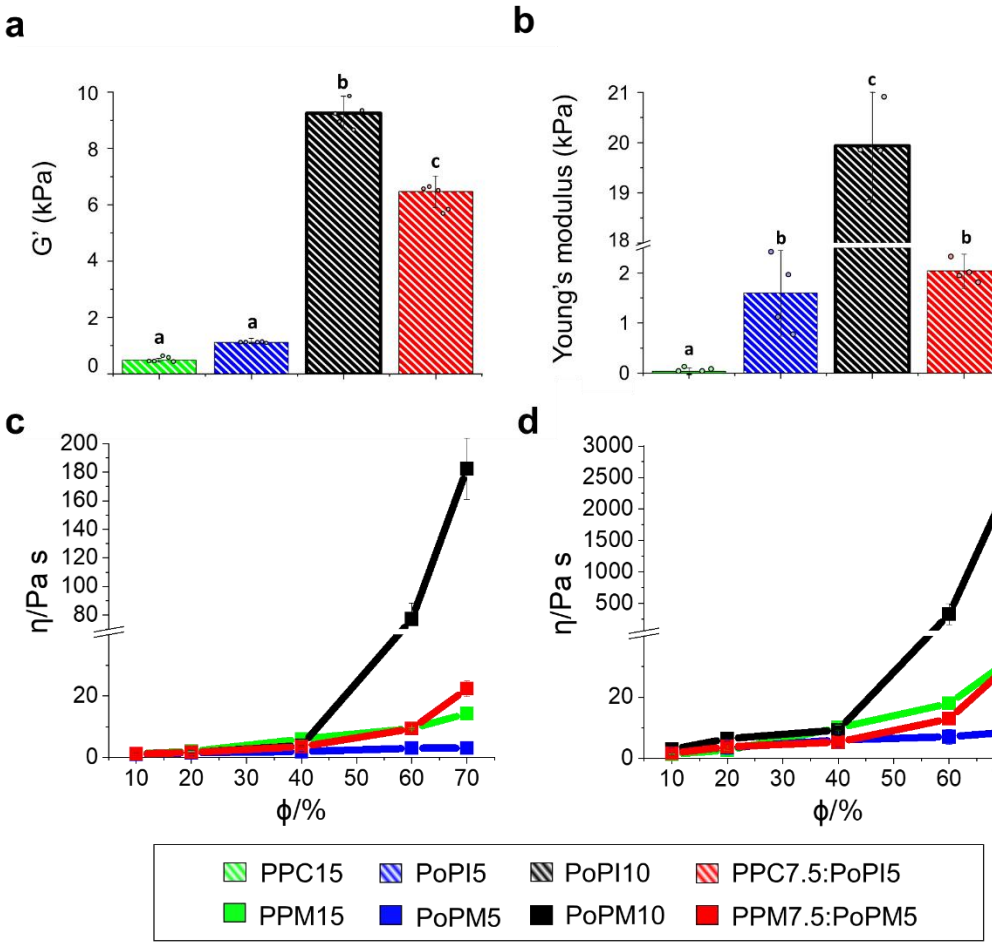

Figure 5.4 Storage modulus (a) and Young's modulus (b) of parent plant protein gels with apparent viscosities (η) of microgels prepared using pea protein concentrate to form a 15.0 wt% total protein microgel, (PPM15), potato protein isolate to form a 5.0 wt% total protein microgel (PoPM5), potato protein isolate to form a 10.0 wt% total protein microgel, (PoPM10), and using a mixture of pea protein concentrate at 7.5 wt% total protein and potato protein isolate at 5.0 wt% total protein microgel (PPM7.5:PoPM5) with corresponding storage modulus (G') of parent plant protein gels (a) as a function of volume fractions (ϕ) at pH 7.0 at shear rates of (c) 0.1 s–1 and (d) 50 s–1, the latter representing orally relevant shear rates performed at 37 °C. Data was recorded with shear rate increasing from 0.1 to 50 s–1, Figures a–b display means and standard deviations of 5 measurements on triplicate samples (n = 5 × 3) where statistical analysis was performed using two tailed unpaired Student's t-test with differing lower-case letters in the same bar chart indicate a statistically significant difference ($p < 0.05$). Figures (c,

d) shows the mean of 6 measurements on triplicate samples (n = 6 × 3) with error bars representing standard deviations. The original temperature ramp and frequency sweeps of the parent heat set gelled proteins are shown in Appendix D Figure D3 and D4, respectively. The true stress-strain curves are shown in Appendix D Figure D5 from which the Young's moduli are computed. Original flow curves for the microgel dispersions at each volume fractions are shown in Appendix D Figure D6.

For model hard spheres, a random packing limit of Φ = 64% causes a steep increase in viscosity as mobility of particles in solution is restricted. It is well known microgels do not to follow this model, instead they show such changes often at lower or higher than Φ = 64% due to their ability to swell, interpenetrate, deform and their soft nature (Bouhid de Aguiar et al., 2017). PoPM10 packing limit is met earlier, most likely due to the high content of soluble protein (100%~ solubility at pH 7 (Kew et al., 2021)) and higher modulus (see **Figure 5.4a**, **4b**) allowing for the markedly higher viscosities recorded.

In summary, the microgels convert the native proteins into much less aggregated structures and the viscosity show Φ dependency only above Φ = 40% except for PoPM5, where the viscosity is independent of Φ.

5.3.3 Tribological performance.

In the field of food soft-tribology, the friction coefficient has important connotations in respect to sensory mouthfeel. More specifically low friction coefficients have found to correlate to pleasurable smoothness, creaminess and fat like properties conversely higher values correspond to roughness, astringency and off-mouthfeel (Sarkar and Krop, 2019). Friction coefficients are used here as a measure of lubrication performance for all the created plant protein microgels (Φ = 10-70%). These measurements were compared for native protein counterparts

(equivalent protein to Φ = 70%) and a 20:80 O/W emulsion to observe both improvements in lubrication and similarities of microgel and O/W lubrication with possible effectiveness as a fat replacer determined between steel and soft PDMS surfaces (Figure 5.4, see Appendix D Table D3 for statistical comparison). The viscosity component was considered in the lubrication performance through scaling, here obtained multiplying the friction coefficient (*μ)* on the abscissa by high shear plateau viscosity at 1000 s^{-1}. For reference, original *μ* against entrainment speeds across 10^{-5} – 10^{2} is provided in Appendix D Figure D7 The buffer, native proteins and emulsions display a typical Stribeck curve, with boundary regime depicted at 0.001 Pa m, mixed regime at 0.01-0.1 Pa m and elastohydrodynamic regime at and above 1.0 Pa m. The microgels **(Figure. 5.5**) showed immediate onset of mixed regime even at very low speed x viscosity magnitude of 0.04 Pa m irrespective of the protein type or volume fractions highlighting their ultra-lubricating behaviour.

Of most importance is that in comparison to native proteins all microgels had significantly lower friction when compared at 0.1 Pa m (*p < 0.01)* and throughout the mixed regime. Remarkably PPM15 obtained more than an order of magnitude decrease in friction in comparison to native protein (*μ* = 0.006-0.01 compared to *μ* = 0.14, (*p < 0.01))* with other microgels obtaining at least a 5 fold reduction (refer to Appendix D Table D3) Additionally when comparing against O/W emulsion microgels display significantly lower friction from 0.1 Pa m through to 0.3 Pa m where here onwards all microgels Φ = 10-40% were also non-significant in lubrication (*p < 0.05*) resembling or outperforming the lubrication of the O/W emulsion (*μ* = 0.03 at 0.1 Pa m)

When comparing differences in volume fraction (**Figure 5.5a-d, 1-3**), microgels were highly efficient in decreasing friction at all Φ. The exception was PoPM10, where at Φ = 70%, significantly higher friction was exhibited than all other microgels measured at 0.1 Pa m ($p < 0.05$). This was likely due to a very high viscosity of PoPM10, which resulted in potential aggregation or jamming and consequently inability to effectively entrain between the surfaces in contact. A small but significant ($p < 0.05$) increase in friction was also observed when increasing the volume fraction from Φ = 10% to Φ = 70% for PPM15 and PPM7.5:PoPM5, which may be attributed to particle-particle adhesion. This would mean the formation of larger aggregates (Sridharan et al., 2021) as previously seen by Zembyla et al. (2021). The lowest friction amongst all samples was obtained for PPM15 at Φ = 10% (μ = 0.0057 at 0.1 Pa m) with friction coefficient half of that of other microgels at the same Φ. At Φ = 40% μ values were between 0.006–0.01 whilst at Φ = 70% all microgels achieve friction of 0.01 with the exception of PoPM10 (μ = 0.035) where despite such varied protein concentrations (3.5–10.5 wt%) microgelation was able to standardise friction amongst all proteins.

Overall at 0.1 Pa m the μ values irrespective of volume fractions is one-to-two orders of magnitude lower than buffer (μ = 0.74) with microgels closely resembling that of O/W emulsion friction values (with exception of PoPM Φ = 70%). This highlights the overall effectiveness that microgelation has on protein to provide lubrication properties even resembling that of O/W emulsions without any lipidic additive, eliminating high friction issues associated with the plant proteins. To our knowledge, such extreme improvement in lubrication performance of delubricating (Vlădescu et al., 2023) plant proteins (down to

lowest μ values of <0.005 in many cases) (**Figure 5.5a-d1**, **a-c2** at 0.3 Pa m), achieved by transforming them into microgels has never been reported in literature to date.

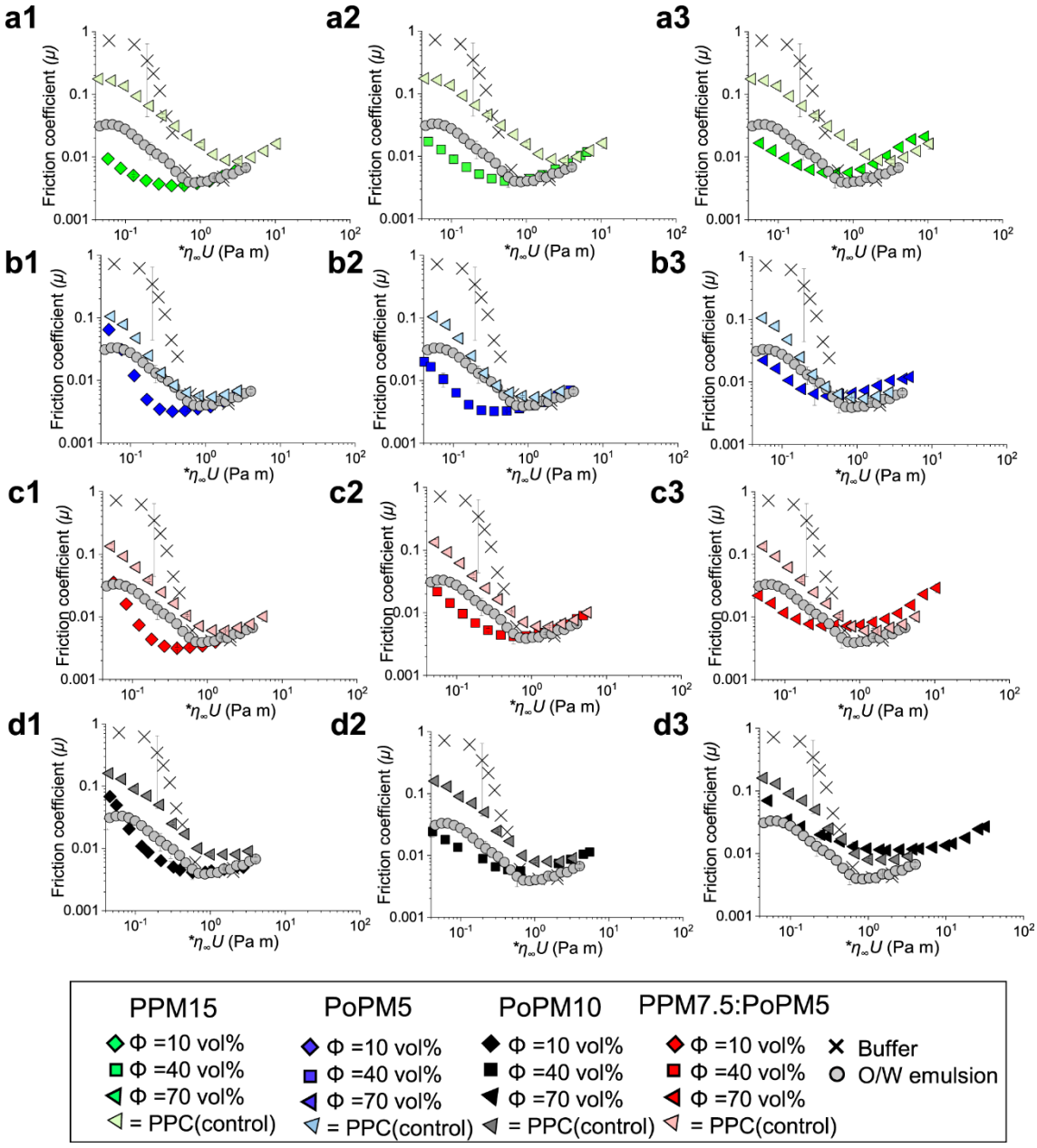

Figure 5.5 Tribological performance of steel ball on PDMS surfaces in the presence of plant protein microgels, native plant protein (matched protein content for Φ = 70 vol% with numbers displayed relating to total protein content) or oil-in-water emulsion. Friction coefficient (μ) as a function of entrainment speed (U) scaled with high rate viscosity (η ∞ = 1000 s − 1) in the presence of plant protein microgels prepared using (a1–a3) pea protein concentrate to form a 15.0 wt% total protein microgel, (PPM15), (b1–b3) potato protein

isolate to form a 5.0 wt% total protein microgel (PoPM5), (c1–c3)), potato protein isolate to form a 10.0 wt% total protein microgel, (PoPM10), and (d1–d3) using a mixture of pea protein concentrate at 7.5 wt% total protein and potato protein isolate at 5.0 wt% total protein microgel (PPM7.5:PoPM5) with 1, 2 and 3 showing increased volume fractions from 10 to 70 vol%, respectively. Frictional responses of the plant proteins at the highest concentration and 20 wt% oil-in-water emulsion (O/W emulsion) and buffer are included in each graph (a-d) as controls. Results are plotted as average of six repeat measurements on triplicate samples (n = 6 × 3) with error bars representing standard deviations. Statistical comparison of mean at 0.1 Pa m is shown in Appendix D Table D3. Original friction coefficient versus entrainment speed curves for the microgel dispersions at each volume fractions are shown in Appendix D Figure D7.

5.3.4 Theoretical fit of lubrication performance of microgels.

The Stribeck curve is often adopted to measure the frictional coefficient μ with increasing entrainment speed U or, the Hersey number, a nondimensional variable formed by the product of the dynamic viscosity η of the fluid with speed U divided by the normal load F_N per length of the contact (Dimina et al., (2022)). The Stribeck curve takes the form shown in equations (Dimina et al., 2022; Akyol et al., 2016; Ashokkumar et al., 2014) (5.3)-(5.5)

$$\mu_{tot} = \mu_{EHL} + \left(\frac{\mu_b - \mu_{EHL}}{1 + (U\eta / B)^m} \right) \tag{5.3}$$

$$\mu_{EHL} = k(U\eta)^n \tag{5.4}$$

$$\mu_b = h(U\eta)^l \tag{5.5}$$

where (k, n) and (h, l) are the elastohydrodynamic regime (EHL) and boundary layer power law coefficients and index respectively, B relates to the threshold value of $U\eta$ for boundary friction and m the mixed regime exponent. These

parameters must be empirically determined. To establish an alternative model, we proceed by calculating expressions for the torque experienced through friction of a rotational disc of radius R (m) on the surface of a fluid with load F_N (N) and, equivalently, for the torque which relates to the fluid properties under rotational shear *i.e.* angular speed ω, viscosity η (N s m^{-2}) and height h (m) of the fluid between the contact surfaces. The coefficient of friction μ is defined as the ratio of the resistive frictional force F opposing the motion of two surfaces experiencing a normal compressive force F_N, namely $\mu = F/ F_N$. Thus,

$$\boldsymbol{F = \sigma A} \tag{5.6}$$

where, σ denotes the stress and A is the contact area, and,

$$\boldsymbol{\sigma = \frac{F}{A} = \frac{\mu F_N}{A} = \frac{\mu F_N}{2\pi R^2}} \tag{5.7}$$

Integrating to obtain the total torque T over the whole surface *i.e.* increasing radial distance r, we have,

$$\boldsymbol{T = \int_0^R 2\pi r^2\, \sigma dr = \int_0^R \frac{2\pi\mu F_N r^2}{2\pi R^2} dr = \frac{\mu F_N}{R^2}\left[\frac{r^3}{3}\right]_0^R = \frac{\mu F_N R}{3}} \tag{5.8}$$

Similarly, using the stress-rate of strain relation we may write,

$$\sigma = \eta\left(\frac{dv}{dz}\right) = \eta\frac{\omega r}{h} \tag{5.9}$$

Considering the Torque T.

$$dT = dF\, r \tag{5.10}$$

$$dF = \sigma dA \tag{5.11}$$

$$dA = 2\pi r dr \tag{5.12}$$

$$dT = 2\pi r^2 \sigma dr = \frac{2\pi r^3 \eta \omega dr}{h} \tag{5.13}$$

$$\boldsymbol{T = \int_0^R \frac{2\pi r^3 \eta \omega}{h} dr = \frac{2\pi \eta \omega}{h}\left[\frac{r^4}{4}\right]_0^R = \frac{\pi \eta \omega R^4}{2h}} \tag{5.14}$$

Equating equations (5.8) and (5.14)

$$\boldsymbol{\mu = \frac{3\pi \eta \omega R^3}{2F_N h}} \tag{5.15}$$

Assuming the fluid follows an Ostwald–de Waele law as can be expected for microgel dispersions being power-law fluid,

$$\boldsymbol{\sigma = K\left(\frac{\partial v}{\partial z}\right)^n = K\left(\frac{\omega r}{h}\right)^n} \tag{5.16}$$

$$dT = 2\pi r^2 \sigma dr = 2\pi K r^2 \left(\frac{\omega r}{h}\right)^n dr = 2\pi K r^{n+2} \left(\frac{\omega}{h}\right)^n dr \tag{5.17}$$

$$T = \int_0^R 2\pi K r^{n+2} \left(\frac{\omega}{h}\right)^n dr = 2\pi K \left(\frac{\omega}{h}\right)^n \left[\frac{r^{n+3}}{n+3}\right]_0^R = 2\pi K \left(\frac{\omega}{h}\right)^n \frac{R^{n+3}}{n+3} \tag{5.18}$$

$$\frac{\mu \mathrm{F}_N R}{3} = 2\pi K \left(\frac{\omega}{h}\right)^n \frac{R^{n+3}}{n+3} \tag{5.19}$$

$$\boldsymbol{\mu = \frac{6\pi K}{\mathrm{F}_N} \left(\frac{\omega}{h}\right)^n \frac{R^{n+2}}{n+3} = \frac{6\pi K R^2}{\mathrm{F}_N (n+3)} \left(\frac{\omega R}{h}\right)^n} \tag{5.20}$$

In lubrication theory, the specific height λ between the two surfaces can be related to the surface roughness and asperities σ_1^2 and σ_2^2 of the two surfaces, and the fixed surface separation *h* as shown in equation (9). If we assume the asperity σ_1 of one surface is fixed *i.e.* belongs to the tribometer device and that of the other is determined by the sample and which will be dependent upon the entrainment speed *U*.

$$\boldsymbol{\lambda = \frac{h}{\sqrt{\sigma_1^2 + \sigma_2^2}}} \tag{5.21}$$

In the current context, since we have conducted experiments under a constant applied load, we do not speculate on the nature of the dependence of the applied load (or in other words normal force) *i.e.* F_N, and simply confine the effective height dependence on entrainment speed. We suggest the specific height λ of the fluid layer takes a functional dependence on the speed *U*, and which may be estimated empirically. A suitable functional form for this function must be such that the friction constant is asymptotically maximal/minimal at zero/high entrainment speeds respectively and, therefore, must take a sigmoidal

form similar to that of equation (5.21) or equivalently other forms which exhibit this behaviour such as a logistic equation or the adopted form used in this work, the Gompertz equation (5.22). Accordingly, substitution of equation (5.20) into equation (8) we arrive with equation (5.23) where the parameters, *a*, *b*, *c* and *K* are empirically determined. **Figure 5.6a** shows the experimental data of the friction coefficient against Log *U* and the associated empirically fitted model described by equation (5.21). Models were fitted using non-linear solvers which optimally minimised summed residuals.

$$\boldsymbol{h(U, \mathrm{F}_N) = ae^{-e^{b-cU}}} \tag{5.22}$$

Here *a* is the maximum value of the asymptote, *b* is the displacement along the velocity axis and *c* the growth rate scaled by U.

Thus,

$$\boldsymbol{\mu = \frac{6\pi KR^2}{\mathrm{F}_N(n+3)}\left(\frac{U}{h(U)}\right)^n} \tag{5.23}$$

In **Figure 5.6a** we show the theoretical modelling of lubrication performance using equation (5,23) at a load of 2.0 N of exemplar plant protein microgels (pea, potato and mixed pea and potato) showing close resemblance to the emulsion as opposed to the large friction coefficients obtained in presence of native protein. In Appendix D Figure D8 we show the normalised (to the initial level) friction coefficient to scale and remove the dependence upon the applied load. It may be observed that the native protein requires higher speeds before a reduction in normalised coefficient is observed in contrast to the microgel and emulsion sample. We suggest that friction-velocity profiles may be fitted using equation (5.23) and that in the boundary regime, the specific height λ is negligible resulting in high friction and, this reduces under shear in the mixed regime as the effective fluid height increases as the fluid is entrained and, which will attain a

minimal asymptotic level when the specific fluid height reaches its maximum and the system is in the elastohydrodynamic region. In the latter case, this will be the case when the available 'free' fluid within the microgel has been released from the structure increasing the depth of the fluid layer and asperities have been reduced. This demonstrates the effective height of microgels vs native proteins is crucial in lubrication, comparing microgel to native protein there is a clear reduction in friction coefficient owing to their water saturated structure demonstrating a striking improvement in lubrication (**Figure 5.6a**). Furthermore a similar frictional response is obtained to a O/W emulsion enhancing the extended use of microgels as a fat mimetic demonstrating clear improvements.

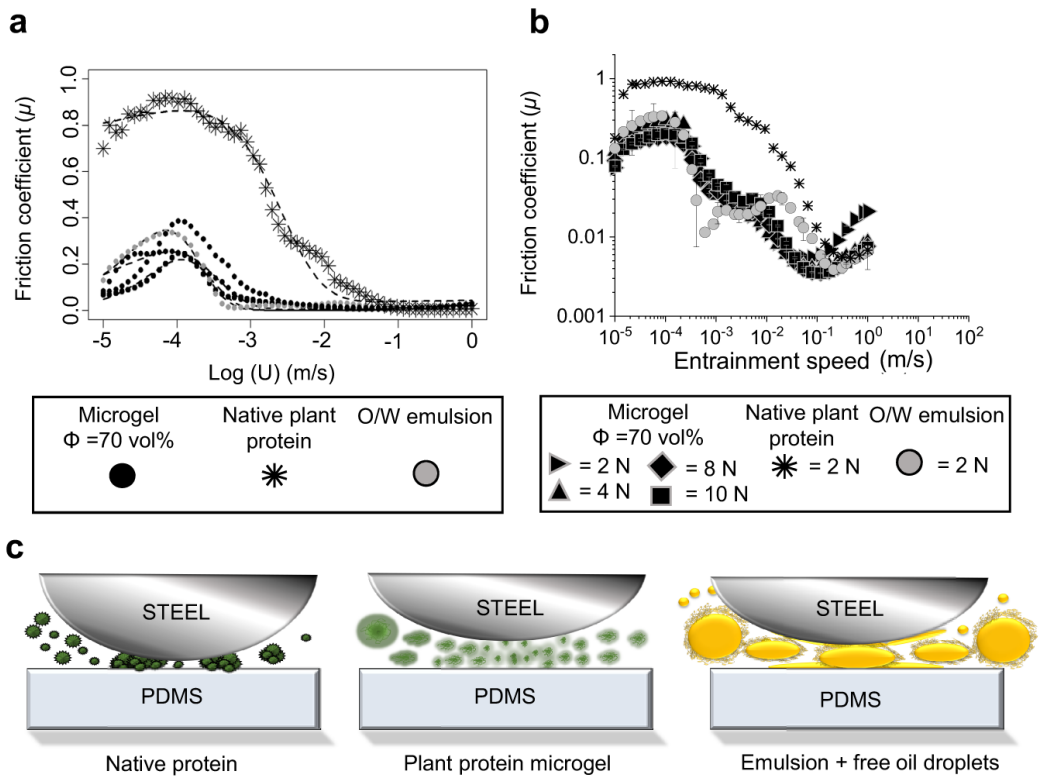

Figure 5.6 Tribological performance of steel ball on PDMS contact surfaces showing (a) theoretical modelling of lubrication performance at a load of 2 N of exemplar plant protein microgels (pea, potato and mixed pea and potato microgel) showing close resemblance to the emulsions as opposed to the large friction coefficients obtained in presence of the native protein. Here the dashed lines show the best theoretical fit using Eq. (5.21) and (Figure 5.6b) load dependency of microgels as compared to the native protein (matched

protein content for Φ = 70 vol%) with 20:80 O/W emulsion as control with (c) schematic illustration of microgel performance as compared to native protein in hard-soft contacts. Friction coefficient (μ) is plotted as a function of entrainment speed (U). Results are plotted as average of three repeat measurements on triplicate measurements (n = 3 × 3) with error bars representing standard deviations.

Next we determine whether microgels release fluids upon tribological stress. A load-dependence procedure was followed where friction under increasing loads (2 – 10 N) were measured (**Figure 5.6b**). It is now clear that microgels as a result of increased load show no significant differences in lubrication throughout boundary and mixed regimes (0.001-0.1). Microgels remained resilient and when compared to native structures, frictional curves did not converge to the native plant protein even at 10 N. This suggests even under high normal force microgels still provide support, despite undergoing changes, whereby under load act as mini-reservoirs of water which promote hydration lubrication (Ma, L. et al., 2015) and behaving differently to native protein.

In order to understand the microgel lubrication mechanism, the deformation was computed by calculating indentation from Hertz theory of contact points (Tatara, 1991) similarly performed previously for microgels and emulsion (Torres et al., 2018). This model allows us to understand how particles and microgels break, squeeze and flow to support lubrication of the load. The normal load supported by lubricant (W_L) and the individual particle/microgel (W_p) as well as the reduced elastic modulus formed between particle/microgel and PDMS surface (E^*) were determined. We also estimate the number of particles/microgels with radius R, forming a monolayer inside the contact with an effective fraction (ϕ_p) covering contact area (a_{TP}), (refer to Supporting Information D1 for theoretical analysis).

The relative indentation can be expressed as equation (5.24):

$$\frac{\boldsymbol{\delta}}{\boldsymbol{R}} = \left(\frac{\boldsymbol{a_H}}{\boldsymbol{R}}\right)^2 - \frac{\boldsymbol{4}}{\boldsymbol{3\pi(1-\nu^2)}}\left(\frac{\boldsymbol{a_H}}{\boldsymbol{R}}\right) \boldsymbol{f}\left(\frac{\boldsymbol{a_H}}{\boldsymbol{R}}\right) \tag{5.24}$$

where, ν is the Poisson ratio estimated for gels and the ratio a_H/R is the radius of contact which is independent of R, relating to fraction of surface covered by particles/microgels ϕ_p, expressed as equation (5.23)

$$\frac{\boldsymbol{a_H}}{\boldsymbol{R}} = \left(\frac{\boldsymbol{3W_L}}{\boldsymbol{4\emptyset_p E^* {a_{TP}}^2}}\right)^{\boldsymbol{1/3}} \tag{5.25}$$

We also estimated the entrainment force of the microgels being dragged into contact using Stokes drag equation (5.24):

$$\boldsymbol{F_d = 6\pi R\eta \bar{U}} \tag{5.26}$$

where, η is the viscosity and $\bar{U}$ the entrainment speed. Based on theoretical and experimental results we have generated indentation and drag force values (**Table 6**) with a subsequent schematic for lubricity (**Figure 5.6c**). We observe that all microgel lubricants support a high percentage (> 90%) of the load (W_L) resulting in the decrease in friction coefficient (**Table 6**). However, due to the difference in viscosity component as well as the elasticity between the emulsion and microgels, the drag force as well as the load supported by individual particles/microgels differed. From the indentation data, it is clear that emulsion droplets most likely deform into an elliptical shape under contact ($\delta R^* = 0.62$) in contrast to the microgels that are rather fully deformed ($\delta R^* > 1$). This suggests

that breakdown of the microgels would promote surface coverage between asperities, allow weeping of water into the contact, therefore increasing localised viscosity enhancing lubricity (**Figure 5.6C**), as a parallel mechanism to the coalescence of oil observed in O/W emulsions to generate low friction by separating contact. In addition, the gel material may further swell generating hydration lubricity observed from adsorption measurements when exposed to free water resulting in a steric viscoelastic hydrated layer separating contact (Appendix D Figure D9). Overall, the one-two orders of magnitude higher drag force (except for PoPM5) and W_p for microgels as compared to the emulsions drives the microgels to the contact and allow supporting the load by virtue of their elasticity and viscosity explains the microgel lubricity mechanism.

Table 6 Calculation of relative Indentation and drag force of the emulsion droplets and microgels

Lubricant	W_L (%)	δR*	η at 1.0 s^{-1} (Pa s)	W_p (N)	F_d (N)
PPM15	95.2	1.18	0.03	7.7×10^{-5}	2.0×10^{-10}
PoPM5	92.2	1.57	0.01	6.1×10^{-5}	2.0×10^{-11}
PoPM10	93.5	3.23	2.26	0.01	8.4×10^{-9}
PPM7.5:PoPM5.0	95.0	2.85	0.03	0.026	2.5×10^{-10}
O/W emulsion	96.4	0.62	0.0001	4.5×10^{-4}	5.0×10^{-11}

5.3.5 Lubrication using biomimetic tongue surface

Oral tribology has provided significant advances in friction medicated sensory responses, which is supported by over a decade of correlating tribology to real sensory attributes (Kokini et al., 1977; Pradal and Stokes, 2016; Sarkar and Krop, 2019). In oral tribology, the paradigm has historically been using smooth, hydrophobic, PDMS tribopairs of high elastic modulus (~ 2 MPa) as a surface to

represent human tongue, however such materials differ in their wettability, contact pressure and topography from a real human tongue (Sarkar et al., 2019; Andablo-Reyes, Efren et al., 2020), thus hindering true friction-sensory correlation in complex soft materials. In the pursuit of improving accuracy and reliability of *in-vitro* oral mouthfeel measurements, specific attention is given on development of biorelevant surfaces (Andablo-Reyes, Efren et al., 2020). Therefore to establish mechanistic understanding behind friction-mouthfeel associations, lubrication of plant microgels and O/W emulsion was measured between a bespoke biomimetic 3D tongue-like surface on steel contact (Figure 5.7) created from a 3D printed mould which incorporates papillae size and spatial distribution, elasticity and wetting properties of human tongue (Andablo-Reyes, Efren et al., 2020). For reference exact values and statistical comparison can be found in Appendix D Table D4. Unlike PDMS-steel contact (Appendix D Figure D7) looking at range of entrainment speed, the biomimetic tongue-steel contact focuses on boundary friction coefficients.

Similarly to PDMS-Steel contact we measure excellent lubrication for microgels showing similarities to O/W emulsion where we observe a non-significant or significantly improved friction at all volume fractions of PPM15, Φ = 70% of PoPM5 and PoPM10 and Φ = 10-40% of PPM7.5:PPM5, again reinforcing such excellent lubricity of plant protein microgels. Also observed from **Figure 5.5 c3**, higher speeds result in increased friction in presence of PoPM10 (**Figure 5.7 c3**) arising from high solution viscosity, limiting easy entrainment between contacts.

This technique does present several differences arising from the properties of the tongue-surface specifically, its wettability, topography and deformability which may incur high frictional sensitivity in the boundary friction. In

particular PoPM5 Φ = 10, PoPM10 Φ = 10 and PPM7.5:PoPM5 Φ = 70 were found to have frictions higher than O/W at lower V_R ($p > 0.05$). We speculate a higher δR* and lower d_H may contribute to an initial ineffective lubrication for potato protein microgels as there may not be sufficient levels of microgel for successful entrainment. However, at higher V_R the friction reduces where a non-significant difference in μ to those in O/W emulsion is observed ($p > 0.05$). For PPM7.5:PoPM5.0, an increase in volume fraction results in increased friction. As this dispersion is made up of two sets of microgels of different moduli and size, a build-up may occur at higher concentrations at the papillae promoting a jamming behaviour opposed to uniformly hydrated ball-bearing-type lubrication if microgel of one protein type(Wan et al., 2022) is present. This phenomenon is not observed in glass and PDMS as is likely the flat surface contact allow separate microgels to flow over one another without disruption improving lubricity.

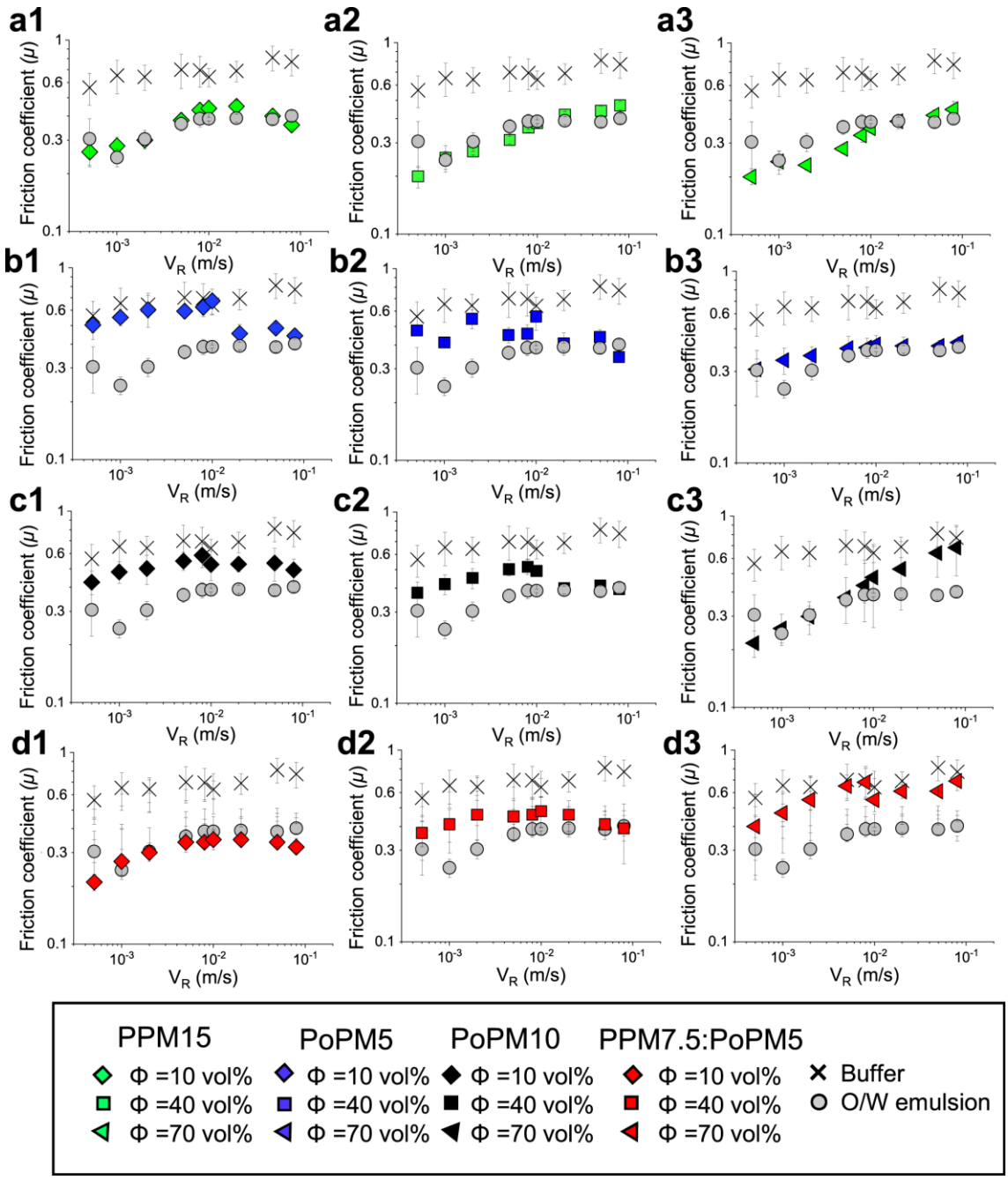

Figure 5.7 Tribological performance in 3D biomimetic tongue-like surfaces. Tribological performance of 3D-printed biomimetic tongue-like polymeric surfaces in presence of plant protein microgels or oil-in-water emulsions. Friction coefficient (μ) as a function of linear speed (VR) in the presence of plant protein microgels prepared using (a1-3) pea protein concentrate to form a 15.0 wt% total protein microgel, (PPM15), (b1-3) potato protein isolate to form a 5.0 wt% total protein microgel (PoPM5), (c1-3)), potato protein isolate to form a 10.0 wt% total protein microgel, (PoPM10), and (d1-3) using a mixture of pea protein concentrate at 7.5 wt% total protein and potato protein isolate at 5.0 wt%

total protein microgel (PPM7.5:PoPM5), respectively. Frictional responses of 20 wt% oil-in-water emulsion (O/W emulsion) and buffer are included in each graphs (a-d) as controls. Results are plotted as average of six measurements (n = 6 x 3) with error bars representing standard deviations. Statistical comparison of means at each lubrication regimes is shown in Appendix D Table D4.

To relate adsorption and lubrication properties, hydrated mass and adsorption kinetics of the protein microgels were analysed using QCM-D on PDMS coated sensors (see Appendix D Figure D9**)** for frequency and dissipation shifts). The hydrated mass has been inversely correlated to mixed and hydrodynamic regimes depicting the point of lowest friction (Stokes et al., 2011) and has been recently used with tribology to understand surface adsorption, particularly in boundary regime (Kew et al., 2021). When comparing single microgels, each possess significantly different hydrated masses *($p > 0.05$)* positively correlating to elastic modulus (**Figure 5.4a**) where viscoelasticity does not-significantly differ (0.08-0.12, *$p > 0.05$)*) (**Table 7**). When comparing frictional values to hydrated mass we see a negative correlation in the highest hydrated mass (PoPM10) and lower hydrated masses of other microgels (0.1 Pa m).

Despite PPM15 showing the most effective lubrication, interestingly hydrated mass and viscoelasticity (11.1 mg m^{-2}, $-\Delta D/\Delta f = 0.08$, **Table 7**) mirror data from that of native pea protein (11.1 mg m^{-2}, $-\Delta D/\Delta f = 0.07$) when comparing in previous study (Kew et al., 2021). However striking differences are observed when applying a final buffer rinse as little change or increase in viscoelasticity observed (Appendix D Figure D9) suggesting further hydration and swelling. Ultimately this may be key as to why microgels lubricate more effectively showing

less binding to the surface even if they support load (**Table 6**) in contrast to native proteins.

Table 7 Quantitative assessment of binding of plant protein microgels to hydrophobic surface. Mean and standard deviation (SD) obtained from three repeat measurements on triplicate samples (n = 3 × 2) of the hydrated mass and viscoelasticity (*-ΔD/Δf*) plant protein microgels prepared using pea protein concentrate to form a 15.0 wt% total protein microgel, (PPM15), potato protein isolate to form a 5.0 wt% total protein microgel (PoPM5), potato protein isolate to form a 10.0 wt% total protein microgel, (PoPM10), and using a mixture of pea protein concentrate at 7.5 wt% total protein and potato protein isolate at 5.0 wt% total protein microgel (PPM7.5:PoPM5). Data was obtained using 3rd, 5th, 7th and 11th overtones. Different lower-case letters in the same column indicate a statistically significant difference ($p < 0.05$). Original frequency and dissipation shift data are shown in Appendix D Figure D9.

Protein microgel	**Hydrated mass (mg m^{-2})**	***-ΔD/Δf***
PPM15	11.1 +/- 2.6^{b}	0.08 +/- 0.050^{ab}
PoPM5	8.4 +/- 0.3^{a}	0.10 +/- 0.003^{a}
PoPM10	24.0 +/- 2.1^{c}	0.12 +/- 0.070^{ac}
PPM7.5:PoPM5	16.7 +/- 6.6^{abc}	0.06 +/- 0.020^{bc}

5.3.6 Contribution to sustainability

With drive to replace animal-based proteins with sustainable plant-based alternatives, the energy used to produce a refined protein powder (over 85% protein) from an original plant-based source must be considered, including the subsequent steps of fabricating these functional microgels. Life Cycle Analysis (LCA) have shown that the plant proteins produce much lower GHG emissions

than meat proteins and such differences mainly is attributed to the primary production and plant-to-animal protein conversion (in-farm stages) rather than subsequent processing stages. It is now well-evidenced that in-farm processing produces the largest environmental impact (Ashokkumar et al., 2014b; Lie-Piang et al., 2021; Pampuri et al., 2021) in contrast to beyond-farm processes. For instance, LCA of plant and meat burgers conducted by Heller et al (Heller and Keoleian, 2018) demonstrated 90% less GHGs, 46% less energy, 93% less land and 99.5% less water when producing a plant-based burger using pea protein concentrate. These impressive improvements in climate markers are also observed for other analogues utilising soy protein isolates (Saerens et al., 2021). Although LCA of microgelation is beyond the scope of this work due to lab-scale production of this technology, LCA of other processing can be used as proxy to understand the environmental implications. Aganovic et al.(Aganovic et al., 2017) conducted a “farm to gate” analysis comparing thermal, pulsed electric field and high-pressure processing and reported that the environmental impact was overshadowed by the production of raw materials (20-64%) and packaging containers (85%). Hence, the additional processing of plant-based proteins towards fabricating these functional and lubricating microgels which is in line with standard food processing practices appears to be negligible in terms of GHG emissions (with considerably lower energy requirements to those in the LCA of the thermally processing studied previously (Aganovic et al., 2017)). Of more importance, the high reward of improving plant protein lubrication performance *via* physical modification (without any chemical additives) offers a viable approach, 1) to create next generation of sustainable, *yet pleasurable*, plant-based foods to enable the much needed large-scale transition from unsustainable animal protein-based diets and 2) reduce food wastage due to unpalatability,

astringency challenges (Tanger et al., 2022; Vlădescu et al., 2023) and associated large scale consumer unacceptability of current plant-based foods (Baune et al., 2023).

5.4 Discussion

Despite the immense effort to use sustainable plant proteins in food, their undesirable mouthfeel is a key bottle neck for consumer acceptability and hinders the transition to plant-based diets. Herein, we have presented a method to convert and optimise lubrication of plant proteins into effective lubricants by physically crosslinking them as microgels. Two commonly and commercially available plant proteins were used to prove this hypothesis, pea and potato, which were hydrated, gelled and homogenised into four types of microgel varying in concentration of protein and a range of volume fractions were tested. Through the use of DLS, AFM and rheology we physically observed these sub-micron sized microgels with low PDI values, suggesting a better control of size and stability over native proteins, latter are highly aggregated and are poorly functional. These microgels were extensively characterised in lubrication including hard-soft contact surfaces as well as 3D biomimetic tongue-like rough and wettable surfaces (Andablo-Reyes, E. et al., 2020) to serve as effective proxies to sensory evaluation(Sarkar and Krop, 2019). The microgel tribology performance was compared to the native protein, known to suffer with poor-lubrication and sensorially astringent properties, and an O/W emulsion with contrasting desirable high-lubrication properties. Additionally theoretical mechanisms of lubricity for each systems were determined using mathematical modelling, load-bearing experiments and surface properties measured using QCM-D.

Firstly, using size characterisation and rheology we show that microgelation is an excellent technique to generate small, discrete, spherical, highly stable plant-based hydrated microgels with limited aggregation and mostly Newtonian behaviour as opposed by the shear-thinning behaviour and poorly stable native proteins that were self-aggregating. Plant microgels show tuneable viscosity modifying properties due to hydration and theorised swelling ability which can be controlled by altering protein type, crosslinking density and volume fraction.

Secondly, we evidence the excellent lubrication properties of microgels. PPM15, PoP5 and PPM7.5:PoPM5 achieved orders of magnitude decrease in friction from native counterpart offering lubricity similar to O/W emulsion without the use of any lipids. We further evidenced the lubrication improvement by comparing two tribology methodologies with use of additional biomimetic surfaces where similarities in friction responses were recorded, which provides strong *in-vitro evidence* for mouthfeel performance. The topographic differences did relay importance as PoPM5, PoPM10 and PPM7.5:PoPM5 displayed reduced lubricity at low and high volume fractions, owing to an imposed papillae friction resulting in a macroscopic-aggregation hypothesis. This unexpected result depicts the importance of the use of alternate biomimetic surfaces for *in vivo* and *in-vitro* comparisons which must be standardised for future soft-tribology research. Nonetheless, understanding the real friction-mediated sensory analysis of plant protein microgels remains as a necessary undertaking, which is outside the scope of this study.

Finally, we evidence a mechanism of lubricity utilising adsorption, theoretical modelling and relative indentation. Adsorption measurements showed that viscoelasticity did not change from microgels but hydrated mass differed,

relating to moduli and ability to take up water which provided a negative correlation to lubrication performance. However a major difference was revealed in that subsequent washing of buffer resulted in little change in mass with evidence of swelling as viscoelasticity increased. Coupled with highly time and heat dependant microgel stability, this behaviour demonstrates the resilience of microgels to aggregate that is typically observed in native plant protein structures which was not observed with microgels. An alternative model for lubrication was determined, showcasing the similarity to O/W emulsion with dramatic lubricity differences converting native to micro-gelled protein owing to the effective height obtained by the swelling of microgels further complimenting observation from adsorption mechanics. Further, from the relative indentation calculations we showcase the excellent loadbearing ability from microgels where microgels weep out water increasing localised viscosity contributing to hydration lubrication. It is presumed the soft, hydrated microgels are able to flow and slide past one another as opposed to the aggregating-rubbing like feature of native plant proteins, reflected in viscosity, tribology, adsorption and theoretical results.

With growing sustainability needs, rise in vegetarianism, global protein malnourishment and inequity, the future world must look to plant based proteins in our growing population. Application of plants are at the forefront of food product development but currently limited by off-mouthfeel and poor functionality among a range of other barriers to adoption. Using a range of experimental and theoretical approaches, we confirm that microgelation is a viable technique to improve the lubricity, application and stability of plant protein in food. Ultimately, converting native plant proteins into microgels offers a facile platform to solve friction-related issues and combining this mechanistic work with sensory studies

in the future will allow rapid transition from animal to palatable plant protein-based diets to promote planetary health.

5.5 References

Aery, S., Parry, A., Araiza-Calahorra, A., Evans, S.D., Gleeson, H.F., Dan, A. and Sarkar, A. 2023. Ultra-stable liquid crystal droplets coated by sustainable plant-based materials for optical sensing of chemical and biological analytes. *Journal of Materials Chemistry* C.

Aganovic, K., Smetana, S., Grauwet, T., Toepfl, S., Mathys, A., Van Loey, A. and Heinz, V. 2017. Pilot scale thermal and alternative pasteurization of tomato and watermelon juice: An energy comparison and life cycle assessment. *Journal of Cleaner Production*. 141, pp.514-525.

Akyol, H., Riciputi, Y., Capanoglu, E., Caboni, M.F. and Verardo, V. 2016. Phenolic compounds in the potato and its byproducts: An overview. *International journal of molecular sciences*. 17(6), p835.

Andablo-Reyes, E., Bryant, M., Neville, A., Hyde, P., Sarkar, R., Francis, M. and Sarkar, A. 2020. 3d biomimetic tongue-emulating surfaces for tribological applications. *ACS Appl Mater Interfaces*. 12(44), pp.49371-49385.

Andablo-Reyes, E., Bryant, M., Neville, A., Hyde, P., Sarkar, R., Francis, M. and Sarkar, A. 2020. 3d biomimetic tongue-emulating surfaces for tribological applications. *ACS Applied Materials & Interfaces*. 12(44), pp.49371-49385.

Andablo-Reyes, E., Yerani, D., Fu, M., Liamas, E., Connell, S., Torres, O. and Sarkar, A. 2019. Microgels as viscosity modifiers influence lubrication performance of continuum. *Soft Matter*. 15(47), pp.9614-9624.

Araiza-Calahorra, A. and Sarkar, A. 2019. Pickering emulsion stabilized by protein nanogel particles for delivery of curcumin: Effects of ph and ionic strength on curcumin retention. *Food Structure*. 21, p100113.

Ashokkumar, K., Tar'an, B., Diapari, M., Arganosa, G. and Warkentin, T.D. 2014a. Effect of cultivar and environment on carotenoid profile of pea and chickpea. *Crop Science*. 54(5), pp.2225-2235.

Ashokkumar, K., Tar'an, B., Diapari, M., Arganosa, G. and Warkentin, T.D. 2014b. Effect of cultivar and environment on carotenoid profile of pea and chickpea. 54(5), pp.2225-2235.

Aufderhorst-Roberts, A., Baker, D., Foster, R.J., Cayre, O., Mattsson, J. and Connell, S.D. 2018. Nanoscale mechanics of microgel particles. *Nanoscale*. 10(34), pp.16050-16061.

Baune, M.-C., Broucke, K., Ebert, S., Gibis, M., Weiss, J., Enneking, U., Profeta, A., Terjung, N. and Heinz, V. 2023. Meat hybrids–an assessment of sensorial aspects, consumer acceptance, and nutritional properties. 10.

Bouhid de Aguiar, I., van de Laar, T., Meireles, M., Bouchoux, A., Sprakel, J. and Schroën, K. 2017. Deswelling and deformation of microgels in concentrated packings. *Scientific Reports*. 7(1), p10223.

Cosson, A., Blumenthal, D., Descamps, N., Souchon, I. and Saint-Eve, A. 2021. Using a mixture design and fraction-based formulation to better understand perceptions of plant-protein-based solutions. *Food Research International*. 141, p110151.

Crippa, M., Solazzo, E., Guizzardi, D., Monforti-Ferrario, F., Tubiello, F.N. and Leip, A. 2021. Food systems are responsible for a third of global anthropogenic ghg emissions. *Nature Food*. 2(3), pp.198-209.

de Vicente, J., Stokes, J.R. and Spikes, H.A. 2006. Soft lubrication of model hydrocolloids. *Food Hydrocolloids*. 20(4), pp.483-491.

Dimina, L., Rémond, D., Huneau, J.-F. and Mariotti, F. 2022. Combining plant proteins to achieve amino acid profiles adapted to various nutritional objectives—an exploratory analysis using linear programming. *Front. Nutr*. 8.

Dresselhuis, D.M., Klok, H.J., Stuart, M.A.C., de Vries, R.J., van Aken, G.A. and de Hoog, E.H.A. 2007. Tribology of o/w emulsions under mouth-like conditions: Determinants of friction. *Food Biophysics*. 2(4), pp.158-171.

Garrec, D.A. and Norton, I.T. 2013. Kappa carrageenan fluid gel material properties. Part 2: Tribology. *Food Hydrocolloids*. 33(1), pp.160-167.

Heller, M.C. and Keoleian, G.A. 2018. Beyond meat's beyond burger life cycle assessment: A detailed comparison between.

Kew, B., Holmes, M., Stieger, M. and Sarkar, A. 2020. Review on fat replacement using protein-based microparticulated powders or microgels: A textural perspective. *Trends in Food Science & Technology*.

Kew, B., Holmes, M., Stieger, M. and Sarkar, A. 2021. Oral tribology, adsorption and rheology of alternative food proteins. *Food Hydrocolloids*. 116, p106636.

Kokini, J.L., Kadane, J.B. and Cussler, E.L. 1977. Liquid texure perceived in the mouth. *Journal of Texture Studies*. 8(2), pp.195-218.

Lam, A.C.Y., Can Karaca, A., Tyler, R.T. and Nickerson, M.T. 2018. Pea protein isolates: Structure, extraction, and functionality. *Food Reviews International*. 34(2), pp.126-147.

Liamas, E., Connell, S.D. and Sarkar, A. 2023. Frictional behaviour of plant proteins in soft contacts: Unveiling nanoscale mechanisms. *Nanoscale* Advances.

Liamas, E., Connell, S.D., Zembyla, M., Ettelaie, R. and Sarkar, A. 2021. Friction between soft contacts at nanoscale on uncoated and protein-coated surfaces. *Nanoscale.* 13(4), pp.2350-2367.

Liang, H.-N. and Tang, C.-H. 2013. Ph-dependent emulsifying properties of pea [pisum sativum (l.)] proteins*. Food Hydrocolloids*. 33(2), pp.309-319.

Lie-Piang, A., Braconi, N., Boom, R.M. and van der Padt, A. 2021. Less refined ingredients have lower environmental impact – a life cycle assessment of protein-rich ingredients from oil- and starch-bearing crops. *Journal of Cleaner Production.* 292, p126046.

Liu, K., Stieger, M., van der Linden, E. and van de Velde, F. 2016a. Effect of microparticulated whey protein on sensory properties of liquid and semi-solid model foods. *Food Hydrocolloids*. 60, pp.186-198.

Liu, K., Tian, Y., Stieger, M., van der Linden, E. and van de Velde, F. 2016b. Evidence for ball-bearing mechanism of microparticulated whey protein as fat replacer in liquid and semi-solid multi-component model foods. *Food Hydrocolloids.* 52, pp.403-414.

Liu, Y., Toro-Gipson, R.S.D. and Drake, M. 2021. Sensory properties and consumer acceptance of ready-to-drink vanilla protein beverages. *Journal of Sensory Studies.* 36(6), pe12704.

Ma, K.K., Greis, M., Lu, J., Nolden, A.A., McClements, D.J. and Kinchla, A.J. 2022. *Functional performance of plant proteins*. 11(4), p594.

Ma, L., Gaisinskaya-Kipnis, A., Kampf, N. and Klein, J. 2015. Origins of hydration lubrication. *Nature Communications*. 6(1), p6060.

Mao, C., Wu, J., Zhang, X., Ma, F. and Cheng, Y. 2020. Improving the solubility and digestibility of potato protein with an online ultrasound-assisted ph shifting treatment at medium temperature. 9(12), p1908.

Pampuri, A., Casson, A., Alamprese, C., Di Mattia, C.D., Piscopo, A., Difonzo, G., Conte, P., Paciulli, M., Tugnolo, A., Beghi, R., Casiraghi, E., Guidetti, R. and Giovenzana, V. 2021. Environmental impact of food preparations enriched with phenolic extracts from olive oil mill waste. 10(5), p980.

Pang, Z., Tong, F., Jiang, S., Chen, C. and Liu, X. 2023. Particle characteristics and tribo-rheological properties of soy protein isolate (spi) dispersions: Effect of heating and incorporation of flaxseed gum*. International Journal of Biological Macromolecules*. 232, p123455.

Pradal, C. and Stokes, J.R. 2016. Oral tribology: Bridging the gap between physical measurements and sensory experience. *Current Opinion in Food Science*. 9, pp.34-41.

S. Tomoskozi, R.H.a.O.B. 2001. Isolation and study of the functional properties of pea proteins. *Nahrung/Food*. 45, pp.399–401.

Saerens, W., Smetana, S., Van Campenhout, L., Lammers, V. and Heinz, V. 2021. Life cycle assessment of burger patties produced with extruded meat substitutes. *Journal of Cleaner Production*. 306, p127177.

Sarkar, A., Andablo-Reyes, E., Bryant, M., Dowson, D. and Neville, A. 2019. Lubrication of soft oral surfaces. *Current Opinion in Colloid & Interface Science*. 39, pp.61-75.

Sarkar, A., Kanti, F., Gulotta, A., Murray, B.S. and Zhang, S. 2017. Aqueous lubrication, structure and rheological properties of whey protein microgel particles. *Langmuir*. 33(51), pp.14699-14708.

Sarkar, A. and Krop, E.M. 2019. Marrying oral tribology to sensory perception: A systematic review. *Current Opinion in Food Science*. 27, pp.64-73.

Sarkar, A., Murray, B., Holmes, M., Ettelaie, R., Abdalla, A. and Yang, X. 2016. In-vitro digestion of pickering emulsions stabilized by soft whey protein microgel particles: Influence of thermal treatment. *Soft Matter.* 12(15), pp.3558-3569.

Schmidt, J.M., Damgaard, H., Greve-Poulsen, M., Sunds, A.V., Larsen, L.B. and Hammershøj, M. 2019. Gel properties of potato protein and the isolated fractions of patatins and protease inhibitors – impact of drying method, protein concentration, ph and ionic strength. *Food Hydrocolloids.* 96, pp.246-258.

Shewan, H.M. and Stokes, J.R. 2013. Review of techniques to manufacture micro-hydrogel particles for the food industry and their applications. *Journal of Food Engineering*. 119(4), pp.781-792.

Sim, S.Y.J., SRV, A., Chiang, J.H. and Henry, C.J. 2021. Plant proteins for future foods: A roadmap. *Foods* 10(8), p1967.

Sridharan, S., Meinders, M.B.J., Sagis, L.M., Bitter, J.H. and Nikiforidis, C.V. 2021. Jammed emulsions with adhesive pea protein particles for elastoplastic edible 3d printed materials. *Advanced Functional Materials.* 31(45), p2101749.

Stokes, J.R., Macakova, L., Chojnicka-Paszun, A., de Kruif, C.G. and de Jongh, H.H.J. 2011. Lubrication, adsorption, and rheology of aqueous polysaccharide solutions. *Langmuir.* 27(7), pp.3474-3484.

Tanger, C., Utz, F., Spaccasassi, A., Kreissl, J., Dombrowski, J., Dawid, C. and Kulozik, U. 2022. Influence of pea and potato protein microparticles on texture

and sensory properties in a fat-reduced model milk dessert. *ACS Food Science & Technology*. 2(1), pp.169-179.

Tatara, Y. 1991. On compression of rubber elastic sphere over a large range of displacements—part 1: Theoretical study. *Journal of Engineering Materials and Technology.* 113(3), pp.285-291.

Torres, O., Andablo-Reyes, E., Murray, B.S. and Sarkar, A. 2018. Emulsion microgel particles as high-performance bio-lubricants. *ACS Applied Materials & Interfaces.* 10(32), pp.26893-26905.

Veldhorst, M., Smeets, A., Soenen, S., Hochstenbach-Waelen, A., Hursel, R., Diepvens, K., Lejeune, M., Luscombe-Marsh, N. and Westerterp-Plantenga, M. 2008. Protein-induced satiety: Effects and mechanisms of different proteins. *Physiology & Behavior.* 94(2), pp.300-307.

Vlădescu, S.-C., Agurto, M.G., Myant, C., Boehm, M.W., Baier, S.K., Yakubov, G.E., Carpenter, G. and Reddyhoff, T. 2023. Protein-induced delubrication: How plant-based and dairy proteins affect mouthfeel. *Food Hydrocolloids*. 134, p107975.

Voigt, W.U. 1889. The relationship between the two elasticity constants isotropic body. *Wiedmann's annalen der phys chem*. 38, pp.573-587.

Waglay, A., Karboune, S. and Alli, I. 2014. Potato protein isolates: Recovery and characterization of their properties. *Food Chemistry*. 142, pp.373-382.

Wan, J., Ningtyas, D.W., Bhandari, B., Liu, C. and Prakash, S. 2022. Oral perception of the textural and flavor characteristics of soy-cow blended emulsions. *Journal of Texture Studies*. 53(1), pp.108-121.

Xu, X., Sharma, P., Shu, S., Lin, T.-S., Ciais, P., Tubiello, F.N., Smith, P., Campbell, N. and Jain, A.K. 2021. Global greenhouse gas emissions from

animal-based foods are twice those of plant-based foods. *Nature Food*. 2(9), pp.724-732.

Zembyla, M., Liamas, E., Andablo-Reyes, E., Gu, K., Krop, E.M., Kew, B. and Sarkar, A. 2021. Surface adsorption and lubrication properties of plant and dairy proteins: A comparative study. *Food Hydrocolloids*. 111, p106364.

Zhang, S., Holmes, M., Ettelaie, R. and Sarkar, A. 2020. Pea protein microgel particles as pickering stabilisers of oil-in-water emulsions: Responsiveness to ph and ionic strength. *Food Hydrocolloids*. 102, p105583.

Chapter 6 : General discussion and future studies

6.1 Introduction

Plant proteins are becoming an integral part of food design driven by the growing emphasis on sustainability and equitable access to protein resources globally, alongside a growing commitment to improving animal welfare. Plant proteins have seen increased use in alternative meat or use in high protein snacks, however their consumption is still severely hampered due to their limited functionality and poor sensory profile, particularly dry, astringent sensations. In the beginning the broad goal of the thesis was to understand why plant proteins suffer from sensory problems by investigating the oral tribology aspects. This followed by fundamental characterisation in tribology, rheology and adsorption of new sustainable proteins, investigating their extensive sensory responses in neural and cellular contexts. This has then lead onto a way to convert plant proteins into microgels successfully improving their functional and textural properties, reducing friction related negative textural responses and wider application as a new plant protein-based fat replacer.

An overview of this thesis is shown in **Figure 6.1** where both *in vivo* and *in-vitro* studies were explored to understand and find a solution for plant protein related friction

In **chapter 2** an initial focus was to understand proteins as fat replacements with clear knowledge gaps presented in plant protein, tribology, sensory. Overall, the direction of the thesis followed the identified knowledge gaps, in particular the tribology and sensory perception of plant proteins. Therefore numerous alternative proteins that are accessible for commercial use, actively utilised, or identified for future utilisation (such as legume, vegetable and insect-derived proteins) were subjected to characterisation based on their tribological, rheological, and adsorption behaviours in **Chapter 3**. This was undertaken to comprehensively grasp the properties including development of an *in-vitro* textural toolbox assessing the effect of protein type and concentration on rheology, sizing, tribology and adsorption behaviour, as highlighted in **Chapter 4**.

These proteins were then subsequently characterised *in vivo* (pea, potato, lupin were selected) validating the *in-vitro* results, undergoing an extensive RATA sensory profiling with 100 participants to understand taste and textural implications when using different alternative plant proteins, at differing concentrations and when mixed. Astringency was found to be the most prominent issue associated with their use even at low concentrations, where astringency was also correlated to high friction response in tribology confirming a frictional related issue predicted during **chapter 3**. Sensory methodology was then followed up with brain imaging using functional near-infrared spectroscopy (fNIRS) that provided neural insights into plant protein and tannic acid induced astringency. It was discovered that such neural astringency caused by tannic acid were akin to those generated by plant proteins. To conclude this investigation into

astringency, we reintroduce whey protein that showed excellent lubricity (**chapter 3**) and widely recognised palatability (Smithers, 2008; Smithers, 2015; Krolczyk et al., 2016) . A comparison was drawn between whey protein, plant protein and tannic acid solutions that were administered to TR146 cell lines inoculated with saliva. The salivary proteins were stained to measure any interaction and loss in the salivary protein film. Both the plant protein and tannic acid solutions exhibited the ability to bind, disrupt, and diminish the salivary protein film. However, even at elevated concentrations, whey protein demonstrated no signs of interaction or loss. In summary, the resemblance between plant protein and tannic acid, coupled with the contrast in behaviour exhibited by whey protein, contributes to the establishment of an astringency mechanism.

Lastly, with high friction, associated astringency and poor lubrication proven to be a problem for plant proteins during **Chapter 3** and **Chapter 4** we addressed a gap (**Figure 2.4., chapter 2**) and a colloidal solution of fabricating plant protein microgels was approached to solve friction related issues. Such microgelation has previously been utilised for animal protein but to reduce friction of plant proteins was novel. Therefore in **Chapter 5** we transformed pea and potato plant protein into highly hydrated ultra-lubricating microgels. Remarkably we found by microgelling native proteins, orders of magnitude reductions in friction were attained, reducing the friction related issues with native proteins. Furthermore such microgels also performed equally as well in lubricity to a 20% oil in water emulsion similar to single cream that ultimately provides potential as a new fat replacer technology. To quantify a mechanism we then applied mathematical, theoretical and indentation calculations where we establish microgels elastic nature and water weeping that optimised hydration lubricity achieving ultra-low frictions despite containing no lipid addition.

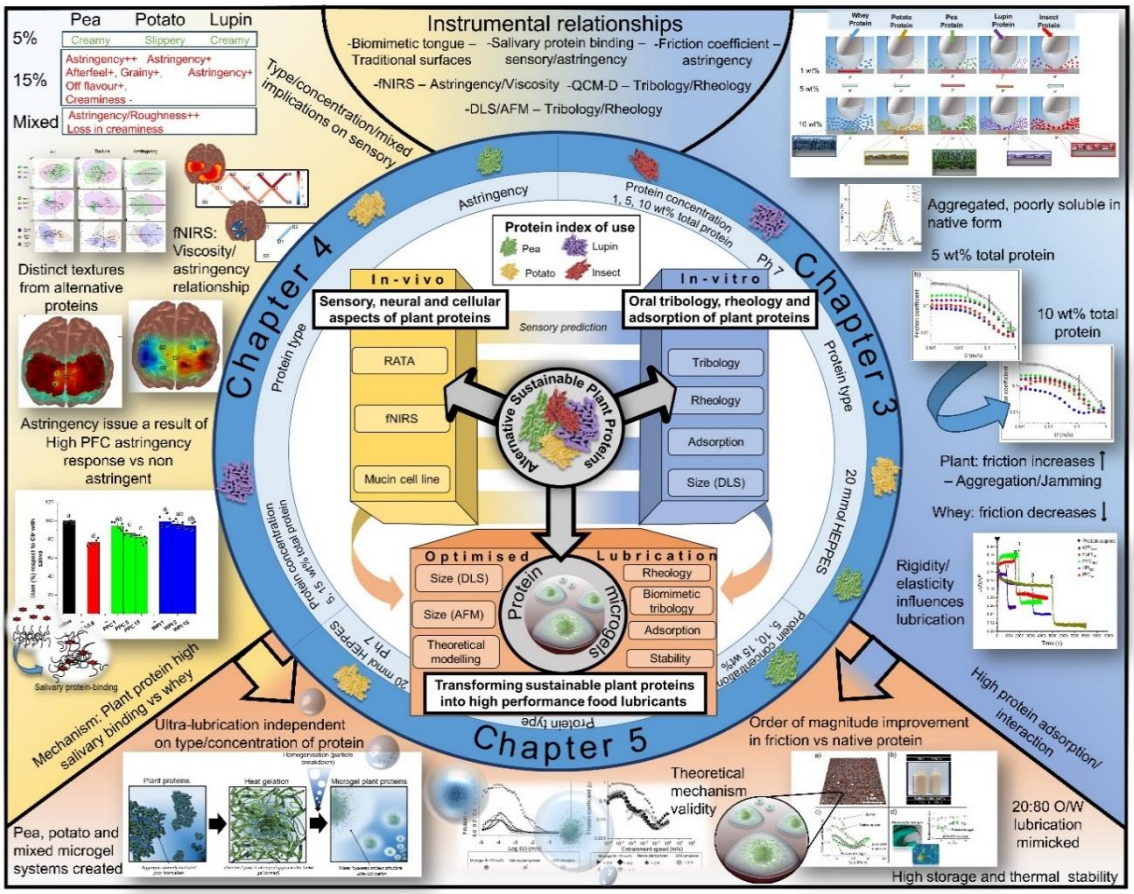

Figure 6.1 thesis summary: *In-vitro* and *in vivo* characterisation of alternative plant proteins varying in type and concentration and processing such plant proteins into ultra lubricating microgels. (Kew et al., 2021; Kew et al., 2023)

6.2 Summary of the main results

6.2.1 Poor lubrication performance found in plant proteins

In **Chapter 3**, the properties of protein powders derived from peas, potatoes, lupin, and insect were examined. These proteins were dispersed in a buffer with a pH of 7, and their behaviour in terms of tribology, rheology, and adsorption was studied. Whey protein, widely regarded as a benchmark animal protein, was used for comparison. The original proteins displayed a tendency to aggregate and had limited solubility and overall showed poor lubricity in comparison to whey even upon extraction of soluble protein fractions. Additionally upon increasing concentration from 5 wt% to 10 wt% total protein friction was found to increase

for a number of plant proteins, opposite to that of whey. This disparity in friction characteristics pointed to plant proteins being associated with higher astringency, roughness, and subpar sensory attributes.

6.2.2 Extensive sensory identifies uses of new alternative proteins

Pea, potato and lupin proteins were extensively characterised by Rate-All-That-Apply (RATA) by investigating 17 sensory attributes from 5-15 wt% concentration and upon mixing. At the 5% concentration, the primary distinguishing factor among the proteins was their texture, while the taste remained relatively uniform across all solutions. Textures included creaminess with thicker legume samples and slipperiness for thinner potato protein. Upon increasing concentration legume proteins, in particular pea protein, encountered increased roughness loss of smoothness and prominent astringency. Lupin retained more desirable characteristics compared to pea and would provide a more suitable legume protein based on sensory qualities. Additionally potato at 15 wt% only encountered notable increases in off-flavour initially making it a hopeful candidate for high-protein applications. However, of most importance, the presence of astringency was consistently noted among most participants, and notably, certain individuals exhibited extremely heightened sensitivity. This poses a significant challenge that hinders the majority of application unless effective ways to reduce astringency are taken and understood.

6.2.3 Neural response in consumption of plant protein

Astringency was a prime issue for plant proteins studied in **chapter 4** which is also well reported for plant proteins in literature with considerable research attention given to the topic itself (Troszynska, 2006; Bajec and Pickering, 2008; Cheynier, 2012; Canon et al., 2021). Neural methodology is a key step to understanding sensory relationships past traditional sensory panels that is

becoming a valuable asset to understand origins of sensory perception. A very strong response in prefrontal cortex (PFC) was found when consuming highly astringent samples, both as a oxyhaemoglobin (HbO) and deoxyhaemoglobin (HbR) inducer, dependant on viscosity. Additionally, a rise in HbR levels was observed at lower concentrations of pea, contrasting with the absence of such an increase in the water (STD) sample. This finding strongly indicates a neural impact of astringency linked to PFC activity, a phenomenon that has not been previously documented. Such PFC response indicates a secondary gustatory response (associated with dorsolateral stimulation) but also trigeminal and tactile response (dorsomedial stimulation). In addition

6.2.4 Degree of astringency correlates to salivary binding in cellular context

Both the astringent tannic acid and pea protein triggered a binding response with saliva proteins, and this binding was directly correlated with the intensity of perceived astringency. A concentration dependant response was also observed with 1-15% pea protein which was also consistent with observations made during the measurement of friction in plant proteins in **chapter 3**. Taken together, sensory and neural findings indicate the failure of saliva itself, or acting as a precursor, leads to the astringent response. The significance of the results was accentuated by the absence of non-significant binding of saliva with water and whey protein even at 15 wt%. It's yet to be determined whether the protein are solely accountable, or if residual polyphenol content contributes to astringent that warrants future measurement and a limitation in this study. However the evidence that transforming proteins by physical alteration into microgels serves as preliminary evidence of a structural role of astringency. Overall the stark contrast of whey emphasises the problem of plant proteins and necessitates thorough

attention and resolution in order to enhance the suitability and acceptability of plant proteins in food.

6.2.5 A process to remove lubrication related issues associated with plant proteins

The process of microgelation applied to plant proteins has demonstrated its remarkable effectiveness in enhancing the frictional properties of these proteins and uncovering a possible physical importance of structure in astringency mechanism. In **chapter 3** and **chapter 4** we show plant proteins at high concentration produce various levels of high friction and astringency that increases upon repeat consumption with further issues in mixed formulations. Microgelation exhibited a universal capacity to significantly reduce friction levels by orders of magnitude, irrespective of the protein source—be it pea, potato, or a combination thereof. This effectively addresses friction-related issues in **chapter 3**. Secondly the range of protein concentrations spanning from 0.5 wt% to 10 wt% exhibited consistently low lubricity. This indicates the resolution of the concentration-related concerns outlined in **chapter 3** and potentially **chapter 4**, thereby rendering microgelation a suitable solution to enhance lubrication in both low and high protein concentration food formulations. Impressively, this improved lubrication mirroring the lubricity of 20% oil-in-water emulsions, suggesting the potential expansion of plant proteins' applications from problematic food components to now functional uses. Moreover, the benefits extended beyond enhanced lubrication. Microgelation facilitated improved dispersibility, prevention of sedimentation and maintained particle sizes over time and under heating conditions. While sensory evaluations are necessary to validate these outcomes, our approach involved the innovative combination of a new biomimetic tongue surface and indentation theory supporting friction data. These elements not only

reinforce the observed improvements but also aided in generating a mechanism for achieving optimal lubrication.

6.2.6 Interconnections between Instruments, methodology, and sensory prediction across the thesis

Within this thesis a number of relatively novel characterisation techniques were employed. This includes quartz crystal microbalance with dissipation (QCM-D) for adsorption, biomimetic surfaces in tribology, use of fNIRS to study astringency in plant proteins and mathematical modelling. As this thesis explored in-vivo and in-vitro methodology this provides a unique comparison into both new instrumental relationships as well as correlations between sensory and the lab.

QCM-D: This novel technique and the relationship to tribology was explored throughout **chapters 3** and **5**. The hydrated mass was found to have links to the onset of the mixed to hydrodynamic regime and the rigidity correlated to boundary lubrication. It was found more elastic plant proteins displayed optimised lubricity at low concentrations (1 wt%) but at higher concentrations (10 wt%) suffer from higher friction. Rigid proteins such as potato poorly lubricated at low concentrations but may improve lubricity at higher levels. However the latter needs validating with a larger range of other proteins. These lubrication effects may be due to subunit protein conformation and so each subunit should be explored in their lubricative effect as well as the aggregated state naturally present. QCM-D was also used to characterise microgels. Hydrated mass was found to increase for potato proteins and for pea proteins although akin to that of native proteins in **chapter 3** there was a reduced level of aggregation and interaction when the microgels were rinsed with buffer. Furthermore, even though there was minimal alteration in the hydrated mass, potato microgels displayed heightened elasticity. This suggests that potato microgels experiences swelling

in the presence of the solvent. In conclusion, the microgels were determined to be remarkably hydrated, capable of swelling, and maintaining their non-aggregated state in contrast to the behaviour of native proteins.

Biomimetic surfaces: During the start of this thesis a new biomimetic tongue surface was generated at Leeds (Andablo-Reyes et al., 2020). To draw comparisons between friction of 3-pin PDMS and steel ball surfaces we also implemented this new surface for studying the frictional properties of microgels and a 20% oil-in-water emulsion. Similar findings and non-significant lubrication differences were found with this new system validating frictional performances. Notably, we speculate that the surface properties induced contrasting behaviour when mixed microgels were introduced, which should be an investigated in the future. Overall this new tribology system was shown to be effective in friction measurements similarly to traditional systems that reflects a more accurate oral surface for tribology research.

Textural relationships of fNIRS, cell line, sensory, tribology and viscosity: Astringency was shown to induce a strong prefrontal cortex (PFC) reaction with both plant proteins and tannic acid. This same astringency was recorded in Rate-All-That-Apply (RATA), squamous cell carcinoma cells with saliva (TR146+S) protein binding as well as friction coefficients upon increasing concentration in chapter 3. Additionally a specific HbR increase activation was found for high viscosity samples. These combinations of techniques would offer a valuable and complementary approach to experimental design for future food science and nutrition research.

Mathematical modelling: In chapter 5 we explored an alternative approach in predicting friction. Moreover, it offered insight into the lubricating mechanism of microgels, considering their capability to modify effective height

following water expulsion and their ability to adjust viscosity. This theoretical work was complimented in deformation behaviour computed by calculating indentation from Hertz theory of contact points that ultimately provided strong validation into microgels effective lubricity.

6.3 Concluding remarks

A schematic overview of the approach of the thesis is presented in **Figure 6.1**. Ultimately the thesis focuses on plant proteins, which expands to their characterisation both *in-vitro* and *in vivo* that concludes with a chapter on microgelation of plant proteins that aim to resolve friction related issues linked to plant proteins. The outer rim of the figure showcases key discoveries while also spotlighting several innovative characterisation tools employed throughout this research.

Overall the thesis highlights the frictional issues related to the use of new alternative proteins at low to high concentrations that severely limit application. These challenges significantly limit their practical utility, as they consistently exhibit contrasting functional and material properties repeatedly observed when compared to the benchmark whey protein. The research notably uncovers the widespread presence of astringency in sensory assessments, triggering pronounced neural reactions where this astringent response is intrinsically linked to salivary binding. The study underscores the indispensable roles of tribology, rheology, and adsorption as essential tools for comprehending this phenomenon. These tools have ultimately paved a way to improve friction by a microgelation process, which not only addresses poor friction but also enhances the functional attributes of an array of plant proteins.

6.4 Future studies

6.4.1 Protein type

Continued characterisation of new alternative proteins, their mixtures and as bipolymers: At the commencement of this thesis, we procured the most up-to-date and prospective commercially available alternative proteins for the purpose of research. Since then, there has been a swift worldwide surge and fascination for novel alternative proteins and by product proteins both in academia and industry. As a result this research compliments a wealth of other work conducted both in these proteins and in new proteins. Therefore the techniques used in this thesis could be applied to such new emerging proteins. Examples include algae, oat, wheat, hemp, yeast, lentil, duckweed and a variety of insect protein powders. Characterising these proteins and future proteins using both in-vitro, in vivo and applied microgelation processing may highlight, improve and fast-track more functional and sensorially pleasing alternative proteins.

It is also important to use combinations of proteins with balanced amino acid compositions that is often unconsidered in research. This would involve examining their compatibility, highlighting any potential synergistic effects that as seen in **chapter 4** that may yield both beneficial and unfavourable outcomes. Studies on individual subunits and their possible interaction with other protein species should be explored.

Biopolymers were not within the scope of this thesis, however these new proteins should be explored in conjunction with other macronutrients, both carbohydrate (from mono to polysaccharides) and lipids (from saturated to unsaturated). These additional structuring agents within food may complex with proteins alleviating various frictional and sensory challenges but also as functional ingredients *i.e.* new fat mimetics, structuring agents, pharmaceutical design of more nutritious foods or even food packaging.

6.4.2 Advanced characterisation tools and methodology

Enhancing tribology techniques for more realistic scenarios: When consuming food the saliva performs a significant role in lubrication and eating. In **chapter 4** we showed strong interactions with saliva and so the friction of protein solutions should also be measured with saliva incorporated (Brown et al., 2021)

In tribology biomimetic tongue surfaces used in **chapter 5** provided useful and more applicable to real life friction coefficients using surfaces with wettability, elasticity and topography to the tongue. The ongoing utilisation of these surfaces holds promise for future research. However, it is crucial to delve deeper by exploring dynamic tribology protocols. This is essential because eating involves a series of environmental shifts, including periods of starvation, changes in the composition of the tongue's tribofilms, fluctuations in saliva levels, alterations in food moisture, and the impact of residual food particles once they are swallowed. Such dynamic protocols have recently been created by Fan et al. (2021) and such protocol has recently been useful in uncovering plant proteins de-lubricating capacities (Vlădescu et al., 2023).

Visualisation in tribology protocols using microscopy would make for a valuable tool in validating frictional changes in ingredients and foods (Bakalova et al., 2014). Our hypothesis suggests that an aggregation mechanism contributes to the elevated friction observed with plant proteins, conversely the expulsion of water and the promotion of hydration lubrication play a significant role in reducing friction in plant protein microgels. It would be useful to prove such mechanisms where imaging would help. Microscopy has been utilised previously in combination with tribology (Soltanahmadi et al., 2023; Vlădescu et al., 2023) but another avenue for exploration would be thermal imaging where frictional heat may be captured and modelled using infrared.

Participant, assessor demographic and sensory impact: In future sensory study, information on age, gender, nationality, language, education and food exposure (measured by food frequency or other dietary questionnaires) could be an interesting variable in astringency, neural and sensory responses of participants. Such factors has recently been explored by Nuvoli et al., (2023) where astringency may vary depending on habitual diets in vegans compared to omnivores, although such studies are missing with plant proteins among other environmental factors. Additionally how different communities respond to astringency/sensory may differ around the world and so to improve sensory experimentation, participants from a broader pool of participants should be selected or individually measured. Furthermore, it might be advantageous to employ trained panellists for protein assessment, encompassing a wider range of model plant protein solutions. This approach has the potential to streamline the evaluation process, resulting in time savings and an overall increase in the output of research findings. Moreover, it allows for the rapid analysis of a diverse range of proteins in comparison to relying on untrained panellists.

Enhancing sensory methodology through use of neural imaging: In **chapter 4** we showed a significant and specific neural response activation after exposure to food solutions controlled in astringency and viscosity within the PFC. fNIRS provided complementary data to RATA profiling of plant proteins and future study could benefit from comparing responses of different participant groups (age/gender/nationality/food exposure/diet) to specific attributes in controlled studies. In future fNIRS studies a consideration of measuring bitterness should be examined. This is often an attribute similarly associated with astringency and so may be required in order to pre-screen super tasters to improve data.

Furthermore, it is worthwhile to contrast the findings with other neural methodologies such as functional magnetic resonance imaging (fMRI) or electrocardiogram (ECG), which offer more precise insights into neural activation across deeper regions of the brain or delve into the examination of electrical brain waves. Overall employing a combination of these approaches would enhance the interpretability of neural responses. Moreover, it would be interesting to incorporate an analysis of brain stimulation over different time intervals, as demonstrated by afterfeel responses differing in time recorded in RATA (**chapter 4**) where evidence of astringency and viscosity might have been overlooked in the initial neural response.

Nonetheless, a significant hurdle in neural data collection is the complexity requiring extensive training, prolonged periods dedicated to data analysis, and adherence to tightly controlled procedures that have so far limited its wider use in sensory research and application commercially. Given the novelty and underuse, a proactive interest in neural imaging should be integrated into sensory research to promote its incorporation, advance neural technology design and understanding of the origin of sensory processing in the future.

6.4.3 Microgels

Physicochemical properties of microgels: In **chapter 5** new plant protein microgel particles were created. These microgels were characterised in size, shape, adsorption, mathematically and in their stability. In food their presents numerous conditions that effect functionality of proteins such as ions, pH and temperature that may alter macroscopic food properties. Further testing on pea protein microgel stability should be assessed including the later in appropriate food relevant conditions and samples.

To elucidate the structure, employing small and wide angle x-ray diffraction (SAXS/WAXS) could prove valuable information comprehending the heating-induced transformations of native proteins into a microgel state. Both X-ray techniques can offer more precise structural insights into the formation and composition of microgels, thereby contributing to the development of enhanced structural models. Other additional techniques also include ultrasonic spectroscopy that could validate interaction and stability of microgels by measuring their acoustic properties or Raman spectroscopy to provide information on chemical composition and surface functional group changes. Additionally circular dichroism spectroscopy can be used to understand denaturation of proteins into microgels which was briefly performed for native pea and potato protein and also flow-induced dispersion analysis (**Figure 6.2, Figure 6.3**) that provides information on molecular weight, hydrodynamic size and also the nature of the aggregates. The latter two are very efficient and effective at understanding protein structure and would benefit characterisation of protein or microgels.

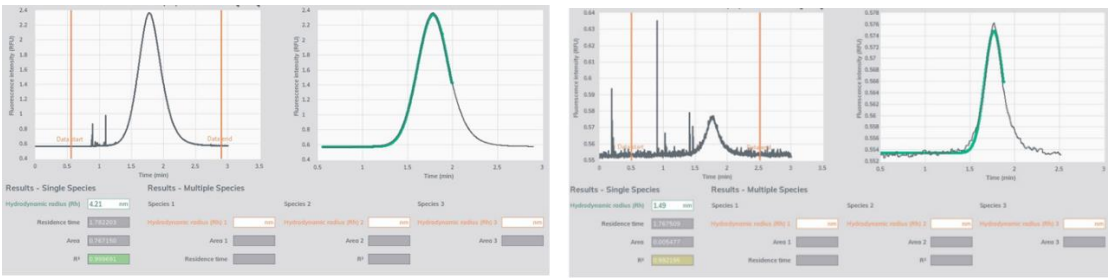

Figure 6.2 Flow induced dispersion results from potato protein isolate and pea protein concentrate as a future characterisation tool. Results display the size of protein and nature of aggregates.

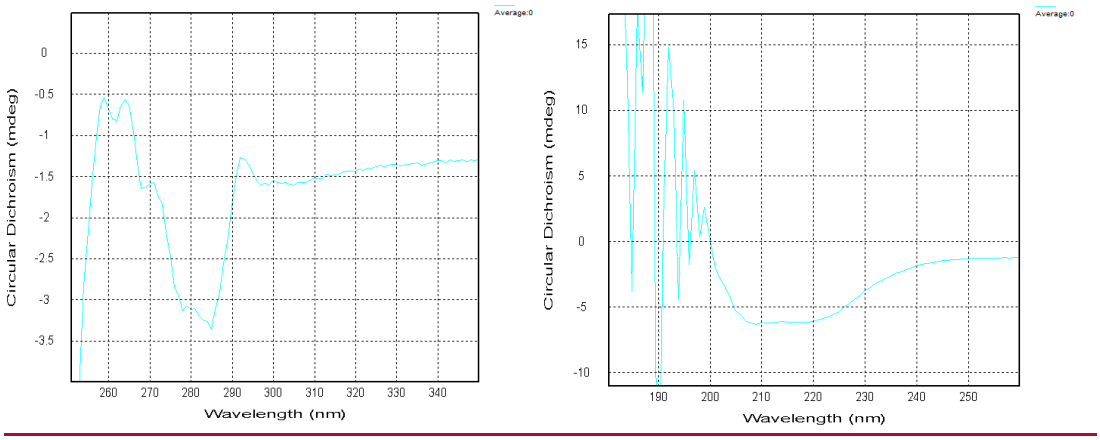

Figure 6.3 Circular dichroism spectroscopy conducted on potato protein isolate (left) and pea protein concentrate (right) as a future characterisation tool. Results indicate the secondary structure of proteins, in this case potato protein is observed as having a alpha helical conformation.

Digestibility and nutritional properties associated with microgelation: Asides from sensory and functional issues, plant proteins can also suffer from poor digestibility and bioavailability typically measured by the digestible indispensable amino acid score (DIAAS value). Potato protein is unique in its DIAAS score above 100 which is similar to egg and casein proteins. However for a lot of alternative new plant proteins, namely lupin, pea, hemp, oat there DIAAS is below 75 thanks to poor digestibility, amino acid sequence and anti-nutritional factors. It is unknown if bulk consumption of protein microgelation with low aggregation, higher surface area states could promote enzyme effectiveness to digest proteins to amino acids in the small intestine. Current research points towards good digestibility (Zhang et al., 2020) although these are as oil in water Pickering stabilisers and so low concentration and structurally modified. Conversely microgelation may hinder digestion and then may find application of controlled release of substances (i.e. drugs). It has also been evidenced that pea microgels possess sustained release abilities due to their gel-steric stabilisation states and that may delay digestion (Shao and Tang, 2016). Additionally

microgels were observed to swell (**Chapter 5**) and so may contribute to the feeling of fullness similar to soluble fibre and if undigested proteins remain, may have prebiotic activity that should be assessed. In general investigating the microgels using an INFOGEST in-vitro model would be beneficial in particular assessing changes upon extremes in environmental pH throughout digestion. Additionally, in human participants amino acid uptake could be measured in the blood to understand rate, efficiency and concentration of amino acid uptake compared to native proteins that may serve as a interesting sports or health supplement applications.

Sensory evaluation compared to native protein: Similar to **chapter 4** such sensory, neural and cellular methodology could be performed on these microgels. Additionally other sensory tests including preference, or discrimination tests can be conducted in fat replacement ability or for preference in food formulations.

Food product development: An obvious next step would be to incorporate these microgels into food products. Several ways these microgels can be incorporated from characteristics displayed in this thesis are proposed:

1) Microgel liquid solution. Additional flavour mitigators and preservation techniques (i.e. pasteurisation/ultra heat treatment – where we showed effective thermal resistance) could enable the solution to serve as a high protein, low fat beverage. This would follow typical styles to current high protein whey milk products but also with thermal stability (and pH dependant stability) that may branch into suitable improved creamy low fat plant based milks or used for a new product category such as high protein hot beverages.

2) low or high protein concentration fat mimetic. These microgels could be added to products as a fat mimetic or in low friction high protein application as

lubrication was excellent at 0.5 to 12 wt% total protein concentrations in **chapter 5** (Calculated from various volume fractions created). Product categories could follow current use that include dairy (ice-cream, yoghurt etc) but also, as an ingredient typically utilised in savoury use, plant protein microgels should be considered for the replacing of plant oils (humus, oil sprays, vinaigrettes, mayonnaise, salad creme etc.) that would also compliment its natural flavour profile. Considering the improved viscosity-modifying characteristics of potato microgels, it's conceivable that novel applications resembling those of soft margarine or butter could be developed. In lattice-style pastries, butter serves as a lubricant amid pastry layers. Upon heating, it liquefies, water vaporises, and delicate layers are produced. Similarly, in choux pastry, it expands into a hollow shell. Analogously, high-volume fraction microgel pastes might exhibit similar traits to more solid saturated fat, potentially facilitating the creation of optimised, lower-fat baked applications.

3) Solid microgel powders. Microgels could be re-solidified by spray/freeze drying either after initial protein extraction or as a step within protein extraction. These resultant powders hold promise for application in dry food contexts, including baked goods and protein fortification as well as improve transportation efficiency.

4) Meat alternative formulations. Whether in liquid or powder form, these microgels have the potential to serve as a lubricant in meat analogues. They could contribute to both the retention of moisture and juiciness, while also serving as a partial substitute for fat, both are major problems associated with vegetarian and vegan meat alternatives.

Taste/flavour/ingredient release. As hydrated gel particles that initially exists as a continuous phase of water, a variety of water soluble compounds or

ingredients could be dispersed before gelling. These flavours could potentially mitigate off-flavours or, depending on their pH resistance, serve as an ingestible protective matrix for antioxidant, probiotic, or medicinal components that are subsequently released later or slowly during the digestion process (Souza Almeida et al., 2021).

Life cycle assessment. In **chapter 5** LCA was hypothesised from past literature to be low for microgels (Heller and Keoleian, 2018; Saerens et al., 2021; Kew et al., 2023), however a full LCA should be assessed if it were to be mass produced to assess true sustainable impact.

6.5 References

A. Troszynska, R.A., G. Lamparski, A. Wołejszo, N. Baryłko-Pikielna. 2006. Investigation of astringency of extracts obtained from selected tannins-rich legume seeds. *Food Quality and Preference*. 17, pp.31-35.

Andablo-Reyes, E., Bryant, M., Neville, A., Hyde, P., Sarkar, R., Francis, M. and Sarkar, A. 2020. 3d biomimetic tongue-emulating surfaces for tribological applications. *ACS Applied Materials & Interfaces.* 12(44), pp.49371-49385.

Bajec, M.R. and Pickering, G.J. 2008. Astringency: Mechanisms and perception. *Critical Reviews in Food Science and Nutrition.* 48(9), pp.858-875.

Bakalova, T., Louda, P., Voleský, L. and Andršová, Z. 2014. The use of optical microscopy to evaluate the tribological properties. *Manufacturing Technology Journal*. 14(3), pp.256-261.

Brown, F.N., Mackie, A.R., He, Q., Branch, A. and Sarkar, A. 2021. Protein–saliva interactions: A systematic review. Food & Function. 12(8), pp.3324-3351.

Canon, F., Belloir, C., Bourillot, E., Brignot, H., Briand, L., Feron, G., Lesniewska, E., Nivet, C., Septier, C., Schwartz, M., Tournier, C., Vargiolu, R., Wang, M.,

Zahouani, H. and Neiers, F. 2021. Perspectives on astringency sensation: An alternative hypothesis on the molecular origin of astringency. *Journal of agricultural and food chemistry*. 69(13), pp.3822-3826.

Cheynier, V. 2012. Phenolic compounds: From plants to foods. *Phytochemistry Reviews.* 11(2), pp.153-177.

Fan, N., Shewan, H.M., Smyth, H.E., Yakubov, G.E. and Stokes, J.R. 2021. Dynamic tribology protocol (dtp): Response of salivary pellicle to dairy protein interactions validated against sensory perception. *Food Hydrocolloids*. 113, p106478.

Heller, M.C. and Keoleian, G.A. 2018. Beyond meat's beyond burger life cycle assessment: A detailed comparison between. (1–38). University of Michigan.

Kew, B., Holmes, M., Liamas, E., Ettelaie, R., Connell, S.D., Dini, D. and Sarkar, A. 2023. Transforming sustainable plant proteins into high performance lubricating microgels. *Nature Communications*. 14(1), p4743.

Kew, B., Holmes, M., Stieger, M. and Sarkar, A. 2021. Oral tribology, adsorption and rheology of alternative food proteins*. Food Hydrocolloids*. 116, p106636.

Krolczyk, J.B., Dawidziuk, T., Janiszewska-Turak, E. and Solowiej, B. 2016. Use of whey and whey preparations in the food industry - a review. *Polish Journal of Food and Nutrition Sciences.* 66(3), pp.157-165.

Nuvoli, C., Fillion, L., Lacoste Gregorutti, C. and Labbe, D. 2023. Comparison of sensitivity to taste and astringency stimuli among vegans and omnivores. *Physiology & Behavior.* 262, p114092.

Saerens, W., Smetana, S., Van Campenhout, L., Lammers, V. and Heinz, V. 2021. Life cycle assessment of burger patties produced with extruded meat substitutes. *Journal of Cleaner Production.* 306, p127177.

Shao, Y. and Tang, C.-H. 2016. Gel-like pea protein pickering emulsions at ph3.0 as a potential intestine-targeted and sustained-release delivery system for β-carotene. *Food Research International.* 79, pp.64-72.

Smithers, G.W. 2008. Whey and whey proteins—from 'gutter-to-gold'. *International Dairy Journal*. 18(7), pp.695-704.

Smithers, G.W. 2015. Whey-ing up the options – yesterday, today and tomorrow. *International Dairy Journal.* 48, pp.2-14.

Soltanahmadi, S., Bryant, M. and Sarkar, A. 2023. Insights into the multiscale lubrication mechanism of edible phase change materials. *ACS Applied Materials & Interfaces.* 15(3), pp.3699-3712.

Souza Almeida, F., Guedes Silva, K.C. and Kawazoe Sato, A.C. 2021. Polysaccharide-peptides-based microgels: Characterization, in-vitro digestibility, and rheological behavior of their suspensions. *Food Biophysics*. 16(4), pp.440-450.

Vlădescu, S.-C., Agurto, M.G., Myant, C., Boehm, M.W., Baier, S.K., Yakubov, G.E., Carpenter, G. and Reddyhoff, T. 2023. Protein-induced delubrication: How plant-based and dairy proteins affect mouthfeel. *Food Hydrocolloids*. 134, p107975.

Zhang, S., Holmes, M., Ettelaie, R. and Sarkar, A. 2020. Pea protein microgel particles as pickering stabilisers of oil-in-water emulsions: Responsiveness to ph and ionic strength. *Food Hydrocolloids.* 102, p105583.

Appendix A Supporting information for chapter 2

Table A1. Characterization techniques used in various studies involving protein—based fat replacers and microgels**.**

Protein types	References	Size	Rheology	Sensory	Tribology
Protein Concentrates/isolates	Zhang, 2015	✓	✓		
	Costa, 2016		✓		
	Fang, 2019	✓	✓	✓	
	Jørgensen, 2015	✓	✓	✓	
	Guo, 2018	✓	✓	✓	
	Liu, 2018	✓	✓	✓	
	Zhu, 2019	✓	✓		✓
	Dabija, 2018		✓	✓	
	Danesh, 2018	✓	✓		
	Schädle, 2020		✓		
Micro-particulated protein	Aggarwal, 2016			✓	
	El-Aidie, 2019	✓	✓	✓	

	Torres, 2018	✓	✓		
	Temiz, 2015		✓	✓	
	Akin, 2015		✓	✓	
	Urgu, 2019	✓	✓	✓	
	Olivares, 2019	✓	✓		✓
	Liu, 2018	✓	✓	✓	
	Beran, 2018	✓		✓	
	Zhang, 2020a	✓	✓		✓
	Schädle, 2020		✓		
Microgels	Torres, 2017	✓	✓		
	Sarkar, 2016	✓			
	Sarkar, 2017	✓	✓		✓
	Sarkar, 2018	✓			

Andablo-Reyes, 2019	✓	✓	✓
Bahri, 2019	✓	✓	
Jiao, 2018	✓		
Li, 2020	✓	✓	
Araiza-Calahorra, 2019	✓	✓	

Appendix B supporting information for chapter 3

Table B1. Mean and standard deviation (SD) of the friction coefficients of buffer and soluble protein solutions at 1 wt% (a), 5 wt% (b), 10 wt% (c) and 10 wt% scaled with viscosity at 1000 s-1 (η∞ U (Pa m)) (d). Soluble protein fraction samples were prepared in the control HEPES buffer at pH 7 at a temperature of 37oC. Different lower case letters in the same column indicate a statistically significant difference ($p < 0.05$).

(a)	**Coefficient of friction of 1 wt% protein$_{sol}$**							
	Boundary lubrication regime (0.01 m s^{-1})		Mixed lubrication regime (0.1 m s^{-1})		Mixed lubrication regime (0.3 m s^{-1})		Hydrodynamic lubrication regime (1.0 m s^{-1})	
	Mean	SD	Mean	SD	Mean	SD	Mean	SD
Buffer	0.509^{c}	0.128	0.182^{d}	0.116	0.056^{abc}	0.035	0.014^{a}	0.005
WPI_{sol}	0.387^{bc}	0.018	0.164^{abd}	0.018	0.051^{ab}	0.007	0.015^{a}	0.001

$PoPI_{sol}$	0.327^{a}	0.005	0.157^{ad}	0.005	0.056^{ab}	0.003	0.013^{a}	0.001
PPC_{sol}	0.332^{a}	0.010	0.164^{bd}	0.001	0.058^{b}	0.001	0.013^{a}	0.001
LPI_{sol}	0.401^{bc}	0.011	0.202^{cd}	0.003	0.066^{c}	0.002	0.013^{a}	0.001
IPC_{sol}	0.335^{a}	0.008	0.149^{ad}	0.005	0.053^{a}	0.002	0.013^{a}	0.001

(b)	**Coefficient of friction of 5 wt% protein$_{sol}$**							
	Boundary lubrication regime (0.01 m s^{-1})		Mixed lubrication regime (0.1 m s^{-1})		Mixed lubrication regime (0.3 m s^{-1})		Hydrodynamic lubrication regime (1.0 m s^{-1})	
	Mean	SD	Mean	SD	Mean	SD	Mean	SD
Buffer	0.509^{f}	0.128	0.182^{e}	0.116	0.056^{d}	0.035	0.014^{c}	0.005
WPI_{sol}	0.069^{a}	0.005	0.024^{a}	0.002	0.010^{a}	0.001	0.008^{ac}	0.001
$PoPI_{sol}$	0.082^{b}	0.006	0.027^{a}	0.001	0.010^{a}	0.001	0.009^{abc}	0.001
PPC_{sol}	0.234^{e}	0.006	0.097^{de}	0.003	0.031^{cd}	0.002	0.011^{bc}	0.001
LPI_{sol}	0.164^{d}	0.006	0.073^{ce}	0.001	0.024^{bd}	0.001	0.009^{abc}	0.001
IPC_{sol}	0.098^{c}	0.003	0.032^{b}	0.001	0.010^{a}	0.001	0.008^{ac}	0.001

(c)	**Coefficient of friction of 10 wt% protein$_{sol}$**			
	Boundary lubrication regime (0.01 m s^{-1})	Mixed lubrication regime (0.1 m s^{-1})	Mixed lubrication regime (0.3 m s^{-1})	Hydrodynamic lubrication regime (1.0 m s^{-1})

	Mean	SD	Mean	SD	Mean	SD	Mean	SD
Buffer	0.509^{f}	0.128	0.182^{f}	0.116	0.056^{d}	0.035	0.014^{b}	0.005
WPI_{sol}	0.051^{a}	0.001	0.011^{a}	0.001	0.010^{a}	0.001	0.016^{bc}	0.002
$PoPI_{sol}$	0.126^{b}	0.002	0.041^{b}	0.001	0.012^{a}	0.001	0.011^{ab}	0.001
PPC_{sol}	0.205^{e}	0.001	0.083^{ef}	0.001	0.020^{cd}	0.001	0.009^{ab}	0.001
LPI_{sol}	0.182^{d}	0.004	0.060^{d}	0.002	0.015^{b}	0.001	0.011^{ab}	0.002
IPC_{sol}	0.152^{c}	0.012	0.054^{c}	0.001	0.015^{b}	0.002	0.010^{ab}	0.001

(d)	**Coefficient of friction of 10 wt% protein$_{sol}$ scaled η_{∞} U (Pa m)**							
	Boundary lubrication regime (0.01 m s^{-1})		Mixed lubrication regime (0.1 m s^{-1})		Mixed lubrication regime (0.3 m s^{-1})		Hydrodynamic lubrication regime (1.0 m s^{-1})	
	Mean	SD	Mean	SD	Mean	SD	Mean	SD
Buffer	0.509^{f}	0.128	0.182^{e}	0.116	0.056^{d}	0.035	0.014^{d}	0.005
WPI_{sol}	0.059^{a}	0.006	0.014^{a}	0.002	0.009^{a}	0.001	0.013^{bcd}	0.002
$PoPI_{sol}$	0.150^{b}	0.004	0.066^{b}	0.001	0.027^{bd}	0.001	0.010^{abd}	0.001
PPC_{sol}	0.260^{d}	0.001	0.163^{de}	0.006	0.096^{e}	0.001	0.026^{e}	0.001
LPI_{sol}	0.199^{c}	0.002	0.125^{ce}	0.003	0.050^{cd}	0.001	0.013^{cd}	0.001
IPC_{sol}	0.159^{b}	0.011	0.064^{b}	0.001	0.023^{bd}	0.003	0.009^{ad}	0.001

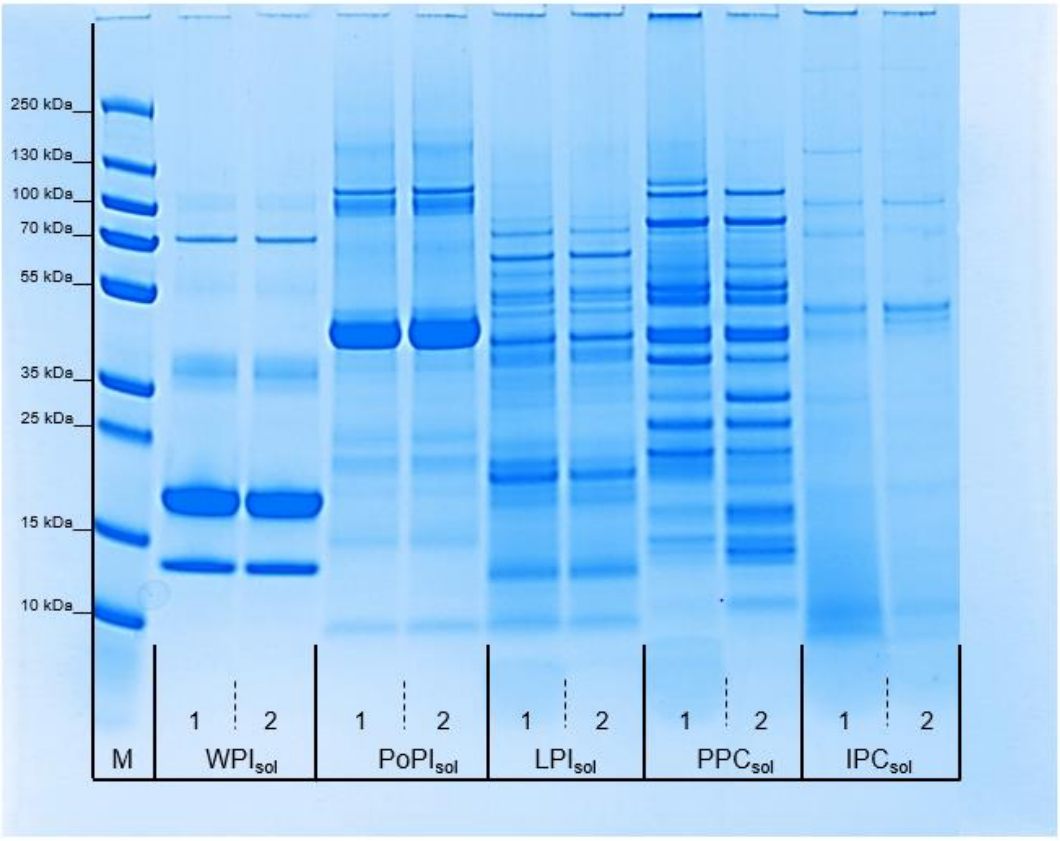

Figure B1. Raw data of the sodium dodecyl sulphate polyacrylamide gel electrophoresis (SDS-PAGE) of protein solutions at pH 7.0. 1 and 2 refers to the uncentrifuged and centrifuged samples, respectively. M represents the protein marker.

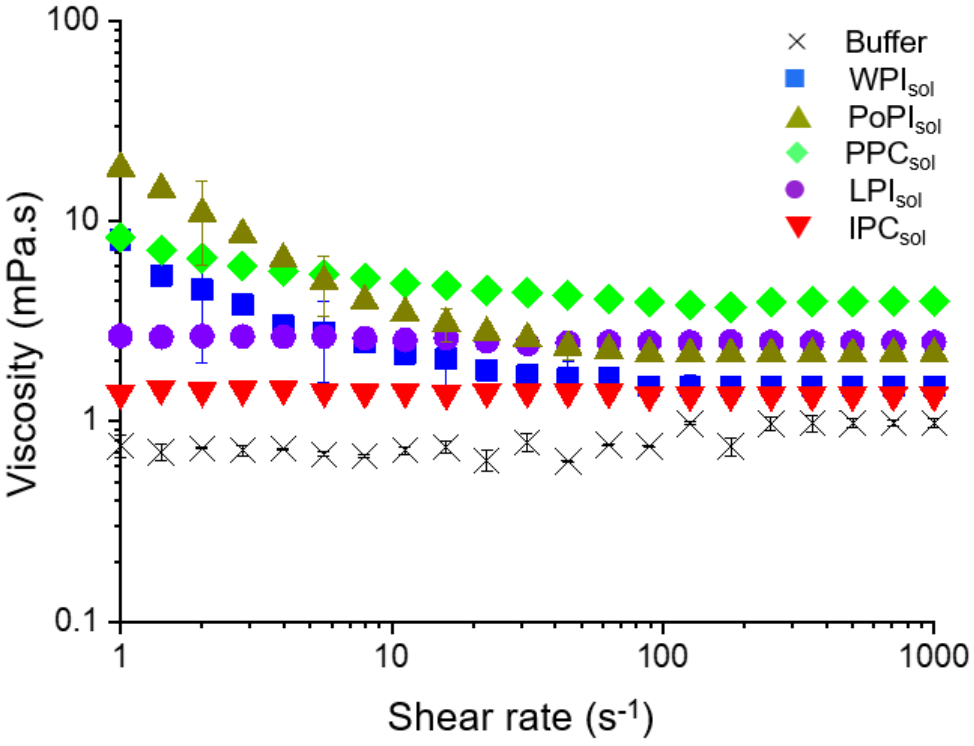

Figure B2. Flow curves of protein solutions (10 wt% protein) at pH 7.0. Error bars indicate standard deviation for triplicate experiments (n = 3 × 3).

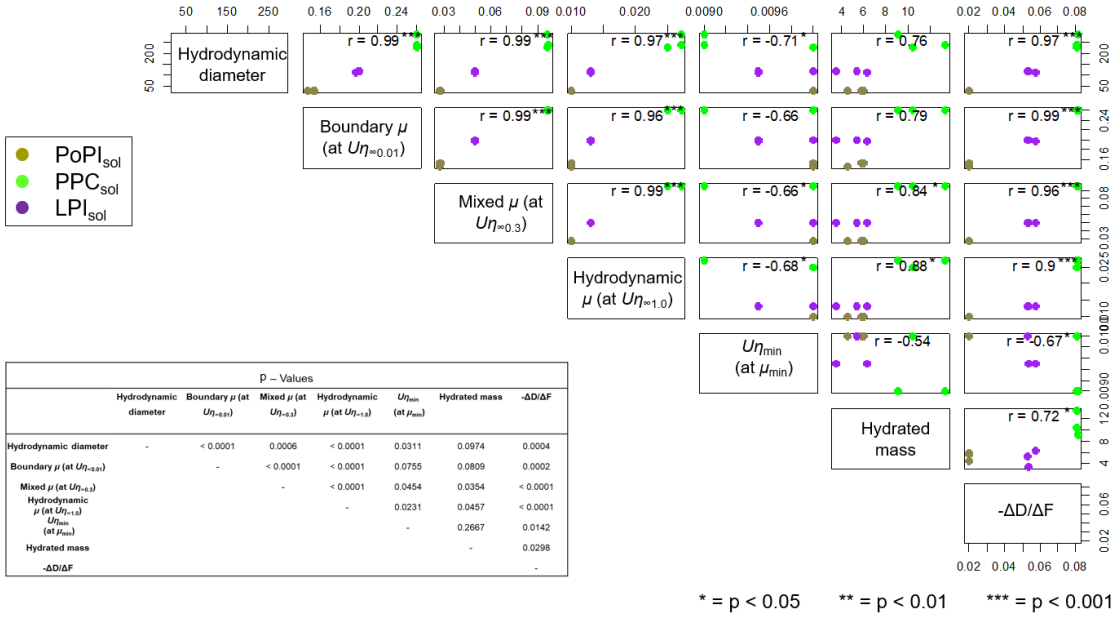

Figure B3. Pearson correlation (r) of instrumental data for 10 wt% protein solutions excluding WPIsol and IPCsol, where per protein data set n = 3. Spearman's rank was

used to obtain p-values shown in the inset table and translated into *, **, *** indicating 0.05-0.001 in order of significance.

Appendix C supporting information for chapter 4

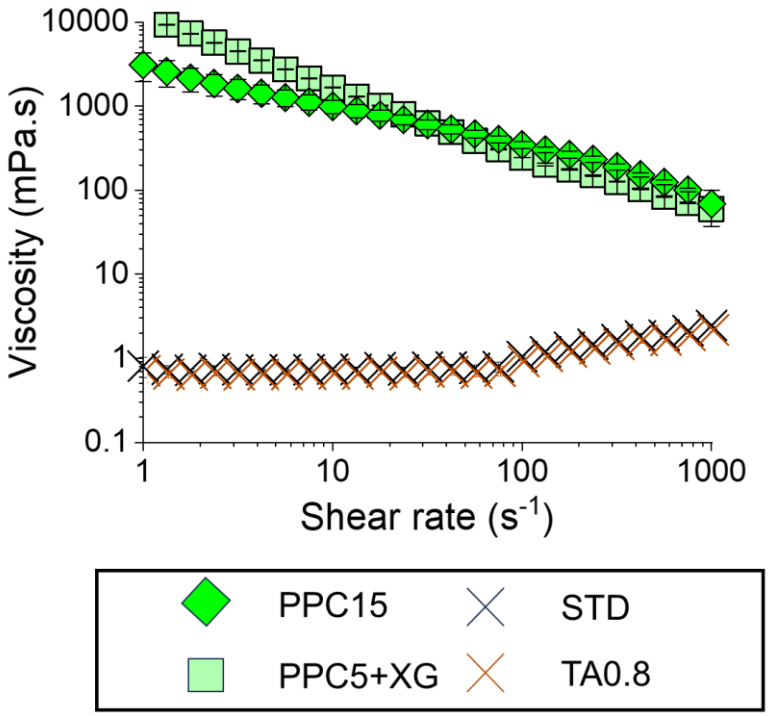

Figure C1 Flow curves of solutions in standardisation of their viscosity. Apparent viscosity of 5 wt% total protein pea protein concentrate with xanthan gum (PPC+XG), 15 wt% total protein pea protein concentrate, standard water (STD) and 0.8 total wt% tannic acid (TA0.8) in controlling viscosity of solutions when measuring neural response using functional near infrared spectroscopy (fNIRS). Shear rates were measured ramping up from 1 s^{-1} to 1000 s^{-1} at 37 ^{o}C with plots as means of three measurements on triplicate samples (n = 6 x 3) with error bars representing standard deviations.

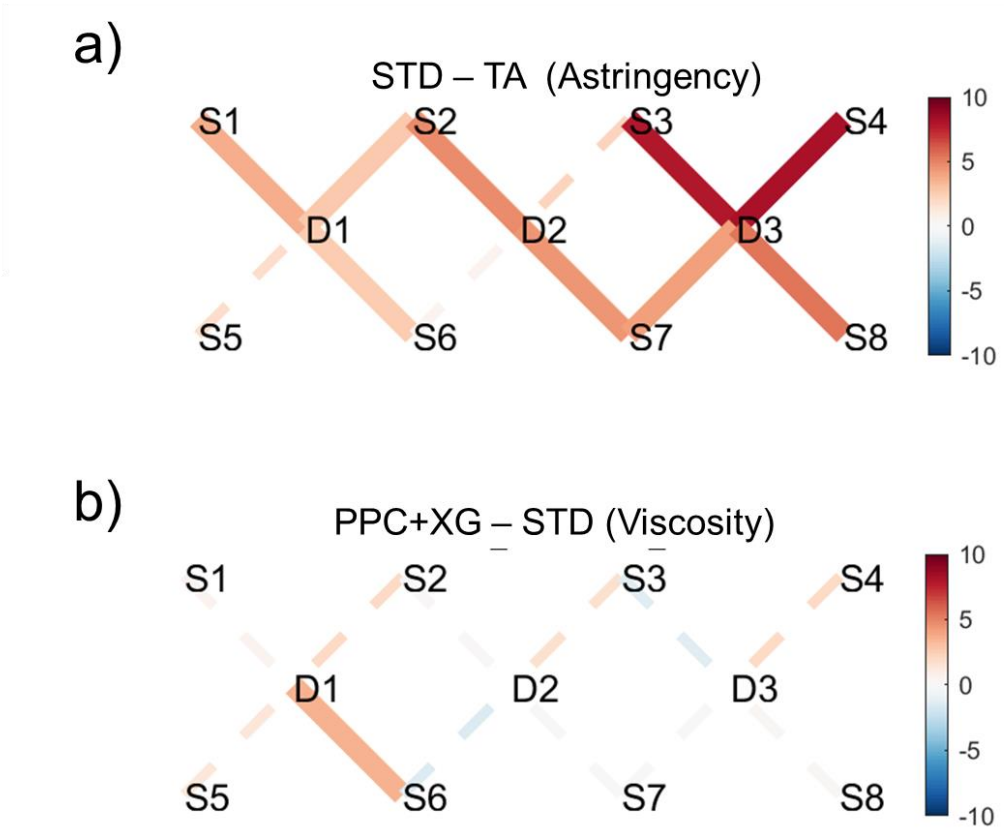

Figure C2 Neural contrasts depicting deoxygenated haemoglobin (HbO) response. Block averaged overall neural effect (T-stat) from 35 participants of (a) astringency calculated by an overall effect contrast between the neural response of water (STD) and 0.8 wt% tannic acid (TA.08), (b) viscosity calculated by an overall effect contrast between the neural response of 5 wt% total protein pea protein concentrate with xanthan gum (PPC+XG) and 15 wt% pea protein concentrate (PPC15). Solid connecting lines represent statistically significant response ($p < 0.05$) with their colour legend indicating magnitude of difference. A positive value (red) reflects increase in HbO whilst a negative value (blue) reflects decreased HbO.

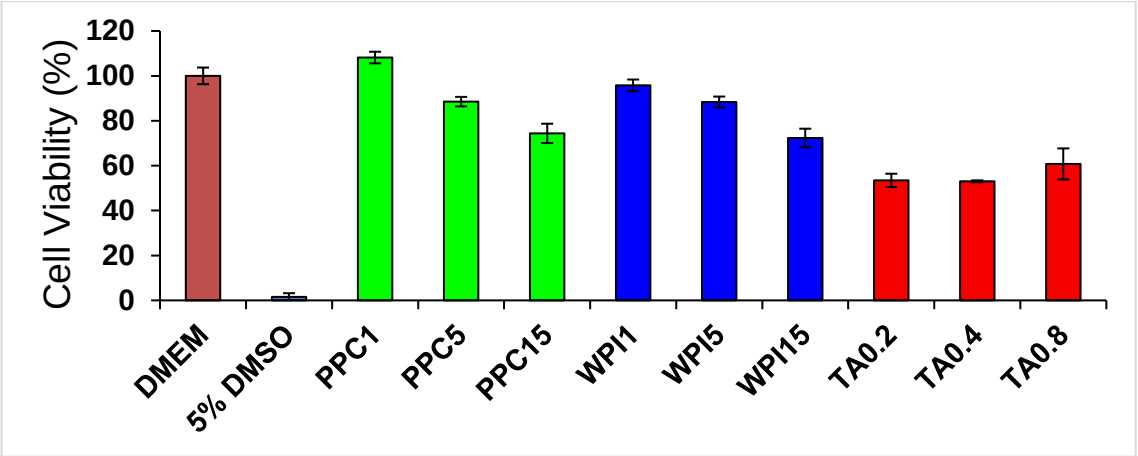

Figure C3 Cytotoxicity assay response of solutions. Cell viability (%) as compared to medium control (Dulbecco's Modified Eagle Medium (DMEM) of 1-15 wt% total protein pea protein concentrate (PPC1, PPC5, PPC15), 1-15 wt% total protein whey protein isolate (WPI1, WPI5, WPI15), 0.2-0.8 wt% tannic acid (TA0.2, TA0.4, TA0.8). Results are plotted as means and standard deviations of 6 repeat measurements on triplicate samples (n = 6 x 3) with error bars representing standard deviations.

Table C1. Overview of sensory terms and definitions used in Rata-All-That-Apply **(RATA)**

Category	RATA Terms	Definitions
Taste	Vanilla flavour	The degree to which the sample tastes like vanilla
	Off flavour	The degree to which the sample tastes undesirable/harsh in flavour
	Cereal flavour	The degree to which the sample tastes like hay/straw
	Sweetness	Sweet sensation from sucrose, sweetener
	Beany flavour	Bean, pea like flavour
Texture	Creamy	The degree to which the sample gives a silky, rich, full mouthfeel.
	Slippery	The degree to which sample can slide easily in the mouth
	Grainy	The presence of granules, particles in the mouth
	Smooth	homogenous; absence of lumpiness and graininess; the sample flows easily in the mouth.
	Thick	The thickness of the sample; the amount of force needed to make the sample flow or deform in the mouth.

	Thin	The lack of force needed to allow the sample to flow in the mouth
	Rough	A drying, little lubricating saliva, sensation in the mouth
	mouthcoating	The feeling that a layer of the sample remains behind in the mouth and palate after swallowing.
	Astringent	Puckering, mouth-drying, rough sensation
After-Feel	Creamy	The degree to which the sample gives a silky, rich, full mouthfeel.
	Rough	A drying, little lubricating saliva, sensation in the mouth
	Astringent	Puckering, mouth-drying, rough sensation

Table C2 Summary of the overall effect (Beta, T-Stats) and statistical differences (standard error (SE), Q-value) of measuring the neural response using functional near-infrared-spectroscopy (fNIRS) of water (STD), 5 wt% total protein pea protein concentrate with xanthan gum (PPC+XG), 15 wt% pea protein concentrate (PPC15) and 0.8 wt% tannic acid.

STD					
Source	Detector	Beta	SE	T stats	Q value
1	1	2.764554	2.270018	1.217856	0.443292
2	1	5.02406	2.183223	2.301213	0.090403
2	2	2.865867	2.342557	1.223392	0.443292
3	2	6.65238	2.449732	2.715554	0.035872
3	3	-8.37293	2.571169	-3.25647	0.00788
4	3	-1.32706	2.414454	-0.54963	0.762368
5	1	0.312155	2.87489	0.10858	0.953491
6	1	4.159245	2.1469	1.937326	0.190782
6	2	-0.37471	2.211513	-0.16944	0.933907
7	2	2.46029	2.453209	1.002886	0.540122
7	3	-0.52051	2.705251	-0.19241	0.924904
8	3	3.397	2.652674	1.280594	0.424532
1	1	2.764554	2.270018	1.217856	0.443292
TA0.8					
Source	Detector	Beta	SE	T stats	Q value
1	1	14.49171	2.228701	6.502311	3.55E-09
2	1	13.30105	2.152639	6.178952	1.56E-08
2	2	18.48557	2.218184	8.33365	5.56E-13
3	2	14.29121	2.422732	5.8988	5.47E-08
3	3	20.64669	2.570726	8.031459	2.44E-12
4	3	25.8114	2.221304	11.61993	5.21E-20
5	1	7.728557	2.947304	2.622246	0.010159
6	1	12.58965	2.38305	5.282997	7.93E-07
6	2	1.2373	2.298801	0.538237	0.591659

7	2	17.79902	2.394737	7.432556	4.42E-11
7	3	15.35323	2.674304	5.741019	1.10E-07
8	3	22.84725	2.478662	9.217574	7.14E-15
PPC5+XG					
Source	Detector	Beta	Se	T stats	Q value
1	1	1.072986	2.236956	0.479663	0.777041
2	1	-0.90492	2.117651	-0.42732	0.784507
2	2	2.470686	2.276936	1.085092	0.518027
3	2	0.966141	2.375224	0.406758	0.792395
3	3	-3.72009	2.56167	-1.45221	0.35475
4	3	-8.01622	2.343136	-3.42115	0.004893
5	1	-4.9647	2.808615	-1.76767	0.2658
6	1	-6.91716	2.300998	-3.00616	0.016206
6	2	4.509416	2.243104	2.010346	0.167822
7	2	3.461466	2.394256	1.445737	0.35475
7	3	-0.08123	2.710983	-0.02996	0.976159
8	3	1.869244	2.492818	0.749852	0.682766
PPC15					
Source	Detector	Beta	SE	T stats	Q value
1	1	3.732236	2.257393	1.653339	0.296672
2	1	-12.3508	1.886992	-6.54523	4.66E-08
2	2	-2.07453	2.078299	-0.99819	0.540122
3	2	1.19604	2.346894	0.509627	0.762368
3	3	-0.86617	2.630441	-0.32929	0.819482
4	3	-9.08842	2.437694	-3.72829	0.002086
5	1	-4.82532	2.870323	-1.68111	0.296672
6	1	-9.06618	2.208746	-4.10467	0.000583
6	2	-5.66858	2.2283	-2.5439	0.052417
7	2	-1.38083	2.398233	-0.57577	0.762368
7	3	4.214403	2.57572	1.636204	0.296672
8	3	1.657845	2.624359	0.631714	0.762368

Table C3 Rate-All-That-Apply (RATA) values attained after consumption of water (STD), 5 wt% total protein pea protein concentrate with xanthan gum (PPC+XG), 15 wt% pea protein concentrate (PPC15) and 0.8 wt% tannic acid undergoing neural functional near-infrared spectroscopy (fNIRS) analysis. Results are plotted as means and standard deviation from 35 participants with different lowercase letters of significant difference (*p = 0.05*)

	PPC5+XG	PPC15	SD	TA
Sweet	4.7 ± 1.6a	3.2 ± 1.7c	6.8 ± 1.4b	2.6 ± 1.6c

Astringent	2.6 ± 1.9a	6.4 ± 2.2b	1.0 ± 1.9a	7.9 ± 1.7c
Thick	6.7 ± 2.0a	7.9 ± 1.2a	1.6 ± 1.0c	1.9 ± 1.6c
Smooth	6.6 ± 2.1a	2.2 ± 1.9c	5.5 ± 2.2b	3.2 ± 1.8d
Creamy	6.3 ± 1.9a	5.7 ± 2.3a	2.6 ± 2.0b	1.7 ± 1.3c

Table C4 Associated *p* values in the Absorbance of Alcian blue stained squamous cell carcinoma cells with saliva (TR146+S) after application and washed with water control (Ctr), 0.8 wt% tannic acid (TA0.8), pea protein concentrate at a total protein concentration of 1 wt% (PPC1), 5 wt% (PPC5) and 15 wt% (PPC15), and whey protein isolate at a total protein concentration of 1 wt% (WPI1), 5 wt% (WPI5) and 15 wt% (WPI15).

	Ctr+ Saliva	**PPC1**	**PPC5**	**PPC15**	**WPI1**	**WPI5**	**WPI15**	**TA0.8**
Ctr+Saliva		0.098	<0.001	<0.001	0.877	0.360	0.100	<0.001
PPC1			0.001	0.009	0.583	0.879	0.534	<0.001
PPC5				0.576	0.003	<0.001	0.001	<0.001
PPC15					0.001	<0.001	0.002	0.003
WPI1						0.326	0.176	<0.001
WPI5							0.508	<0.001
WPI15								<0.001
TA0.8								

Supporting information C1 Questionnaire for Rate-All-That-Apply

Qualtrics XM

Thank you for taking part in this sensory trial!

You will be tasting vanilla flavoured protein beverages consisting of new, vegan and sustainable "proteins of tomorrow" (types of new, emerging plant protein for future food use!). You are contributing to research that will improve plant proteins which are also ethical, energy efficient and more accessible in developing countries.

I hope you enjoy trying these new proteins and we will also give you £5 voucher for your time.

Personal details

In this section you will be asked for your personal details such as name and surname, email and phone number. All information will be kept strictly confidentially. This information is need for two reasons:

1. In case you are eligible and decide to take part into the study you will be paid **£5** in vouchers, after completing the study. Please make sure you give your name and surname correctly.
2. In case you decide to withdraw from the study, we need to be able to identify the right person and withdraw the right responses.

Note: We ask for your phone number as the research team will call/message you before each session for a short Covid-19 health screening, to make sure each participants is Covid-19 free

In this section we ask specific questions that is important to our study

Where is your home country

Whats your current level of education? (e.g. College/Undergraduate/Postgraduate)

Roughly how many portions of vegetables do you consume per day (80g/handfull of one vegetable type = 1 portion)

Are you following any specific diet (e.g. vegetarian/vegan)

- Vegetarian
- Vegan
- Other (please specify)

What is your name

What is your surname

What is your email

What is your mobile phone number? Note: We ask for your phone number as the research team will call/message you before each session for a short Covid-19 health screening, to make sure each participants is Covid-19 free.

What is your gender

- Male
- Female
- Non-binary / third gender
- Prefer not to say

In this last section you will be asked some health screening related questions.

Do you smoke (y/n)

Do you have any oral infections/diseases (y/n)

Do you have chronic or acute health condition that may affect ability to sense, eat, digest, absorb or excrete food? (y/n)

Do you suffer from IBS (y/n)

Are you pregnant (y/n)

Are you currently breast feeding (y/n)

Are you on any special diet or taking protein and/or fibre supplements? (y/n)

Can you tolerate protein liquids (potato/lupin/pea) (y/n)

May we keep this information on file and contact you about future studies? (y/n)

Participant number: ____ **Sample:___**

Taste/Flavour									
Attribute	**Tick if applies**	**Circle number in how you rate the intensity of the ticked attribute (1 being lowest intensity and 9 being highest intensity)**							
		Lowest →							**Highest**
Sweetness		1	2	3	4	5	6	7	8	9
Notes:									
Vanilla Flavour		1	2	3	4	5	6	7	8	9
Notes									
Cereal-Flavour		1	2	3	4	5	6	7	8	9
Notes:									
Off-Flavour		1	2	3	4	5	6	7	8	9
Notes:									
Beany Flavour		1	2	3	4	5	6	7	8	9
Notes:									

Texture									
Creamy		1	2	3	4	5	6	7	8	9
Notes:									
Slippery		1	2	3	4	5	6	7	8	9
Notes									
Grainy		1	2	3	4	5	6	7	8	9
Notes:									
Smooth		1	2	3	4	5	6	7	8	9
Notes:									
Rough		1	2	3	4	5	6	7	8	9
Notes:									
Thick		1	2	3	4	5	6	7	8	9
Notes:									
Thin		1	2	3	4	5	6	7	8	9
Notes:									
Mouthcoating		1	2	3	4	5	6	7	8	9
Notes:									
Astringent		1	2	3	4	5	6	7	8	9
Notes:									

Afterfeel (10 seconds after consumption)									
Attribute	**Tick if applies**	**Circle number in how you rate the intensity of the ticked attribute (1 being lowest intensity and 9 being highest intensity)**							
		Lowest			→				**Highest**
Creamy		1	2	3	4	5	6	7	8	9
Notes:									
Rough		1	2	3	4	5	6	7	8	9
Notes									
Astringent		1	2	3	4	5	6	7	8	9
Notes:									

Supporting information C2 Questionnaire for Check-All-That-Apply (CATA)

Appearance		Taste/flavour		Texture		Afterfeel (after 10 seconds)	
Glossy	☐	Dairy	☐	Creamy	☐	Creamy	☐
Creamy	☐	Vanilla	☐	Slippery	☐	Fatty	☐
Smooth	☐	Earthy	☐	Fatty	☐	Rough	☐
Transparent	☐	Vegetal	☐	Grainy	☐	Sticky	☐
Thick	☐	Savoury	☐	Slimy	☐	Slimy	☐
Thin	☐	Cardboard/paper	☐	Smooth	☐		☐
	☐	Nutty	☐	Thick	☐		☐
	☐	Salty	☐	Thin	☐		☐
	☐	Off-flavour	☐	Sticky	☐		☐
	☐	Hay-flavour	☐	mouthcoating	☐		☐
Other descriptors/notes		Other descriptors/notes		Other descriptors/notes		Other descriptors/notes	

Supporting information C3 Questionnaire for fNIRS

Study Title: Understanding astringency of plant proteins using brain imaging

Carefully read all criteria and tick box to agree before continuing

☐ I confirm I am over the age of 18 and generally in good health I'm not a smoker I have no oral infections/ diseases I'm not pregnant or lactating that Im not suffering from any chronic or acute illness or taking any medication

☐ I confirm that I have read and understand the Participant Information Sheet explaining the above research project and I have had the opportunity to ask questions about the project

☐ I confirm that I have been presented with a list of conditions which make my participation in this study prohibited for my own safety and I do not have a history of ANY of these conditions

☐ I confirm that I have read and fully understood the information sheet given to me regarding this piece of research

☐ I understand fNIRS will be used and I have been informed of how and why this technique will be used

☐ I have been informed of the risks of fNIRS and still consent to taking part in this study

☐ I have been informed that I will drink food-grade solutions and protein beverages and record my subjective assessment of taste perception

☐ I understand that my participation is voluntary and that I am free to withdraw at any time during data collection without giving any reason and without there being any negative consequences In addition should I not wish to answer any particular question or questions I am free to decline

☐ I agree that I have had adequate opportunity to ask the researcher(s) any questions I may have about this research and if applicable been given an appropriate answer

☐ I understand that my responses will be kept strictly confidential I give permission for members of the research team to have access to my anonymised responses

☐ I understand that my name will not be linked with the research materials and that an anonymous participant code will be used instead and I will not be identified or identifiable in the report or reports that result from the research

☐ I understand that the anonymized data will be stored in University Repository and other genuine researchers will have access to this anonymized data only if they agree to preserve the confidentiality of the information as requested in this form

☐ I understand that relevant sections of the data collected during the study may be looked at by individuals from the University of Leeds or from regulatory authorities where it is relevant to my taking part in this research I give permission for these individuals to have access to my records

☐ I have not had long-covid related symptoms and have no issues that may affect my response in normal consumption of food

☐ I give my consent to take part in this study.

Participant code (please ask researcher)

Participant signature (please write name)_____

Date_____

Email:_____

*You can contact Prof. Anwesha Sarkar (A.Sarkar@leeds.ac.uk, 0113 3432748) Dr Melanie Burke (M.R.Burke@leeds.ac.uk; 0113 3435738) if you have any further questions. If you decide to withdraw, your data are going to be deleted permanently until the anonymized data has been used in publications (i.e. 2 months' time from the completion of the study).

If you would like a copy of this consent form please let the researcher know and one shall be emailed to you

Appendix D supporting information for chapter 5

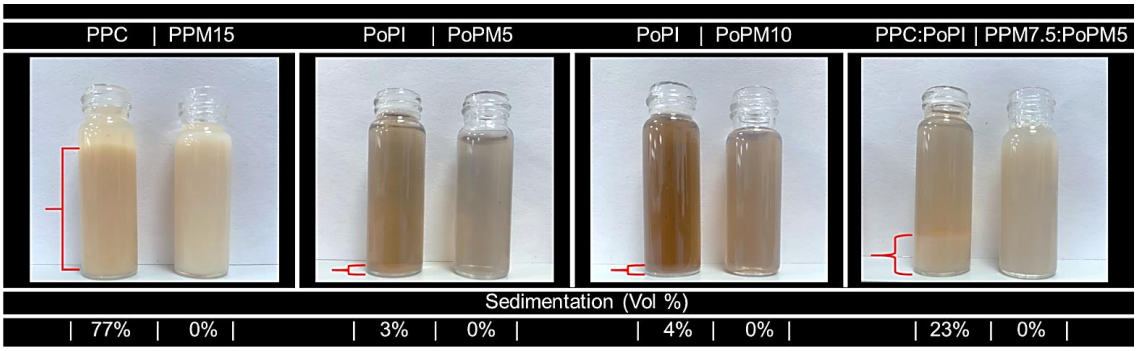

Figure D1 Sedimentation in native plant protein solutions as compared to corresponding microgel dispersions. Images and sedimentation (vol %) of native plant protein and plant protein microgel solutions prepared using pea protein concentrate to form a 15.0 wt% total protein microgel, (PPM15), potato protein isolate to form a 5.0 wt% total protein microgel (PoPM5), potato protein isolate to form a 10.0 wt% total protein microgel, (PoPM10), and using a mixture of pea protein concentrate at 7.5 wt% total protein and potato protein isolate at 5.0 wt% total protein microgel (PPM7.5:PoPM5). Microgels were prepared with volume fraction Φ = 40 and compared to native protein solutions of the same protein concentration. Photographs were captured when native proteins were left for 1 day whilst microgels were left for 28 days, such stability in microgels persisted for months. Red brackets highlight sedimentation in native protein solutions compared to undetectable levels present in microgel solutions

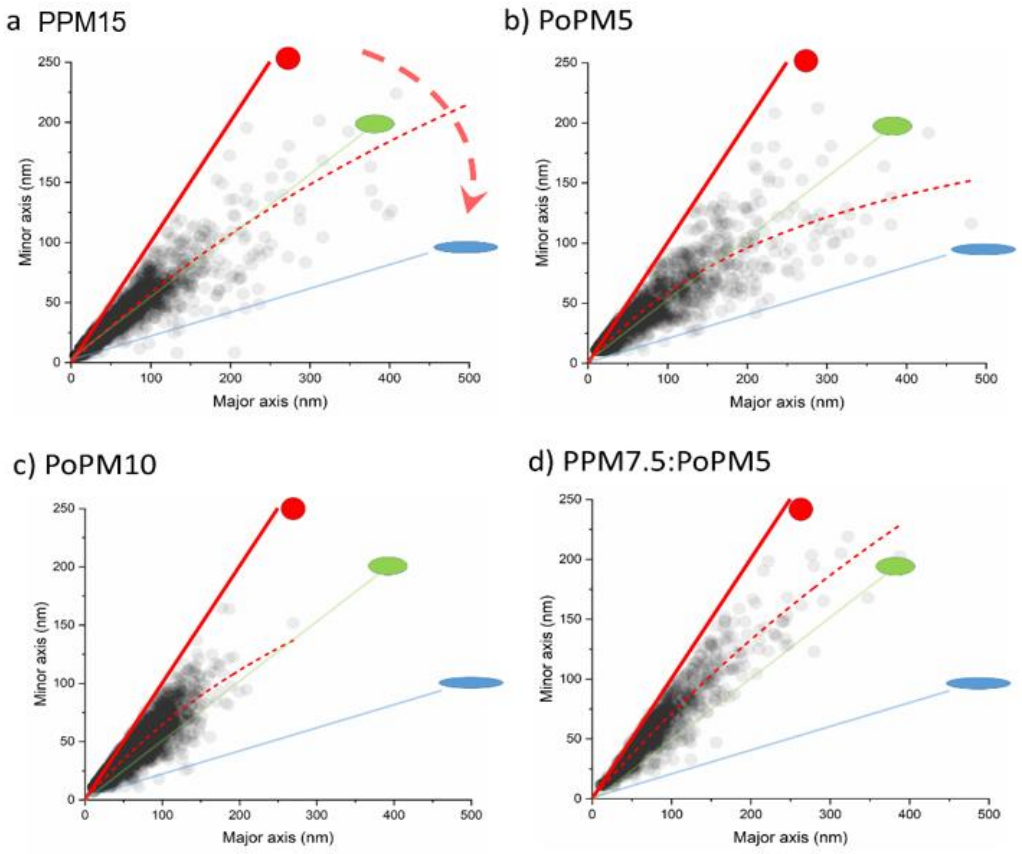

Figure D2 Shape analysis of microgel particle size distribution. Shape analysis performed on several thousand microgels per sample shown in Fig 3, microgels prepared using (a) pea protein concentrate to form a 15.0 wt% total protein microgel, (PPM15), (b) potato protein isolate to form a 5.0 wt% total protein microgel (PoPM5), (c) potato protein isolate to form a 10.0 wt% total protein microgel, (PoPM10), and (d) a mixture of pea protein concentrate at 7.5 wt% total protein and potato protein isolate at 5.0 wt% total protein. Ellipses were fitted to each microgel, and the graph plots the short or minor axis vs the long or major axis. Hence, the perfectly spherical microgels will follow the red line with a 1:1 aspect ratio. Most microgels in all samples were between spherical and a 2:1 aspect ratio represented by the green line. A general trend found is the increase in aspect ratio as particle size increases, represented the dashed red fit lines (note: the Michaelis-Menten fit equation used is not physically relevant). This could be explained by the larger microgels being randomly shaped aggregates of the smaller microgels.

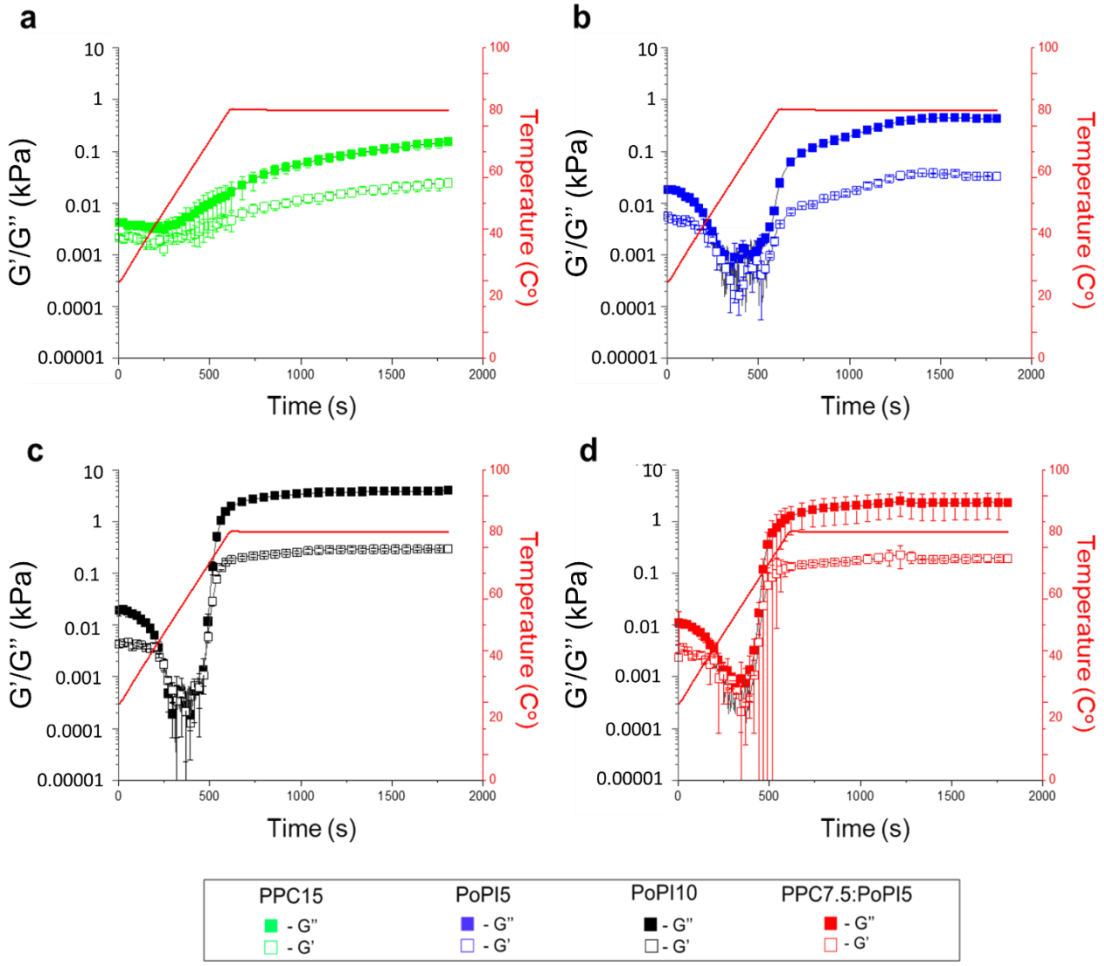

Figure D3 Temperature ramp with constant strain (0.1% at 1Hz) applied to native protein solutions prepared showing storage (G') and loss (G'') moduli of (a) pea protein concentrate to form a 15.0 wt% total protein microgel, (PPM15), (b) potato protein isolate to form a 5.0 wt% total protein microgel (PoPM5),(c) potato protein isolate to form a 10.0 wt% total protein microgel, (PoPM10), and (d) using a mixture of pea protein concentrate at 7.5 wt% total protein and potato protein isolate at 5.0 wt% total protein microgel (PPM7.5:PoPM5).Results are plotted as average of three repeat measurements on triplicate samples (n = 3 × 2) with error bars representing standard deviations.

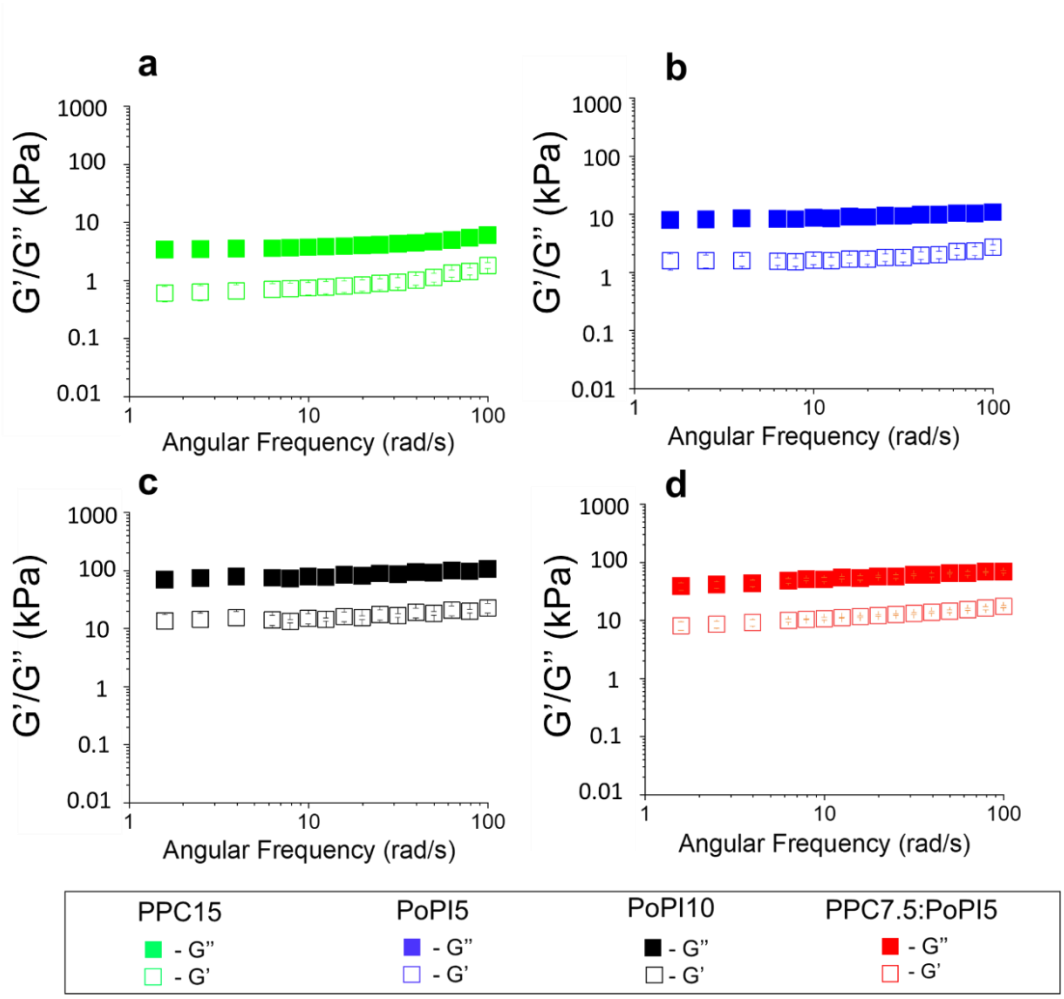

Figure D4 Viscoelasticity of plant protein-based parent hydrogels. Frequency sweep of heat-set gels prepared using (a) pea protein concentrate to form a 15.0 wt% total protein microgel, (PPM15), (b) potato protein isolate to form a 5.0 wt% total protein microgel (PoPM5), (c) potato protein isolate to form a 10.0 wt% total protein microgel, (PoPM10), and (d) using a mixture of pea protein concentrate at 7.5 wt% total protein and potato protein isolate at 5.0 wt% total protein microgel (PPM7.5:PoPM5).Protein dispersions were added onto a cone-and-plate geometry (diameter 50 mm, angle 1o), and gelation was initiated using a temperature ramp (25 – 80oC at a rate of 0.08 oC/ s and held at 80 oC for 30 min) and cooled to 37 oC where a frequency sweep at a strain of 0.1% was initialised. Results are plotted as average of six measurements on triplicate samples (n = 6 × 3) with error bars representing standard deviations.

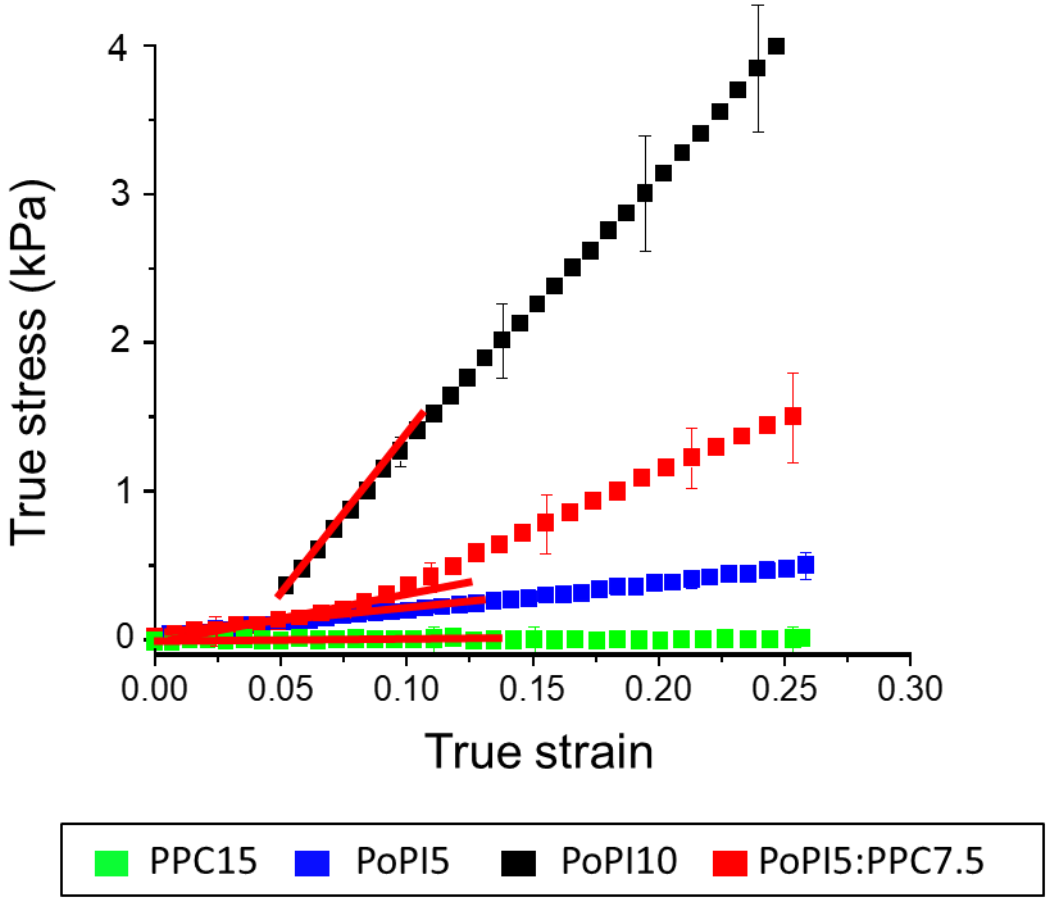

Figure D5 Large scale deformation of the parent protein gels. Stress-strain curves of plant protein gels prepared using pea protein concentrate to form a 15.0 wt% gel, (PPM15), potato protein isolate to form a 5.0 wt% gel (PoPM5), potato protein isolate to form a 10.0 wt% gel, (PoPM10), and using a mixture of pea protein concentrate at 7.5 wt% total protein and potato protein isolate at 5.0 wt% total protein gel (PPM7.5:PoPM5). Values where Young's modulus was calculated is indicated by the red vector. Results are plotted as average of three repeat measurements on triplicate samples (n = 3 × 2) with error bars representing standard deviations.

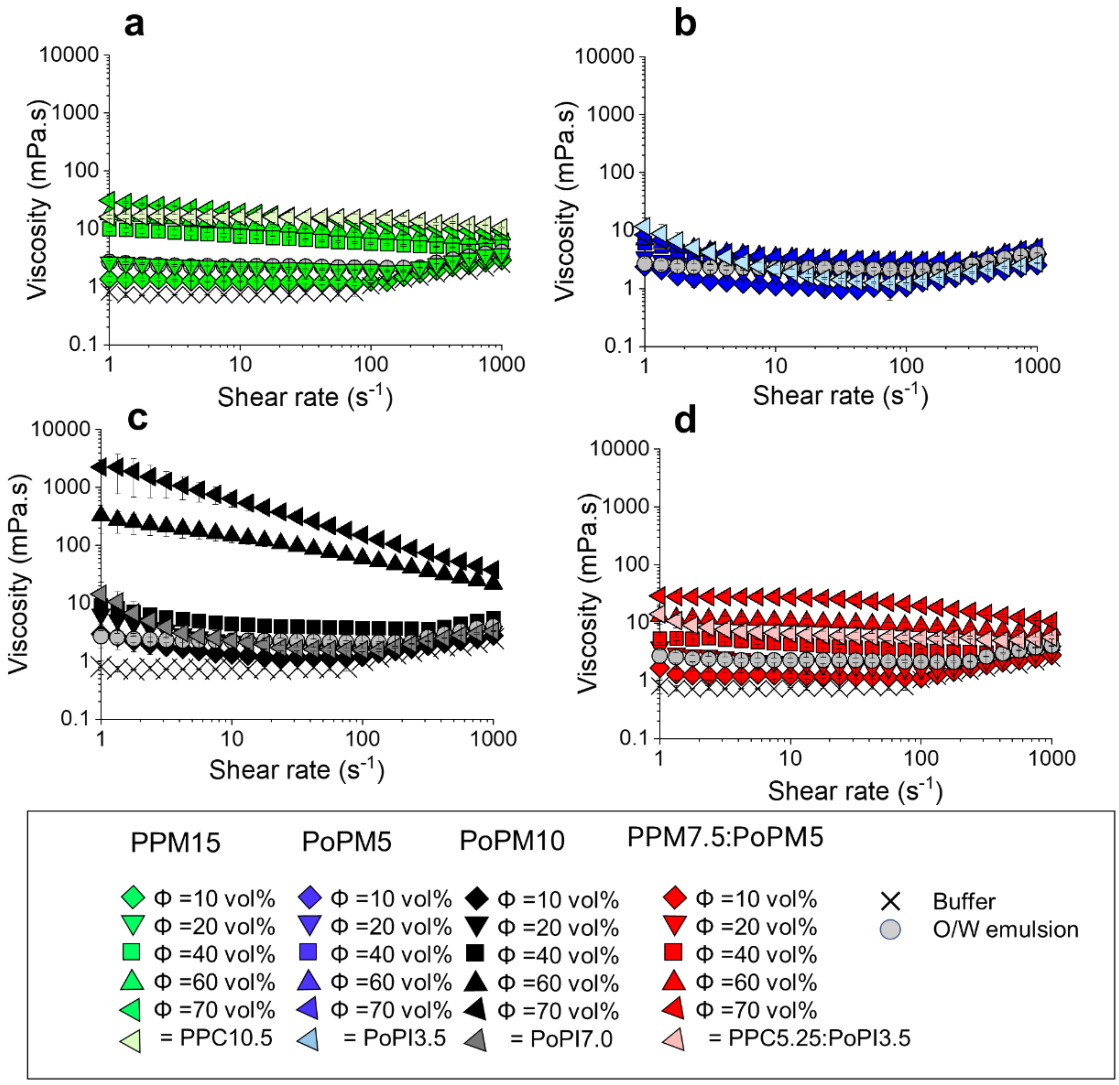

Figure D6 Flow curves of plant protein microgels. Apparent viscosity of plant protein microgels prepared using (a) pea protein concentrate to form a 15.0 wt% total protein microgel, (PPM15) (b) potato protein isolate to form a 5.0 wt% total protein microgel (PoPM5), (c) potato protein isolate to form a 10.0 wt% total protein microgel, (PoPM10) and (d) using a mixture of pea protein concentrate at 7.5 wt% total protein and potato protein isolate at 5.0 wt% total protein microgel (PPM7.5:PoPM5), as function of shear rate, respectively. Plant protein microgels were compared to native proteins (matched protein content for Φ =70 vol% with numbers displayed relating to the total protein content). 20.0 wt% oil-in-water (O/W) emulsion and buffer are shown in each plots (a-d) as controls. Shear rates were measured from ramping up from 1 s-1 to 1000 s-1 at 37 °C with plots as average of six measurements on triplicate samples (n = 6 × 3) with error bars representing standard deviations.

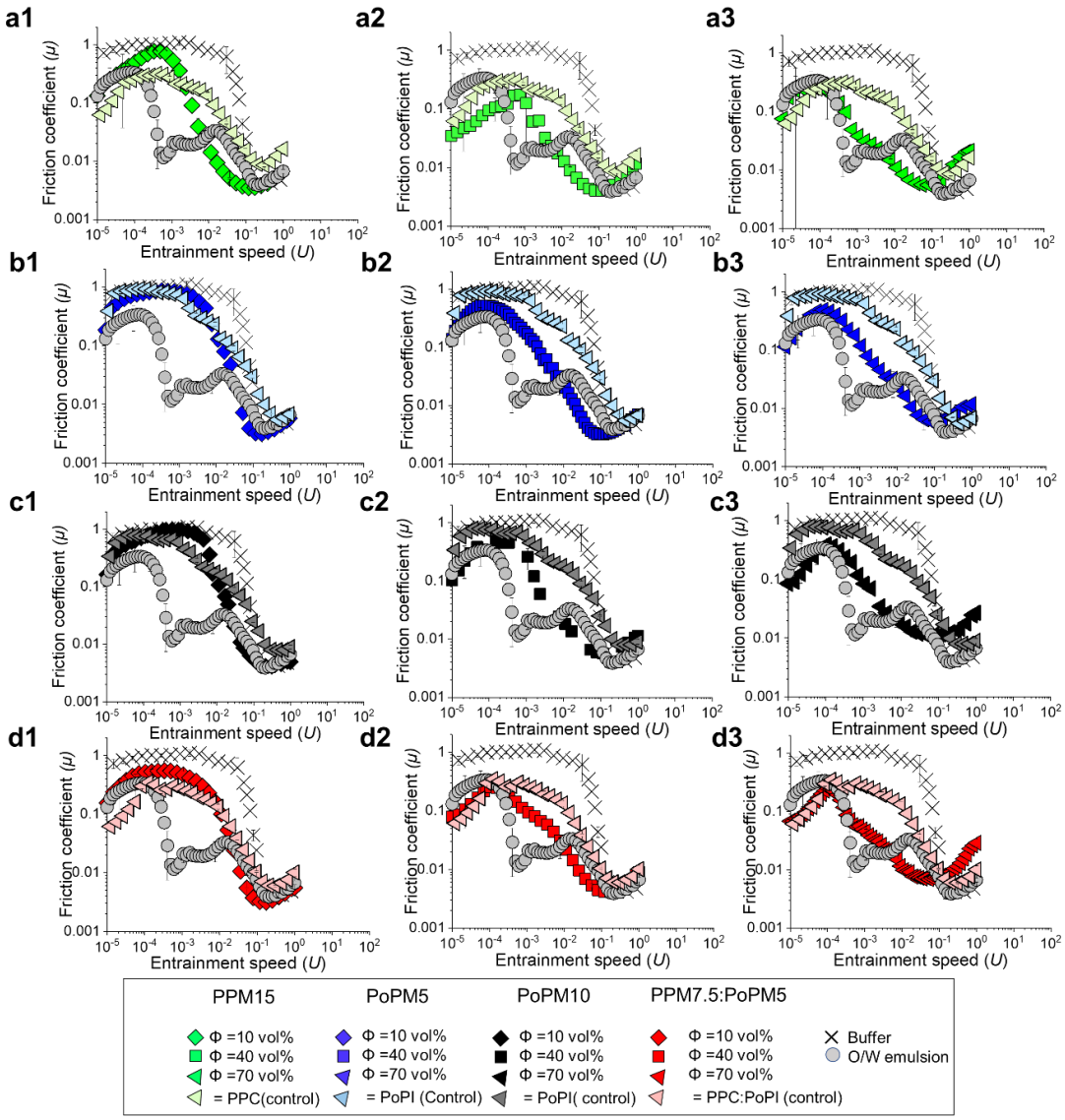

Figure D7 Frictional behaviour in hard-soft contact surfaces in presence of plant protein microgels. Tribological performance of steel ball on PDMS surfaces in the presence of plant protein microgels, native plant protein (matched protein content for Φ =70 vol% with numbers displayed relating to total protein content or oil-in-water emulsion. Friction coefficient (μ) as a function of entrainment in the presence of plant protein microgels prepared using (a1-3) pea protein concentrate to form a 15.0 wt% total protein microgel, (PPM15), (b1-3) potato protein isolate to form a 5.0 wt% total protein microgel (PoPM5), (c1-3)), potato protein isolate to form a 10.0 wt% total protein microgel, (PoPM10), and (d1-3) using a mixture of pea protein concentrate at 7.5 wt% total protein and potato protein isolate at 5.0 wt% total protein microgel (PPM7.5:PoPM5) with 1, 2 and 3 showing increased volume fractions from 10 to 70 vol%, respectively. Frictional responses of the

plant proteins at the highest concentration and 20 wt% oil-in-water emulsion (O/W emulsion) and buffer are included in each graph (a-d) as controls. Results are plotted as average of six repeat measurements on triplicate samples (n = 6 × 3) with error bars representing standard deviations.

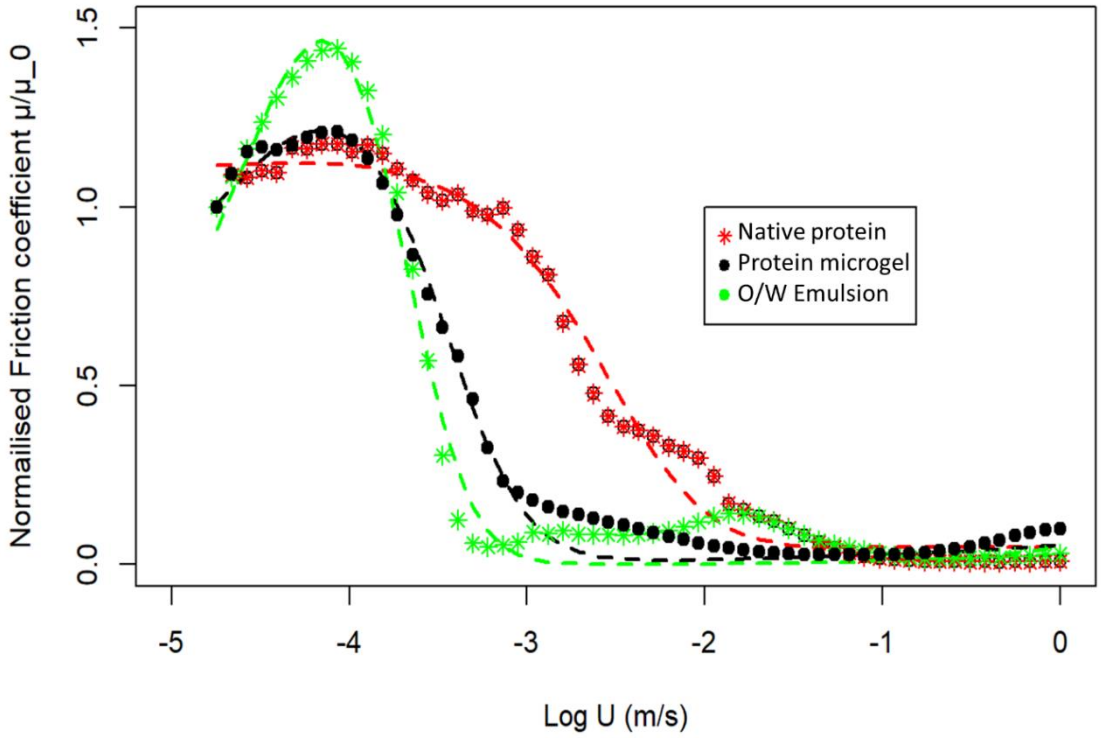

Figure D8 Normalised friction force of microgels compared against emulsions and native protein. Tribological performance of hard/soft (steel ball-on-PDMS) contact surfaces showing theoretical modelling of the normalised ratio of friction coefficients against the initial level at a load of 2.0 N. Microgel and emulsions show close resemblance in friction coefficients in comparison to those obtained in the presence of native protein, in the latter a greater speed is required before a reduction in normalized friction is observed. Here the dashed lines show the best theoretical fit using equation 5.21 in the main text.

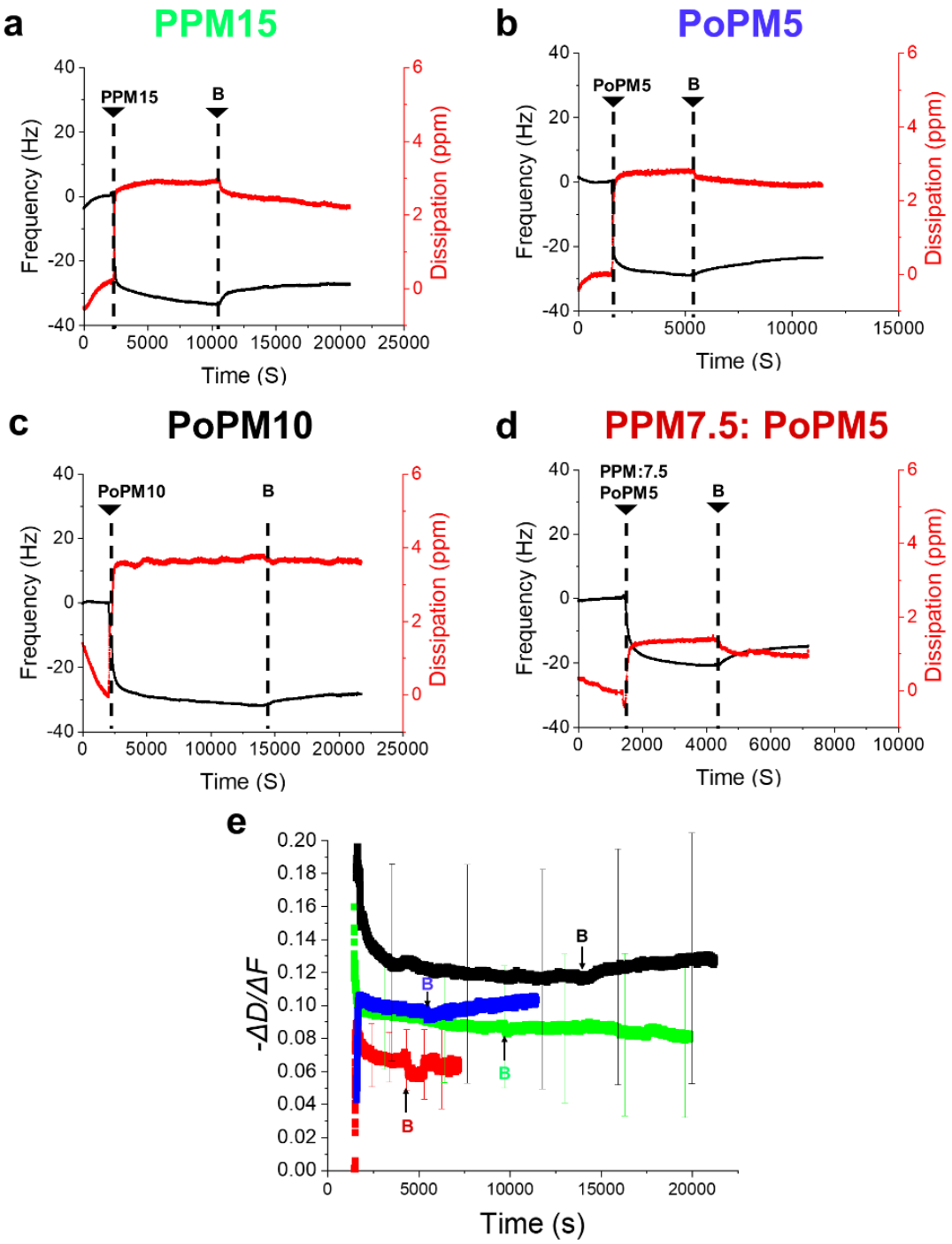

Figure D9 Adsorption properties of plant protein microgels. Mean frequency and dissipation (5th overtone shown) of plant protein microgels prepared using (a) pea protein concentrate to form a 15.0 wt% total protein microgel, (PPM15), (b) potato protein isolate to form a 5.0 wt% total protein microgel (PoPM5), (c) potato protein isolate to form a 10.0 wt% total protein microgel, (PoPM10), and (d) using a mixture of pea protein concentrate at 7.5 wt% total protein and potato protein isolate at 5.0 wt% total protein microgel (PPM7.5:PoPM5) on PDMS-coated hydrophobic sensors with B implying

injection of HEPES buffer. Viscoelasticity of the films (e) is represented by dissipation shift (ΔD)/frequency shift ratio (Δf) i.e. –ΔD/Δf of protein microgel solutions with step B representing the final buffer rinse stage. Results are plotted as average of three repeat measurements on triplicate samples (n = 3 × 2) with error bars representing standard deviations.

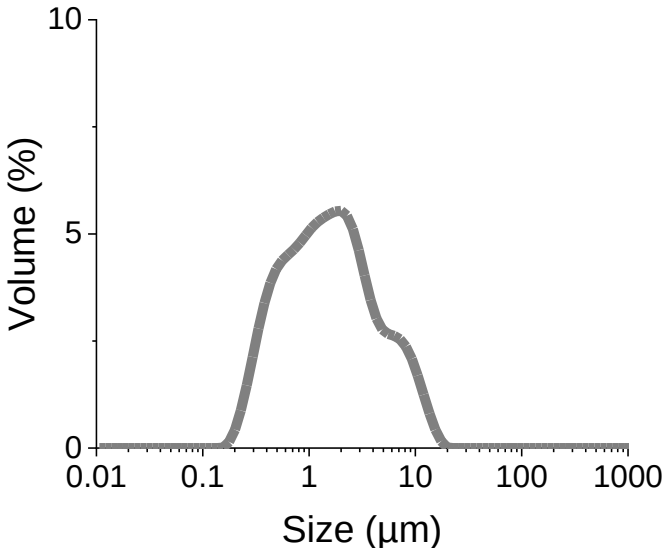

Figure D10 Droplet size distribution of 20:80 O/W Emulsion. Mean droplet size distribution of 20:80 O/W emulsions stabilised using 1.5 wt% potato protein. Results are plotted as average of three repeat measurements on triplicate samples (n = 3 × 2).

Table D1. Evolution of size of plant protein microgels with time. Mean and standard deviation (SD) of the change in hydrodynamic diameter (dH) of plant protein microgels as a function of storage time (T, days) at room temperature (22 ºC). Plant protein microgels were prepared using pea protein concentrate to form a 15.0 wt% total protein microgel, (PPM15), potato protein isolate to form a 5.0 wt% total protein microgel (PoPM5), potato protein isolate to form a 10.0 wt% total protein microgel, (PoPM10), and using a mixture of pea protein concentrate at 7.5 wt% total protein and potato protein isolate at 5.0 wt% total protein microgel (PPM7.5:PoPM5). Different lower-case letters in the same column indicate a statistically significant difference ($p < 0.05$)

	PPM15	**PoPM5**	**PoPM10**	**PPM7.5:PoPM5.0**

Storage time (Days)	d_H	PDI	d_H	PDI	d_H	PDI	d_H (Peak 1)	d_H (Peak 2)
T = 0	204 ± 7 [a]	0.22 ± 0.02 [a]	60 ± 1 [a]	0.23 ± 0.01 [a]	132 ± 2.5 [a]	0.21 ± 0.01 [a]	238 ± 4 [a]	48 ± 12 [a]
T = 7	236 ± 5 [a]	0.30 ± 0.04 [s]	67 ± 5 [ab]	0.27 ± 0.01 [b]	89.7 ± 4 [b]	0.22 ± 0.01 [ab]	260 ± 14 [b]	100 ± 10 [b]
T = 14	210 ± 5 [a]	0.24 ± 0.03 [a]	72 ± 2 [b]	0.25 ± 0.01 [b]	98 ± 2 [c]	0.24 ± 0.01 [b]	300 ± 10 [c]	96 ± 13 [b]
T = 28	222 ± 6 [a]	0.26 ± 0.02 [a]	78 ± 1 [b]	0.24 ± 0.01 [b]	105 ± 7 [a]	0.25 ± 0.01 [b]	315 ± 15 [c]	115 ± 17 [b]

Table D2 Stability of plant protein microgels when subjected to processing. Mean and standard deviation (SD) of the change in hydrodynamic diameter of of plant protein microgels when heated at 90 oC for 30 min. Plant protein microgels were prepared using pea protein concentrate containing 15.0 wt% protein (PPM15), potato protein isolate containing 5.0 wt% protein (PoPM5), potato protein isolate containing 10.0 wt% protein (PoPM10), and mixed pea protein concentrate containing 7.5 wt% protein and potato protein isolate containing 5.0 wt% protein (PPM7.5:PoPM5). Different lower-case letters in the same column indicate a statistically significant difference ($p < 0.05$).

	PPM15	PoPM5	PoPM10	PPM7.5:PoPM5.0

Time (s)	d_H	PDI	d_H	PDI	d_H	PDI	d_H (Peak 1)	d_H (Peak 2)
T = 0	204 +/- 7[a]	0.22 +/- 0.01[a]	60 +/- 1 [a]	0.23 +/- 0.01[a]	115 +/- 5	0.21 +/- 0.01[a]	238 +/- 4[a]	48 +/- 12[a]
T = 600	211 +/- 5 [a]	0.25 +/- 0.01[b]	76 +/- 1 [b]	0.23 +/- 0.01[a]	119 +/- 1	0.24 +/- 0.01[b]	239 +/- 8[a]	48 +/- 9[a]
T = 1800	198 +/- 3 [a]	0.22 +/- 0.02[a]	86 +/- 2 [c]	0.24 +/- 0.01[a]	130 +/- 5	0.23 +/- 0.01[b]	235 +/- 7[a]	56 +/- 5[a]

Table D3 Comparison of frictional coefficients of plant protein microgels in hard-soft contact surfaces. Mean and standard deviation (SD) of the friction coefficients of plant protein microgels prepared using (a) pea protein concentrate to form a 15.0 wt% total protein microgel, (PPM15), (b) potato protein isolate to form a 5.0 wt% total protein microgel (PoPM5), (c) potato protein isolate to form a 10.0 wt% total protein microgel, (PoPM10), and (d) using a mixture of pea protein concentrate at 7.5 wt% total protein and potato protein isolate at 5.0 wt% total protein microgel (PPM7.5:PoPM5). Different Φ of microgels were compared against buffer, native protein (at Φ = 70 equivalent) and O/W emulsion. Different lower-case letters in the same column indicate a statistically significant difference ($p < 0.05$).

Coefficient of friction of PPM15		
	Mixed lubrication regime (0.1 Pa m)	
	Mean	SD
Φ =10 vol%	0.00573[a]	0.001
Φ =40 vol%	0.00893[b]	0.00122
Φ =70 vol%	0.01096[c]	0.001
Buffer	0.744[d]	0.300
O/W emulsion	0.02771[e]	0.00533
PPC10.5	0.1358[f]	0.01681
Coefficient of friction of PoPM5		
	Mixed lubrication regime (0.1 Pa m)	

	Mean	SD
Φ =10 vol%	0.01193[a]	0.0027
Φ =40 vol%	0.0064[b]	0.00269
Φ =70 vol%	0.01296[a]	0.00388
Buffer	0.744[c]	0.300
O/W emulsion	0.02771[d]	0.00533
PoPI3.5	0.06511[e]	0.01022
Coefficient of friction of PoPM10		
	Mixed lubrication regime (0.1 Pa m)	
	Mean	SD
Φ =10 vol%	0.01084[a]	0.00119
Φ =40 vol%	0.0116[a]	0.00166
Φ =70 vol%	0.03457[b]	0.00597
Buffer	0.744[c]	0.300
O/W emulsion	0.02771[d]	0.00533
PoPI7.0	0.08773[e]	0.00882
Coefficient of friction of PPM7.5:PoPM5		
	Mixed lubrication regime (0.1 Pa m)	
	Mean	SD
Φ =10 vol%	0.01063[a]	0.001
Φ =40 vol%	0.01177[b]	0.001
Φ =70 vol%	0.01161[b]	0.0028
Buffer	0.744[c]	0.300
O/W emulsion	0.02771[d]	0.00533
PPC5.25: PoPI3.5	0.06172[e]	0.00192

Table D4 Comparison of frictional coefficients of plant protein microgels at a range of speeds in 3D biomimetic tongue-like surfaces. Mean and standard deviation (SD) of the friction coefficients of plant protein microgels prepared using (a) pea protein concentrate to form a 15.0 wt% total protein microgel, (PPM15), (b) potato protein isolate to form a 5.0 wt% total protein microgel (PoPM5), (c) potato protein isolate to form a 10.0 wt% total protein microgel, (PoPM10), and (d) using a mixture of pea protein concentrate at 7.5 wt% total protein and potato protein isolate at 5.0 wt% total protein microgel (PPM7.5:PoPM5) in the boundary and mixed regimes. Different Φ of microgels were compared against buffer and O/W emulsion. Different lowercase letters in the same row indicate a statistically significant difference ($p < 0.05$).

	Buffer		**20% O/W emulsion**		**PPM15**						**PoPM5**					
VR (M/S)		**SD**		**SD**	**10**	**SD**	**40**	**SD**	**70**	**SD**	**10**	**SD**	**40**	**SD**	**70**	**SD**
0.0005	0.56[a]	0.11	0.30[b]	0.08	0.26[cb]	0.04	0.20[d]	0.03	0.20[d]	0.02	0.50[a]	0.08	0.48[a]	0.03	0.31[e]	0.04

0.001	0.65[a]	0.13	0.24[b]	0.03	0.28[cb]	0.03	0.25[cb]	0.03	0.24[c]	0.03	0.55[a]	0.05	0.41[d]	0.01	0.34[e]	0.05
0.002	0.64[a]	0.10	0.30[b]	0.03	0.30[cb]	0.02	0.27[cb]	0.01	0.23[d]	0.01	0.60[a]	0.11	0.55[ab]	0.06	0.36[e]	0.04
0.0050	0.70[a]	0.14	0.36[b]	0.03	0.38[cb]	0.04	0.31[d]	0.01	0.28[e]	0.02	0.59[f]	0.05	0.45[c]	0.04	0.40[bc]	0.06
0.008	0.70[a]	0.13	0.39[b]	0.04	0.43[cb]	0.04	0.36[db]	0.02	0.33[d]	0.03	0.62[a]	0.07	0.46[c]	0.05	0.40[c,b]	0.05
0.0099	0.64[a]	0.07	0.39[b]	0.01	0.44[b]	0.05	0.38[cb]	0.02	0.36[c]	0.02	0.67[a]	0.10	0.56[a]	0.09	0.41[b,c]	0.05
0.02	0.69[a]	0.08	0.39[b]	0.02	0.45[c]	0.03	0.42[b]	0.01	0.39[b]	0.04	0.45[c]	0.05	0.41[b]	0.05	0.41[b]	0.04
0.0495	0.81[a]	0.12	0.39[b]	0.02	0.40[b]	0.03	0.44[b]	0.03	0.42[b]	0.03	0.49[c]	0.02	0.44[b]	0.04	0.41[b]	0.03
0.0798	0.77[a]	0.12	0.40[b]	0.02	0.36[b]	0.02	0.47[c]	0.02	0.45[c]	0.05	0.44[c]	0.04	0.35[d]	0.01	0.42[b]	0.03

	PoPM10						**PoPM5:PPM7.5**					
VR (M/S)	**10**	**SD**	**40**	**SD**	**70**	**SD**	**10**	**SD**	**40**	**SD**	**70**	**SD**
0.0005	0.43[a]	0.06	0.38[e]	0.05	0.22[cd]	0.03	0.21[d]	0.02	0.37[e]	0.06	0.40[abce]	0.19
0.001	0.48[d]	0.06	0.42[d]	0.05	0.26[b,c]	0.05	0.27[b,c]	0.04	0.41[d]	0.08	0.47[d]	0.12
0.002	0.50[a]	0.09	0.45[e]	0.06	0.30[cf]	0.06	0.30[cf]	0.02	0.46[be]	0.12	0.55[ae]	0.17
0.00501	0.55[f]	0.06	0.50[c]	0.04	0.38	0.10	0.34[cd]	0.04	0.45[bc]	0.10	0.65[a]	0.09
0.008	0.59[a]	0.08	0.52[c]	0.05	0.43[bcd]	0.15	0.34[d]	0.02	0.46[c]	0.09	0.68[a]	0.12
0.0099	0.53[b]	0.09	0.49[b]	0.03	0.48[bcde]	0.21	0.35[d]	0.04	0.48[bde]	0.09	0.55[e]	0.03
0.02	0.53[c]	0.05	0.40[b]	0.02	0.53[abc]	0.21	0.35[d]	0.01	0.46[bc]	0.08	0.61[a]	0.05
0.0495	0.53[c]	0.10	0.41[b]	0.01	0.64[c]	0.16	0.34[d]	0.01	0.41[b]	0.07	0.61[e]	0.01
0.0798	0.49[c]	0.07	0.40[b]	0.01	0.68[a]	0.19	0.32[d]	0.02	0.39[bc]	0.14	0.69[a]	0.07

Supporting information D1 Theoretical analysis of indentation and drag force of lubricants.

The total load (W_T) in mixed regime is supported by both lubricant and the asperities. As lubricant was substantially lower in friction than the buffer, the following expression was used to calculate load:

$$W_L = \frac{\mu B - \mu}{\mu B} W_T \qquad \text{(D1.1)}$$

where, μ is the friction of buffer or lubricant at a defined entrainment speed.

To understand the physical properties of lubricant separating contact surfaces, the mechanical analysis can be performed using Hertz theory at the contact point.

The radius (a_H) and the indentation δ are obtained using equations D1.2 and D1.3 for a point of contact supporting load W.

$$a_H{}^3 = \frac{3}{4}\frac{WR^*}{E^*} \quad \text{(D1.2)}$$

$$\delta = \frac{a_H{}^2}{R^*} - f\left(\frac{a_H}{R}\right)\frac{W}{\pi R^* E(1-v^2)} \quad \text{(D1.3)}$$

With

$$f\left(\frac{a_H}{R}\right) = \frac{2\,(1+v)}{\left(4+\left(\frac{a_H}{R}\right)^2\right)^{3/2}} + \frac{(1-v^2)}{\left(4+\left(\frac{a_H}{R}\right)^2\right)^{1/2}} \quad \text{(D1.4)}$$

R* represents reduced radius $\left(\frac{1}{R\prime} + \frac{1}{R\prime\prime}\right)^{-1}$ from PDMS and steel ball contact, *v* is the Poisson ratio and E^* the elastic modulus between lubricant and PDMS surface. E^*, obtained from the expression $\left(\frac{1-v^2}{E\prime} + \frac{1-v^2}{E\prime\prime}\right)^{-1}$ is the reduced elastic modulus of PDMS and lubricant. For the microgels the elastic modulus measured from heated parent plant proteins was used and for emulsion this was estimated from $E = 2G'_f(1+v)$ where $G'_f = \frac{2y}{R}$ where y is the interfacial surface tension of oil stabilised by potato protein measured at y = 27 mN m^{-1} with R being radius of particle.

The load supported by each lubricant (W_p) was estimated using the following equation where $a_{tp}{}^2$ is the Hertz contact radius between glass ball and PDMS calculated using equation D1.2 :

$$Wp = \frac{W_p}{N_p} = \frac{1}{\emptyset_p}\frac{W_T R^2}{a_{tp}{}^2} \quad \text{(D1.5)}$$

Combining equations D1.5, D1.2 and D1.3, the relative indentation of the monolayer of microgel particles or emulsion can be expressed as:

$$\frac{\delta}{R} = \left(\frac{a_H}{R}\right)^2 - \frac{4}{3\pi(1-\nu^2)}\left(\frac{a_H}{R}\right)^3 f\left(\frac{a_H}{R}\right) \quad \text{(D1.6)}$$

Where, a_H/R is independent of R and is the relative indentation of the surface particles independent of particle radius

$$\frac{a_H}{R} = \left(\frac{3W_L}{4\emptyset_p E^* atp^2}\right)^{1/3} \quad \text{(D1.7)}$$